ROLE OF KCNRG IN B-CELL CHRONIC LYMPHOCYTIC LEUKEMIA

by

Aybike Birerdinc

A Dissertation
Submitted to the
Graduate Faculty
of
George Mason University
in Partial Fulfillment of
The Requirements for the Degree
of
Doctor of Philosophy
Biosciences

Committee:

Dr. Ancha Baranova,
Dissertation Director

Dr. Alan H Christensen,
Committee Member

Dr. Jenefir D. Isbister,
Committee Member

Dr. Barney Bishop,
Committee Member

Dr. Kirsten Edmiston,
Committee Member

Dr. James A. Willett,
Department Chairperson

Dr. Peter Becker, Associate Dean
for Graduate Programs, College
of Science

Dr. Vikas Chandhoke, Dean,
College of Science

Date: December 2, 2008

Fall Semester 2008
George Mason University
Fairfax, VA

Role of KCNRG in B-CELL Chronic Lymphocytic Leukemia

A dissertation submitted in partial fulfillment of the requirements for the degree of Doctor of Philosophy at George Mason University

By

Aybike Birerdinc
Master of Science
Georgetown University, 2001

Director: Ancha Baranova, Assistant Professor
Department of Molecular and Microbiology

Fall Semester 2008
George Mason University
Fairfax, VA

Copyright: 2008 Aybike Birerdinc
All Rights Reserved

DEDICATION

This is dedicated to my loving family, who has given me unwavering trust, support and patience. Thank you for believing in me, always.

ACKNOWLEDGEMENTS

I would like to thank Stephanie Coon who collaborated on cell line DNA preparation and sequence analysis, Masoomeh Sikaroodi, who performed automated sequencing, Amy J VanMeter for the work on the protein arrays, Manpreet Rhandawa. for her help with the FACS analysis and all of my colleagues who have gracefully shared their time and experience.

I would like to thank my committee members for their contributions, and Dr. Baranova, my dissertation adviser, who always goes above and beyond the call of duty in sharing her time and experience with me and the rest of her students. And last but certainly not least, I would like to thank my family for their boundless support and encouragement.

TABLE OF CONTENTS

Page
List of Tables……vi
List of Figures……vii
List of Abbreviations……viii
Abstract……x
Chapter 1: Background and Significance……1
Chapter 2: Materials and Methods…… 21
Chapter 3: Results and Discussion……44
Chapter 4: Conclusion……83
Appendix 1: KCNRG isoforms: Blastp search……86
Appendix 2: KCNRG isoforms: Allignment……91
Appendix 3: Proteins Containing COOL Domain…… 101
Appendix 4: Analysis of COOL Domain……110
Appendix 5: KCNRG Variant 2 Sequence…… 118
Appendix 6: Cell Proliferation Assay: BrdU ELISA……119
Appendix 7: FACS Analsysis: Cell Cycle PI…… 121
Appendix 8: Apoptosis FACS Analysis: Annexin V / 7-AAD…… 136
Appendix 9: Protein Array: KCNRG V1 & V2 Cell Lines…… 139
Appendix 10: Microarray: Cancer Pathway…… 142
Appendix 11: RT-Array vs. Microarray……153
List of References……156
Curriculum Vitae……175

LIST OF TABLES

Table Page
Table 1: Primers.....37
Table 2: Tissue type and disease stage 40
Table 3: SuperArray RT-PCR.....80

LIST OF FIGURES

Figure Page
Figure 1: Map of 13q14 regions....5
Figure 2: Isoforms of KCNRG and RFP2 and overlapping regions....13
Figure 3: Kv Shaker type channel with α, β and T1 domains. 15
Figure 4: Comparative analysis of RFP2/KCNRG locus 45
Figure 5: KCNRG conserved domain homology....47
Figure 6: RASMOL image of T1 domain tetramer 48
Figure 7: Evolution tree KCNRG COOL-domain....50
Figure 8: Alignment of KCNRG and KCTD family 51
Figure 9: Phylogenetic tree: KCNRG-like proteins....51
Figure 10: Multiple cloning site pcDNA 3.1 version A....57
Figure 11: Insert site of KCNRG Variant 1 58
Figure 12: Proliferation: BrdU ELISA assay....60
Figure 13: HL60 FACS PI....61
Figure 14: Quantification of HL60 FACS 63
Figure 15: HL60 Annexin V / 7-AAD....65
Figure 16: Fluorescent stains: Hl60 66
Figure 17: Fluorescent stains: RPMI 8226 67
Figure 18: Fluorescent stains: LNCaP 68
Figure 19: Live cell pictures 69
Figure 20: LNcaP Anoikis 71
Figure 21: Topographic map: Selected Genes 73
Figure 22: Effects of normalization 74
Figure 23: Mann-Whitney shortlist genes....75
Figure 24: Caspase cascade 77
Figure 25: RT-PCR validation 78
Figure 26: BAX isoforms....79
Figure 27: Real-time PCR human lymphoma....81

LIST OF ABBREVIATIONS

7-AAD – 7-amino-actinomysin
ATCC – American Type Culture Collection
B-CLL – B-cell Chronic Lymphocyte Leukemia
BMSCs – Bone marrow stromal cells
BTB/POZ – BTB, for BR-C, ttk and bab, and the POZ also known as poxvirus and zinc finger
CLL – Chronic Lymphocyte Leukemia
COOL – Proteins homologous to C-end of KCNRG isoform S
DAPI – 4',6-diamidino-2-phenylindole
DiOC18 – 3-dioctadecyloxacarbocyanine perchlorate
DLBL – Diffuse Large B-cell Lymphomas
DLEU1 – BCMS (B-Cell Multiple Splicing)
DLEU2 – BCMSUN (BCMS-Upstream Neighbor) gene
ECM – Extracellular Matrix
ELISA – Enzyme-Linked ImmunoSorbent Assay
ELM – Eukaryotic Linear Motif Resource
ER – Endoplasmic reticulum
ERAD – ER-associated degradation pathway
EST – Express sequence tags
EthD-1 – Ethidium Homodimer
EV – Empty Vector
FACS – Fluorescence-activated cell sorting
FDR – False Discovery Rate
FISH – Fluorescent in situ Hybridization
FL – Follicular Lymphomas
FSC – Forward Scatter
GIST – Gastrointestinal Stromal Tumors
GWA – Genome Wide Association
HCC – Hepatocellular Carcinoma
HL – Hodgkin Lymphomas
HL-60 – Human Promyelocytic Leukemia
ICRF – Imperial Cancer Research Foundation, United Kingdom
INR – Core Promoter Initiator Element
KCNRG V1 – KCNRG variant 1, corresponding to protein product KCNRG - S
KCNRG V2 – KCNRG variant 2, corresponding to protein product KCNRG – L
Kir – two trans-membrane helix inward rectifier channel class
Kv – six trans-membrane helix voltage gated potassium channel class
LANL – Los Alamos National Laboratory, United States

LNCaP – Androgen-sensitive human prostate adenocarcinoma derived from lymph node metastasis
LOH – The loss of heterozygosity
MB – Medulloblastoma
MCL – Mantle Cell Lymphoma
MCL – Mantle Cell Lymphomas
MDR – Minimally Deleted Regions
MM – Multiple Myeloma
MZBL – Marginal Zone B-cell Lymphomas
NCBI – National Center for Biotechnology Information
NZB – New Zealand black mouse
NZW – New Zealand white mouse
ORF – Open reading frame
PAH – Pulmonary Arterial Hypertension
PBL – Peripheral Blood Lymphocytes
PBS – Phosphate buffered saline
PI – Propidium iodide
PME – Progressive myoclonic epilepsy
RAMS – Russian Academy for Medical Science
RB1 – Retinoblastoma gene 1
RBCC/TRIM – zinc-binding RING domains, a B-box, and a coiled-coil domain
RCMG – Russian Center for Medical Genetics, Moscow, Russia
RFP2 – Ret Finger Protein 2
RPA – Reverse Phase-protein Array
RPMI-8226 – Multiple Myeloma cell line with lymphoblast-like appearance
RT-PCR – Real time Polymerase Chain Reaction
SAM – Significance Analysis of Microarrays
SLL – Small Lymphocytic Lymphomas
SNPs – Single Nucleotide Polymorphisms
SSC – Side Scatter
SSCP – Single-strand conformational polymorphism
SSDSPA – Class IV WW domain interaction motif involved in phosphorylation-dependent interaction
STK2 – serine-threonine kinase
STS – Sequence tagged site
T1 – Tetramerization Domain
T2D – Type 2 diabetes
TL – T-cell Lymphomas
T-PLL – T-cell Prolymphocytic Leukemia
TSG – Tumor suppressor gene
VDAC – Mitochondrial Voltage-Dependent Anion Channels
YAC – Yeast Artificial Chromosome

ABSTRACT

ROLE OF KCNRG IN B-CELL CHRONIC LYMPHOCYTIC LEUKEMIA

Aybike Birerdinc, PhD

George Mason University, 2008

Dissertation Director: Ancha Baranova

B-cell chronic lymphocyte leukemia (B-CLL) accounts for approximately 30% of all leukemias in the Western world and has so far been treated with variable success. The newly characterized *KCNRG* gene has been mapped to chromosome 13q14.3. *KCNRG* is thought to be a tumor suppressor gene involved in the development of B-cell chronic lymphocytic leukemia due to its significant homology to the tetramerization (T1) domain of the voltage-gated potassium channels (Kv channels) and an ability to suppress growth-stimulating Kv currents. Since point mutations of *KCNRG* have not been found in B-CLL samples, a novel approach for its study based on a haploinsufficiency model was suggested. The aim of this study is to determine whether the KCNRG gene functions as growth suppressor in tumor cell lines and to elucidate a putative role for the loss of this gene in the development and the progression of B-CLL. Overexpression studies of *KCNRG* were performed in an attempted to determine the involvement of *KCNRG* in

apoptosis, differentiation, and invasion of cultured human tumor cells, and the effects of overexpression of *KCNRG* on gene expression and proteomics profiles were quantified.

CHAPTER 1: Background and Significance

B-cell Chronic Lymphocytic Leukemia (B-CLL) is one of the most commonly diagnosed leukemias in the Western world (Byrd et al. 2004). This disease accounts for ~30% of all human leukemias and is most commonly seen amongst the elderly; about two-thirds of the patients are older the age of 60 (Zwiebel et al. 1998). The clinical course of CLL is subdivided into five stages: during stage O, only bone marrow and blood lymphocytosis is seen; during stage I, it is possible to detect lymphocytosis with enlarged nodes; at stage II, lymphocytosis with enlarged spleen and/or liver involvement can be detected; at stage III, lymphocytosis with anemia is observed; and at stage IV lymphocytosis with thrombocytopenia can be seen (Rai KR et al. 1975, Binet at al. 1981). As can be observed from the clinical staging CLL develops progressively.

On a cellular level the disease progresses due to the prolonged survival of B-CLL cells arrested in the G0 stage of the cell cycle (Gale et al. 1987). This prolonged survival causes the accumulation of slowly proliferating CD5(+) B lymphocytes in the blood, bone marrow, and lymphatic tissues leading to the clinical manifestations of the disease. These quiescent small lymphocytes, CD5(+) B lymphocytes are frozen at an early step of maturation and have decreased susceptibility to apoptotic cell death. Latter features are commonly attributed to the imbalance in various cytoplasmic pro-survival and pro-death pathways, including the BCR-signaling pathway (Danilov AV et al. 2006; Ougolkov

2007, Iglesias-Serret 2007). In addition, a small number of "atypical", Ki-67 expressing lymphocytes are frequently observed in the bone marrow of CLL patients (Bueso-Ramos CE. et al. 2004). Proliferation rates of these lymphocytes vary among patients and even among subpopulations of cells within the leukemic clones of individual patients (Chiorazzi N, Ferrarini M 2006). A newly evolving point of view stresses that blood lymphocyte count in B-CLL patients represents a dynamic interplay between ongoing birth and death within the clones rather than a linear, monotonous accumulation of inert leukemic cells (Chiorazzi N, Ferrarini M 2006).

Historically CLL has been treated with mixed success. More often than not, classical chemotherapy methods are only marginally effective and rarely yield complete responses. Typically the survival times are ~5-8 years although this is highly variable (Dighiero et al. 1998; Montserrat E. 2004). Therefore, understanding the genetic pathways involved in B-CLL is necessary to design more effective therapeutic approaches.

Genetic aberrations seen in CLL

From a genetic perspective, an abnormal karyotype, as detected by fluorescent in situ hybridization (FISH), can be observed in the tumor cells of the majority (90%) of patients with CLL cases (Döhner et al. 1999). The most common chromosomal abnormalities are deletions of the chromosomal band 13q14 which occur in ~50-70% of all cases of CLL (Liu Y et al. 1997). The next most common deletions are found in 11q22-q23 region accounting for ~19% and are usually associated with extensive lymph

node involvement and an aggressive form of the disease (Cuneo A. et al. 2002; Dohner H. et al. 2000). The deletions in 11q22-q23 region may not be a primary event, and may actually arise as a secondary event in cases where there is already an aberration in 13q14 (Cuneo A. et al. 2002).

Other aberrations include trisomy 12, which is considered to be atypical CLL and is usually associated with poor prognosis. Trisomy 12 in CLL coincides with the expression of the CD11a marker (O'Connor S.J. et al. 2000). In 1999 Caligaris-Cappio et al. showed that trisomy 12 is associated with the un-mutated status of the immunoglobulin variable heavy chain (VH) genes, and corresponds to atypical cellular morphology (Caligaris-Cappio et al. 1999). Another type of aberration, one that involves deletions in the 17p13 region, seems to be more common in the late stage of the disease and is believed to involve the TP53 tumor suppressor gene. This type of deletion is also associated with shortened survival (Shaw GR and Kronberger DL 2000 and Haslinger et al. 2004). Finally, the deletions in 6q21 are found to occur in 7% of B-CLL cases. Deletions of 6q21 are associated with larger tumor size (lymphadenopathy), however, no correlation with negative prognosis has been evident (Stilgenbauer et al. 1999).

Using FISH, deletions in 13q14.3 are detected in > 95% of the clonal population of malignant cells, hence giving rise to the belief that deletions in 13q14.3 may be an early or even initiating event in CLL. In contrast, other chromosomal abnormalities are less prevalent, being present in only a small proportion of the CLL cohort (Jabbar SA et al. 1995).

Fine mapping of 13q14.3 region deleted in CLL

The search for a TSG involved in B-CLL was stimulated by the fact that the retinoblastoma gene (RB1), a well-known TSG residing in13q14.3, remains functional in some B-CLL patients, while a region adjacent to RB1 on the telomere side is often deleted (L.A. Hawthorn et al. 1993, Y. Liu et al. 1992). This region was assumed to contain a TSG critical for B-CLL development. At the time, the 13q14.3 region, as well as most of the human genome landscape, was uncharted territory: markers suitable for physical mapping were several mega-bases apart from each other, which hindered precise localization of the chromosomal breakpoints in CLL cells.

Through concerted efforts by a number of research teams, several STS-markers were mapped to the region of interest and used as anchors for yeast artificial chromosome (YAC) contigs (V.M. Brodyanskii et al. 1995). These markers were also used as probes for Southern blotting of DNA of patients in order to pinpoint the area deleted in B-CLL cases (Y. Liu et al. 1995; M.M Corcoran et al. 1991). Fine structural analysis of the 13q14 region of the human genome was a necessary step in initial attempts to clone CLL TSG. Those attempts were supported in the frame of Chromosome 13 Mapping and Sequencing Project of the Human Genome Program. First, a contig overlapping the 13q14.3 region was built using cosmid libraries constructed by the Los Alamos National Laboratory (LANL, United States) and the Imperial Cancer Research Foundation (ICRF, United Kingdom). About 30,000 individual cosmids (equivalent to approximately nine spans of chromosome 13) individually stored in 96-well plates were used as probes for cross hybridization, revealing overlapping cloned DNA fragments covering more than

600 kb of the chromosome 13 region frequently deleted in B-CLL (B.I. Kapanadze et al. 1997). Further delineation of the region was achieved by analysis of the loss of heterozygosity (LOH) patterns and fluorescence in situ hybridization (FISH) studies. As a result, the minimal region lost in B-CLL was reduced to 300 kb (M.M Corcoran et al. 1991; M.C. Devilder et al. 1995).

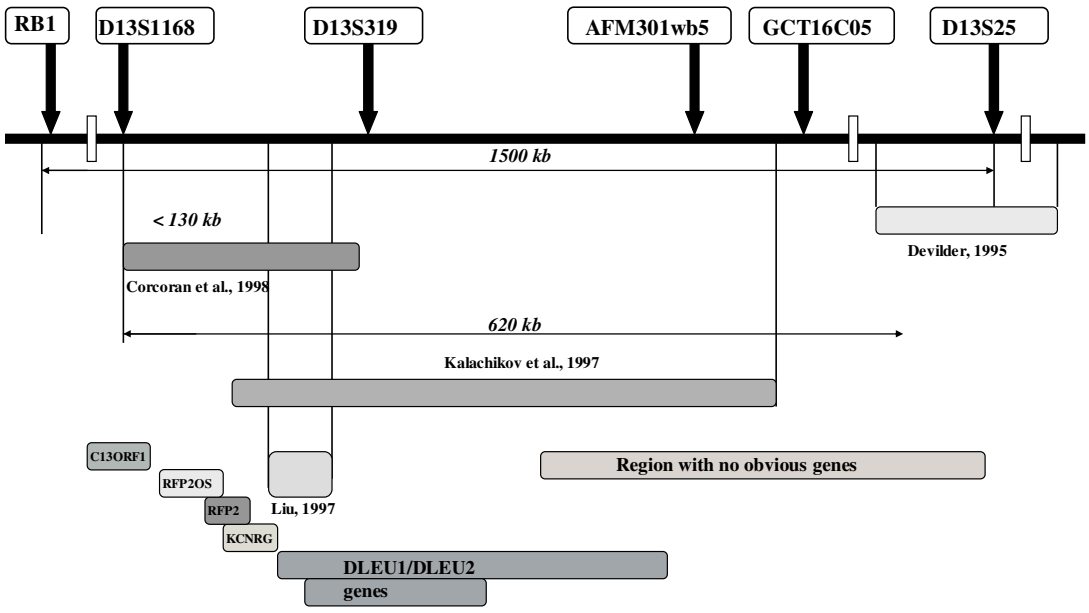

Fig.1. Map of regions identified as having deletions by various independent researchers.

The mimimally deleted region was localized between two STSs, D13S1149 and D13S25 (Fig. 1); another marker, D13S319, proved to be the one most often eliminated by deletion. Further minimization attempts were performed in different labs which examined independent groups of B-CLL patients. Surprisingly, each group succeeded in chopping the minimally deleted region down to less than 300 kb, but the resulting regions

were minimally overlapping, and in extreme cases, deleted regions were mapped 200 kb apart (M.C. Devilder et al. 1995; I. Bouyge-Moreau et al. 1997). Since further minimization of the deleted region yielded discrepant results, a physical map with a higher resolution was necessary. Southern hybridization of DNA probes representing 300bp-2 kb fragments of cosmid clones with genomic DNA of B-CLL patients allowed precise localization of the rearrangements in individual patients. As a result, genome rearrangements were localized on a map of EcoRI/HindIII digestion sites with a resolution of 1-2 kb (Y. Liu et al. 1995). Such a resolution cannot be obtained by FISH or LOH analysis. Rearranged genomic DNA fragments were observed in three out of 206 B-CLL patients examined in the Karolinska Hospital, Sweden. The minimal area of overlap between deletions in these three patients was only 10 kb. In 46% of cases (95 out of 206 tumor DNA specimens), deletions of the 10-kb region affected either both chromosomes (28 cases) or only one (67 cases) (Y. Liu, M et al. 1997). Interestingly, the minimally deleted region identified in this study was located upstream of D13S319 (i.e., on its centromere side), whereas most other authors mapped the CLL TSG downstream of this marker.

Tumor suppressor gene candidates located in 13q14

Through the efforts of various labs and researchers, a more informative physical map of the deleted region in CLL was subsequently generated. On this map, all deletions found in patients with B-CLL were mapped within the 620-kb interval between D13S1168 and D13S25. Interestingly, in some cases the minimally deleted regions

mapped by different research groups were not overlapping, in fact, in some cases these regions were located a hundred kilo-bases apart. These findings may be interpreted in three different ways: either there are multiple TSGs involved in CLL and are located in 13q14 (unlikely), either the expression of the B-CLL-associated TSG is sensitive to chromosome rearrangements in its vicinity, or that the B-CLL-associated gene is rather large, and consequently deletions in its first or last exon may similarly impair its function. In either case, identification of the TSG associated with B-CLL required the mapping of all RNA transcripts located within the 620-kb area of interest. This work started in 1996, when the process of mapping and initial characterization of transcripts was laborious. Hence, the first attempts to hunt down the CLL TSG were restricted to the analysis of the most probable candidates, located in the chromosome region most commonly eliminated by deletions.

DLEU1 and DLEU2

Researchers used various different methods of mapping in an attempt to locate precisely the deleted regions in 13q14. Despite initial difficulties with positional cloning due to the unique features of this region such as unusually high content of repeats, researchers were able to compose a valuable picture. Independent studies by various labs produced the map of non-overlapping but adjacent minimally deleted regions (MDRs) (Fig.1). Two candidate tumor suppressor genes, DLEU1 and DLEU2, were suggested as a result of the analysis of the smallest (10kb) MDR region et al. 1997). Nucleotide sequencing of DLEU1 and DLEU2 did not reveal homology to any known genes. The

putative open reading frames of DLEU1 and DLEU2 seem to encode for hypothetical proteins of only 72 and 84 residues, respectively. The open reading frames of DLEU1 and DLEU2 are associated with weak Kozak sequence context, casting doubts on their ability to function as translated proteins. Single-strand conformational polymorphism (SSCP) analysis of these ORFs and adjacent non-coding sequences did not reveal any point mutations in samples from B-CLL patients (Y. Liu, M et al. 1997; Migliazza, A et al. 2001). In-depth analysis into DLEU1 showed it to be a fragment of a much larger 560-kb gene thought to contain at least 50 exons and be expressed as up to 20 different non-coding RNAs. (S. Wolf et al. 2001). This gene was re-named BCMS (B-Cell Multiple Splicing) (S. Wolf et al. 2001).

The DLEU2 gene was also extensively studied. The extended sequence of this gene was deposited in GenBank in 2000 under the name BCMSUN (BCMS-Upstream Neighbor) (D. Mertens et al. 2000). Like DLEU1, DLEU2 is expressed as multiple alternatively spliced RNAs lacking reading frames. Interestingly, despite the DLEU2 ortholog being present in the mouse genome, human and mouse RNA isoforms of DLEU2 only have a few exons in common, (B. Kapanadze et al. 2000) thus indicating that the 13q14 region harboring the putative CLL TSG underwent relatively recent rearrangements in the course of evolution. Despite a number of interesting findings describing peculiar expression patterns of the first line candidates DLEU1 and DLEU2, a lack of open reading frames and presence of mutations in the DNA of CLL cells prompted the removal of these genes from the list of likely CLL TSG candidates.

MicroRNAs

The obvious absence of protein coding genes within the minimal deletion in CLL cells initiated an exhaustive search for non-coding sequences with regulatory potential in CLL. A recent study examining the expression profiles of microRNAs and the ability of these profiles to help distinguish normal B cells from malignant B cells in CLL, found that there indeed was a unique microRNA change associated with 13q14.3 deletions. The microRNA genes miR-15a and miR-16-1 were located to the 30-kb core of the minimally deleted region (Calin et al. 2005; G.A. Calin et al. 2002). MicroRNAs represent a new class of gene products that are typically excised from 60- to 70-nt fold-back RNA precursor structures by Dicer RNase III and the Argonaute family members (T.P. Chendrimada et al. 2005). Interstingly, miR-15a and miR-16-1 are down-regulated or deleted in the majority of B-CLL cases. In addition, a clearly identifiable band of 70 bp was seen in many CLL samples, suggesting that miR-15a might be inefficiently processed in some CLLs (G.A. Calin et al. 2002). On the other hand, a C->T homozygous substitution was detected in premiR-16-1 in 2 out of 75 screened CLL patients, but in none of the 160 normal subjects. In both of these CLL patients, normal cells from the buccal mucosa were heterozygous for this abnormality. Therefore, the C->T change is a germ-line mutation; the mother and sister of one of these patients had CLL and breast cancer, respectively, supporting the possible causal role of this mutation in predisposition to CLL (G.A. Calin et al. 2005) as opposed to sporadic CLL.

MiR-16-1 is a member of the family of miRNA-16-like genes which share sequence identity, so it would be extremely difficult to study the trans-regulation effects

of miR-16-1 located in 13q14 apart from the effects of its paralogues. Collectively, the miR-16 family down-regulates a number of targets located on various human chromosomes and causes an accumulation of cells in G(0)/G(1) (P.S. Linsley et al. 2007). To what extent this cell cycle block depends on the individual effect of miR-16-1 remains unknown. Both miR-15 and miR-16 were shown to negatively regulate Bcl2 at a post-transcriptional level and induce apoptosis (G.A. Calin et al 2006). Recently, the genome of the CLL model animal, the New Zealand black (NZB) mouse, was shown to have a point mutation in the 3' flanking sequence of the orthologous microRNA, miR-16-1. This mutation is not present in other strains, including the nearest relative, the New Zealand white (NZW) mouse. A decrease in the levels of miR-16 was noted in NZB lymphoid tissue (E.S. Raveche et al. 2007; B.J. Scaglione et al. 2007). All these findings suggest that alteration of the normal expression suppressor function of miRNAs located within 13q14 is intimately linked to CLL.

Interestingly, the same RNA molecules that encode pre-miRNA may exert additional cis-regulatory effects on other genes located in 13q14, as they are located within the area covered by the DLEU2/miR-15a/miR-16-1 transcript described above. This very complex transcription unit overlaps with the RFP2/KCNRG/RFP2OS unit described in the following chapters.

RFP2

RFP2 (Ret Finger Protein 2) (Kapanadze et al. 1998; Baranova et al. 2004) is situated 10 kb away from the minimal deletion region (Fig. 1). Its open reading frame encodes a

protein of 407 amino acid residues and contains zinc-binding RING domains, a B-box, and a coiled-coil domain (A. Baranova et al. 2003). This combination of domains is known as the RBCC/TRIM domain and is found in a number of Rfp-like proteins which take part in cell differentiation, regulation of early embryo development, immune response, and neoplastic transformation. As a general rule, RBCC/TRIM domain-containing proteins appear to function as parts of large protein complexes and possess E2-dependent E3 ubiquitin ligase activity (K.M. Short and T.C. Cox, 2006). RFP2 has been shown recently to encode an unstable protein with autopolyubiquitination activity. (M Lerner 2008). Rfp2 protein interacts with other proteins localized to the endoplasmic reticulum (ER) and is involved in the ER-associated degradation (ERAD) pathway, which serves as a primary mean of quality control within the secretory pathway and decreases ER stress by clearing terminally mis-folded proteins from the ER (M. Lerner et al. 2007).

Despite its promising location, no mutations were found in *RFP2* during screening of patients with CLL (A.Baranova, 2003; Migliazza, A et al. 2001; van Everdink WJ et al. 2003). Additionally, direct sequencing of *RFP2* revealed no mutations in six patients and four multiple myeloma (MM) cell lines harboring 13q14 deletions (M.O. Elnenaei et al. 2003). These findings decrease the probability that *RFP2* is actually a tumor suppressor gene. However, a study of *RFP2* has revealed many interesting features of that locus which might be relevant to CLL, as they point to the unexpectedly high complexity of this expressed region of chromosome 13. This region proved to be transcribed in both directions, as *RFP2* overlaps with at least two anti-sense RNAs

encoded by the opposite DNA strand, *DLEU2* (M.M Corcoran et al. 1991) and *RFP2OS* (A. Baranova et al. 2003). Furthermore, the *RFP2* promoter contains multiple quadruplex forming GGGGA-repeats and possesses very low nucleosome-forming potential, allowing for its unusual strength (M. Skoblov et al. 2006)

The *RFP2/LEU5* transcript may be alternatively spliced to yield either a monocistronic transcript or a theoretically predicted bicistronic transcript encoding two separate open-reading frames. Furthermore, the DLEU2 gene may produce a noncoding antisense RNA, whereby one of its exons, previously described as *RFP2OS*, directly overlaps the first exon of the RFP2/LEU5 gene in the opposite orientation (Corcoran et al. 2004; Baranova et al. 2004). *RFP2* may be involved in the activation of the NF-kB pathway, implicating this region within the chromosome in various disease pathways (Matsuda et al. 2003).

KCNRG

The gene KCNRG is located adjacent to *RFP2* and is thought to encode a potassium channel regulating protein (Ivanov et al. 2003). Due to the close proximity of these two genes it is not clear whether KCNRG mRNA is transcribed using a promoter in the RFP2 3' untranslated region, or whether RFP2 and KCNRG share a promoter. KCNRG encodes two protein isoforms KCNRG-L (272 aa) and KCNRG-S (229aa), corresponding to variant 1 and variant 2 respectively (Fig.2); Previous studies showed differential expression of KCNRG mRNA isoforms between tumor and normal cells (Ivanov et al. 2003). Isoforms S and L were found in normal human lungs, in lymphocytes and in

prostate cells, however they were not found in the cell line LNCaP which is a prostate cancer cell line. In the ovarian cancer cell line SKOV-3 and osteosarcoma cell line T1-13, expression of KCNRG was not found at all. Interestingly, in the A431 epidermoid carcinoma the levels of expression of the larger mRNA isoform were decreased compared to other samples, and in the osteosarcoma cell line SAOS-2, larger of two mRNA isoforms can not be detected by amplification.

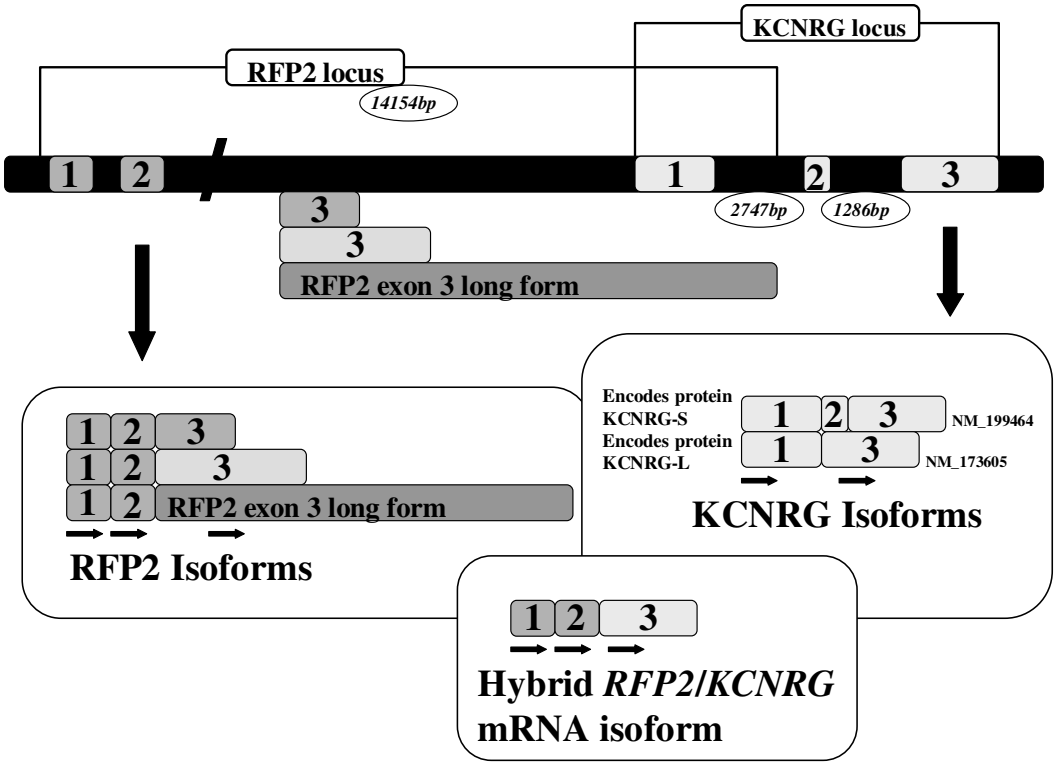

Fig.2. Isoforms of KCNRG and RFP2 and overlapping regions

KCNRG exerts an inhibitory effect on Kv potassium channels (Ivanov et al. 2003). It encodes a protein which resembles the T1 (tetramerization) domain of the voltage gated K+ channels, suggesting that the protein encoded by KCNRG may interfere

with the normal assembly of these channels and thereby suppresses Kv currents (Ivanov et al. 2003).

Potassium channels are one of the most varied members of the ion channel family, and generally can be divided into two broad categories: the 'delayed' group and the 'transient' group (Perney T.M et al. 1991; Luneau C et al. 1991; Stuhmer W et al. 1989). The diversity found in potassium channels is thought to be caused by small amino acid changes that affect not only the voltage-dependent gating mechanism, but that also modify other properties such as channel conductance and the ability of channels to interact with various toxins. The understanding of the regulatory processes of K+ channels is a constantly expanding field and includes mechanisms of plasma membrane depolarization, hyper-polarization, actions of intracellular kinases, and actions of GTP binding proteins and various other second messengers (Schwarz T.L et al. 1988).

K+ channels can be further categorized into two classes based on their trans-membrane topology: the six trans-membrane helix voltage gated (Kv) class, and the two trans-membrane helix inward rectifier (Kir) class (Papazian DM et al. 1987, Pongs O et al. 1988, Ho K et al. 1993). All K+ channels posses a distinct sequence (TMxTVGYG) between two trans-membrane helices at the carboxy-terminus (Heginbotham L. et al 1994). The trans-membrane region of the Kv channel, containing tetrameric components is composed of the α-subunits which form a pore (Fig. 3). Each of these α-subunits contains six hydrophobic trans-membrane units: S1, S2, S3, S4, S5, S6 with a P-domain inserted between S5 and S6 (Sansom MS, 2000). S1, S2, S3, S5 and S6, are thought to function in the closing and opening of the pore whereas unit S4 is thought to be the

voltage sensing component in these channels, and is not exposed to the lipid bilayer (Miller C., 2000).

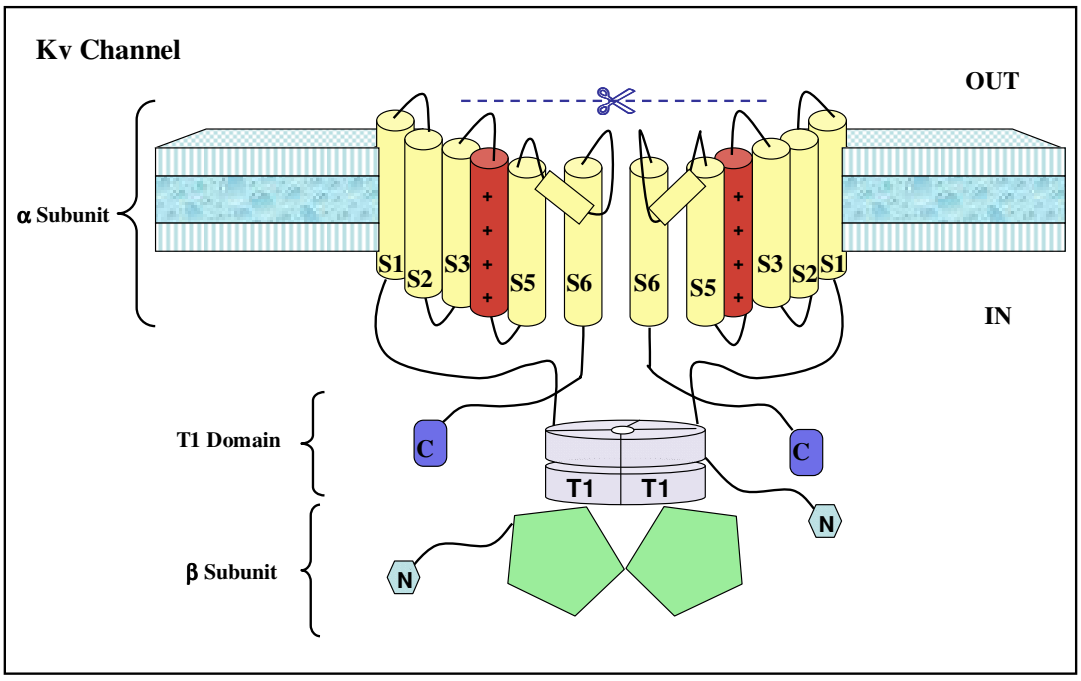

Fig. 3: Kv Shaker type channel with α, β and T1 domains.

The Kv type of potassium channel can be further subdivided based on sequence similarity and function into four classical subfamilies: Kv1 (Shaker), Kv2 (Shab), Kv3 (Shaw) and Kv4 (Shal) (Miller C., 2000). All Kv channels, however, have a highly conserved T1 domain whose function is still being elucidated but is thought to be involved in determining the subfamily specific assembly of the alpha-subunits and shares homology with proteins that contain a BTB/POZ domain (Bixby K.A. et al. 1999).

The T1 domains in eukaryotic Kv channels seem to serve as a link, via the S1 subunit, between the pore forming units and the B subunit (Gulbis JM et al. 2000; Sewing S et al. 1996; Yu W et al. 1996). Although emerging research seems to not only indicate

an additional regulatory function in terms of channel gating but also seems to suggest that the conformation of the T1 domain influences the operation of the channel itself (Wang G et al. 2006; Cushman SJ et al. 2000; Minor DL. et al. 2000). The B subunit is a tetrameric arrangement of proteins that are thought to be related to aldo-keto reductase enzymes (Rehm H. et all 1988; Parcej DN et al. 1992; Scott VE et al. 1994; McCormack T. et al 1994; Chouinard SW. et al 1995; Gulbis JM et al. 1999). Although more and more features of the B subunit structure and composition are being elucidated, its exact function remains elusive (Long SB et al. 2005).

In addition to the classical roles of K+ channels such as their involvement in neural signaling, generation of cardiac rhythm, signal transduction pathways via G protein coupled receptors; K+ channels are now thought to play a crucial role in cell cycle processes, apoptosis and cancer (Attali B et al. 1992; Felipe A et al. 2006). In fact, Kv channels are being implicated in a diverse range of diseases and metabolic pathways. In a recent study Kv channels were proposed to play a role in pulmonary arterial hypertension (PAH), which is an antiapoptotic, proliferative, and inflammatory disease (Bonnet S et al. 2007). A recent study on breast cancer proposed a definite connection between Kv channels and deregulation in apoptosis in certain types of breast tumors (Brevet M et al. 2008). Additional regulatory roles for Kv channels have been proposed where the Kv channels play a role in proliferation by maintaining the driving force for calcium influx (Cahalan MD and Lewis RS, 1990).

These new roles for Kv channels open up a vista of possible mechanisms by which KCNRG can play a role in B-CLL formation. Primary among these is KCNRG

dependent suppression of Kv currents that affect calcium-dependent cell cycle control. For example, Kv channels were previously implicated in metastasis and proliferation of hepatocarcinoma cells. In these cells the blockage of Kv channels prevents both adhesion and proliferation (Zhou Q et al. 2003).

Despite the promising advances on the characterization of KCNRG, there has yet been no evidence of KCNRG mutations in B-CLL cases sampled. This suggests that perhaps a new approach needs to be adopted when attempting to determine the characteristics and effects of KCNRG.

Haploinsufficiency

Finding a somatic point mutation in the majority of a tumor of a given type is commonly considered a final proof of the involvement of a candidate gene in tumor suppression. However, in some cases, point mutations of a gene clearly capable of tumor suppression in both *in vitro* and *in vivo* experimental settings are never or almost never found in tumor DNA samples. During the last five years the haploinsufficiency mechanism of tumor suppressor gene inactivation has come to be the focus of many cancer-related studies (M. Santarosa and A. Ashworth, 2004). According to this model, inactivation of one copy of the tumor suppressor gene via deletion or methylation is enough to provide selective advantage or prevent apoptosis in progenitor cells of the tumor. Often in such cases tumor cells contain a large chromosomal of one copy of the gene while the second copy remains intact with no point mutations. This might indeed be the case with CLL, since non-imprinting type of the monoallelic silencing of genes

localized in the critical region has been observed (D. Mertens et al. 2000). Therefore, deletion of the single active copy of 13q14.3 may result in significant down-regulation of the candidate genes and loss of their function (D. Mertens et al. 2000; D.V. Ivanov et al. 2003). The involvement of the haploinsufficient genes in the process of tumorigenesis cannot be proven by mutation screenings showing that both copies of TSG are inactivated by one or another mechanism, but requires thorough functional studies.

There are several examples of diseases in particular, cancers that arise due to haploinsufficiency. An example of such a case is acute myeloid leukemia where the haploinsufficiency of the gene AML1 instigates the genetic cause of the disease (Barton K and Nucifora G., 2000). Another piece of information which supports the haploinsuficiency approach is the observation that in cases of haploinsufficiency often the gene in question is dramatically down-regulated in disease samples. Although mutations were not shown in RFP2, several genes including RFP2 were shown to be consistently downregulated in B-CLL patients, and furthermore RFP2 was the most significantly downregulated gene (Mertens et al. 2000). Unfortunately KCNRG was not examined at this time as this gene was not known, however the adjacent location of these two genes, and the detection of their fusion mRNA isoforms suggest that RFP2 and KCNRG may be co-regulated. Downregulation of KCNRG was mentioned during the study of its expression in cancer cell lines (Ivanov et al. 2003).

A recent study on hepatocellular carcinoma (HCC) was conducted by analyzing the mutation, allelic loss and expression pattern of the KCNRG gene as well as performing in vitro assays. Interestingly, the outcome of the study did indeed indicate an

allelic loss of KCNRG in HCC, but more importantly, the results seem to indicate a correlation between allelic loss and severity of disease. Moreover, one somatic missense mutation c.275G>A (p.R92H) and a lower frequency (26.5%) of allelic losses were found in the Korean population of informative HCC cases. As the corresponding normal sample showed no evidence of mutations by repeated SSCP analysis, the mutation was likely a somatic event. Interestingly, the HCC case with a KCNRG mutation showed a LOH at D13S272 and only aberrant bands of the mutant allele as determined by SSCP, suggesting a mutation in one allele and loss of the other. The authors concluded that loss or alteration of the KCNRG gene may play a previously unforeseen role in the development and/or progression of some cases of HCCs (Cho YG et al. 2006).

13q14 deletions in other malignancies

Many previously described human tumor suppressor genes play a role in the development of more than one type of human malignancy. The list of such polyfunctional TSGs includes TP53 (M. Olivier et al. 2004), PTEN (I. Sansal and W.R. Sellers, 2004), CDKN2A (N.E. Sharpless, 2005) and others. If the putative tumor suppressor for CLL is indeed located in 13q14.3, it might play a role in the development of other tumors harboring a deletion in this segment of the human genome.

Rearrangements and/or deletions in the region of 13q14.3 are found in many types of hematopoietic malignancies. These deletions account for 38% in mantle cell lymphoma (MCL) (Rosenwald et al. 1999; A. Cuneo et al. 1999), and approximately 54% in multiple myeloma cases (MM), as detected by FISH (Harrison C.J. et al. 2003;

Fiserova A. et al. 2002; M.O. Elnenaei et al. 2003; L. Chen et al. 2007). In the majority of these cases 13q14 deletions are associated with a poor chemotherapy response profile. Deletions of 13q14.3 could contribute to the development of overt leukemia in T-cell prolymphocytic leukemia (T-PLL) (V. Brito-Babapulle et al. 2001).

Allelic imbalance at 13q14.3 is an important event in the progression of localized prostate cancer (N. Brookman-Amissah et al. 2007) and in high-grade high-stage carcinoma originating from prostatic tissue (J.T. Dong et al. 2001). Interestingly, some studies indicate that 13q14 loss is also associated with the initiation of prostate tumors (W. Lu et al. 2006). The region within 13q14, distal to the RB1-locus, is of importance to the development of low-malignant lipomatous tumors (A. Dahlen et al. 2003).

A study of the KCNRG allelic loss in 13q14 revealed deletions in 13 (25.5%) out of the 51 HBV-positive HCCs of grade II and in 4 (66.7%) out of 6 HCCs of grade III. There was a significant correlation between an allelic loss and the histology grades ($P = 0.0078$) and stages ($P = 0.0071$). Furthermore, the number of allelic losses was higher in those cases with an intrahepatic metastasis than in the cases without metastasis ($P = 0.0247$) (Y.G. Cho et al. 2006). Taken together, these observations indicate that the elusive TSG located in 13q14.3 may have an importance not limited to CLL. Therefore, all CLL TSG candidates discussed above should be subjected to both mutational screening and functional studies in the malignant cells of non-lymphatic origin.

Chapter 2: Materials and Methods

Cloning and sequencing of human KCNRG

The basic molecular biology and microbiology procedures such as plasmid isolation, cloning, *E. coli* transformation and cultivation, were performed according to standard protocols (Sambrook et al., 1989). Human KCNRG variant 1 and KCNRG variant 2 were cloned into a pcDNA3.1/myc-His vector (Invitrogen, San Diego, CA). The cloning of KCNRG variant 1 was performed by OriGene (Rockville, MD, USA). The cDNA used was a full-length archived cDNA clone which corresponds to the mRNA isoform NM_173605. The cloning of KCNRG variant 2 was performed by our collaborators Andre Marakhonov and Dr. Mikhail Skoblov (Russian Center for Medical Genetics, Moscow, Russia) by amplifying its full length ORF from the coding sequence of human brain cDNA. This product was cloned into a pGemT-Easy vector (Promega, Madison, WI), and then transferred into a pcDNA3.1/myc-His plasmid. According to the manufacturer's protocol, bidirectional sequencing of the plasmids and PCR clones with vector or gene-specific primers were performed by fluorescence-tagged chain termination (Big Dye Terminator, Applied Biosystems) and the fragments detected using a ABI 310 automated DNA sequencer (Applied Biosystems).

The recombinant plasmids containing KCNRG V1 and KCNRG V2 were stored at -80 until transformation. The *E. coli* strain used for transformation was JM109, standard K-12 non-pathogenic recA–, endA– *E. coli* appropriate for routine cloning

applications. JM109 cells contain the $LacI^{q}Z\Delta M15$ gene on the F´ episome, allowing blue-white screening for recombinant plasmids.

Following transformation the *E. coli* cells were grown on imMedia™ Amp Agar for selection and imMedia™ Amp Liquid for propagation (Invitrogen, CA). The plasmids were extracted using EndoFree Plasmid Maxi Kit (QIAGEN).

HL-60, RPMI-8226 and LNCaP cells stably expressing KCNRG V1 and KCNRG V2

Cell lines LNCaP, HL-60 and RPMI-8226 were obtained from the American Type Culture Collection (Manassas, VA). LNCaP cells are androgen-sensitive human prostate adenocarcinoma derived from the lymph node metastasis. They are adherent epithelial cells growing in aggregates and as single cells. Functional differentiation of LNCaP cells is preserved. HL-60 (human promyelocytic leukemia) cell line proliferates continuously in suspension culture with the doubling time of about 36-48 hours. HL-60 cells are predominantly a neutrophilic promyelocyte (precursor). RPMI-8226 is a multiple myeloma cell line with lymphoblast-like appearance.

All of the cells were grown and maintained in RPMI1640 media containing 2 mM glutamine, 10 mM HEPES and 10% fetal calf serum (Invitrogen, CA). Transfections of the cell lines were initially attempted using a liposome-mediated transfection system, Lipofectamine™ Reagent (Invitrogen) according to the manufacturer's protocols. Optimization of transfection conditions was performed with positive control lacZ-containing vector provided with the pcDNA.3.1/myc-His/ system. Despite the

manufacturer's claims of low toxicity, transfection reactions with Lipofectamine (Invitrogen) yielded stable transfectants only with RPMI-8226 cells. A very high rate of cell death was observed for mock-Lipofectamine transfected cells (designated: EV for empty vector pcDNA.3.1/myc-His) for the first days following transfection, indicating high levels of reagent toxicity. This was most evident in HL60 cells, in which none of the transfectants survived the first week of transfection regardless of the minimal concentrations of the transfectant.

Following this discovery, a less toxic system was deemed necessary, and consequently the cDNA-containing or empty control plasmids were transfected into LNCaP, HL-60 and RPMI-8226 cells with Transfectol reagent (Gene Choice, Frederick, MD). This transfection system was optimized to yield the highest number of transfectants and the lowest number of cell deaths due to toxicity. After the cells were transfected, they were incubated in growth media containing RPMI1640 media with 15% fetal calf serum for 24 hours to aid their recovery. Following the recovery period cells were centrifuged and re-suspended in RPMI1640 media with 10% fetal calf and a selection specific antibiotic. Stably transfected cells were selected using 500 ug/mL of Geneticin (Sigma) and were subsequently maintained in 75 cm^2 flasks in medium with antibiotic in incubators with 5% CO_2 and humidity for the duration of the experiments. The continual growth of cells in selective antibiotic assured the maintenance of selective pressure and prevented the loss of the transfected plasmid.

HL-60, RPMI-8226 and LNCaP cells transiently expressing KCNRG V1 and KCNRG V2

The same transfection reagents were used for the preparation of the transiently transfected cells. The transfection was carried out in a 96 well plate as per the manufacturer's instructions. In addition to the empty vector plasmid, KCNRG V1 plasmid and KCNRG V2 plasmid, cells were mock transfected using only the Transfectol reagents to determine toxicity effects of the reagents. The transiently transfected cells were immediately used for experiments 48 hours after transfection and were not selected with Geneticin.

Generation of Clonal Populations

Following stable transfection, a serial dilution of the mixed cell populations was performed on a 96-well cell culture plate in an attempt to isolate and generate a clonal population. RPMI-8226 was the only cell line in which this was successfully achieved, as LNCaP and HL60 cells did not survive being isolated into single cell units. Forty three clones were generated for the RPMI-8226 cell line; out of these three clones were selected based on their rate of proliferation as compared to the mixed population: fast growing (S1B9), same as mixed population (S2A11), and slow growing (S3A10).

Cell proliferation and apoptosis assays

Cell proliferation assays were performed using the Chemiluminescence-based Cell Proliferation ELISA, BrdU kit (Roche). The chemiluminescence-based assay was

chosen as it is has been found to be more sensitive than its colorimetric version (Unteregger G, Profit S., 2001).

Proliferation rates of the cells transfected with empty vector and stable KCNRG variant 1 and 2 overexperessing cells were determined by quantifying the BrdU incorporated into the newly synthesized DNA of replicating cells. The experiment was conducted according the manufacturers protocol. The cells were seeded into 96-well black plates with clear bottoms (Thermo Electron) at a density of 2×10^4 per well. Cells or blanks (100 μL) and 10 μL of the BrdU labeling solution were added to the wells. The incubation time was determined experimentally. Due to the longer replication periods of the transfected cells, the optimum time for BrdU incorporation in HL60 and RPMI-8662 was 48 hours and the optimal time for LNCaP was 72 hours. Each cell type was tested in replicates of eight. Chemoluminescence was quantified using a Fluoroskan Ascent microplate fluorometer (Thermo Scientific).

To determine apoptosis in KCNRG V1, V2 and empty vector transfected cells, the Caspase-Glo® 3/7 Assay was used (Promega, Madison, WI). This assay focuses on the caspase-3 and -7 activities and the level of caspase activity in the sample is proportional to the luminescence produced by caspase cleavage of the substrate For the apoptosis assays, cells were seeded in 96-well black plates with clear bottoms (Thermo Electron) at a density of 3.5×10^4 per well in 50 μL of RPMI1640 media with 10% fetal calf serum. As per the manufacturers protocol, the Caspase-Glo reagent was added in a 1:1 ratio. All of the cell lines were incubated for 2 hours at room temperature and chemoluminescence was quantified using a Fluoroskan Ascent microplate fluorometer (Thermo Scientific).

In experiments where the cells were transiently transfected, immediately following transfection proliferation and apoptosis assays were performed using conditions identical to those of the stable transfection experiments. The only exception to this protocol was the addition of an extra set of 16 wells with mock-transfected cells. Chemoluminescence was quantified as described above.

FACS / flow cytometry

Cell cycle distribution was analyzed by flow cytometry (Kim Y. et al 1992). All of the cell lines were grown to optimum densities. Cells were brought to concentrations of 1.5x 10^6 cells/mL and were transferred to 15 mL conical tubes. Cells were washed twice with cold PBS, centrifuged at 1000g for 5 min and resuspended in 1 mL of PI staining solution (PBS + 50ug/mL PI + 100ug/mL RNAse A). Cells were incubated at 4C in the dark for 20 minutes and were analyzed on FACSCalibur (Becton Dickinson) within 15-30 minutes of staining. All of the cells were kept on ice and away from light during the entire experiment.

Quantification of cell death was determined by staining with Annexin V/7-AAD kit (BD Pharmingen, San Jose, CA). Annexin V aids in the detection of one of the primary events in apoptosis, namely, the translocation of the membrane phospholipid phosphatidylserine (PS) from the inner surface to the outer surface of the plasma membrane. This allows for Annexin V, a 35-36 kDa, Ca 2+-dependent, phospholipid binding protein to bind to PS. However, since translocation of PS also occurs during necrosis, 7-amino-actinomysin (7-AAD), which binds to nucleic acids only in the case of

a failure in the membrane integrity was used in conjunction with Annexin V. The dual use of Annexin V and 7-AAD aided in clearly establishing the population of cells going through apoptosis versus those going through necrosis. Cells were once again counted and prepared in densities of 1.5 x 10^6 cells/mL. All of the cells were washed and the centrifuged pellets were re-suspended in 0.1mL of 1x binding buffer, 10 μL of annexin V and 5 μL of 7-AAD were added to each sample. Cells and reagents were gently mixed and incubated at room temperature for 15 minutes in the dark. Following incubation 0.9 mL of 1x binding buffer were added to the cells. The samples were analyzed within 1 hour of staining. Controls stained with Annexin V only and 7-AAD only were performed for calibration purposes. During the experiments cells were kept on ice and away from light sources.

Cell Imaging

Cells were stained with fluorescent dyes in an attempt to visualize any morphological changes that may have been caused by transfection with KCNRG V1 and KCNRG V2. With this goal in mind, three regions of interest on the cell were observed. DAPI, a blue-fluorescent nucleic acid stain was selected to stain the nucleus (Invitrogen). DAPI preferentially stains dsDNA and is believed to associate with the AT clusters in the minor groove (Kubista M et al. 1987). When DAPI binds to dsDNA it produces a ~20-fold fluorescence enhancement, which is thought to be due to the displacement of water molecules from DAPI and the minor groove (Tanious FA et al. 1992). DAPI has also been successfully used in conjunction with other dyes, and when used according the

manufacturers protocols, stains nuclei specifically. The plasma membranes were stained with 3-dioctadecyloxacarbocyanine perchlorate (DiOC18) (Invitrogen). DIOC 18 is highly lipophilic and can diffuse laterally through out the membrane and most importantly does not influence the viability of the cells (Zhang W et al 2005). Hence it was deemed optimal for observing minute morphological changes in the membrane structures of the cell, be it plasma membrane or inter cellular membranes. The third goal of the fluorescent imaging of the cells was to determine the overall changes in the structure of the cells. As such, Rhodamine phalloidin was used to visualize the F-actin content of the cells. Rhodamine phalloidin is a phallotoxin, a bicyclic peptide which is isolated from the deadly *Amanita phalloides* mushroom and has a very high affinity to F-actin filaments (Wieland T., 1977). Phallotoxins stabilize F-actin filaments, thereby preventing depolymerization while retaining functionality and overall structural integrity of the cell (Mahaffy RE et al. 2008; Oda T et al. 2005).

RPMI-8662 and HL60 cells were centrifuged and the cell pellets rinsed with PBS to remove media components. The cells were fixed in freshly prepared 4% paraformaldehyde/PBS solution for 15 min at room temperature. Cells were permeabilized by adding 0.1% Triton-X100 in PBS for 1 min. A PBS diluted solution of Rhodamine-phalloidin (1:100 in PBS), 5 μL of 300 nM DAPI and 4 μL of diluted DIOC 18 solution were added to the permeabilized cells. The mixture was incubated for 15 min at room temperature. Following staining the cells were rinsed in PBS three times and mounted onto slides with coverslips. LNCaP cells were grown directly on cell culture treated slides and were washed and consequently treated in the same manner as the other

two cell lines. Slides were kept in the dark and in the freezer until imaging. Images were taken on a Nikon Eclipse 90i microscope equipped with a Nikon C1 confocal scan head and laser lines at 406nm, 488nm and 568nm.

Invasion and migration assays

To evaluate the migratory and invasive properties of the cells over-expressing KCNRG, fluorimetric CytoSelect 96well Cell Migration and Invasion, CytoSelect 24-wells Anoikis and CytoSelect Leukocyte Transmigration Assays (Cell Biolabs, Inc, San Diego, CA) were used according to the manufacturer's protocols. The CytoSelect™ 96-well Cell Migration Assay Kit uses a polycarbonate membrane chamber (8 μM pores) as a barrier to separate cells with the ability to migrate from cells that are non-migratory. This platform is based on the ability of migratory cells to extend protrusions towards chemo-attractants via cellular processes such as microfilament reorganization thereby passing through the pores of the membrane. Once through the membrane, these migratory cells are dissociated from the membrane and detected with CyQuant® GR Dye. A similar theory underlies the platform for the invasion assay where an insert membrane, coated with a layer of dried basement membrane matrix solution is used to separate cells that have the ability to degrade matrix proteins and therefore the ability to pass through the membrane from those that do not have these abilities. Due to the larger pore size of these assays HL60 cells were not tested with this assay, but instead were tested using the CytoSelect Leukocyte Transmigration Assays (Cell Biolabs, Inc, San Diego, CA) which

not only has a smaller pore size, but also has an endothelial monolayer of cells which provides additional information on the cells ability for extravasation.

An anoikis assay was performed on the LNCaP cells to observe any changes in apoptosis resulting from the loss of cell adhesion to the extracellular matrix (ECM). The CytoSelect™ 24-Well Anoikis Assay uses a poly-Hema coated plate in conjunction with a cell culture control plate and allows the measurement of cell viability using either MTT or Calcein AM. MTT (3-(4, 5-dimethylthiazolyl-2)-2, 5-diphenyltetrazolium bromide) is a yellow tetrazolium salt that is reduced by metabolically active cells and is used in determining cell proliferation. Calcein AM is an acetomethoxy derivate of calcein and is transported through cellular membranes of live cells, upon binding to calcium within the cell it emits a strong green fluorescence signal thereby "labeling" only live cells. Levels of anoikis related cell death is measured by ethidium homodimer (EthD-1), a red fluorescent dye that can penetrate only damaged cell membranes. Upon binding to ssDNA, dsDNA, RNA, oligonucleotides, and triplex DNA, EthD-1 fluoresces with a 40-fold increase. This property also causes a fairly low background as the dye has almost no fluorescence in its non-bound state.

A cell suspension of $2x10^6$ cell/mL in culture media was prepared. Cell suspension (0.5 mL) was added to each well of the anchorage resistant plate and the 24 well control plate. The cells were cultured for 72 hours at 37ºC and 5% CO_2. As per the manufacturers protocol, 50 µL of the MTT Reagent was added to each well of the anchorage resistant plate and control plate. The plates were incubated for 2 hours at 37ºC. Following incubation 500 µL of detergent solution was added to each well and mixed.

The plates were covered and incubated for an additional 2 hours at room temperature. An aliquot (200 μL) of each sample was transferred to a 96-well plate and the absorbance was determined at 570 nm (Fluoroskan Ascent, Thermo Scientific).

For the Calcein AM / EthD-1 Fluorometric Detection, 1 μL of Calcein AM/EthD-1 solution was added to each well of the 24-well anchorage resistant plate and the control plate. These plates were incubated for 30 minutes at 37ºC. The cells were microscopically observed for the presence of the green Calcein AM (Ex: 485 nm and Em: 515 nm) or red EthD-1 (Ex: 525 nm and Em: 590 nm) for fluorescence. The fluorescence was also read quantitatively with a fluorescence microplate reader (Fluoroskan Ascent, Thermo Scientific).

Proteome analysis

The protein analysis was performed by our collaborators at the Center for Applied Proteomics & Molecular Medicine. Amy J. VanMeter prepared the samples. For reverse-phase protein microarrays the protein lysates were loaded into 384-well plates and each lysate was serially diluted in lysis buffer to a 5-point dilution curve (neat, 1/2, 1/4, 1/8, and 1/16). Each dilution series was printed in duplicate onto nitrocellulose-coated glass slides (Whatman, Inc., Sanford, ME) with a 2470 Arrayer (Aushon BioSystems, Burlington, MA). Slides were dessicated and stored at -20°C. Before antibody staining, the lysate arrays were treated with mild Reblot Antibody Stripping Solution (Chemicon, Temecula, CA) for 15 minutes at room temperature, washed twice for 5 minutes in phosphate buffered saline, and then incubated for at least 5 hours in blocking solution [1g

I-block (Tropix, Bedford, MA), 0.1% Tween-20 in 500 ml phosphate-buffered saline] at room temperature with constant rocking.

Blocked arrays were stained with antibodies on an automated slide stainer (Dako Cytomation, Carpinteria, CA) using the Catalyzed Signal Amplification System kit according to the manufacturer's recommendation (CSA; Dako Cytomation). The endogenous biotin was blocked for 10 minutes with the biotin blocking kit (Dako Cytomation). This was followed by application of protein block for 5 minutes. The primary antibodies were diluted in antibody diluent and incubated on slides for 30 minutes, and the biotinylated secondary antibodies were incubated for 15 minutes. Signal amplification was achieved by incubation with a streptavidin-biotin-peroxidase complex provided in the CSA kit for 15 minutes, and amplification reagent, (biotinyl-tyramide/hydrogen peroxide, streptavidin-peroxidase) for 15 minutes each. Development was completed using diaminobenzadine/ hydrogen peroxide as the chromogen/substrate. Slides were then allowed to air dry. Primary antibodies (n = 38) were specifically chosen to be analyzed to cover the broad signaling pathways thought to be involved in the proliferation and apoptosis-related signaling. Secondary antibodies and dilutions included: biotinlyated goat antirabbit IgG (H_L) 1:5,000 (Vector Laboratories, Burlingame, CA); and biotinylated rabbit anti-mouse IgG 1:10 (Dako Cytomation).

Stained slides were scanned individually on a UMAX PowerLook III scanner (UMAX, Dallas, TX) at 600 dpi and saved as TIF files in Photoshop 6.0 (Adobe, San Jose, CA). The TIF images for antibody stained slides and SYPRO-stained slide images were analyzed using MicroVigene image analysis software, version 2.200 (Vigenetech,

North Billerica, MA), and Microsoft Excel 2000 software. The images were imported into Microvigene, which was used for spot finding, local background subtractions, replicate averaging, and total protein normalization. This analysis produced a single value for each sample at each endpoint.

Pathway -Specific Microarray Gene Expression Profiling

Two separate experiments with pathway specific microarrays were performed, the Oligo GEArray® Human Cancer Microarray (OHS-802) and the Oligo GEArray Human Hematopoietic Stem Cells and Hematopoiesis Microarray (OHS-054). The general protocol for both of these arrays was the same and proceeded as follows.

Cells were grown to confluency and $1x10^6$ cells were counted and separated. RNA was extracted using RNAeasy RNA extraction kits (Qiagen) according to the manufacturer's protocol. The RNA concentration and purity were determined by UV spectrophotometry (GeneQuant). RNA extractions were verified to have a A_{260}:A_{280} ratio greater than 2.0 and a A_{260}:A_{230} ratio greater than 1.7. In addition, aliquots of the extracted RNA samples were run on an agarose gel to visually determine a clear distinction between the 18S and 28S ribosomal RNA (rRNA) bands and that the sample did not have any smearing indicating sample degradation.

According to the manufacturer's protocol an annealing mixture was prepared using 3.0 μg RNA and 1.0 μL Component G1. The volume was brought to 10 uL by the addition of RNase-free water. The mixture was mixed and briefly centrifuged and incubated at 70°C for 10 min. Following the incubation, the mixture was again

centrifuged briefly (~2 sec) and was immediately placed on ice. A cDNA synthesis master mix was prepared by combining 4 µL of RNase-free water, 4 µL of 5X cDNA Synthesis Buffer (G3), 1 µL of RNase Inhibitor (RI) and 1 µL of cDNA Synthesis Enzyme Mix (G2) to a final volume of 10 µL. The master mix solution was mixed, briefly centrifuged and placed on ice. A cDNA synthesis reaction was made by adding 10 µL of cDNA synthesis master mix solution to each tube which also contained 10 µL of annealing mixture. The tubes were mixed gently by pipetting several times and were briefly centrifuged. Each sample was incubated at 42 °C for 50 minutes followed by 75 ºC for 5 minutes and then cooled to 37 ºC. The amplification master mix was prepared on ice by adding 16 µL of 2.5X RNA Polymerase Buffer (G24), 2 µL of Biotinylated-UTP (10 mM) and 2 µL RNA Polymerase Enzyme (G25) into a final volume of 20 µL. The cRNA Synthesis Reaction was prepared by add 20 µL Amplification Master Mix to each tube containing 20 µL of cDNA Synthesis Reaction. The solutions were mixed, centrifuged and were incubated overnight at 37 °C. Purification of the samples was performed using spin columns. The cRNA was bound to the spin column by adding 60 µL of RNase-free water to each cRNA synthesis reaction tube to bring the volume to 100 µL. Contents of the tubes were transferred to a 1.5 mL RNase-free tube. Lysis & Binding Buffer (G6; 350 µL) was added to each reaction mixture followed by 350 µL of room temperature ACS-Grade 100% ethanol. Contents were mixed and loaded to the spin columns. Spin columns were centrifuged for ~ 30 sec at 8,000 x g and the flow through solution was discarded. The columns were washed in several consecutive steps by adding 600 µL Washing Buffer (G17 with ethanol), centrifuging for ~ 30 sec at 8,000 x g and

adding another 200 µL Washing Buffer (G17 with ethanol) and centrifuging for 1 min at 11,000 x g. The cRNA was eluted into a fresh RNase-free tube by adding 50 µL of room temperature RNase-free 10 mM Tris buffer pH 8.0 (G26). The filter was allowed to soak completely by incubating at room temperature for 2 min. This was followed by centrifugation for 1 min at 8000 x g. The resultant samples were stored on ice. The cRNA concentration was determined by UV Spectrophotometry (GeneQuant).

A pre-hybridization step was performed by adding 2 mL of pre-warmed GEAhyb Hybridization Solution to each filter array and incubating for 30 minutes at 60 ºC with shaking at 500 rpm on the GEArray® Express Thermoshaker. A target hybridization mix was prepared by adding 4 µg cRNA target to a 2.0 mL aliquot of warm GEAhyb Hybridization Solution. Each sample target was added to a separate hybridization chamber containing a GEArray® and was sealed with a GEArray® Multi-Chamber Seal. The arrays were incubated for 24 hours at 60 ºC with shaking at 500 rpm. Arrays were rinsed with 4 mL of pre-warmed Wash Solution, followed by 2 mL of pre-warmed Wash Solution 2 and incubated for 5 min at 60 ºC with shaking at 1000 rpm. The wash buffer was removed and the arrays were allowed to reach room temperature. Dilute AP-Streptavidin (2 mL) was added to each GEArray® and incubated for exactly 10 min on the bench top. This solution was removed and 2 mLs of room temperature 1X Buffer F was added and arrays were incubated for 5 min at 37 ºC with shaking at 700 rpm; this step was repeated three times.

To perform the buffer equilibration 2 mL of room temperature Buffer G was added and the arrays incubated for ~ 1 minute at 37 ºC with shaking at 700 rpm. Buffer G

was removed and 1.0 mL of CDP-Star®, was added and the arrays incubated with shaking at 37 ºC for 1 min. Upon the removal CDP-Star® the arrays were incubated in the HybPlate without shaking at 37 ºC for 4 minutes. Immediately following this incubation the GEArray® chemiluminescent images were acquired using a cooled CCD camera system (Kodak). The images were saved in TIFF format, and the array filters were allowed to dry and were stored in sealed plastic packets. Spot finding and spot intensity measurements were performed with the integrated GEArray Expression Analysis Suite (SuperArray).

Real-time PCR profiling of KCNRG in human lymphoma samples and cell lines

Total RNA was isolated by Qiagen RNeasy Mini Kit (Valencia, CA) from wild-type cell lines LNCaP, HL-60 and RPMI-8226 (ATTC, Manassas, VA) as well as from their derivatives stably expressing KCNRG V1, KCNRG V2 and the pcDNA3.1 empty vector control. Reverse transcription reactions were performed using 2 μg of total RNA. Reactions were heated at 70 C for 5 min in a total volume of 12.5 μL in the presence of 100 ng of random hexamers (Invitrogen) and cooled at room temperature for 1 min. After a mini-centrifuge spin, 4 μL of 5X first strand buffer (Invitrogen), 2 μL of 0.1 M DTT and 0.5 μL of 25 mM dNTP mix (Fisher Scientific) were added to the reaction. The mixture was then incubated at 42 C for 1 h. The resulting cDNA was stored frozen (-80 C) until assayed by real-time PCR.

In addition to KCNRG primers, primers for genes selected from the analysis of the microarray data were used to perform real-time PCR reactions in a 96-well format in

the BioRad iCycler iQ RealTime Detection System (BioRad Laboratories, Hercules, CA)(Table 1). The real-time PCR mixtures contained 1 μL of the reverse transcribed RNA sample, 400 nM each of forward and reverse primers and 1X iQ SYBR Green Super Mix and were carried out in a total volume of 15 μL. Amplification of 18S RNA in parallel with the genes of interest was performed as an internal control as described (Grace et al., 2003). For each gene of interest and 18S RNA, three-to-four independent PCR experiments from the same RT sample were performed.

Table 1: Primer sequences with calculated and validated Tm.

Primer Name		Primer Sequence	Calculated	Validated
			Tm °C	Tm °C
KCNRG V1	**F**	TTT TCC CTC CTC AGA TGA CC	59.07	60
	R	TCC AGT TTG GTT ATC AGT AGT GC	58.33	60
KCNRG V2	**F**	CCT GGT TTT CCA GTG TGG TT	59.86	60
	R	GCT GAG GCA GGA GAA TCA CT	59.56	60
18S	**F**	GCC TCA CTA AAC CAT CCA A	54.53	55-60
	R	AGG AAT TCC CAG TAA GTG CG	57.72	55-60
etv6	**F**	CCA CCA TTG AAC TGT TGC AC	60	58
	R	CTG GTG GTT GTT CTC CTG GT		
notch1	**F**	GGA GGC ATC CTA CCC TTT TC	60	58
	R	TGT GTT GCT GGA GCA TCT TC		
cdkn1b	**F**	CAG GTA GTT TGG GGC AAA AA	60	58
	R	ACA GCC CGA AGT GAA AAG AA		
TK1	**F**	ACC TTC CAG AGG AAG CCA TT	60	58
	R	CCT CGA CCT CCT TCT CTG TG		
TNFRSF10A	**F**	AGA GAG AAG TCC CTG CAC CA	60	58
	R	GTC ACT CCA GGG CGT ACA AT		
P53	**F**	CTC TCC CCA GAA GCT CAC AC	60	58
	R	GAA ACC AAA CTG GGA CAG GA		
BAX 225	**F**	GCC CTT TTG CTT CAG GGT TT	60	58
	R	TCC AAT GTC CAG CCC ATG AT		
BAX 430	**F**	GCT GGA CAT TGG ACT TCC TC	60	58

	R	CTC AGC CCA TCT TCT TCC AG		
KITLG	**F**	TGC CAT CTC CAA CTA CAT CCT	60	58
	R	AAA AAT GGT GGC AAG TGG AC		
TNF	**F**	TCC TTC AGA CAC CCT CAA CC	60	58
	R	AGG CCC CAG TTT GAA TTC TT		
TNFRSF1A	**F**	CTC AGG AGC ATG GGG ATA AA	60	58
	R	AGC CAG CCA GTC TGA CAT CT		
STAT2	**F**	TTC AGC CCT TTT CCC AGG AT	55	55
	R	TGT TCC AAC CCG TGG TCA AT		
JUN	**F**	CTA CGC AAA CCT CAG CAA C	58	58
	R	CTT CCT CTC CGC CTT GAT		
CDKN1	**F**	AGC CAG CGC AAG TGG AAT TT	58	58
	R	TTG GGG AAC CGT CTG AAA CA		
NQO1	**F**	AAA AGA AGC TGG AAG CCG CA	55	58
	R	AGG ATT TGA ATT CGG GCG TC		
ABL1	**F**	AGC CCC CGT TCT ATA TCA TC	58	58
	R	GCC AAA ATC AGC TAC CTT CA		

To further confirm microarray data a pathway focused gene expression profiling real-time PCR system was used (RT2 Profiler™ PCR Array System, SuperArray). The RT2 Profiler PCR Array Human Apoptosis pathway was selected based on the number of overlapping genes between the RT-PCR platform and the microarray platform. The 96-well array platform consisted of wells A1 through G12 containing a real-time PCR mix for genes from the same biological pathway, wells H1 through H5 containing housekeeping genes for normalization, well H6 containing a genomic DNA control, wells H7 through H9 containing replicate reverse transcription controls and wells H10 through H12 containing replicate positive PCR Controls. The genomic DNA was eliminated in each 5 µL sample by adding 2.0 µL of GE (5X gDNA Elimination Buffer) and bringing the final volume to 10.0 µL with RNase-free water. An RT-PCR reaction cocktail was

prepared per sample by adding 4 µL of 5X RT buffer (BC3), 1 µL of primer and external control mix (P2), 2 µL of RT enzyme mix (RE3), and 3 µL of RNase-free H20. The RT cocktail (10 µL) was added to each of the 10 µL genomic DNA elimination mixtures and was incubated at 42 °C for 15 min followed by heating at 95 °C for 5 minutes in order to degrade the initial RNA and to inactivate the reverse transcriptase. Following inactivation 91 µL of ultra-pure water was added to each 20 µL of cDNA synthesis reaction and solution was stored on ice. The RT-PCR assay mixture was prepared for a 96-well format by adding 1275 µL of 2x SuperArray RT^2 qPCR master mix, 102 µL of diluted first strand cDNA synthesis reaction, and 1173 µL of ddH20 for a final volume of 2550 µL. The reaction mixture (25 µL) was added to each experimental well of the 96-well assay and sealed with the film provided. The RT-PCR was performed on the BioRad iCycler iQ Real-Time Detection System according to the manufacturers protocol (BioRad Laboratories, Hercules, CA).

To assess KCNRG gene expression in human lymphoma samples, TissueScan Tissue qPCR Arrays Panels were purchased from OriGene Technologies, Inc (Rockville, MD). The normalized cDNAs per each panel were composed of 6 normal, 10 follicular lymphomas, 11 diffuse large B-cell lymphomas, 3 small lymphocytic lymphomas, 6 Hodgkin lymphomas, 8 marginal zone B-cell lymphomas, 2 mantle cell lymphomas and 3 T-cell lymphomas (Table 2). Reactions were performed in a 96-well format in 30 µL volumes in the BioRad iCycler iQ Real-Time Detection System (BioRad Laboratories, Hercules, CA). The cycling program for the reaction was determined experimentally for the previously mentioned KCNRG primers. For KCNRG isoforms, three independent

PCR experiments on individual pre-normalized Tissue Scan plates from the same manufacturer's batch were performed. As an additional control, β-actin mRNA levels were also tested in triplicate. The presence of a single, specific PCR product was verified by melting curve analysis and confirmed on agarose gels.

Table 2: Tissue type and disease stage for RT-PCR profiling.

Disease Stage	Disease Type	Location	Source
N	Normal	C1	Male-50
N	Normal	C2	Female-18
N	Normal	C3	Male-43
N	Normal	C4	Male-52
N	Normal	C5	Male-41
N	Normal	C6	Male-56
I	Lymphoma, anaplastic large cell	C7	Male-58
I	Lymphoma, follicular	C8	Male-37
I	Lymphoma, follicular	C9	Male-38
I	Lymphoma, follicular	C10	Male-42
I	Lymphoma, follicular	C11	Not Sp-67
I	Lymphoma, follicular	C12	Female-53
I	Lymphoma, Hodgkin	D1	Female-82
I	Lymphoma, Hodgkin, nodular lymphocyte predominant	D2	Male-21
I	Lymphoma, Hodgkin, nodular lymphocyte predominant	D3	Male-48
I	Lymphoma, Hodgkin, nodular sclerosing	D4	Female-65
I	Lymphoma, Hodgkin, recurrent	D5	Male-16
I	Lymphoma, large B-cell, diffuse	D6	Male-30
I	Lymphoma, large B-cell, diffuse	D7	Male-56
I	Lymphoma, large B-cell, diffuse	D8	Female-57
I	Lymphoma, large B-cell, diffuse	D9	Female-77
I	Lymphoma, large B-cell, diffuse	D10	Female-65

I	Lymphoma, nodal marginal zone B-cell	D11	Male-76
I	Lymphoma, nodal marginal zone B-cell	D12	Male-76
I	Lymphoma, nodal marginal zone B-cell	E1	Female-74
I	Lymphoma, peripheral T-cell	E2	Male-51
I	Lymphoma, peripheral T-cell	E3	Male-71
I	Lymphoma, small lymphocytic	E4	Female-72
I	Lymphoma, small lymphocytic	E5	Male-47
I	Lymphoma, small lymphocytic	E6	Male-57
IE	Lymphoma, extranodal marginal zone B-cell	E7	Female-76
IE	Lymphoma, extranodal marginal zone B-cell	E8	Male-29
IE	Lymphoma, follicular	E9	Male-78
IE	Lymphoma, large B-cell, diffuse	E10	Female-66
IE	Lymphoma, large B-cell, diffuse	E11	Male-70
IE	Lymphoma, large B-cell, diffuse	E12	Male-63
IE	Lymphoma, marginal zone B-cell, splenic	F1	Male-45
IE	Lymphoma, peripheral T-cell	F2	Male-51
II	Lymphoma, follicular	F3	Female-48
II	Lymphoma, mantle cell	F4	Not Sp-83
IIE	Lymphoma, extranodal marginal zone B-cell	F5	Female-75
IIE	Lymphoma, large B-cell, diffuse	F6	Female-74
IIE	Lymphoma, mantle cell	F7	Male-52
IIE	Lymphoma, marginal zone B-cell, splenic	F8	Male-55
IV	Lymphoma, follicular	F9	Female-76
IV	Lymphoma, follicular	F10	Female-58
IV	Lymphoma, Hodgkin, nodular sclerosing	F11	Female-56
IV	Lymphoma, large B-cell, diffuse	F12	Male-55

Computer programs and statistic analysis

Comparative analysis *in silico* and an analysis of the structure of the KCNRG gene were performed using genomic, mRNA and EST databases

(http://www.ncbi.nlm.nih.gov and http://genome.ucsc.edu). The KCNRG promoter was predicted by Core Promoter (http://www.cshl.edu/OTT/html/corepromoter.html) and NNPP (http://www.fruitfly.org/seq_tools/promoter.html) services. Multiple alignments of the protein sequences were performed using ClustalW v.1.83. A phylogenetic tree of prealigned T1 domains of KCNRG-like proteins was reconstructed by the neighbor-joining method and visualized by the same software. Group comparisons were performed by non-parametric Mann-Whitney hypothesis tests. Unless otherwise noted, P values < 0.05 were considered significant.

A novel method for the analysis of the dual channel microarray data was developed by James Baughman. The microarray dataset was analyzed by normalization based on the average of the selected gene expressions across all of the arrays. Selected genes were picked from the built in list of 'housekeeping' genes provided by the SuperArray oligo platform. Genes were selected based on their performance as true housekeeping genes, and their ability to accurately indicate the signal intensity of their representative arrays. Therefore, the sensitivity of individual gene expression in the control arrays (HR1, HR2,…) versus the arrays with transfected genes (HT1, HT2,…) is highlighted vis-à-vis this normalization method. The method does not take into account the selected gene expression within the array, but rather uses the overall variance of selected gene expression across arrays as a means to quantify the comparative expression of each individual array. Normalization was based on the following process: The mean of the selected gene expression for each array was calculated ($\mu 1$, $\mu 2$, $\mu 3$ …). The mean of the selected gene expression of all arrays (μT) was then calculated. The expression of

each gene (selected & non-selected) was multiplied by the mean selected gene expression of all arrays divided by the mean selected gene expression of its array ([μT / μ1], [μT / μ2], [μT/μ3]…). This was normalized by dividing by the mean expression of each array (selected & non-selected) and multiplying the result by 100. The minimum expression was set at 10.

Chapter 3: Results and Discussion

Comparative analysis of the KCNRG mRNA and protein isoforms

Candidate tumor suppressor gene KCNRG resides within the 3' end of the largest transcript of human RFP2 gene described earlier (Baranova et al., 2003; Lerner et al., 2007). Major mRNA isoforms of KCNRG are transcribed independently of RFP2, starting at the promoter located within 3'-untranslated region RFP2 (Fig.2). This sequence coincides with the *in silico* predicted promoter located in the position approximately –100 nt upstream of the putative 5' end of the KCNRG transcripts according to an alignment of the KCNRG ESTs to the genomic sequence (Core Promoter score 1.000, NNPP score 0.97).

Additionally, collaborators at the Russian Center of Medical Genetics (RCMG) demonstrated an existence of a hybrid mRNA isoform that includes exons from both RFP2 and KCNRG (Fig.2) (M.Skoblov, personal communication). This isoform originates from the quadruplex containing promoter of RFP2, possibly due to its unusual properties described earlier (Skoblov et al., 2006). In all examined species of mammals with the exception of human and chimps, KCNRG and RFP2 genes are encoded by separate loci (Fig.4).

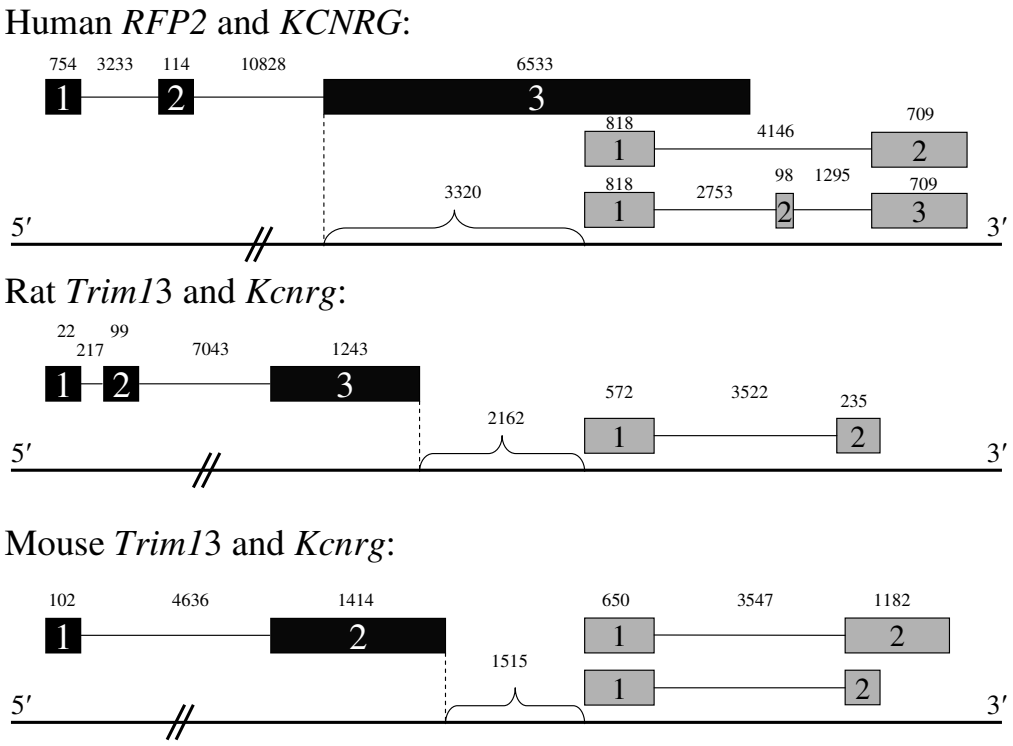

Fig. 4. Comparative analysis of the RFP2/KCNRG locus found in human, rat and mouse genomes. Exons are shown as boxes and introns or intergenic regions as lines. Exons of RFP2 or its orthologs (Trim13 in mouse and rat) are depicted in black while exons of KCNRG and its orthologs are illustrated in gray. Sizes are scaled to the human genome distances.

Human KCNRG encodes two protein isoforms KCNRG-L (272 aa) and KCNRG-S (229aa), corresponding to variant 1 and variant 2 respectively, that differ in their C-ends and possess common N-end of 184 aa. A T1 tetramerization domain covers amino acid positions 7 to 98. KCNRG loci of other mammals including chimpanzee, encode only one protein isoform corresponding to human KCNRG-L. In chimps, KCNRG-L differs from its human ortholog by one amino acid substitution (Pro→Leu) in the position 158. Comparison of human and rat KCNRG orthologs revealed 85.4% identity in a 268 residue overlap, while comparison with the mouse ortholog was characterized by 73.2%

identity in a 264 residue overlap. Murine KCNRG locus encodes two protein isoforms, 264 and 191 residues in length, both of which are variants of human KCNRG-L isoform.

Interestingly, human KCNRG-S and KCNRG–L isoforms share only the first 191 residues, while being different in their C-termini. This difference is due to out-of-frame insertion of the alternatively spliced exon 2 that is present only in the human genome and is derived from an AluSp SINE repeat. According to results of RT-PCR experiments performed by colleagues in RCMG, RAMS (data not shown) mRNA isoforms encoding two KCNRG proteins are co-expressed in human tissues. Levels of Alu-containing KCNRG-S mRNA isoforms are substantially lower than that of KCNRG-L mRNA.

Computational analysis of the KCNRG protein

Computational analysis of the sequence of KCNRG was performed in order to discern any regions of interest within its open reading frame. The amino acid sequences of KCNRG-L (272 aa) and KCNRG-S (229) aa isoform have been used for a blastp search against the protein database. The data resulting from this blastp analysis were examined to determine the highest matching sequences. The highest matching sequences were obtained using the (E) values calculated from the blastp search. The (E) value is a parameter that refers to the possible expected number of hits one can obtain from searching a given database, this value decreases as the significance of the hit increases. Hence the lower the (E) value, the stronger the match.

The resulting data were tabulated and separated into two sets in accordance with the region of homology. The first set comprised the sequence similarity between amino

acids 1 and 190. This segment of the sequence displayed two regions thought to be conserved domains: the BTB/POZ domain with an (E) value of 8e-7 and a K+ channel tetramerization domain with an (E) value of 9e-14 (Fig.5). The data presented in the following homology analysis were obtained using the shorter of the two isoforms (229 aa).

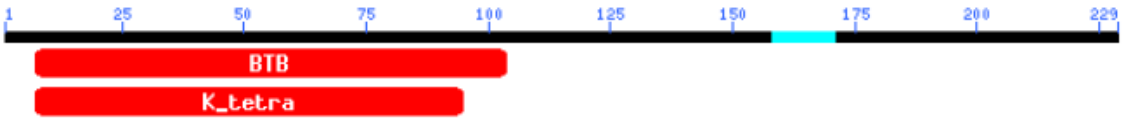

Fig.5. The regions of KCNRG containing conserved domain homology

The BTB/POZ (The BTB (for BR-C, ttk and bab, and the POZ also known as poxvirus and zinc finger) domain consists of a protein-protein interaction motif located at the N-termini of certain transcription factors as well as certain types of potassium channels. The structure is comprised of a tightly intertwined dimer created by the interactions between the N-terminal strand and helix structures (Bardwell et al. 1994 and Koonin et all 1999). The cytoplasmic tetramerization domain (T1) of voltage-gated K+ channels, also known as K+ tetramerization domain, is thought to code for the molecular components used for the subfamily-specific assembly of the alpha-subunits into functional tetrameric channels. It is also thought to be related to the BTB/POZ domain (Kobertz et al. 1999 and Zerangue et al. 2000). Using a molecular visualization program, images of the Kv channels can be generated and the locations of the tetramerization domains can be seen with respect to the rest of the channel (See Fig. 6) (Kobertz et al. 1999).

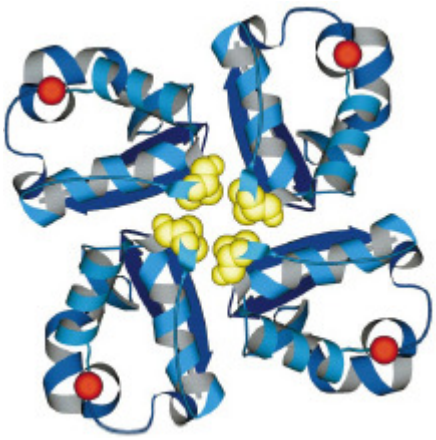

Fig.6. RASMOL image of a view along the four-fold axis of the T1 domain tetramer. Yellow designates the Asn 167 side chains that form the tightest constriction along the axis. Red marks the C-termini that attach to the channel protein ~20 residues before the beginning of the S1 transmembrane helix. (Kobertz et al. 1999).

Interestingly, detailed blastp analysis of the shorter version of KCNRG protein (isoform S, 229 aa in size) revealed a novel, very highly conservative domain located between amino acids 190 and 229. As no known conserved domain signatures were recognized in this region, we considered this domain as novel and called it COOL (because we think it is very interesting - "cool", and because it's located close to C-end). The list of the proteins homologous to the C-tail of KCNRG isoform S includes those that belong to protein families with various functions. COOL domains with the proposed structure most closely resembling that of C-end of KCNRG-S isoform are found in human serine-threonine kinase STK2 (NIMA-type kinase 4), protein BCAS4 that is often amplified or fused in breast carcinomas and TRIM61/RNF35 RING finger protein that is translated temporally in the pre-implantation embryos (Hayashi et al., Barlund et al., Choo et al.). Nucleotide analysis of the exon encoding the COOL-domain suggests its

possible origin from the insert of a partial Alu-repeat into the 3' area of its open reading frame.

The complete list of the COOL domain containing proteins and corresponding alignments can be found in Appendix 1, 2 and 3. The preliminary analyses of the COOL proteins indicate no clues as to functions. This domain may serve regulatory functions, e.g. it may contain an important site for post-translational modification or protein-protein interaction.

According to Motif Scan analysis (http://scansite.mit.edu/cgi-bin/motifscan_seq) both KCNRG isoforms are with high probability able to interact with SH3 domains of Amphiphysin, Cbl-Associated protein C, and IL2-inducible T-cell kinase ITK/LYK (also known as PSCTK2, ETK) (Fig.7). Both Serine/threonine-protein kinase STK2/Nek4/NRK2 and BCAS4 proteins that include COOL-like domains also contain a SH3 binding site. The same site is also present in a variety of the potassium voltage-gated channel proteins.

Analysis using the NetPhos 2.0 Server indicated possible phosphorylation sites at 5 Ser, 3 Thr and 2 Tyr residues, with one of the Ser phosphorylation sites located within the COOL domain. Four highly significant O-ß-GlcNAc attachment sites, 3 of them located in the COOL domain were predicted using the YinOYang 1.2 server (http://www.cbs.dtu.dk/services/YinOYang/). A search for a short protein motif performed by ELM (Eukaryotic Linear Motif Resource, http://elm.eu.org/) revealed, among others, a highly conserved SSDSPA motif that is embedded within COOL domain. According to ELM, SSDSPA motif is classified as Class IV WW domain

interaction motif involved in phosphorylation-dependent interactions. The complete list of the motifs and functional sites found in KCNRG can be found in Appendix 4.

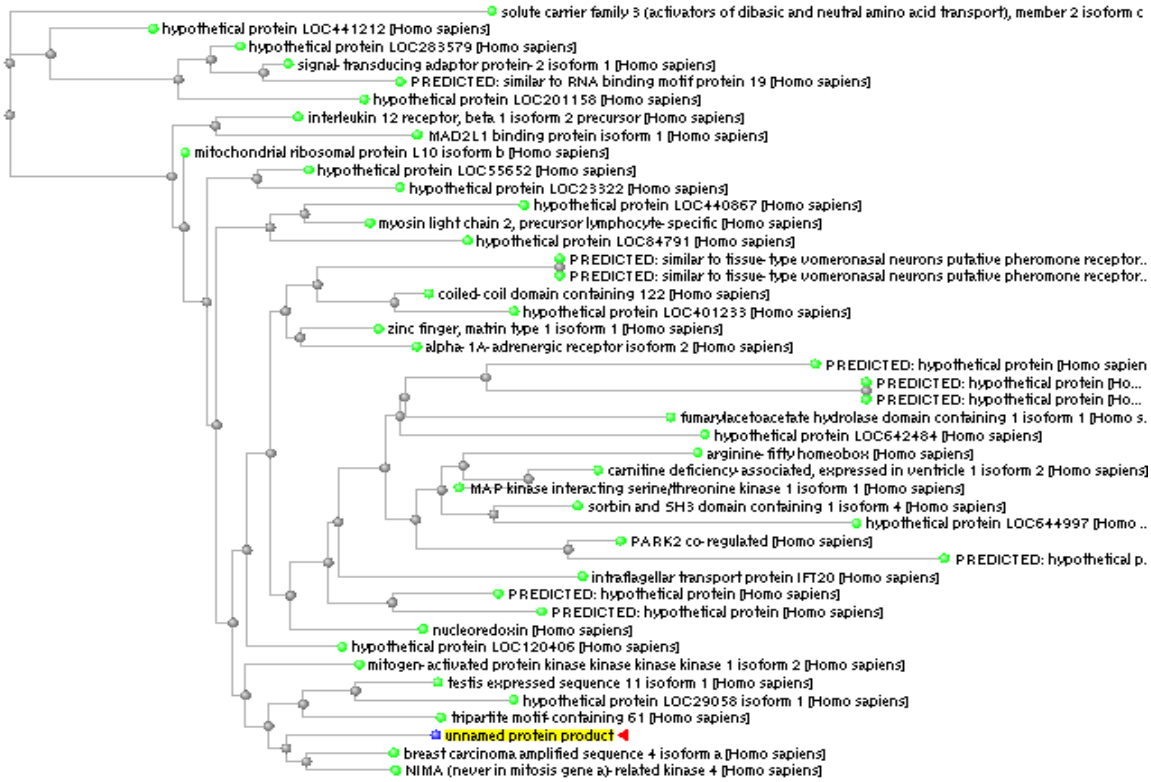

Fig.7. Fast minimum evolution tree of KCNRG COOL-domain.

KCNRG is a member of the KCTD protein family

Human KCNRG is a member of the KCTD gene family that encodes predicted proteins with an N-terminal domain that is homologous to the T1 domain in voltage-gated potassium channels. The KCTD family of proteins belong to a larger group of non-channel T1/BTB proteins. KCTD family members are similar to Pfam K_tetra consensus (PF02214) rather than that of BTB/POZ (Stogios et al., 2005). Our analysis (Fig.8 and 9)

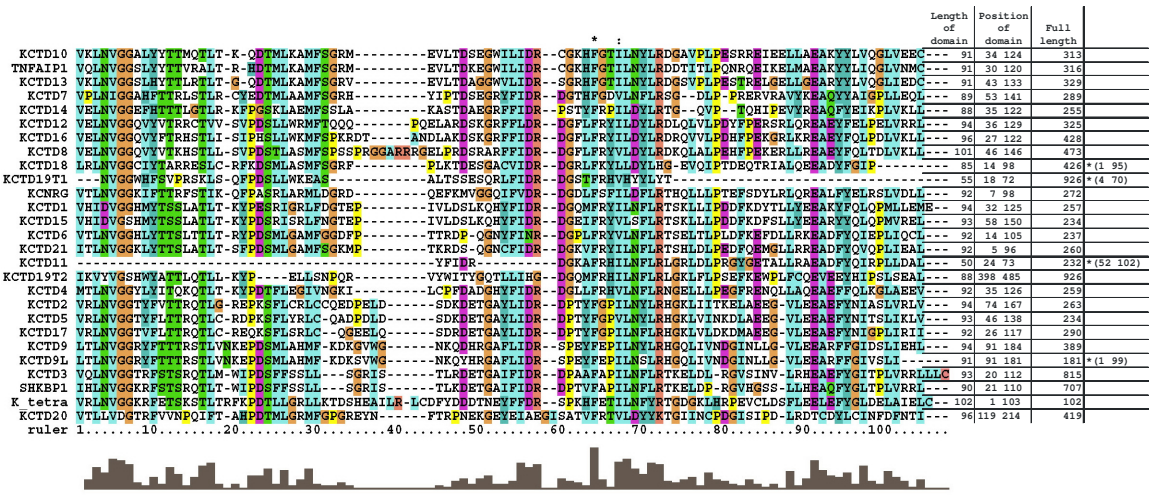

Fig. 8. An alignment of KCNRG with other proteins of KCTD family. Degree of shading indicates different degree of conservation for a given amino acid position: invariant positions are darkest, other conserved positions are shaded lighter, non conserved positions are not shaded. Total length of T1 domain, its position and full length of the proteins are summarized in the table adjacent to the aligned protein sequences. Truncated versions of T1 domain are marked by star (*).

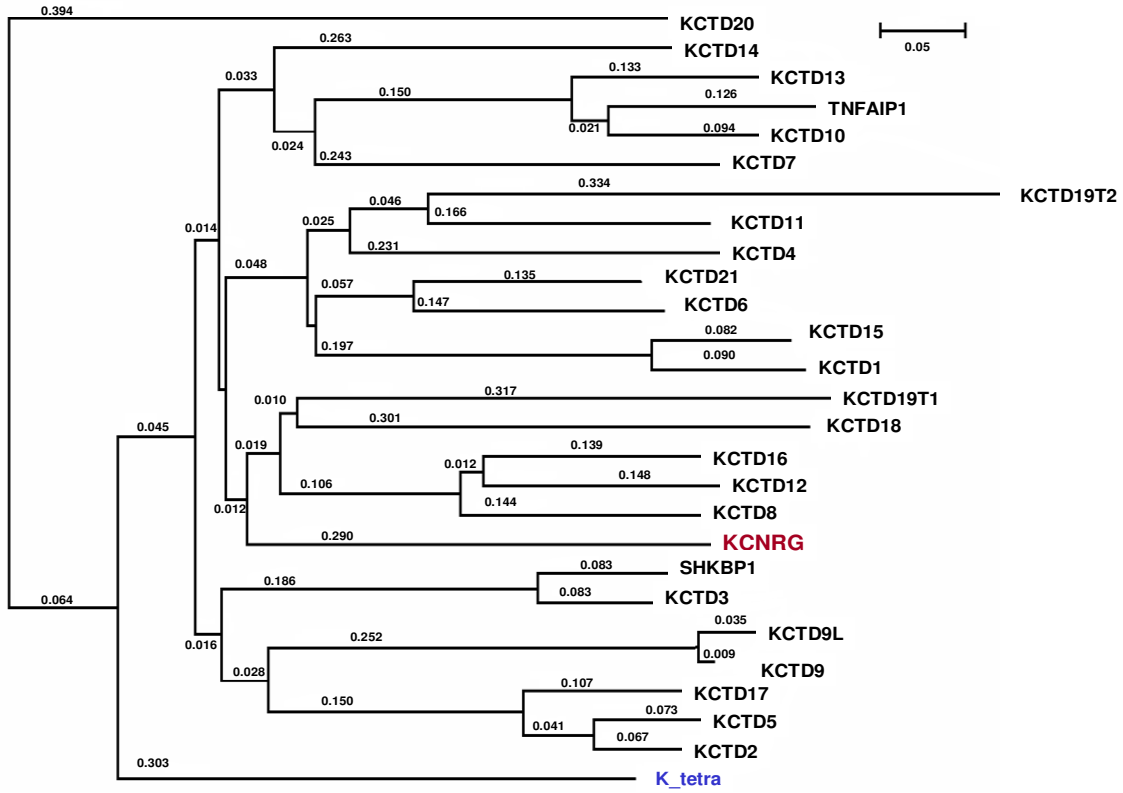

Fig. 9. A phylogenetic tree of prealigned T1 domains of KCNRG-like proteins.

revealed two additional KCNRG-like proteins that should be classified as KCTD family members, TNFAIP1 (Tumor necrosis factor-alpha-induced protein 1) and SHKPB1 (SH3KBP1 binding protein 1), while the protein C6orf69 previously classified as KCTD20 represents an out-group and should be excluded from the T1 family in a *sensu stricto*.

Previous research has implicated TNFAIP1 in the progression of cancer and linked its overexpression to increased rates of apoptosis (Yang LP et al. 2006). An interesting study on HBV showed increased TNFAIP1 expression via RT-PCR detection in patients that are immune to HBV, indicating a role for TNFAIP1 in the innate immunity against HBV (Lin MC et al. 2005). Recently a study of a comparative genome-scale transcriptional analysis of two T-cell subsets CD4+ and CD8+ against each other and against CD3+ cells found TNFAIP1 to be one of the set of proteins implicated in the communication between these two subsets, indicating a possible role for TNFAIP1 in T-cell activation and immune response (Wang M et al. 2008).

SH3KBP1, a gene with many alternative names (Gene names: SH3KBP1, CIN85, Protein names: Human Src family kinase-binding protein 1 (HSB-1), CD2-binding protein 3 (CD2BP3), Cbl-interacting protein of 85 kDa) encodes an adapter protein involved in regulating diverse signal transduction pathways (UniProt, Watanabe S et al. 2000). Recent studies have implicated SH3KBP1 in ASAP1 mediated EGF receptor recycling, leading the investigators to propose a scaffold protein role for SH3KBP1 (Kowanetz K et. al 2004). Additionally, another study has shown that SH3KBP1 interacts

with TNFR1, leading to the hypothesis that this association may modulate TNF-α-induced apoptosis (Narita T et al. 2005).

KCTD20 is a BTB/POZ domain-containing protein residing on chromosome 6p21.31 (GeneCards). It has been identified as part of a complex containing MARK4. This complex regulates microtubules, participates in the defining of the cell polarity and has a higher expression level in human gliomas (Beghini A et al. 2003; Brajenovic M. et al. 2004). KCTD13 (located on 16p11.2), alternatively known as FKSG86 and PDIP1, is a TNFAIP1-like protein, and interacts with POLD2 and PCNA. A role has been proposed for it in cytokine activation and DNA replication (He H et al. 2001). Similarly, like other TNFAIP1-like proteins, KCTD10 (12q24.11) is inducible by TNF-α and interacts with the small subunit of DNA polymerase delta and PCNA (Zhou J et al. 2005).

KCTD7 is located on 7q11.21 and is thought to be a cytoplasmic protein. Interestingly in a study attempting to shed light on the identity of the causal gene in autosomal recessive progressive myoclonic epilepsy (PME), linkage analyses identified a new locus on 7q11.2, where researchers found a C to T mutation in exon 2 of the KCTD7 gene (Van Bogaert P et al. 2007).

Recent research has found KCTD11 (also known as REN), located on 17p13.1, to play a regulatory role in neuronal differentiation via signaling by retinoic acid, epidermal growth factor/EGF and NGFB/nerve growth factor (Gallo R et al. 2002). Additionally, studies of medulloblastoma (MB) tumors revealed that KCTD11 suppresses the tumor-promoting Hedgehog signaling pathway, while in granule cell progenitors overexpression of KCTD11 seems to increase apoptosis and decrease proliferation (Di

Marcotullio L et al. 2004; Argenti B et al. 2005). A similar study of medulloblastoma samples found a reduction of KCTD11 expression in tumor cells as compared to normal adult cerebellum cells. Even more significant reduction of KCTD11 expression in neural stem cells lead the researchers to propose that haploinsufficiency of KCTD11 may play a role in MB tumorigenesis (Zawlik I et. al 2006). The most close paralogs for the KCTD11 gene include KCTD21 (11q14.1), KCTD15 (19q13.11), KCTD6 (3p14.3) and KCTD1 (18q11.2) a nuclear protein that has recently been found to act as a transcriptional repressor in addition to mediating protein-protein interactions through its BTB domain (Ding XF et al. 2008).

KCTD12, also known as Pfetin, C13orf2, KIAA1778, and PFET1, is located on 13q22.3 and is paralogous to KCTD8 (4p13) KCTD16 (5q32) and KCTD14 (11q14.1) (GeneCards). KCTD12 was cloned from human fetal cochlear cDNA clones. Its 6-kb transcript was found to be present in several fetal organs, the highest expression levels being in the cochlea and brain; however very low expression levels were detected in adult tissues such as brain and lung (Resendes BL et al. 2004). A study aiming to find markers for transplantable bone marrow stromal cells (BMSCs) found KCTD12 to be a reliable indicator (Igarashi A et al. 2007). Recent research on type 2 diabetes (T2D), a Genome Wide Association (GWA) study identified new single nucleotide polymorphisms (SNPs) with 14 risk loci, one of these loci being KCTD12 (Cauchi S et al. 2008). A proteomic study aimed at developing prognostic biomarkers for gastrointestinal stromal tumors (GIST) found that KCTD12 was not only a strong marker for GISTs but was also

informative in distinguishing between GISTs with good and poor prognosis (Suehara Y et al. 2008).

KCTD3 (1q41) was found to be a tumor antigen recognized by the humoral immune system in a study with patients with renal cancer, thereby acquiring the name NY-REN-45 (Scanlan MJ et al. 1999). KCTD3 is co-expressed with the transcription factor Oct4 (Pou5f1) (with a % correlation of +91), a mediator that has been implicated in lineage specific differentiation, adult stem cell identity, and cancer (Pearl A et al. 2007).

KCTD9 is located on 8p21.1 and, in addition to the BTB/POZ domain, contains 3 pentapeptide repeat domains (Uniprot). Although detailed information on the function of KCTD9 has not yet been elucidated it has been independently identified in several cancer related array based genomic studies. These studies includes an attempt to determine signature genes distinguishing types or grades of tumors where KCTD9 was amongst the 10 most frequent genes as ranked by score (Junior Barrera et al. 2007).

A study on organ-confined prostate cancer observing whole genome copy number changes in the genomes of hormone-naive lymph node metastases found KCTD9 to be amongst the genes exhibiting increased copy number aberrations (CNAs) for primary tumors that progressed and metastasized (Pamela L et al. 2006). In a study on sporadic breast cancer using array-based comparative genomic hybridization, researchers found KCTD9 to be amongst the genes with a 11.1% homozygous loss in the cell lines studied, and a 36% hemizygous loss in the tumors studied (Tara L Naylor et al. 2005).

Recently, KCTD5 (16p13.3) was found to interact with the adeno-associated virus 2 REP proteins (AAV-2 Rep78/Rep68) and upon interaction was found to undergo

translocation to the nucleus, thereby indicating a regulatory role for this protein (Weger S et al. 2007). In addition, new research has suggested that KCTD5 may also be a substrate-specific adaptor for cullin3-based E3 ligases (Bayón Y et al. 2008). Aside from their structural properties KCTD17 (22q12.3), KCTD18 (2q33.1), KCTD4 (13q14.12) and KCTD2 (17q25.1) have yet to reveal any functional properties.

Most of the KCTD proteins are relatively short (on average, 355 amino acids), their T1 domains are located close to the N-end of the protein and are not accompanied by any other Pfam domains. All KCTD proteins except KCTD19 contain only one T1 domain. The first of two T1 domains of KCTD19 is truncated. T1 domains of 3 out of 25 KCTD proteins (KCTD18, KCTD11 and KCTD9L) are truncated. KCNRG is a typical member of the KCTD family, with solitary T1 domain unaccompanied by any other recognizable protein structure. The function of these proteins is still unknown.

Cloning of KCNRG isoforms

The initial cloning of KCNRG V1 was contracted to the Maryland based company OriGene. The company was provided with the pCDNA3.1/myc-His A vector (Invitrogen), the structure and multiple cloning site of this vector can be seen below (Fig.10).

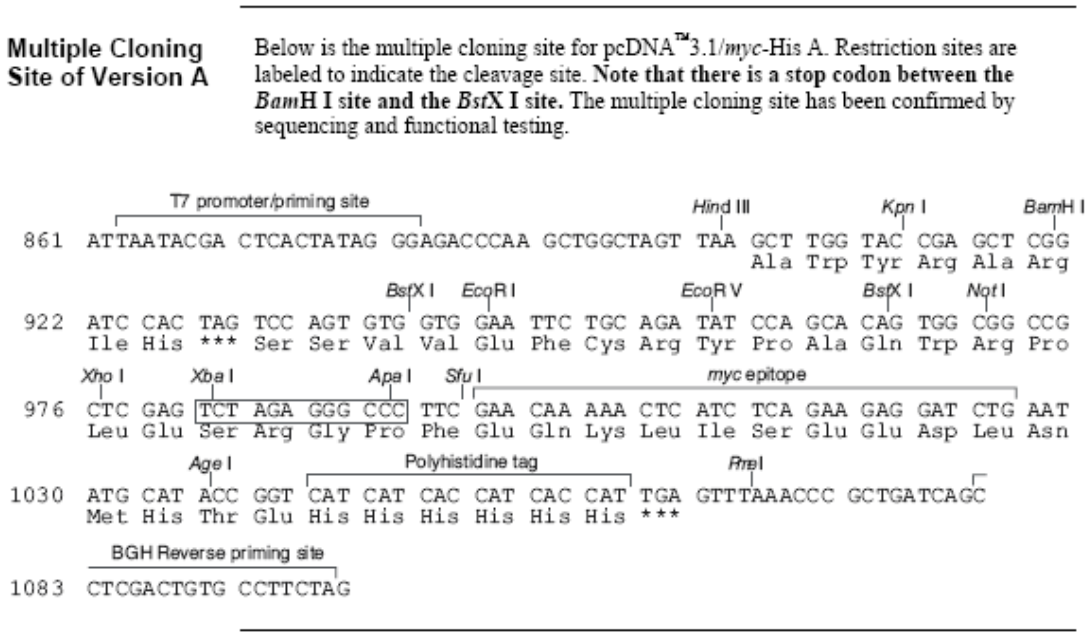

Fig. 10. Multiple cloning site of pcDNA 3.1 version A (Invitrogen).

The KCNRG gene was cloned in between the BamH1 and Xho1 restriction sites.

The resulting recombinant plasmid obtained from OriGene can be seen below (Fig.11).

-BamH1--Start-

AATACGACTCACTATAGGGAGACCCAAGCTGGCTAGTTAAGCTTGGTACCGAGCTC*GGATCC*AGA*ATG*AGT*AGT*CAG*GAA*CTG*GTC*ACT*TTG*AAT*GTG*GGA*GGG*AAG*ATA*TTC*ACG*ACA*AGG*TTT*TCT*ACG*ATA*AAG*CAG*TTT*CCT*GCT*TCT*CGT*TTG*GCA*CGC*ATG*TTA*GAT*GGC*AGA*GAC*CAA*GAA*TTC*AAG*ATG*GTT*GGT*GGC*CAG*ATT*TTT*GTA*GAC*AGA*GAT*GGT*GAT*TTG*TTT*AGT*TTC*ATC*TTA*GAT*TTT*TTG*AGA*ACT*CAC*CAG*CTT*TTA*TTA*CCC*ACT*GAA*TTT*TCA*GAC*TAT*CTT*AGG*CTT*CAG*AGA*GAG*GCT*CTT*TTC*TAT*GAA*CTT*CGT*TCT*CTA*GTT*GAT*CTC*TTA*AAC*CCA*TAC*CTG*CTA*CAG*CCA*AGA*CCT*GCT*CTT*GTG*GAG*GTA*CAT*TTC*CTA*AGC*CGG*AAC*ACT*CAA*GCT*TTT*TTC*AGG*GTG*TTT*GGC*TCT*TGC*AGC*AAA*ACA*ATT*GAG*ATG*CTA*ACA*GGG*AGG*ATT*ACA*GTG*TTT*ACA*GAA*CAA*CCT*TCA*GCG*CCG*ACC*TGG*AAT*GGT*AAC*TTT*TTC*CCT*CCT*CAG*ATG*ACC*TTA*CTT*CCA*CTG*CCT*CCA*CAA*AGA*CCT*TCT*TAC*CAT*GAC*CTG*GTT*TTC*CAG*TGT*GGT*TCT*GAC*AGC*ACT*ACT*GAT*AAC*CAA*ACT*GGA*GTC*AGG*TAT*GTT*TCT*ATA*AAA*CCT*GAT*AAC*CGA*AAA*TTG*GCC*AAC*GGA*ACA*AAT*GTC*CTC*GGC*TTA*CTG*ATT*GAC*ACT*TTA*TTA*AAG*GAA*GGC*TTT*CAT*TTG*GTC*AGC*ACT*AGA*ACA*GTA*TCT*TCT*GAA*GAC*AAA*AC

T*GAA*TGC*TAT*AGC*TTT*GAA*AGG*ATA*AAA*AGC*CCT*GAA*GTG*CTC*A
TC*ACG*AAT*GAA*ACA*CCA*AAA*CCA*GAG*ACT*ATC*ATC*ATA*CCA*GAG*
CAA*TCT*CAG*ATA*AAG*AAA*CTC*GAG*TCT*AGA*GGG*CCC*TTC*GAA*CAA*AAA*C
TC*ATC*TCA*GAA*GAG*GAT*CTG*AAT*ATG*CAT*ACC*GGT*CAT*CAT*CAC*CAT*CAC*C
- Polyhistidine Tag ---
AT***TGA***GTTTAAACCCGCTGATCAGCCTCGACTGTGCCTTCTAGTTGCCAGCCATCTGTTGTTTGCCC
---**Stop-**

Fig. 11. Insert site for KCNRG Variant 1 in plasmid pcDNA 3.1/myc-His A.

The resulting vector was sequenced to confirm that the insert was placed properly, particularly, that there are no stop codons within the gene and before the polyhistidine tag, and that the insert is in frame with the myc epitope and the polyhistidine tag. A restriction digest of the plasmid was performed to verify the size of the insert before the use of the plasmids for overexpression studies. This sequence analysis confirms that the KCNRG V1 gene in the pCDNA3.1/myc-His A vector is indeed placed optimally. A blast search against the nucleotide database of NCBI confirms that this gene is the longer isoform (Variant 1) of KCNRG. The cloning of KCNRG variant 2 was performed by our collaborators Andre Marakhonov and Dr. Mikhail Skoblov (Russian Center for Medical Genetics, Moscow, Russia) as described in the Materials and Methods section, the product was subjected to the same analysis as KCNRG V1 (Appendix 5).

A search for variations in the KCNRG locus

Mutations within open reading frame of KCNRG and adjacent parts of its introns were screened in 35 CLL patients by conventional PCR-SSCP in the collaborating lab at RCMG, RAS. No aberrant bands were seen. DNA was prepared from RPMI-8226 and two other multiple myeloma cell lines, U266 and CRL-9068, and this DNA was

subjected to automated sequencing. Direct sequencing of KCNRG exons revealed a point mutation delT in the +30 position of the 5' non-coding area of KCNR gene in RPMI-8226 cell line (position indicated according to mRNA Ac. Num. NM_199464). The search for known human SNPs was negative for any match in this nucleotide position. Interestingly, an analysis of matches to transcription factor binding matrices with MatInspector software revealed the core promoter initiator element (INR) that overlaps the mutated position. Deletion of T decreases the matrix similarity of the match from 0.945 to 0.941, and, therefore, might negatively influence expression of KCNRG in RPMI-8226 cells.

A low complexity repeat (A)33(TA)8(CA)8TATGTA(CA)2TACA (TA)4CA(TA)3 located at the position – 1006 relative to the major start of KCNRG mRNAs and within 3' untranslated area of RFP2 was amplified by PCR with subsequent band resolution in polyacrylamide gel in 21 DNA sample of CLL patients and 50 DNA samples of normal donors at RCMG, RAMS. Unusually high levels of the polymorphism have been observed, as the profiling of a total of 142 chromosomes revealed 12 alleles of this repeat. The heterozygous state of this repeat was seen in 52/71 (73%) samples tested indicating high informativeness of this polymorphic DNA marker. In the future this marker can be used to test possible monoallelic losses of KCNRG gene in CLL samples.

Expression of KCNRG inhibits proliferation and enhances apoptosis in cultured tumor cells

Open reading frames corresponding to both protein isoforms of KCNRG were cloned into the pcDNA3.1 backbone, stably transfected in to LNCaP, HL-60 and RPMI-

8226 cells and studied in various functional assays. The cells transfected with pcDNA3.1 vector alone were used as a control and are designated as EV for Empty Vector. As quantified by chemilumionescent BrdU cell proliferation ELISA assay, growth of all three cell lines was significantly inhibited by an overexpression of KCNRG-V1 isoform (RPMI-8226: decrease of 37%, $P < 0.001$; HL-60: decrease of 26%, $P < 0.0025$; LNCaP: decrease of 38%, $P < 0.009$). The KCNRG-V2 isoform exerted less prominent growth suppressive effect in these cells (RPMI-8226: decrease of 27%; HL-60: decrease of 12%; LNCaP: decrease of 24%). In the case of KCNRG-V2 isoform, the difference between observed values were significant only for KCNRG-V2 overexpression in LNCaP ($P < 0.05$) and RPMI-8226 ($P < 0.02$) (Fig. 12 a,b,c).

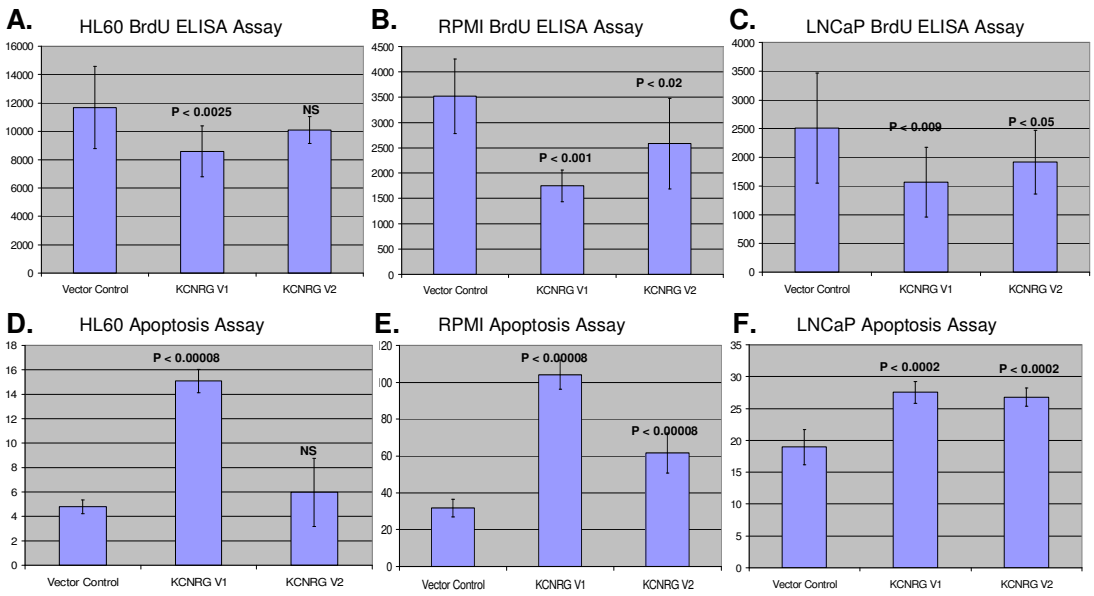

Fig. 12. Expression of KCNRG inhibits proliferation (BrdU ELISA assay, A, B, C) and enhances apoptosis (caspase 3/7 assay, D, E and F) in cultured tumor cells. A and D: HL-60. B and E: RPMI-8226. C and F: LnCaP. Complete tables can be found in Appendix 6.

Cell survival was analyzed by measurement of the activities of caspases 3 and 7. An increase in the apoptotic events was found in the cells that were stably transfected with any KCNRG isoform, but in KCNRG-V1 cells these changes were more profound (KCNRG-V1/RPMI-8226: increase of 180%, $P < 0.0008$; KCNRG-V1/HL-60: increase of 216%, $P < 0.0008$; KCNRG-V1/LNCaP: increase of 46%, $P < 0.0002$; KCNRG-V2/RPMI-8226: increase of 94%, $P < 0.0008$; KCNRG-V2/HL-60: increase of 25%, NS; KCNRG-V2/LNCaP: increase of 41%, $P < 0.0002$) (Fig. 12 d,e,f). Complete tables can be found in Appendix 6.

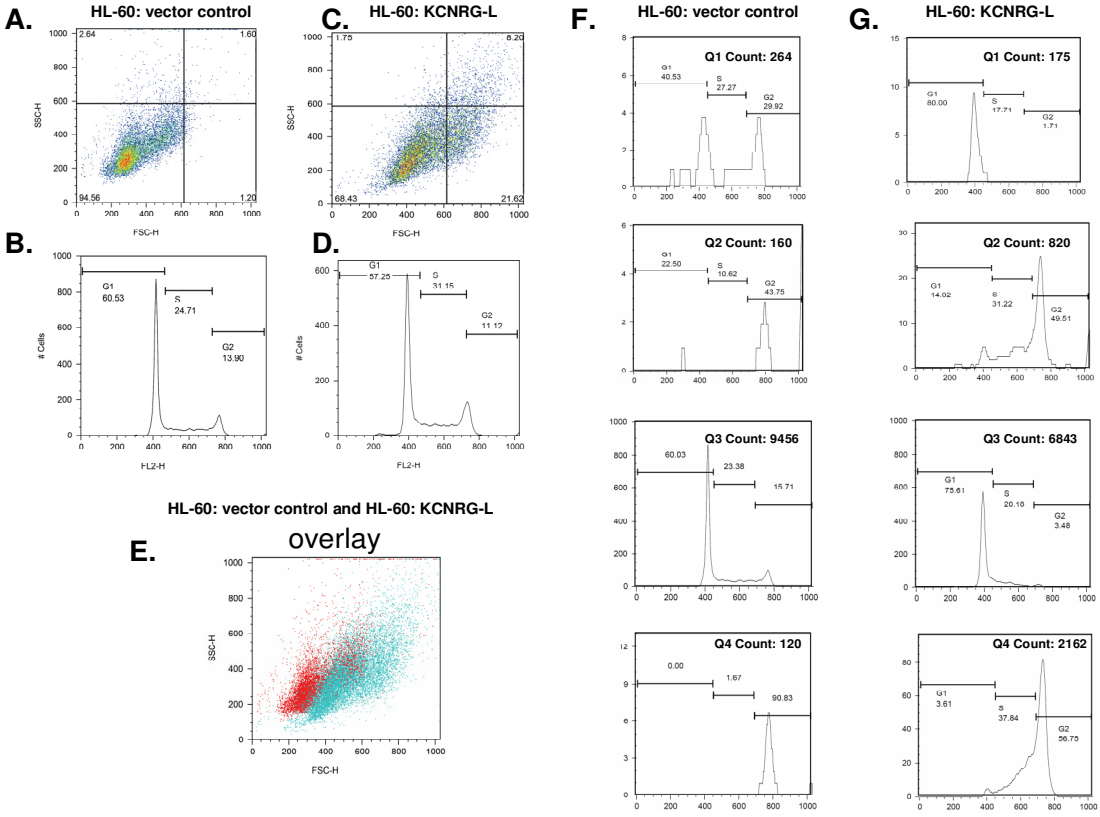

Fig. 13 A. HL60 empty vector control in Side Scatter (SSC) vs. Forward Scatter (FSC) plot. B. Histogram of HL60 EV control C. HL60 transfected with KCNRG V11 in Side Scatter (SSC) vs. Forward Scatter plot. D. Histogram of HL60 transfected with KCNRG V1. E. Overlay of scatter plot for HL60 empty vector control and HL60 V1. F. Histogram analysis of each quadrant of HL60 empty vector control scatterplot. G. Histogram analysis of each quadrant of HL60 V1 scatterplot.

Observations described above were confirmed by FACS analysis of the cell lines over expressing KCNRG isoforms and the vector control (Figs. 13).

Interestingly, the suppression of the proliferation of the suspension cell lines HL-60 and RPMI-8226 has been accompanied by the dramatic changes in the size and the shape of the cells. An increase of KCNRG-V1 expression in HL-60 cell line resulted in the formation of two cell populations, a normal-like population mainly residing in G1 phase (Fig. 13F and 13G, quadrants 1 and 3) and larger, abnormal cells residing in G2 (Fig. 13F and 13G, quadrants 2 and 4). In order to see this effect more clearly the cells were analyzed by charting them on a SSC (Side Scatter) and FSC (Forward Scatter) plot (Fig. 13A and 13B). The plot was gated into four quadrants, and each cell line was subjected to the same gating conditions. The histogram of each quadrant clearly indicates more than one population of cells undergoing cell cycle changes. Similarly, an overexpression of KCNRG-V1 in RPMI-8226 also produced a population of abnormal cells (see Appendix 7) as compared to KCNRG-V2 and KCNRG-EV. The changes in LNCaP-V1 and V2 cells were more subtle, and composed mainly of a decrease in overall cell size for LNCaP-V1 cells, indicated by the slight shift downward of the scatter-plot (see Appendix 7). The quantification of the results for HL60 empty vector control and HL60 transfected with KCNRG V1 and V2 is presented in two tables (Fig. 14A and 14B), one summarizing the complete population, and one summarizing the gated populations (Tables summarizing PI FACS information on RPMI-8226 and LNCaP cell lines can be found in Appendix 7).

A.

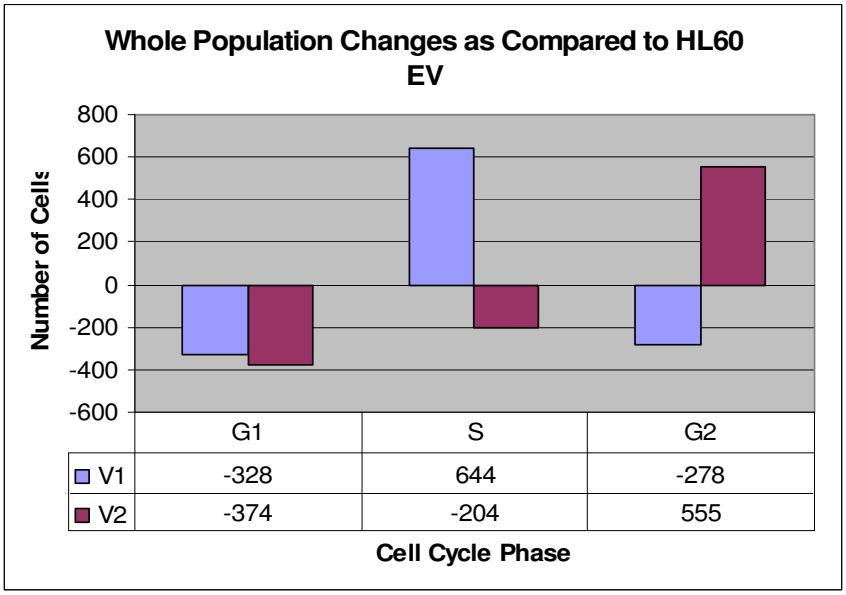

B.

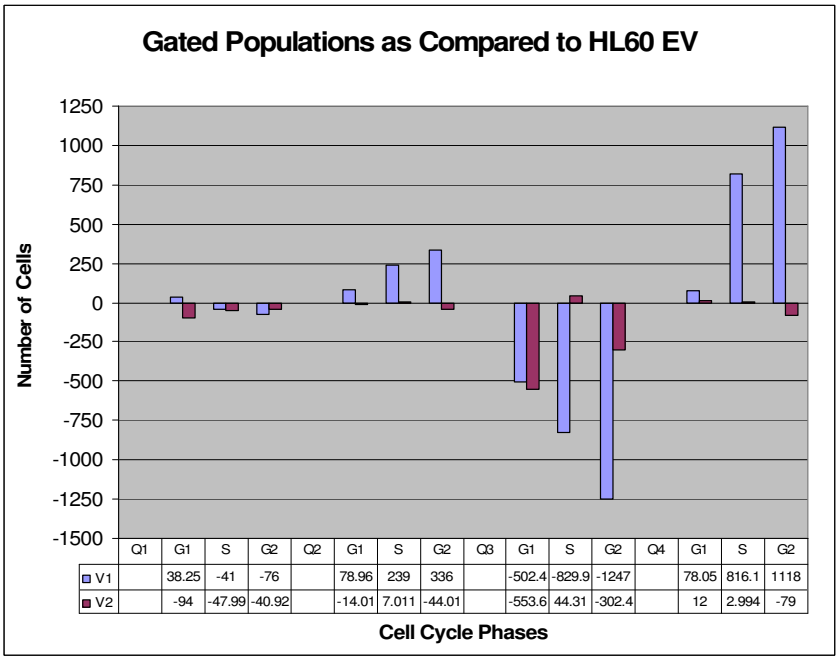

Fig.14. Quantification of HL60 EV and HL60 V1 scatterplots A. Quantification of non-gated data. B. Quantification of gated data.

The apoptosis data obtained by the chemiluminescent detection of caspase activity were also confirmed by FACS analysis using annexin V and 7-AAD. Quadrant 1 shows cells that have absorbed higher levels of 7-AAD, indicating cell wall disruptions, and therefore necrosis. Quadrants 2 shows cells that have absorbed equal amounts of annexin V and 7-AAD, and are cells at the stage of late apoptosis. Quadrant 3 shows healthy live cells, and quadrant 4 shows cells that have absorbed a larger amount of annexin V, indicating early apoptosis. HL60 cells transfected with KCNRG V1 have significantly higher levels of late apoptotic death (Fig. 15).

Interestingly, HL60 cells transfected with KCNRG V2 show slightly higher levels of early apoptosis, and slightly lower levels of necrosis as compared to the cells transfected with KCNRG V2 (See Fig. 15D). In addition, a slight but significant elongation of the healthy cell population can be observed in quadrant three for cell lines transfected with either isoform of KCNRG, once again indicating a more varied cell size in these populations (Fig. 15 A,B,C). The effects of KCNRG V1 and the trend towards increased late apoptosis was observed in RPMI-8226 and LNCaP cell lines as well, and can be found in Appendix 8.

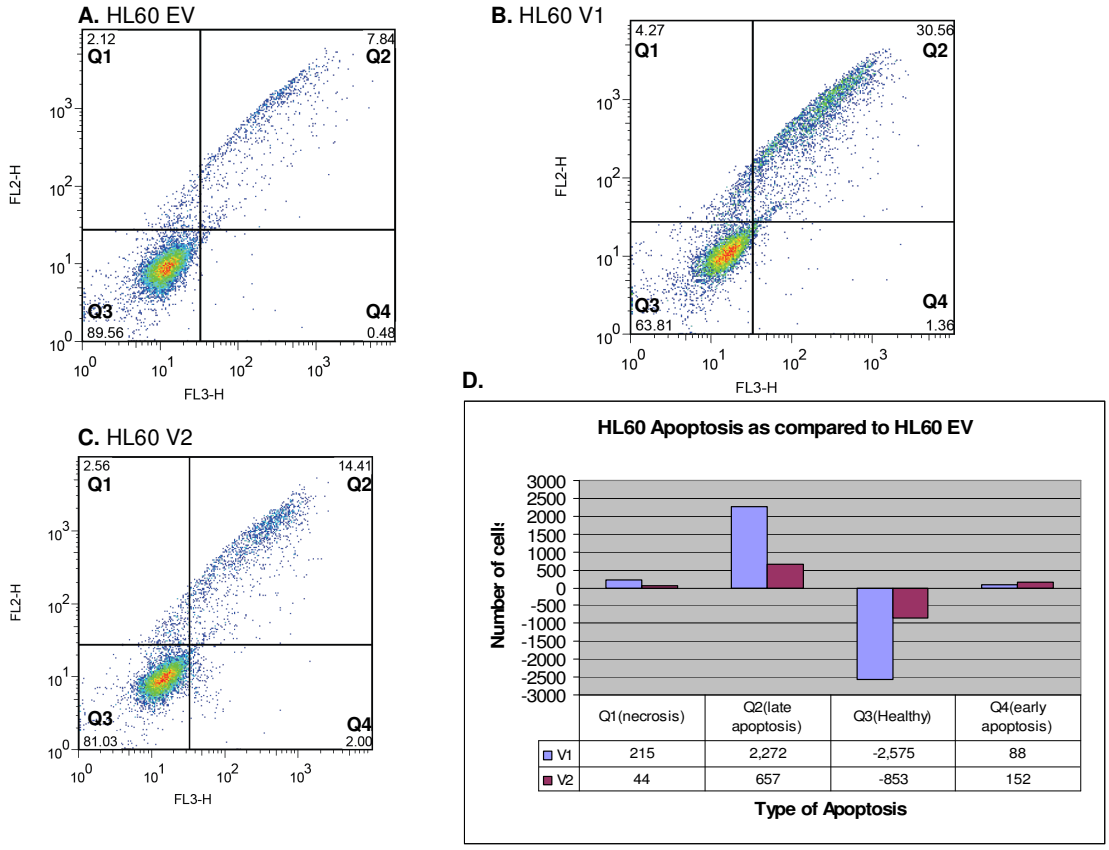

Fig. 15. Scatterplots of annexin V and 7-AAD for FACS analysis of HL60 cells A. Scatterplot for HL60 empty vector control. B. Scatterplot for HL60 transfected with KCNRG V1. C. Scatterplot for HL60 transfected with KCNRG V2. D. Summary of quadrant totals from scatterplots for HL60 EV, V1, V2.

Cell imaging studies indicated a change of morphology in KCNRG overexpressing cells and generally confirmed FACS findings (Fig.16). The first frames in each set show cells stained with Dioc 18 (red), indicating the membranes of the cells. The second frame in each set show the DAPI (blue) stain, and allows the observation of the nucleus. The third frame in each set shows the rhodamine phalloidin (green) where the actin content of the cell can be observed. The fourth frame in each set is the overlay of all three previous frames, and is a more comprehensive picture of the cells. As can be observed, some cell lines exhibit more dramatic changes than others, most particularly, RPMI-8226 clone

S1B9, isolated from the population of RPMI-8226 stably transfected with KCNRG V1, shows several giant cells with multiple nuclei (Fig. 17 E-H). This phenomenon was also observed in other RPMI-8226 V1 clones, and to a lesser extent, with RPMI-8226 V2 clones (Fig. 17 I-T).

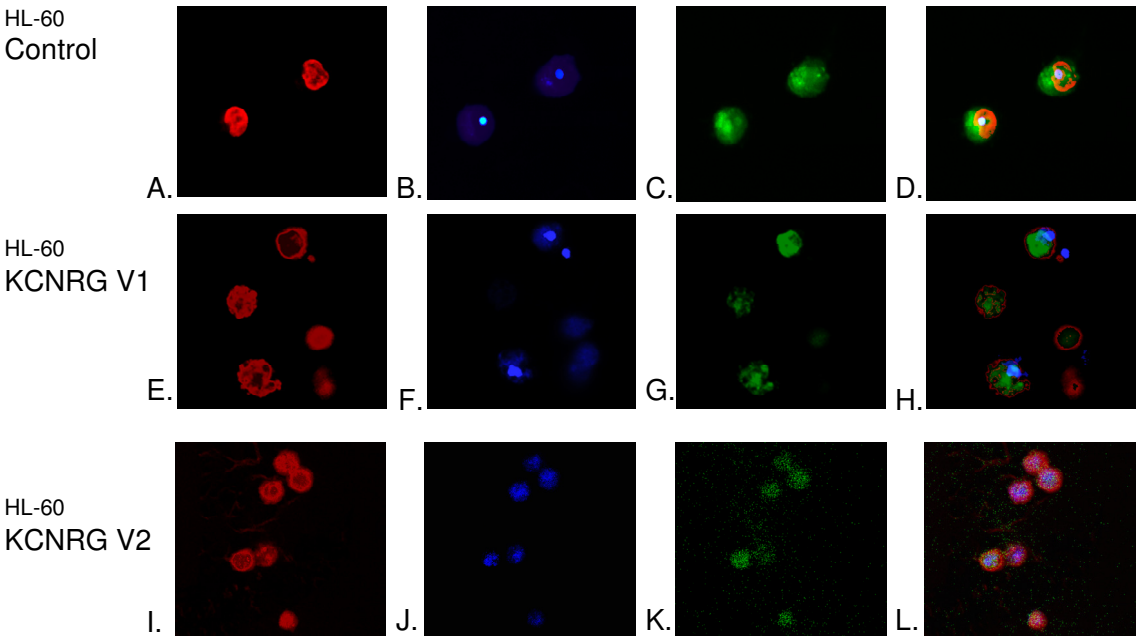

Fig. 16. A-D. HL60 vector control cells stained with Dioc18 (red), DAPI (blue), Rhodamine Phalloidin (green), and overlay of all channels. E-H. HL60 cells transfected with KCNRG V1 stained with Dioc18 (red), DAPI (blue), Rhodamine Phalloidin (green), and overlay of all channels. I-L. HL60 cells transfected with KCNRG V2 stained with Dioc18 (red), DAPI (blue), Rhodamine Phalloidin (green), and overlay of all channels.

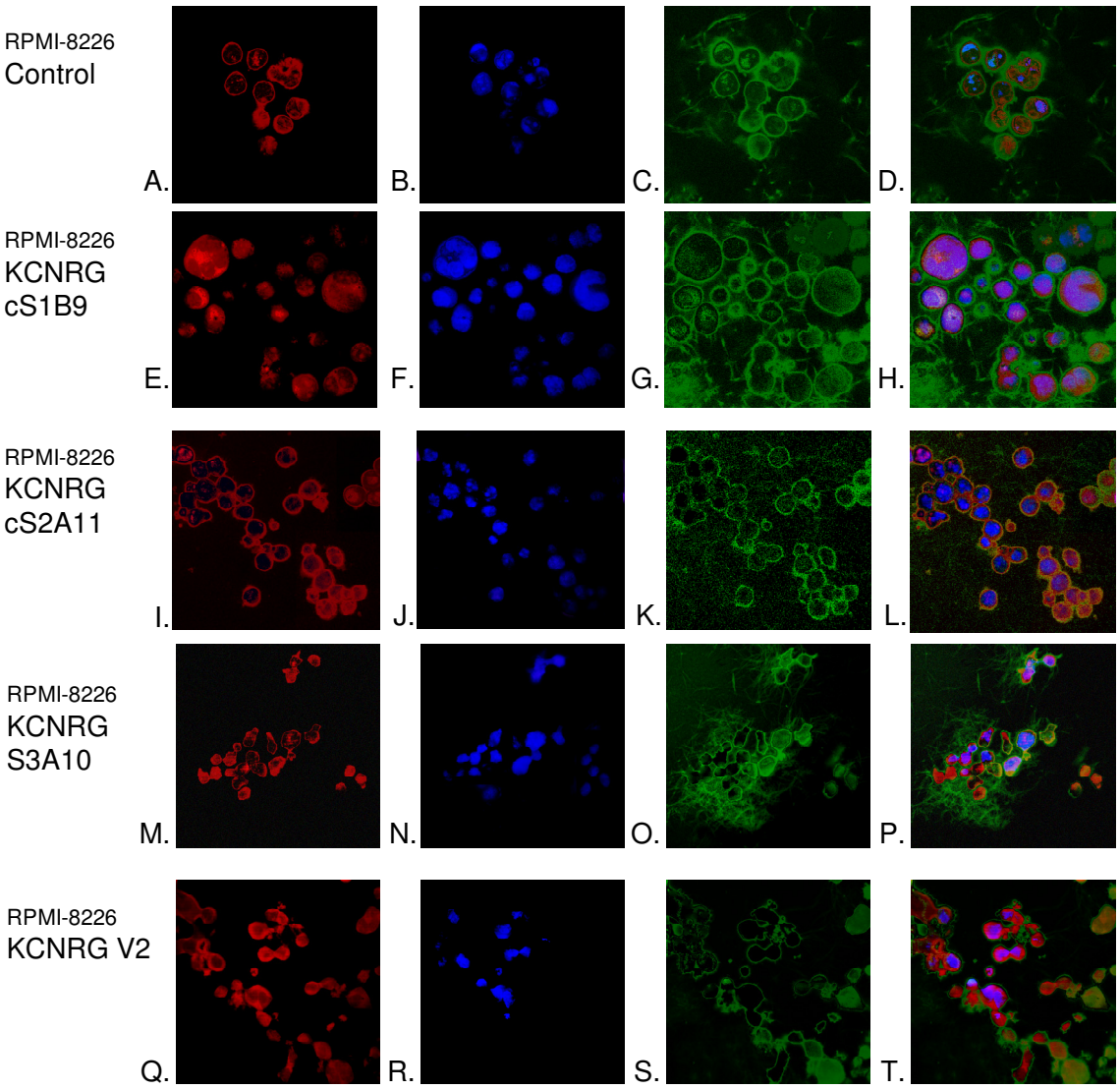

Fig. 17. A-D. RPMI-8226 vector control cells stained with Dioc18 (red), DAPI (blue), Rhodamine Phalloidin (green), and overlay of all channels. E-H. RPMI-8226 V1 - clone S1B9. I-L. RPMI-8226 V1 - clone S2A11 cells. M-P. RPMI-8226 V1 - clone S3A10 cells. Q-T. RPMI-8226 transfected with KCNRG V2 cells.

As can be observed in the LNCaP pictures (Fig.18), cells transfected with either isoform of KCNRG seem to exhibit more extracellular actin content, which may be relevant to their increased contact inhibition. Since LNCaP cells tend to grow in clusters it is difficult to ascertain the presence of multiple nuclei.

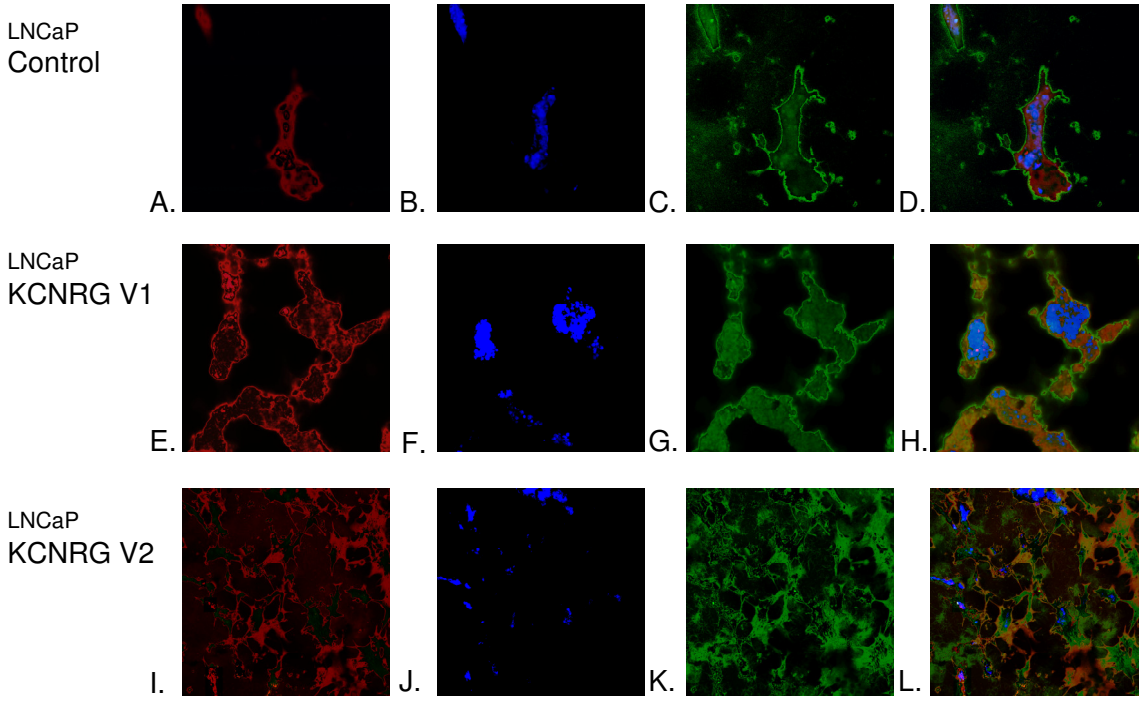

Fig. 18. A-D. LNCaP vector control cells stained with Dioc18 (red), DAPI (blue), Rhodamine Phalloidin (green), and overlay of all channels. E-H. LNCaP cells transfected with KCNRG V1. I-L. LNCaP cells transfected with KCNRG V2.

Pictures of live cells (Fig.19) provide some visual evidence supporting our notions of the behavior of these cells in culture. Giant multi-nucleated cells lose the ability to divide, and over the course of 2-3 days exhibit membrane blebbing and consequently cell death. Since the cells photographed in fig. 19 are not synchronized, these processes can be seen at various stages.

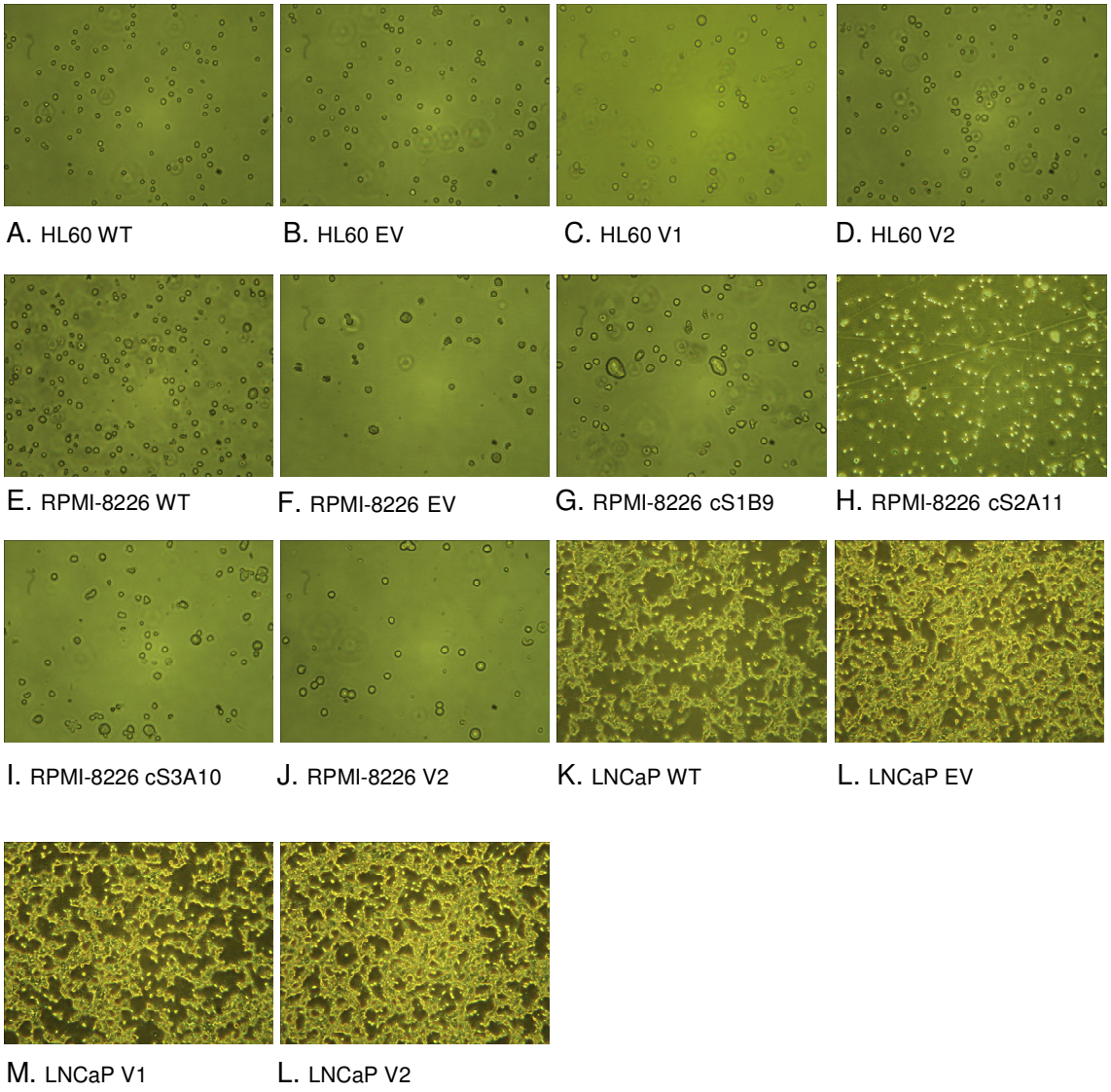

Fig. 19. Live cell pictures for cell lines of HL60, RPMI-8226 and LNCaP.

Expression of KCNRG does not influence invasion of LNCaP cells, but affects migration of the suspension cell lines HL-60 and RPMI-8226

Migration of RPMI-8226 cells stably transfected KCNRG-V2 and KCNRG-V1 as well as vector controls has been studied using 0.2-2.0x10^6 cells/ml and Fetal Bovine

Serum as a chemoattractant. Migration of KCNRG-V1 overexpressing RPMI-8226 cells were not different from that of the control cells, while migration abilities of KCNRG-V2 cells were significantly lower (KCNRG-V2, N=28, 3.46 +/-0.408 vs. Control, N=28, 2.75+/-0.67, $P < 0.004$). Analysis of the transmigration of the vector control and KCNRG overexpressing HL-60 cells through the monolayer of endothelial cell revealed that KCNRG-V1 decreases ability of the cells to penetrate the endothelium (KCNRG-V1, N=5, 17.19 +/- 0.26 vs. Control, N=5, 18.41 +/- 0.59, $P < 0.01$), while overexpression of KCNRG-V2 leads to an non-significant increase in the transmigratory abilities of this cell line. Study of the adherent LNCaP cells revealed that overexpression of the KCNRG isoforms does not influence their ability to cross basement membrane.

Study of anoikis in LNCaP cells showed that both KCNRG overexpressing and vector control cells die upon detachment. Thus there was no influence of KCNRG on anoikis in these cells. An interesting phenomenon that supports observations during routine cell culturing was seen upon imaging of the control plates. Although transfection with either isoform of KCNRG does not change the anoikis behavior of LNCaP cells, cells that are transfected with KCNRG V1 are more prone to contact inhibition, either via other cells, or proximity to the culture vessel walls. This can be observed in the pictures of the control plates for the anoikis assay, where Calcein AM (green) is used to stain live cells and EthD-1 (red) is used to stain cells that have died via anoikis (Fig. 20). All images were taken at the same plate coordinates.

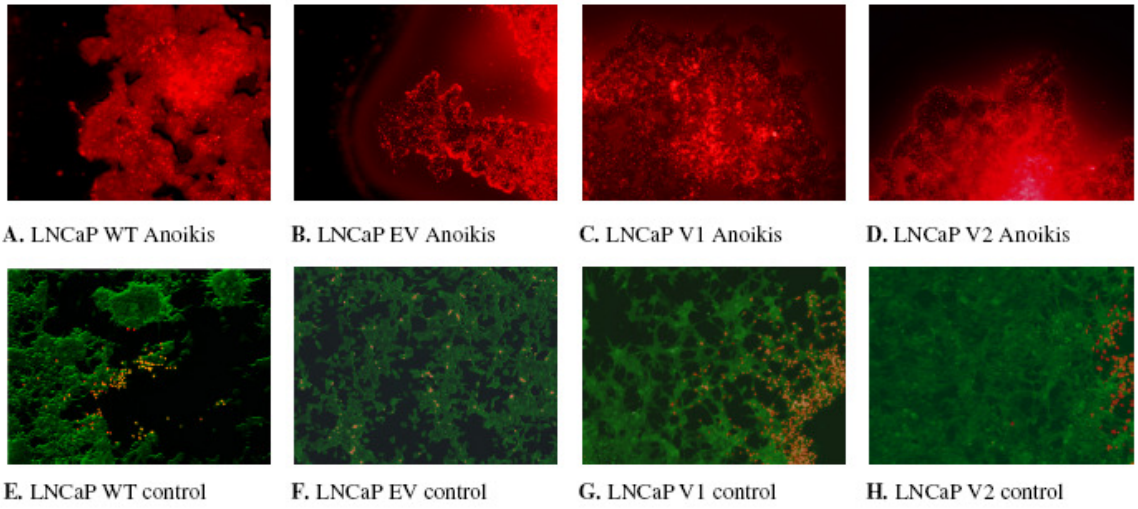

Fig. 20. LNcaP cell line anoikis assay. A-D. Anoikis test plate stained with EthD-1 and Calcein AM. E-H. Control plate stained with EthD-1 and Calcein AM.

Proteome changes associated with KCNRG overexpression

To evaluate differences in intracellular molecular networks associated with overexpression of KCNRG, RPA profiling was attempted to assess the changes in the broad spectrum of the cellular signaling events, with emphasis on the phosphorylation and proteolytic events associated with proliferation and apoptosis. In all three cell lines an overexpression of either isoform of KCNRG was associated with decreased activation of mTOR by phosphorylation of Ser 2481 and 2448 and decreased phosphorylation of Tyr 1175 in VEGFR2. In RPMI-8226, overexpression of KCNRG isoforms lead to the coordinated increase of cleavage events in caspases 3,6,7,9 and the caspase target protein PARP. In LNCaP cells, overexpression of KCNRG resulted in a paradoxical profound increase in ERK signaling as revealed by the phosphorylation of Thr 202 and Tyr 204. (See appendix 9 for complete data protein data)

Microarray analysis of KCNRG V1

Analysis of the gene expression profiles was performed using pathway specific single channel microarrays. The first pathway, Oligo GEArray Human Hematopoietic Stem Cells and Hematopoiesis Microarray, consisted of 128 probes; the second pathway, Oligo GEArray ® Human Cancer Microarray, consisted of 480 probes. Comparisons were performed between cells transfected with KCNRG V1 and wild-type cells of the same lineage. The Superarray software analysis platform offers three standard methods of normalization of arrays, “to the mean”, “to the median” and “to the values for the set of the selected genes”. Traditionally, housekeeping genes have been employed as endogenous reference (“selected genes”) genes for normalization in gene expression studies.

Unfortunately, for most of the housekeeping genes the variability in expression is significant between different cell lines, despite the equalization of quantities of input RNA (Aerts JL et al. 2004). The importance of this phenomenon is most prominent in case of studies of cancer cells and their phenotypes, as profound changes occur in even the most basic metabolism of the cell as it becomes malignant (Gillies RJ et al., 2008). For example, GAPDH and ACTB, genes most frequently used for normalization, are heavily regulated during carcinogenesis and tumor progression (Aerts J.L. et al., 2004; Gao Q. et al., 2008; Lyng MB et al., 2008). These findings are not surprising as recent evidence indicates new and intriguing roles for GAPDH in fundamental mammalian cell processes, including DNA repair, translational control of gene expression, DNA replication and endocytosis (Sirover et al. 2006).

Since the utilization of single housekeeping gene cannot assure an unbiased result, finding a good set of reference genes is a non-trivial problem requiring case-by-case study. Here we tested housekeeping genes against the overall intensity of the array, and a subset indicative of each array was selected for normalization. Figure 21 shows the topographic map of the housekeeping gene expression across all arrays.

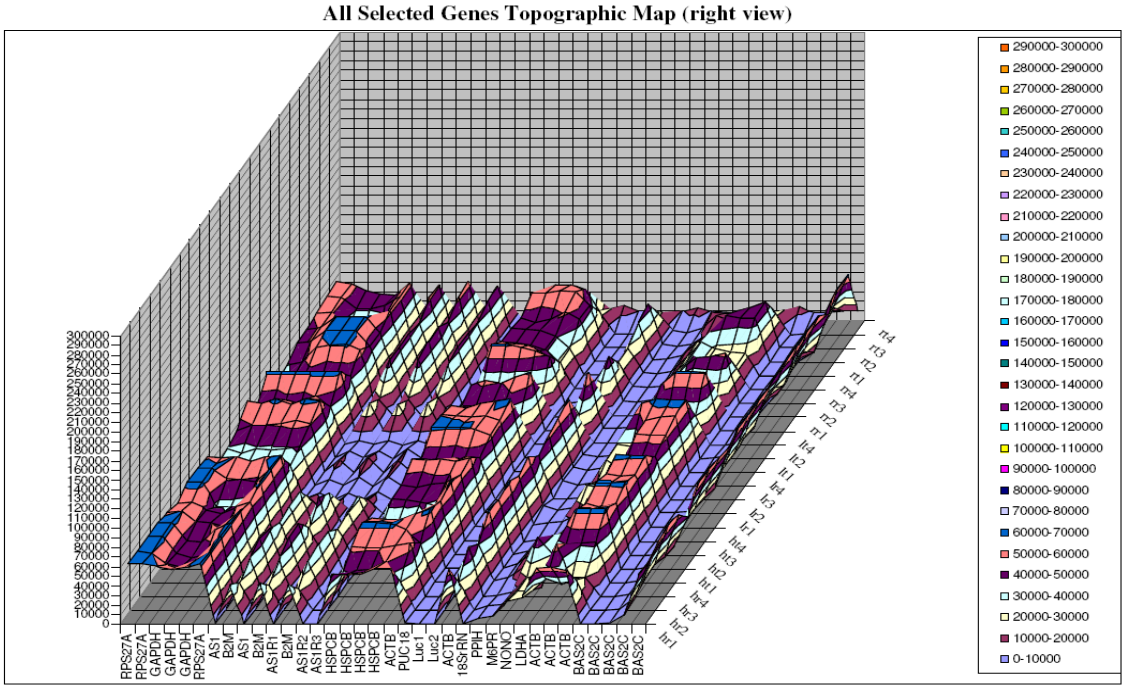

Fig. 21. Topographic map of housekeeping genes and their behavior in all arrays. RR = RPMI Control, HR = HL60 Control, LR = LNCaP control, RT = RPMI transfected, HT = Hl60 transfected, LT = LNCaP transfected.

In addition to their expression pattern, housekeeping genes were selected based on their ability to correctly reflect the overall intensity of their representative arrays. Background correction was performed by the SuperArray proprietary software, and

normalized versus non-normalized values for blank controls, overall array intensities and selected housekeeping genes were determined (Fig.22).

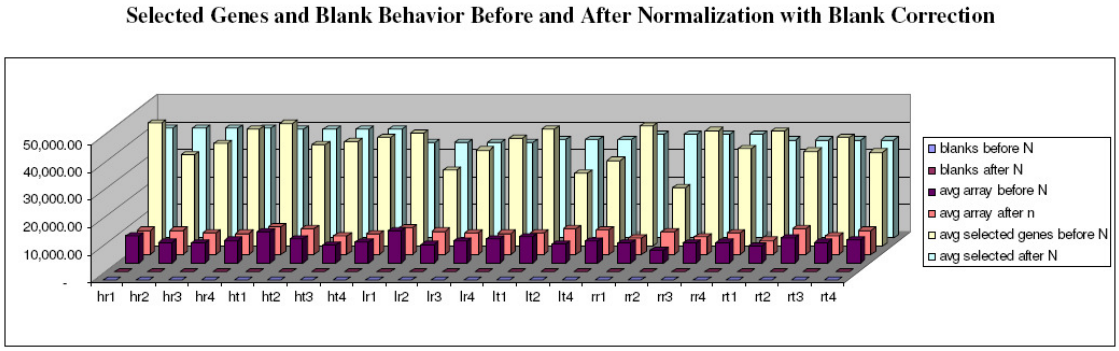

Fig. 22. Effects of normalization on selected genes (housekeeping genes), blanks and array average.

Following background correction and normalization, spreadsheets displaying fold differences between control cases and test cases were generated (for complete lists of differentially expressed genes present on each array please see Appendix r). Initially, statistical analysis was performed by the Significance Analysis of Microarrays (SAM), a popular method for detecting significantly expressed genes and controlling the false discovery rate (FDR) (Rodninger OK et al., 2005; Tusher et al., 2001). False discovery rate (FDR) is defined as the expected percentage of false positives among all the claimed positives. Calculations were performed with the much appreciated help of G. Manyam (PhD student, MMB, GMU). However, recent opinion on statistical testing for small batch microarrays seems to be moving away from permutation based approaches such as SAM (Tan YD et al. 2008). The consensus seems to be that these permutation based approaches often create data sets with very heavy tails, and negatively biased data. Hence

a non-parametric Mann-Whitney test was used for the statistical validation of the microarray data.

In addition to spot finding and numerical value assignation, the SuperArray software sorts each spot as "absent" or "present" based on the intensity of its immediate background environment. This proved problematic in some cases due to over saturation in adjacent spots, as the parameters for this function are non-negotiable; consequently we believe that some spots were mislabeled as absent. The resultant genes from both arrays were compiled and a list with the most significant p-values was created (See Fig 23).

Cell line & change	RR negative change	RR positive change	HR negative change	HR positive change	LR negative change	LR positive change
Gene	BTK	ABL1	DHCR7	COX7A2	CDKN1A	ABL1
	GAS6	ASNS	GCN5L2	ERBB3	KPNA2	RHOB
	SFN	BAX	KIT	FGR	NQO1	JUN
	TIMP1	BRCA1	PKMYT1	GSK3A	PIM1	
	VDAC1	CCND1	RET	HSPA5	RELB	
	LDHA	CDK5	TK1	HYOU1	SARS	
		CEBPG		ILK	SLC20A1	
		CTSD		PDPK1	THBS1	
		E2F1		PPARG	TK1	
		E2F3		PRDX4	TLE1	
		ERCC3		STAT2	WEE1	
		ETV6		TCF7L2	M6PR	
		FRAP1		TIMP1		
		GRB2		TNF		
		HSPA5		TNFRSF1A		
		IGF2R				
		LAMP2				
		LCK				
		LCN2				
		LTF				
		SMAD1				
		MARS				
		MDM4				
		MICB				
		MME				
		MYB				
		MYL9				
		NINJ1				
		NR1D1				
		PIK3CG				
		PRKCBP1				
		PRNP				
		PRSS15				
		RAB5A				
		RRM1				
		SARS				
		TNFSF7				
		UBE2L6				
		WNT1				

Fig. 23. List of Mann-Whitney significant genes compiled from microarray experiments.

Although all three cell lines responded similarly to transfection with KCNRG isoforms, i.e., a general trend of increased apoptosis and decreased proliferation, very few genes seem to be up- or down-regulated in the same direction in all three cell lines, possibly indicating very different expression pathway involved in the proliferation and apoptosis in each type of cell. HSPA5, one of the few genes that is up-regulated in both HL60 and RPMI cells, is a member of the heat-shock protein-70 (HSP70) family. It is thought to aid in protein assembly in the endoplasmic reticulum and may play a role in protein transport in the cell (GeneCard). Conversely, TK1, a cytosolic thymidine kinase known to have a high activity in rapidly proliferating cells and very low activity in resting cells, was down-regulated in both HL60 and LNCaP cells.

The BAX gene behaves differently in HL60 cells as compared to LNCaP and RPMI-8226 cells. BAX functions as a pro-apoptotic gene by forming a heterodimer with BCL2 and is thought to interact with mitochondrial voltage-dependent anion channels (VDAC), causing a loss in membrane potential and thereby releasing Cytochrome C. BAX is thought to be regulated by the p53 tumor suppressor protein (Fig. 24).

Surprisingly, HL60 cells show a down-regulation of BAX, whereas RPMI-8226 and LNCaP cells show a marked up-regulation of BAX in keeping with the more classical model of BAX-mediated apotosis. None of the cell lines show any change in BCL2 levels, although LNCaP cells seem to have a drastically lower amount of native BCL2 expression.

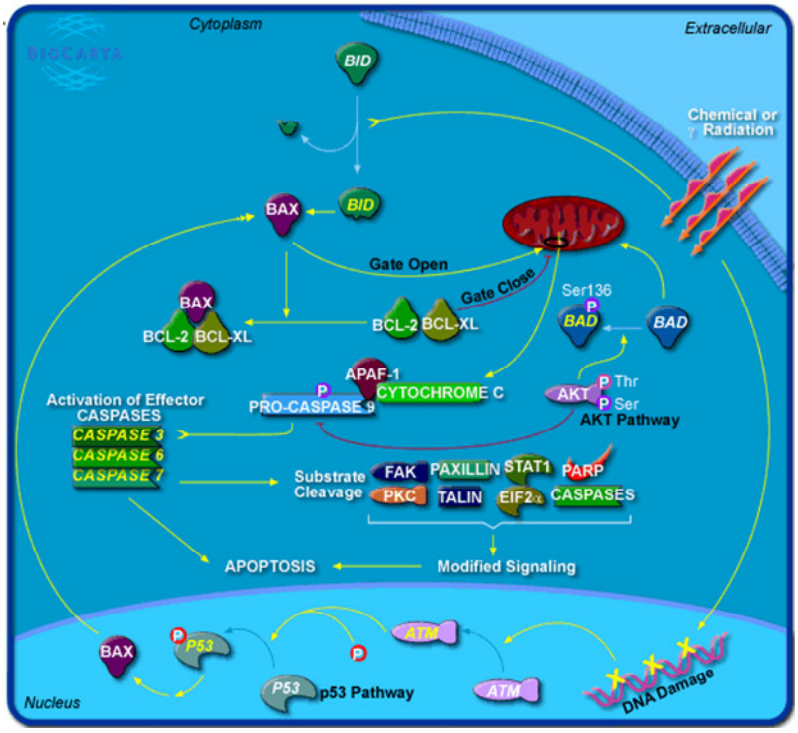

Fig.24 Classical p53 mediated cellular activation of the caspase cascade resulting apoptosis (Biocarta).

According to both to microarray and RT-PCR data, native BAX levels in wild-type HL60 seem to be very high as compared to other cell lines; this is in accordance with similar observation made by other researchers (Campos L et al. 1999). In several studies a decrease in BAX levels have been observed despite increased levels of apoptosis, prompting some researchers to suggest and alternate "death" pathway involving TNF-a, as responsible for this behavior (Legdeur MC et al. 1996, Mengubas K et al. 1996, Ma E et al. 2008). Interestingly, the microarray data for HL60 shows a dramatic and significant increase for both TNF and TNFRSF1A (38.62 and 2.26 fold respectively) (please see Appendix 10 for full microarray).

Independent and array based RT-PCR profiling of genes from microarray

Sixteen genes with the highest degree of commonality were selected from the microarray short list to be verified by RT-PCR. The results of the RT-PCR were compared to those of the microarrays (Fig. 25).

INDIVIDUAL RT-PCR DATA COMPILED AND COMPARED TO MICROARRAYS

(All Fold Differences Compared to transfected with empty plasmid)

	HV1	HV2	Microarray	S1B9	S2A11	S3A10	RV2	Microarray	LV1	LV2	Microarray
etv6	1.209994	1.071773	up	1.380317	2.918041	2.72735	1.148035	up			
notch1	1.866066	1.148698	up	1.394744	1.018068	1.211393	1.583738	down?	1.241141	1.103179	down
cdkn1b				1.381913	1.142082	1.731073	3.048994	up			
TK1	1.652901	5.278032	down	1.915207	2.305373	1.358957	4.062872	no change	5.080604	3.488242	down
TNFRSF10A	2.106722	3.668016	up - not sig by MW								
P53	5.856343	8.282119	no change	1.70527	1.101905	3.305801	1.935223	no change	1.29684	1.481953	up - not sig by MW
BAX 430	1.168777	1.128964	?	8.876556	1.909683	9.031715	13619		7.451341	2.370186	?
BAX 225	4.756828	1.624505	down	39.39662	5.010658	1.624505	1888.904	up	2.732081	1.431473	up
KITLG	1.596597	2.07053	down	3821.703	8.139838	5.755734	955.4258	up			
TNF	4.756828	28.34456	up								
TNFRSF1A	1.128964	5.37029	up								
STAT2	32	9.513657	up	53.81737	14.92853	368.367	50.21338	up			
JUN	2.419988	2.877867	down	1.274561	1.771535	2.505329	1.652901	up	3.452162	1.278986	up
CDKN1									1.812943	1.672106	down
NQO1				23.84861	3.428316	2.605692	1.93858	up	2.378414	2.046748	down
ABL1				1.061301	5.61778	2.599679	1.065601	up	3.976962	1.447269	up

Fig. 25. RT-PCR validated genes selected from microarray short list

In addition to validating the microarray data the apparent discrepancies between the microarray data and RT-PCR data needed to be analyzed further. The oligonucleotide sequences used by SuperArray are proprietary, hence the exact sequences are not available for this work and they could not be matched to a particular area of the corresponding transcript. The BAX oligonucleotide used as a probe for the Superarray was designed by the manufacturer to identify only two out of five BAX isoforms. To see whether this could account for part of the discrepancy two separate BAX primers were used: BAX 430 and BAX 225, designed to amplify BAX transcript variant beta and

alpha, respectively (see Appendix 11). The two BAX variants were found to behave in a very different fashion in HL60 cells transfected with KCNRG V1 (Fig 26).

INDIVIDUAL RT-PCR DATA COMPILED AND COMPARED TO MICROARRAYS

(All Fold Differences Compared to transfected with empty plasmid)

	HV1	HV2	Microarray	S1B9	S2A11	S3A10	RV2	Microarray	LV1	LV2	Microarray
etv6	1.209994	1.071773	up	1.380317	2.918041	2.72735	1.148035	up			
notch1	1.866066	1.148698	up	1.394744	1.018068	1.211393	1.583738	down?	1.241141	1.103179	down
cdkn1b				1.381913	1.142082	1.731073	3.048994	up			
TK1	[illegible]	[illegible]	[illegible]	[illegible]	[illegible]	[illegible]	4.062872	no change	5.080604	3.488242	down
TNFRSF10A	[illegible]										
P53	[illegible]						1.935223	no change	1.29684	1.481953	up - not sig by MW
BAX 430	[illegible]						13619		7.451341	2.370186	?
BAX 225	[illegible]						1888.904	up	2.732081	1.431473	up
KITLG	1.596597	2.07053	down	3821.703	8.139838	5.755734	955.4258	up			
TNF	4.756828	28.34456	up								
TNFRSF1A	1.128964	5.37029	up								
STAT2	32	9.513657	up	53.81737	14.92853	368.367	50.21338	up			
JUN	2.419988	2.877867	down	1.274561	1.771535	2.505329	1.652901	up	3.452162	1.278986	up
CDKN1									1.812943	1.672106	down
NQO1				23.84861	3.428316	2.605692	1.93858	up	2.378414	2.046748	down
ABL1				1.061301	5.61778	2.599679	1.065601	up	3.976962	1.447269	up

1.168777	1.128964	?
4.756828	1.624505	down

Fig. 26. RT-PCR validated genes selected from microarray short list, zoom on HV1 and BAX primers for BAX isoforms alpha and beta.

This behavior suggests the possibility that some of these unresolved disagreements between RT-PCR data and microarray data may be due to microarrays and RT-PCR profiling different isoforms of the mRNA for a particular gene.

To further confirm the microarray data, a set of SuperArray RT-PCR arrays were performed. The Human Apoptosis pathway RT-PCR array was chosen based on the number of overlapping genes found between the RT-PCR and microarray platforms. Once again the manufacturer did not disclose the primers present on the RT-PCR array, however, the manufacturer did disclose that these primers bore no similarities to the sequences found on the microarray and were not guaranteed to isolate the same isoforms of the genes. Keeping this in mind, the 18 genes in common to both platforms, and 2/3 of these agreed in the direction of change (For full results see Appendix 11). In the case of

HL60 cells, a large percentage of genes were in agreement according to the directionality of gene expression changes (Table 3).

Table 3. SuperArray RT-PCR and Oligo Array results compiled.

RT-PCR arrays compared to Microarrays			
Genes	**RT-PCR - HV1**	**RT-PCR - HV2**	**HL60 Microarray**
ABL1	-6.19	-2.30	-1.17
AKT1	1.08	-1.41	-1.34
BAX	-1.96	-1.74	-2.02
BCL2	-2.41	-3.03	-1.32
BRAF	-1.93	-1.62	-11.06
FAS	1.54	-1.15	-1.01
IGF1R	-3.89	-2.14	-1.01
TNF	-25.99	-10.56	38.62
TNFRSF10A	1.67	1.52	16.51
TNFRSF10B	-6.23	-2.46	1.61
TNFRSF1A	-3.66	-3.73	2.26
TP53	1.06	-1.32	-1.01
TP53BP2	-2.69	-1.32	1.69
TP73	2.36	-1.32	-1.01
TRADD	-1.72	-1.62	2.29
B2M	-2.77	-1.87	-1.03
GAPDH	-3.63	-1.32	-1.08
ACTB	1.00	1.00	1.28

Interestingly, there are small but significant changes in expression between HL60 cells transfected with KCNRG V1 versus KCNRG V2. In a significant number of cases, the effects of KCNRG V1 on gene expression profiles were more dramatic than the effects of KCNRG V2.

Real-time PCR profiling of KCNRG mRNAs in human lymphoma samples

Relative levels of KCNRG isoforms were quantified in human lymphoma samples arrayed on TissueScan qPCR Panels (Fig. 27) As expression of the major isoform of KCNRG mRNA encoding KCNRG V1 was approximately 300 times higher than that of the minor mRNA isoform (KCNRG V2), estimates of the mRNA levels obtained using primer pair KCNRG V1/V2 can be approximated to the expression of KCNRG-V1 encoding isoform.

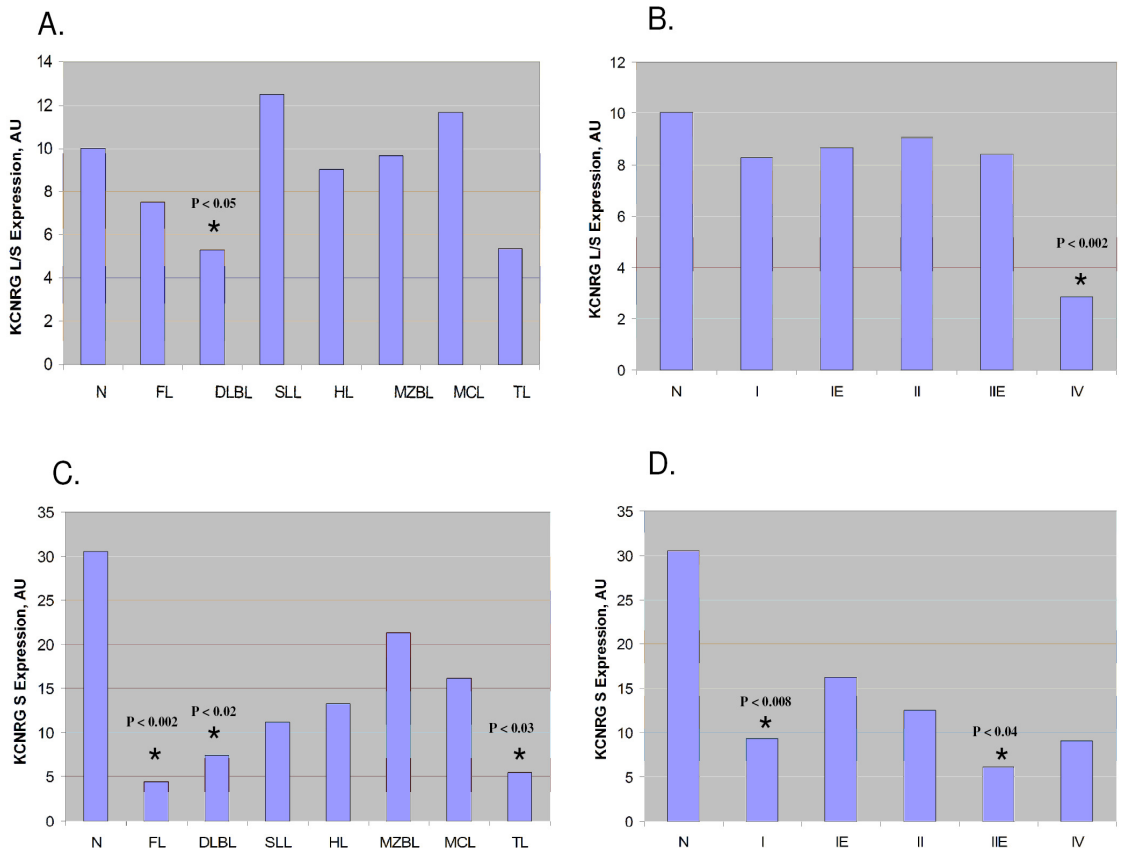

Fig. 27. Real-time PCR profiling of KCNRG mRNAs in human lymphoma samples. N: Normal PBL. FL: follicular lymphoma. DLBL: diffuse large B-cell lymphoma. SLL: small lymphocytic lymphoma. HL: Hodgkin lymphoma. MZBL: marginal zone B-cell lymphoma. MCL: mantle cell lymphoma. TL: T-cell lymphoma. A and B: profiling using primer pair KCNRG-V1/V2 that amplifies both isoforms of KCNRG mRNA. C and D: profliing using primer pair KCNRG V2 that amplifies only mRNA isoform KCNRG V2. Statistically significant changes denoted by star (*) symbol.

Significant down regulation of KCNRG-V1 mRNA ($P < 0.05$) was revealed in the most advanced lymphomas of the stage IV ($N = 4$) as compared to normal PBL samples ($N=6$). When the same set of samples were stratified according to the type of lymphoma, a significant down-regulation of KCNRG V1 was registered only in DLBL ($N=11$) as compared to normal PBL samples ($P < 0.002$).

Interestingly, only one case of DLBL was classified as a stage IV disease, while 6 of these cases were stage I and 4 were staged as IE or IIE. A trend towards down-regulation of the KCNRG V2 encoding mRNA was seen in all lymphoma types profiled, with statistically significant differences seen in FL ($P < 0.002$), DLBL ($P < 0.02$) and T-cell lymphoma ($P < 0.03$) groups. A significant decrease in the level of mRNA for KCNRG V2 was seen in stage I ($P < 0.008$) and IIE ($P < 0.04$) groups.

Chapter 4: Conclusion

Previous studies of the tumor suppressor effects conveyed by the presence of intact chromosome 13 region q14.3 revealed a number of potential candidate genes whose expression is lost in a substantial percentage of CLL cases. Despite significant effort undertaken by multiple laboratories a screening of the mutations in the studied candidate genes in primary tumor cells has not yet been successful. These findings prompted some investigators to propose that a major mode of inactivation of 13q14 tumor suppressor gene(s) is by the deletion of one copy of the gene causing decrease in the production of gene' mRNA and partial loss of its function. This mechanism of gene inactivation is known as haploinsufficiency.

Candidate TSG KCNRG (potassium channel regulating gene) is located very close to the 10-kb region previously described as minimally deleted in CLL and within the larger region deleted in the majority of CLL cases with 13q114.3 aberrations.

Functional analysis of KCNRG pointed at the possibility that it might exert a tumor suppressor effect relevant to CLL and MM. Here KCNRG has been shown to possesses anti-proliferative activity when overexpressed in RPMI-8226, HL-60 and to a lesser extent, LNCaP cells. Moreover, overexpression of KCNRG stimulates apoptosis in these cells and leads to dramatic changes in their size and shape. A substantial proportion

of both RPMI-8226 and HL-60 cells over expressing KCNRG V1 isoform were arrested in G2 phase, possibly indicative of G2/M checkpoint activation.

Additionally, the migration of KCNRG overexpressing cells has also significantly decreased. Microarray and RT-PCR data, taken together with the proliferation and caspase assays, suggests that these events may be occurring via different mechanisms for each cell line, possibly indicating a broader, rather than a pathway specific, role for KCNRG. Finally, KCNRG overexpression increased a propensity of the cells to undergo apoptosis after stress, in particular, affecting its ability to recover after storage in a frozen state.

One way to confirm the relevance of these characteristics of human KCNRG in the suppression of CLL and MM *in vivo* is to find its point mutations in primary tumor cells. Attempts to do so by this lab as well as others have been unsuccessful. However, a number of circumstantial evidence points at KCNRG as an important player in hematological malignancies. First, real-time PCR profiling of KCNRG mRNAs revealed that levels of the major isoform of KCNRG mRNA in DLBL lymphomas are lower compared to normal PBL samples, while levels of its minor mRNA decreased across the broad range of the lymphoma types.

Levels of KCNRG mRNA were also decreased in lymphomas of stage IV. Second, the multiple myeloma cell line RPMI-8226 contains a delT mutation in the core promoter initiator element that might influence levels of KCNRG expression in this model line. Third, proteomics endpoint analysis by RPA indicated an involvement of KCNRG in the suppression of mTOR and VEGFR pathways as well as in caspase

activation in a broad sense. In light of these observations, the identification of the particular mode of KCNRG inactivation in tumor samples becomes a priority.

Despite a number of studies that delineated 13q14 deletions in CLL and MM and quantified relative expression levels of some candidate genes residing in this area, the critical insights related to the role of 13q14 in human malignancies are still to be gained. Here in this work is described a novel, highly informative polymorphic repeat, located at the position –1006 relative to the major start of KCNRG mRNAs and within the 3' untranslated area of RFP2. As the structure of this repeat allows its relatively simple visualization in agarose gels following conventional PCR, it might become a valuable marker for the hemizygous deletion of KCNRG in primary tumor samples.

Interestingly, KCNRG belongs to a rather large subfamily of poorly characterized human genes. Some of these genes function in tumorigenesis. As cellular functions for the majority of the KCNRG-like proteins have never been studied, it is important to determine their relevance to tumorigenesis and lymphomagenesis in humans.

In conclusion, a functional study of the tumor suppressor gene candidate KCNRG was conducted and its growth suppressive and pro-apoptotic effects in the cellular models relevant to CLL and MM was demonstrated. This study demonstrates that the loss of KCNRG might be relevant to the progression of these hematological malignancies at least in a subset of the patients with these disorders.

APPENDIX 1
KCNRG ISOFORM S: BLASTP SEARCH

ACCESSION	Organism	a.a.	Blastp Match	% Match	Chr.	Region	Sc.Match	Genes R.	E value
CAD38633	H. sapiens	216	gi|21733273|emb|CAD38633.1| hypothetical protein [Homo sapiens] Length = 216 Score = 353 bits (907), Expect = 1e-96 Identities = 179/193 (92%), Positives = 179/193 (92%) Query: 1 MSSQELVTLNVGGKIFTTRFSTIKQFPASRLARMLDGRDQEFKMVGGQIFVDRDGDLFSF 60 MSSQELVTLNVGGKIFTTRFSTIKQFPASRLARMLDGRDQEFKMVGGQIFVDRDGDLFSF Sbjct: 4 MSSQELVTLNVGGKIFTTRFSTIKQFPASRLARMLDGRDQEFKMVGGQIFVDRDGDLFSF 63 Query: 61 ILDFLRTHQLLLPTEFSDYLRLQREALFYELRSLVDLLNPYLLQPRPALVEVHFLSRNTQ 120 ILDFLRTHQLLLPTEFSDYLRLQREALFYELRSLVDLLNPYLLQPRPALVEVHFLSRNTQ Sbjct: 64 ILDFLRTHQLLLPTEFSDYLRLQREALFYELRSLVDLLNPYLLQPRPALVEVHFLSRNTQ 123 Query: 121 AFFRVFGSCSKTIEMLTGRITVFTEQPSAPTWNGNFFXXXXXXXXXXXXXSYHDLVFQC 180 AFFRVFGSCSKTIEMLTGRITVFTEQPSAPTWNGNFF SYHDLVFQC Sbjct: 124 AFFRVFGSCSKTIEMLTGRITVFTEQPSAPTWNGNFFPPQMTLLPLPPQRPSYHDLVFQC 183 Query: 181 GSDSTTDNQTGVR 193 GSDSTTDNQTGVR Sbjct: 184 GSDSTTDNQTGVR 196	92	Chr 13	Chr 13q14.2 49,487K-49,490K bp	all	3 genes btw -RFP2 -KCNRG	1.00E-96
NP 699162	H. sapiens	237	>gi|40255153|ref|NP_699162.2| potassium channel tetramerisation domain containing 6 [Homo sapiens] gi|22760703|dbj|BAC11301.1| unnamed protein product [Homo sapiens] Length = 237 Score = 88.6 bits (218), Expect = 1e-16 Identities = 53/152 (34%), Positives = 82/152 (53%), Gaps = 6/152 (3%) Query: 7 VTLNVGGKIFTTRFSTIKQFPASRLARMLDGRDQEFKMVGGQIFVDRDGDLFSFILDFLR 66 VTLNVGG ++TI +I+ ++P S L M G + G E++KDG LF ++L+FLR Sbjct: 14 VTLNVGGHLYTTSLTTLTRYPDSMLGAMFGGDFPTTRDPQGNYFINRDGPLFRYVLNFLR 73 Query: 67 THQLLLPTEFSDYLRLQREALFYELRSLVDLLN-PYLLQPRPALVEVHFLSRNTQAFFRV 125 T +L LP +F ++ L++EA FY++ L+ LN P L P EV LS R Sbjct: 74 TSELTLPLDFKEFDLLRKEADFYQIEPLIQCLNDPKPLYPMDTFEEVVELSST-----RK 128 Query: 126 FGSCSKTIEMLTGRITVFTEQPSAPTWNGNFF 157 S + ++ ++T+ T+ S N+F Sbjct: 129 LSKYSNPVAVIITQLTITTKVHSLLEGISNYF 160	53	Chr 3, Chr 11	Chr 3p14.3 58,458K-58,463K bp Chr 11q23.3 118,379,811-118,380,181 bp	con.	Chr 3 3 genes KCTD6 Chr 11 2 genes DLNB14	1.00E-16
XP 374915	H. sapiens	381	>gi|51468856|ref|XP_374915.2| PREDICTED: similar to KCTD11 protein [Homo sapiens] Length = 381 Score = 84.0 bits (206), Expect = 3e-15 Identities = 41/92 (44%), Positives = 60/92 (65%) Query: 7 VTLNVGGKIFTTRFSTIKQFPASRLARMLDGRDQEFKMVGGQIFVDRDGDLFSFILDFLR 66 +TLNVGGK++TT +T+ FP S L M G+ + G F+DRDG +F +IL+FLR Sbjct: 126 ITLNVGGKLYTTSLATLTSFPDSMLGAMFSGKMPTKRDSQGNCFIDRDGKVFRYILNFLR 185 Query: 67 THQLLLPTEFSDYLRLQREALFYELRSLVDLL 98 T L LP +F + L+REA FY+++ L++ L Sbjct: 186 TSHLDLPEDFQEMGLLRREADFYQVQPLIEAL 217	65	Chr 11	Chr 11q14.1 77560-77564 and 77577-77578	con.	4 genes LOC283219 USP35	3.00E-15
AAQ15187	H. sapiens	325	>gi|33341268|gb|AAQ15187.1| C13orf2 [Homo sapiens] gi|19923973|ref|NP_612453.1| potassium channel tetramerisation domain containing 12 [Homo sapiens] gi|15489330|gb|AAH13764.1| Potassium channel tetramerisation domain containing 12 [Homo sapiens] gi|50401124|sp|Q96CX2|KD12_HUMAN Potassium channel tetramerisation domain containing protein 12 (Pfetin) (Predominantly fetal expressed T1 domain) Length = 325 Score = 75.1 bits (183), Expect = 1e-12 Identities = 42/93 (45%), Positives = 59/93 (63%), Gaps = 2/93 (2%) Query: 5 ELVTLNVGGKIFTTRFSTIKQFPASRLARMLDGRDQE--FKMVGGQIFVDRDGDLFSFIL 62 ++V LNVGG+++ TR T+ P S L RM + + + G+ F+DRDG LF +IL Sbjct: 34 DIVELNVGGQVYVTRRCTVVSVPDSLLWRMFTQQQPQELARDSKGRFFLDRDGFLFRYIL 93 Query: 63 DFLRTHQLLLPTEFSDYLRLQREALFYELRSLV 95 D+LR QL+LP F + RLQREA ++EL LV Sbjct: 94 DYLRDLQLVLPDYFPERSRLQREAEYFELPELV 126	63	Chr 13	Chr 13q22.3 76,357,185-76,358,407 bp	con.	2 genes KCTD12	1.00E-12
XP_372125	H. sapiens	277	>gi|51467220|ref|XP_372125.2| PREDICTED: similar to potassium channel tetramerisation domain containing 1; chromosome 18 open reading frame 5 [Homo sapiens] Length = 277 Score = 67.4 bits (163), Expect = 3e-10 Identities = 32/90 (35%), Positives = 56/90 (62%), Gaps = 1/90 (1%) Query: 7 VTLNVGGKIFTTRFSTIKQFPASRLARMLDGRDQ-EFKMVGGQIFVDRDGDLFSFILDFL 65 V +VG ++T+ +T+ ++P SR+ R+ DG + + F DRDG +F +IL+FL Sbjct: 32 VHTDVGSHMYTSSLATLTKYPVSRIRRLCDGTEPIVLDSLKQHYFTDRDGQMFRYILNFL 91 Query: 66 RTHQLLLPTEFSDYLRLQREALFYELRSLV 95 RT +LL+ +F DY L EA +++L+ ++ Sbjct: 92 RTSKLLILDDFKDYTLLYEEAKYFQLQPML 121	62	Chr 9, Chr 18	Chr 9q22.1 88,020K-88,070K bp Chr 18q11.2 22,260K-22,360K bp	con.	Chr 9 3 genes LOC389768 Chr 18 5 genes KCTD1	3.00E-10

NP_076419	H. sapiens	225	>gi|13027592|ref|NP_076419.1| potassium channel tetramerisation domain containing 14 [Homo sapiens] gi|12804953|gb|AAH01929.1| Hypothetical protein MGC2376 [Homo sapiens] gi|12654469|gb|AAH01062.1| Hypothetical protein MGC2376 [Homo sapiens] gi|50401147|sp|Q9BQ13|KD14_HUMAN Potassium channel tetramerisation domain containing protein 14 Length = 225 Score = 66.6 bits (161), Expect = 5e-10 Identities = 39/93 (41%), Positives = 54/93 (58%), Gaps = 4/93 (4%) Query: 6 LVTLNVGGKIFTTRFSTIKQFPASRLARMLDGRDQEFKMVGGQIFVDRDGDLFSFILDFL 65 +V LNVGG+ TT T+++FP S+LA M + G+ F+DR F ILD+L Sbjct: 4 VVELNVGGEFHTTTLGTLRKFPGSKLAEMFSSLAKASTDAEGRFFIDRPSTYFRPILDYL 63 Query: 66 RTHQLLLPTEFSDYLRLQREALFYELRSLVDLL 98 RT Q +PT+ + REA FYE++ LV LL Sbjct: 64 RTGQ--VPTQHIP--EVYREAQFYEIKPLVKLL 92	58	Chr 9	Chr 11q14.1 77,403K-77,412K bp	con.	3 genes KCTD14	5.00E-10
NP_055301	H. sapiens	375	>gi|7656859|ref|NP_055301.1| neuronal thread protein AD7c-NTP [Homo sapiens] gi|3002527|gb|AAC08737.1| neuronal thread protein AD7c-NTP [Homo sapiens] Length = 375 Score = 59.3 bits (142), Expect = 8e-08 Identities = 30/35 (85%), Positives = 30/35 (85%) Query: 193 RLVCNGVISAHHNLRLWGSSDSPASASRVAGITGM 227 RL CNG ISAH NLRL GSSDSPASAS VAGITGM Sbjct: 9 RLECNGAISAHRNLRLPGSSDSPASASPVAGITGM 43	85	Chr 1	1p36 23,777,128-23,778,924 bp	end	2 genes AD7C-NTP	8.00E-08
AAD42876	H. sapiens	815	>gi|5360115|gb|AAD42876.1| NY-REN-45 antigen [Homo sapiens] Length = 815 Score = 57.8 bits (138), Expect = 2e-07 Identities = 39/93 (41%), Positives = 51/93 (54%), Gaps = 2/93 (2%) Query: 3 SQELVTLNVGGKIFTTRFSTIKQFPASRLARMLDGRDQEFKMVGGQIFVDRDGDLFSFIL 62 S E+V LNVGG F+T T+ P S + +L GR + G IF+DRD F+ IL Sbjct: 16 SGEIVQLNVGGTRFSTSRQTLMWIPDSFFSSLLSGRISTLRDETGAIFIDRDPAAFAPIL 75 Query: 63 DFLRTHQLLLPTEFSDYLRLQREALFYELRSLV 95 +FLRT +L L + LR EA FY + LV Sbjct: 76 NFLRTKELDLRGVSINVLR--HEAEFYGITPLV 106	54	Chr 1,	1q41 212,122K-212,190K bp Xq22.3 109,244K-109,247K bp	con.	Chr X 3 genes AMMECR1 FLJ22679 Chr 1 20 genes KCTD3	2.00E-07
BAC11374	H. sapiens	305	>gi|22760899|dbj|BAC11374.1| unnamed protein product [Homo sapiens] Length = 305 DBSOURCE accession AK075057.1 /tissue_type="ovary, tumor tissue Score = 57.4 bits (137), Expect = 3e-07 Identities = 38/91 (41%), Positives = 49/91 (53%), Gaps = 2/91 (2%) Query: 5 ELVTLNVGGKIFTTRFSTIKQFPASRLARMLDGRDQEFKMVGGQIFVDRDGDLFSFILDF 64 E++ LNVGGK F+T T+ P S + +L GR K G IF+DRD +F+ IL+F Sbjct: 19 EVIHLNVGGKRFSTSRQTLTWIPDSFFSSLLSGRISTLKGETGAIFIDRDPTVFAPILNF 78 Query: 65 LRTHQLLLPTEFSDYLRLQREALFYELRSLV 95 LRT + L L EA FY L LV Sbjct: 79 LRTKE--LDPRGVHGSSLLHEAQFYGLTPLV 107	53	Chr 19	19q13.2 45,773K-45,781K bp	con.	LOC92799 SPTBN4	3.00E-07
NP_612401	H. sapiens	707	>gi|19923917|ref|NP_612401.1| SH3KBP1 binding protein 1 [Homo sapiens] gi|18605539|gb|AAH22855.1| SH3KBP1 binding protein 1 [Homo sapiens] Length = 707 Score = 57.4 bits (137), Expect = 3e-07 Identities = 38/91 (41%), Positives = 49/91 (53%), Gaps = 2/91 (2%) Query: 5 ELVTLNVGGKIFTTRFSTIKQFPASRLARMLDGRDQEFKMVGGQIFVDRDGDLFSFILDF 64 E++ LNVGGK F+T T+ P S + +L GR K G IF+DRD +F+ IL+F Sbjct: 19 EVIHLNVGGKRFSTSRQTLTWIPDSFFSSLLSGRISTLKDETGAIFIDRDPTVFAPILNF 78 Query: 65 LRTHQLLLPTEFSDYLRLQREALFYELRSLV 95 LRT + L L EA FY L LV Sbjct: 79 LRTKE--LDPRGVHGSSLLHEAQFYGLTPLV 107	53	Chr 19	19q13.2 45,772K-45,790K bp	con.	21 genes LOC92799	3.00E-07
AAG23756	H. sapiens	707	>gi|10834652|gb|AAG23756.1| PP203 [Homo sapiens] Length = 707 TITLE Novel human cDNA clones with function of inhibiting cancer cell growth Score = 57.4 bits (137), Expect = 3e-07 Identities = 38/91 (41%), Positives = 49/91 (53%), Gaps = 2/91 (2%) Query: 5 ELVTLNVGGKIFTTRFSTIKQFPASRLARMLDGRDQEFKMVGGQIFVDRDGDLFSFILDF 64 E++ LNVGGK F+T T+ P S + +L GR K G IF+DRD +F+ IL+F Sbjct: 19 EVIHLNVGGKRFSTSRQTLTWIPDSFFSSLLSGRISTLKDETGAIFIDRDPTVFAPILNF 78 Query: 65 LRTHQLLLPTEFSDYLRLQREALFYELRSLV 95 LRT + L L EA FY L LV Sbjct: 79 LRTKE--LDPRGVHGSSLLHEAQFYGLTPLV 107	53	Chr 19	19q13.2 45,772K-45,790K bp	con.	20 genes LOC92799	3.00E-07
CAI20569	H. sapiens	312	>gi|56202411|emb|CAI20569.1| novel protein (MGC34648) [Homo sapiens] gi|4200238|emb|CAA22914.1| hypothetical protein [Homo sapiens] Length = 312 Score = 56.2 bits (134), Expect = 6e-07 Identities = 28/35 (80%), Positives = 30/35 (85%) Query: 193 RLVCNGVISAHHNLRLWGSSDSPASASRVAGITGM 227 RL CNG ISAH NL L GSSDSPAS+SRVAGITG+ Sbjct: 49 RLECNGTISAHCNLHLPGSSDSPASSSRVAGITGI 83	85	Chr 1,	Chr 1 1p35.3 27,732K-27,775K bp Chr 3 3q22.1 134,747,589-134,747,839 bp	end	Chr 1 9 genes MGC34648 Chr 3 2 genes H41 LOC391578	6.00E-07

EAL23735	H. sapiens	289	>gi|51094478|gb|EAL23735.1| potassium channel tetramerisation domain containing 7 [Homo sapiens] gi|16552087|dbj|BAB71236.1| unnamed protein product [Homo sapiens] gi|23308551|ref|NP_694578.1| potassium channel tetramerisation domain containing 7 [Homo sapiens] Length = 289 Score = 55.8 bits (133), Expect = 8e-07 Identities = 36/94 (38%), Positives = 53/94 (56%), Gaps = 3/94 (3%) Query: 5 ELVTLNVGGKIFTTRFSTIKQFPASRLARMLDGRDQEFKMVGGQIFVDRDGDLFSFILDF 64 E+V LN+GG FTTR ST++ + + LA M GR G+ F+DRDG F +L+F Sbjct: 51 EVVPLNIGGAHFTTRLSTLRCYEDTMLAAMFSGRHYIPTDSEGRYFIDRDGTHFGDVLNF 110 Query: 65 LRTHQLLLPTEFSDYLRLQREALFYELRSLVDLL 98 LR+ L P E + +EA +Y + L++ L Sbjct: 111 LRSGD-LPPRE--RVRAVYKEAQYYAIGPLLEQL 141	56	Chr 7	7q11.21 65,536K-65,549K bp	con.	5 genes KCTD7	8.00E-07
NP_803191	H. sapiens	155	>gi|29294653|ref|NP_803191.1| FtsJ homolog 2 isoform b [Homo sapiens] Length = 155 Score = 55.8 bits (133), Expect = 8e-07 Identities = 29/34 (85%), Positives = 30/34 (88%) Query: 193 RLVCNGVISAHHNLRLWGSSDSPASASRVAGITG 226 RL CNGVISAH NL L GSSDSPASAS+VAGITG Sbjct: 107 RLQCNGVISAHCNLCLPGSSDSPASASQVAGITG 140	88	Chr 7	7p22 2,052,254-2,052,621 bp	end	2 genes FTSJ2	8.00E-07
BAC05206	H. sapiens	152	>gi|21757878|dbj|BAC05206.1| unnamed protein product [Homo sapiens] Length = 152 tissue_type="thymus Score = 55.8 bits (133), Expect = 8e-07 Identities = 28/33 (84%), Positives = 29/33 (87%) Query: 194 LVCNGVISAHHNLRLWGSSDSPASASRVAGITG 226 L C+G ISAH NLRL GSSDSPASASRVAGITG Sbjct: 75 LECSGTISAHSNLRLPGSSDSPASASRVAGITG 107	87	Chr 17	17q25 72,949,642-72,950,215 bp	end	2 genes MSF	8.00E-07
AAV38923	Synth.	317	>gi|54697102|gb|AAV38923.1| tumor necrosis factor, alpha-induced protein 1 (endothelial) [synthetic construct] Length = 317 Score = 47.0 bits (110), Expect = 4e-04 Identities = 29/91 (31%), Positives = 45/91 (49%), Gaps = 1/91 (1%) Query: 7 VTLNVGGKIFTTRFSTIKQFPASRLARMLDGRDQEFKMVGGQIFVDRDGDLFSFILDFLR 66 V LNVGG ++ T + + + L M GR + G I +DR G F IL++LR Sbjct: 30 VQLNVGGSLYYTTVRALTRHD-TMLKAMFSGRMEVLTDKEGWILIDRCGKHFGTILNYLR 88 Query: 67 THQLLLPTEFSDYLRLQREALFYELRSLVDL 97 + LP + L EA +Y ++ LV++ Sbjct: 89 DDTITLPQNRQEIKELMAEAKYYLIQGLVNM 119	49	Chr 17	17q22-q23 23,690K-23,696K bp	con.	7 genes TNFAIP1	4.00E-04
AAL55831	H. sapiens	128	>gi|18027740|gb|AAL55831.1| unknown [Homo sapiens] Length = 128 TITLE Novel human cDNA clones with function of inhibiting cancer cell growth Score = 55.8 bits (133), Expect = 8e-07 Identities = 28/34 (82%), Positives = 29/34 (85%) Query: 193 RLVCNGVISAHHNLRLWGSSDSPASASRVAGITG 226 RL C+G ISAH NLRL GSSDSPASASRVAGI G Sbjct: 70 RLECSGAISAHCNLRLLGSSDSPASASRVAGIAG 103	85	Chr 19	19p13.13 13,743K-13,746K bp	end	4 genes between HSPC023 MGC3207	8.00E-07
NP_003148	H. sapiens	841	>gi|4507277|ref|NP_003148.1| NIMA (never in mitosis gene a)-related kinase 4 [Homo sapiens] gi|7427997|pir||I78885 serine/threonine-specific protein kinase (EC 2.7.1.-) STK2 - human gi|1709347|sp|P51957|NEK4_HUMAN Serine/threonine-protein kinase Nek4 (NimA-related protein kinase 4) (Serine/threonine-protein kinase 2) (Serine/threonine-protein kinase NRK2) gi|348245|gb|AAA36658.1| protein serine/threonine kinase Length = 841 Score = 55.5 bits (132), Expect = 1e-06 Identities = 27/35 (77%), Positives = 30/35 (85%) Query: 193 RLVCNGVISAHHNLRLWGSSDSPASASRVAGITGM 227 +L C+G I AH NLRL GSSDSPASASRVAGITG+ Sbjct: 463 KLECSGTILAHSNLRLLGSSDSPASASRVAGITGV 497	85	Chr 3, Chr 21	Chr 3p21.1 52,713K-52,787K bp Chr 21q21.1 17,504,550-17,505,648 bp	end	Chr 3 SPC12 NEK4 ITIH1 chr 21 1 gene CXADR	1.00E-06
AAH45189	H. sapiens	426	>gi|45946234|gb|AAH45189.1| Potassium channel tetramerisation domain containing 18 [Homo sapiens] Length = 426 Score = 55.1 bits (131), Expect = 1e-06 Identities = 31/85 (36%), Positives = 49/85 (57%), Gaps = 1/85 (1%) Query: 5 ELVTLNVGGKIFTTRFSTIKQFPASRLARMLDGRDQEFKMVGGQIFVDRDGDLFSFILDF 64 +++ LNVGG I+T R ++ +F S LA M GR G +DRDG LF ++LD+ Sbjct: 12 DVLRLNVGGCIYTARRESLCRFKDSMLASMFSGRFPLKTDESGACVIDRDGRLFKYLLDY 71 Query: 65 LRTHQLLLPTEFSDYLRLQREALFY 89 L ++ +PT+ + LQ EA ++ Sbjct: 72 LH-GEVQIPTDEQTRIALQEEADYF 95	57	Chr 2	Chr 2q33.1 201,178K-201,199K bp	con.	7 genes FLJ31322	1.00E-06

AAH67755	H. sapiens	426	>gi|45709593|gb|AAH67755.1| KCTD18 protein [Homo sapiens] Length = 426 Score = 55.1 bits (131), Expect = 1e-06 Identities = 31/85 (36%), Positives = 49/85 (57%), Gaps = 1/85 (1%) Query: 5 ELVTLNVGGKIFTTRFSTIKQFPASRLARMLDGRDQEFKMVGGQIFVDRDGDLFSFILDF 64 +++ LNVGG I+T R ++ +F S LA M GR G +DRDG LF ++LD+ Sbjct: 12 DVLRLNVGGCIYTARRESLCRFKDSMLASMFSGRFPLKTDESGACVIDRDGRLFKYLLDY 71 Query: 65 LRTHQLLLPTEFSDYLRLQREALFY 89 L ++ +PT+ + LQ EA ++ Sbjct: 72 LH-GEVQIPTDEQTRIALQEEADYF 95	57	Chr 2	2q33.1 201,176K-201,202K bp	con.	8 genes FLJ31322	1.00E-06
BAC87535	H. sapiens	136	>gi|34536088|dbj|BAC87535.1| unnamed protein product [Homo sapiens] Length = 136 Score = 54.7 bits (130), Expect = 2e-06 Identities = 28/40 (70%), Positives = 34/40 (85%) Query: 186 TDNQTGVRLVCNGVISAHHNLRLWGSSDSPASASRVAGIT 225 T++++G RL +GVISAH NLRL GSSDSPA+ASRVAG T Sbjct: 51 TESRSGTRLKGSGVISAHCNLRLPGSSDSPATASRVAGTT 90	85	Chr 2	2q36.3 227,556,112-227,556,626 bp	end	2 genes DKFZp547E052	2.00E-06
AAG13405	H. sapiens	581	>gi|10121865|gb|AAG13405.1| topoisomerase II alpha-4 [Homo sapiens] Length = 581 Score = 54.3 bits (129), Expect = 2e-06 Identities = 27/34 (79%), Positives = 28/34 (82%) Query: 193 RLVCNGVISAHHNLRLWGSSDSPASASRVAGITG 226 R +CNG I AH NLRL GSSDSPASASRVAGI G Sbjct: 356 RELCNGAILAHCNLRLMGSSDSPASASRVAGIAG 389	82	Chr 17	Chr 17q21-q22 35,816K-35,827K bp	end	12 genes TOP2A	2.00E-06
AAO13802	H. sapiens	1275	>gi|27448209|gb|AAO13802.1| myosin IIIB variant MYO3B.4 [Homo sapiens] Length = 1275 Score = 52.4 bits (124), Expect = 9e-06 Identities = 27/36 (75%), Positives = 30/36 (83%) Query: 192 VRLVCNGVISAHHNLRLWGSSDSPASASRVAGITGM 227 +RL CN +ISA NLR GSSDSPASASRVAGITG+ Sbjct: 1199 LRLECNSMISADCNLRPLGSSDSPASASRVAGITGI 1234	83	Chr 2	Chr 2q31.1-q31.2 170,814K-171,271K bp	con.	33 genes MYO3B	9.00E-06
AAG17216	H. sapiens	130	>gi|10441877|gb|AAG17216.1| unknown [Homo sapiens] Length = 130 Score = 51.6 bits (122), Expect = 2e-05 Identities = 27/35 (77%), Positives = 28/35 (80%) Query: 193 RLVCNGVISAHHNLRLWGSSDSPASASRVAGITGM 227 RL C+G ISAH NL L GSS SPASASRV GITGM Sbjct: 40 RLECSGTISAHCNLCLLGSSYSPASASRVTGITGM 74	80	Chr 1	1p32.3 54,282,114-54,282,604 bp	end	1 gene FLJ32112	2.00E-05
NP_009112	H. sapiens	833	>gi|6005810|ref|NP_009112.1| mitogen-activated protein kinase kinase kinase kinase 1 [Homo sapiens] gi|1575563|gb|AAB97983.1| hematopoietic progenitor kinase gi|29427916|sp|Q92918|M4K1_HUMAN Mitogen-activated protein kinase kinase kinase kinase 1 (MAPK/ERK kinase kinase kinase 1) (MEK kinase kinase 1) (MEKKK 1) (Hematopoietic progenitor kinase) Length = 833 Score = 51.2 bits (121), Expect = 2e-05 Identities = 26/35 (74%), Positives = 29/35 (82%) Query: 193 RLVCNGVISAHHNLRLWGSSDSPASASRVAGITGM 227 RL C+G IS H NL L GSS+SPASASRVAGITG+ Sbjct: 799 RLECSGTISPHCNLLLPGSSNSPASASRVAGITGL 833	82	Chr 19	Chr 19q13.1-q13.4 43,766K-43,804K bp	end	34 genes MAP4K1	2.00E-05
CAI21728	H. sapiens	326	>gi|56204217|emb|CAI21728.1| beta 1,3-N-acetylgalactosaminyltransferase-II (MGC39558) [Homo sapiens] Length = 326 Score = 51.2 bits (121), Expect = 2e-05 Identities = 25/33 (75%), Positives = 27/33 (81%) Query: 193 RLVCNGVISAHHNLRLWGSSDSPASASRVAGIT 225 RL CNG +SAH NL L GS DSPASAS+VAGIT Sbjct: 46 RLECNGAVSAHPNLHLPGSRDSPASASQVAGIT 78	81	Chr 1, Chr 6	Chr 1q42.3 231,950K-231,998K bp Chr 6q22.33 130,163,693-130,164,560 bp	end	Chr 1 MGC39558 8 genes Chr 6 1 gene	2.00E-05
AAH16974	H. sapiens	382	>gi|16877456|gb|AAH16974.1| B3GALNT2 protein [Homo sapiens] Length = 382 tissue_type="Breast, mammary adenocarcinoma Score = 51.2 bits (121), Expect = 2e-05 Identities = 25/33 (75%), Positives = 27/33 (81%) Query: 193 RLVCNGVISAHHNLRLWGSSDSPASASRVAGIT 225 RL CNG +SAH NL L GS DSPASAS+VAGIT Sbjct: 102 RLECNGAVSAHPNLHLPGSRDSPASASQVAGIT 134	81	Chr 1, Chr 7	Chr 1q42.3 231,950K-231,998K bp Chr 6q22.33 130,163,693-130,164,560 bp	end	Chr 1 MGC39558 8 genes Chr 6 1 gene	2.00E-05

NP_001002914	H. sapiens	232	>gi|51036594|ref|NP_001002914.1| potassium channel tetramerisation domain containing 11 [Homo sapiens] gi|50363135|gb|AAT75307.1| potassium channel tetramerization domain containing 11; retinoic acid, EGF, NGF induced gene protein; REN/KCTD11 [Homo sapiens] Length = 232 Score = 50.4 bits (119), Expect = 4e-05 Identities = 25/53 (47%), Positives = 34/53 (64%) Query: 46 GGQIFVDRDGDLFSFILDFLRTHQLLLPTEFSDYLRLQREALFYELRSLVDLL 98 GG F+DRDG F IL+FLR +L LP + + L+ EA FY++R L+D L Sbjct: 21 GGHYFIDRDGKAFRHILNFLRLGRLDLPRGYGETALLRAEADFYQIRPLLDAL 73	64	Chr 17	Chr 17p13.1 7,195K-7,199K bp	mid	3 genes KCTD11 LOC339168	4.00E-05

APPENDIX 2
KCNRG ISOFORM S: ALLIGNMENT

KCNRG isoform 2 (229 aa) contains short domain with probable regulatory function
Alignment of aa 180-227

```
  1 mssqelvtln vggkifttrf stikqfpasr larmldgrdq efkmvggqif vdrdgdlfsf
 61 ildflrthql llptefsdyl rlqrealfye lrslvdllnp yllqprpalv evhflsrntq
121 affrvfgscs ktiemltgri tvfteqpsap twngnffppq mtllplppqr psyhdlvfqc
181 gsdsttdnqt gvrlvcngvi sahhnlrlwg ssdspasasr vagitgmfl
```

>☑ gi|4507277|ref|NP_003148.1| U G NIMA (never in mitosis gene a)-related kinase 4 , alias STK2 kinase [Homo sapiens]
Length=841

```
 Score = 55.5 bits (132),  Expect = 3e-08
 Identities = 27/35 (77%), Positives = 30/35 (85%), Gaps = 0/35 (0%)

Query  193  RLVCNGVISAHHNLRLWGSSDSPASASRVAGITGM  227
            +L C+G I AH NLRL GSSDSPASASRVAGITG+
Sbjct  463  KLECSGTILAHSNLRLLGSSDSPASASRVAGITGV  497
```

>☑ gi|111118986|ref|NP_150646.3| G alpha-1A-adrenergic receptor isoform 2 [Homo sapiens]
Length=475

```
 Score = 51.6 bits (122),  Expect = 5e-07
 Identities = 26/42 (61%), Positives = 32/42 (76%), Gaps = 0/42 (0%)

Query  186  TDNQTGVRLVCNGVISAHHNLRLWGSSDSPASASRVAGITGM  227
            T +++  RL C+G+I AH NLRL GS DSPASAS+ AG TGM
Sbjct  424  TKSRSVTRLECSGMILAHCNLRLPGSRDSPASASQAAGTTGM  465
```

>☑ gi|6005810|ref|NP_009112.1| G mitogen-activated protein kinase kinase kinase kinase 1 isoform
2 [Homo sapiens]
Length=833

```
 Score = 51.2 bits (121),  Expect = 6e-07
 Identities = 26/35 (74%), Positives = 29/35 (82%), Gaps = 0/35 (0%)

Query  193  RLVCNGVISAHHNLRLWGSSDSPASASRVAGITGM  227
            RL C+G IS H NL L GSS+SPASASRVAGITG+
Sbjct  799  RLECSGTISPHCNLLLPGSSNSPASASRVAGITGL  833
```

>☑ gi|8923452|ref|NP_060312.1| U G hypothetical protein LOC55652 [Homo sapiens]
Length=239

```
 Score = 49.3 bits (116),  Expect = 2e-06
 Identities = 25/35 (71%), Positives = 29/35 (82%), Gaps = 0/35 (0%)

Query  193  RLVCNGVISAHHNLRLWGSSDSPASASRVAGITGM  227
            RL C+  ISAH NLRL GSS+SPA AS+VAGITG+
Sbjct  129  RLECSSAISAHCNLRLPGSSNSPALASQVAGITGI  163
```

> gi|22547125|ref|NP_683685.1| mitochondrial ribosomal protein L10 isoform b [Homo sapiens]

```
Length=271

 Score = 45.1 bits (105),  Expect = 4e-05
 Identities = 23/28 (82%), Positives = 25/28 (89%), Gaps = 0/28 (0%)

Query  199  VISAHHNLRLWGSSDSPASASRVAGITG  226
            +ISAH NL L GSSDSPASAS+VAGITG
Sbjct  1    MISAHCNLHLPGSSDSPASASQVAGITG  28
```

> gi|51243063|ref|NP_001003690.1| MAD2L1 binding protein isoform 1 [Homo sapiens]

```
Length=306

 Score = 44.7 bits (104),  Expect = 6e-05
 Identities = 23/32 (71%), Positives = 25/32 (78%), Gaps = 0/32 (0%)

Query  193  RLVCNGVISAHHNLRLWGSSDSPASASRVAGI  224
            RL  NG+ SAHHN RL GS DSPASAS+VA I
Sbjct  15   RLEHNGMTSAHHNFRLPGSRDSPASASQVAEI  46
```

> gi|24497440|ref|NP_714912.1| interleukin 12 receptor, beta 1 isoform 2 precursor [Homo sapiens]

```
Length=381

 Score = 47.0 bits (110),  Expect = 1e-05
 Identities = 24/31 (77%), Positives = 27/31 (87%), Gaps = 0/31 (0%)

Query  197  NGVISAHHNLRLWGSSDSPASASRVAGITGM  227
            +G+ISAH NLRL  S DSPASASRVAGITG+
Sbjct  341  DGMISAHCNLRLPDSRDSPASASRVAGITGI  371
```

> gi|58533176|ref|NP_001011657.1| zinc finger, matrin type 1 isoform 1 [Homo sapiens]

```
Length=638

 Score = 47.0 bits (110),  Expect = 1e-05
 Identities = 23/33 (69%), Positives = 27/33 (81%), Gaps = 0/33 (0%)

Query  193  RLVCNGVISAHHNLRLWGSSDSPASASRVAGIT  225
            RL C+G ISAH +L L GSSDSPASAS++AG T
Sbjct  8    RLECSGAISAHCSLHLPGSSDSPASASQIAGTT  40
```

> gi|42660332|ref|XP_375099.1| PREDICTED: hypothetical protein [Homo sapiens]

gi|89037832|ref|XP_944459.1| PREDICTED: hypothetical protein [Homo sapiens]
Length=98

 Score = 45.8 bits (107), Expect = 3e-05
 Identities = 25/46 (54%), Positives = 28/46 (60%), Gaps = 0/46 (0%)

```
Query  182  SDSTTDNQTGVRLVCNGVISAHHNLRLWGSSDSPASASRVAGITGM  227
            S+   D     +L C G+I AH NL L GS DSP SAS VAG TGM
Sbjct  47   SNIQVDLTLSPKLECTGMILAHCNLCLLGSGDSPTSASPVAGTTGM  92
```

> gi|58294160|ref|NP_060313.3| breast carcinoma amplified sequence 4 isoform a [Homo sapiens]
Length=211

 Score = 45.4 bits (106), Expect = 3e-05
 Identities = 23/30 (76%), Positives = 25/30 (83%), Gaps = 0/30 (0%)

```
Query  196  CNGVISAHHNLRLWGSSDSPASASRVAGIT  225
            C+G I A  NLRL GSSDSPASAS+VAGIT
Sbjct  166  CSGTIPARCNLRLPGSSDSPASASQVAGIT  195
```

> gi|56119090|ref|NP_056087.1| hypothetical protein LOC23322 [Homo sapiens]
Length=1315

 Score = 44.7 bits (104), Expect = 6e-05
 Identities = 23/33 (69%), Positives = 25/33 (75%), Gaps = 0/33 (0%)

```
Query  194   LVCNGVISAHHNLRLWGSSDSPASASRVAGITG  226
             L C+  ISAH N RL GSSD PASAS+V GITG
Sbjct  1106  LGCSSAISAHCNFRLPGSSDFPASASQVDGITG  1138
```

> gi|88965894|ref|XP_293581.5| PREDICTED: similar to tissue-type vomeronasal neurons putative
pheromone receptor V2R2 [Homo sapiens]
Length=774

 Score = 42.4 bits (98), Expect = 3e-04
 Identities = 24/51 (47%), Positives = 33/51 (64%), Gaps = 0/51 (0%)

```
Query  176  LVFQCGSDSTTDNQTGVRLVCNGVISAHHNLRLWGSSDSPASASRVAGITG  226
            + F+     TT++++   L  +G ISAH +L L GSS+SPASA  VAG TG
Sbjct  314  IYFRMNCRVTTESRSVAMLEYSGEISAHCHLCLLGSSNSPASAPLVAGTTG  364
```

> gi|28372523|ref|NP_777547.1| intraflagellar transport protein IFT20 [Homo sapiens]
Length=148

 Score = 42.0 bits (97), Expect = 4e-04
 Identities = 22/34 (64%), Positives = 22/34 (64%), Gaps = 0/34 (0%)

```
Query  193  RLVCNGVISAHHNLRLWGSSDSPASASRVAGITG  226
            RL C G ISAH  L L  SSDSP S SRV G TG
Sbjct  78   RLECTGAISAHCKLCLSDSSDSPTSPSRVGGTTG  111
```

>gi|51972262|ref|NP_001004345.1| hypothetical protein LOC440867 [Homo sapiens]
Length=123

 Score = 41.2 bits (95), Expect = 6e-04
 Identities = 27/62 (43%), Positives = 30/62 (48%), Gaps = 0/62 (0%)

Query 165 PLPPQRPSYHDLVFQCGSDSTTDNQTGVRLVCNGVISAHHNLRLWGSSDSPASASRVAGI 224
            P P   P   +   + S   RL CNG ISA NL   GSSDSPASAS+ A
Sbjct 4   PCPHLPPPLSSCIMNETAASLLPEVLHFRLGCNGSISAQCNLCFPGSSDSPASASQAAVN 63

Query 225 TG 226
            TG
Sbjct 64   TG 65

>gi|94680985|ref|NP_078841.3| cyclin J-like [Homo sapiens]
Length=435

 Score = 40.0 bits (92), Expect = 0.001
 Identities = 24/43 (55%), Positives = 28/43 (65%), Gaps = 7/43 (16%)

Query 193 RLVCNGVISAHHNLRLWGSSDSPASA-------SRVAGITGMF 228
            RL C+G+ISAH NL L GSS+SPASA   +VA TG F
Sbjct 102 RLKCSGMISAHCNLHLPGSSNSPASAPHPPPTPPQVAETTGKF 144

>gi|21699054|ref|NP_659411.1| coiled-coil domain containing 122 [Homo sapiens]
Length=284

 Score = 40.0 bits (92), Expect = 0.001
 Identities = 22/34 (64%), Positives = 23/34 (67%), Gaps = 0/34 (0%)

Query 193 RLVCNGVISAHHNLRLWGSSDSPASASRVAGITG 226
            RL C+ ISAH L L GS SPASAS VAG TG
Sbjct 231 RLECSSAISAHCKLCLPGSRHSPASASGVAGTTG 264

>gi|61966807|ref|NP_001013702.1| hypothetical protein LOC401233 [Homo sapiens]
Length=334

 Score = 39.3 bits (90), Expect = 0.002
 Identities = 21/34 (61%), Positives = 22/34 (64%), Gaps = 0/34 (0%)

Query 193 RLVCNGVISAHHNLRLWGSSDSPASASRVAGITG 226
            RL C+G ISAH L   S SPASASRVAG G
Sbjct 260 RLECSGAISAHCKLCFPASRHSPASASRVAGTAG 293

>gi|61969666|ref|NP_001012677.1| arginine-fifty homeobox [Homo sapiens]
Length=315

 Score = 38.5 bits (88), Expect = 0.004
 Identities = 18/35 (51%), Positives = 25/35 (71%), Gaps = 0/35 (0%)

Query 193 RLVCNGVISAHHNLRLWGSSDSPASASRVAGITGM 227
            +L C+G +SA+ +L L GS+D P SASRVA T +

```
Sbjct  41   KLECSGTVSAYCSLNLPGSTDPPTSASRVAATTAI  75

>  gi|34147532|ref|NP_612412.2|  myosin light chain 2, precursor lymphocyte-
specific [Homo sapiens]
Length=226

 Score = 37.7 bits (86),  Expect = 0.007
 Identities = 20/28 (71%), Positives = 23/28 (82%), Gaps = 0/28 (0%)

Query  193  RLVCNGVISAHHNLRLWGSSDSPASASR  220
            RL  NG+ISAH NL L GSS+SPASAS+
Sbjct  64   RLERNGMISAHCNLCLTGSSNSPASASQ  91

>  gi|27480484|ref|XP_209640.1|  PREDICTED: hypothetical protein [Homo sapiens]
 gi|88981318|ref|XP_944988.1|  PREDICTED: hypothetical protein [Homo sapiens]
Length=109

 Score = 37.4 bits (85),  Expect = 0.009
 Identities = 20/35 (57%), Positives = 23/35 (65%), Gaps = 0/35 (0%)

Query  192  VRLVCNGVISAHHNLRLWGSSDSPASASRVAGITG  226
            V+L C+G I AH NL L GS     SAS+VAG TG
Sbjct  20   VKLECSGPILAHCNLCLLGSRHPSTSASQVAGTTG  54

>  gi|51477721|ref|NP_001003811.1|  testis expressed sequence 11 isoform 1 [Homo
sapiens]
Length=940

 Score = 37.0 bits (84),  Expect = 0.012
 Identities = 20/27 (74%), Positives = 22/27 (81%), Gaps = 0/27 (0%)

Query  199  VISAHHNLRLWGSSDSPASASRVAGIT  225
            +ISAH NLRL  SSDS ASAS+VAG T
Sbjct  1    MISAHCNLRLLCSSDSSASASQVAGTT  27

>  gi|78000165|ref|NP_001030127.1|  sorbin and SH3 domain containing 1 isoform 4
[Homo sapiens]
Length=1151

 Score = 36.6 bits (83),  Expect = 0.016
 Identities = 17/31 (54%), Positives = 23/31 (74%), Gaps = 0/31 (0%)

Query  193  RLVCNGVISAHHNLRLWGSSDSPASASRVAG  223
            RL C+G + AH +L+L  SS+ P SAS+VAG
Sbjct  443  RLECSGTVIAHCSLKLLDSSNPPTSASQVAG  473


>  gi|58331120|ref|NP_001009923.1|  hypothetical protein LOC29058 isoform 1 [Homo
sapiens]
Length=183

 Score = 36.6 bits (83),  Expect = 0.016
 Identities = 20/29 (68%), Positives = 22/29 (75%), Gaps = 0/29 (0%)

Query  193  RLVCNGVISAHHNLRLWGSSDSPASASRV  221
```

```
            RL  +GVISAH NL L  SSDS ASASR+
Sbjct  31   RLEPSGVISAHCNLHLLASSDSSASASRL  59


>  gi|60099474|ref|NP_001012414.1|  tripartite motif-containing 61 [Homo sapiens]
Length=209

 Score = 36.6 bits (83),  Expect = 0.016
 Identities = 19/27 (70%), Positives = 20/27 (74%), Gaps = 0/27 (0%)

Query  193  RLVCNGVISAHHNLRLWGSSDSPASAS  219
            RL C+  ISAH NLRL GSSDS AS S
Sbjct  183  RLECSCTISAHFNLRLPGSSDSSASGS  209
>  gi|34147403|ref|NP_113661.2|  carnitine deficiency-associated, expressed in
ventricle 1 isoform
2 [Homo sapiens]
Length=431

 Score = 36.2 bits (82),  Expect = 0.021
 Identities = 19/37 (51%), Positives = 22/37 (59%), Gaps = 0/37 (0%)

Query  183  DSTTDNQTGVRLVCNGVISAHHNLRLWGSSDSPASAS  219
            D   D     RL C GVI A+ +L+L GSSD P SAS
Sbjct  395  DERQDLTLSPRLECGGVIMAYCSLKLLGSSDPPTSAS  431


>  gi|113421662|ref|XP_001126811.1|  PREDICTED: hypothetical protein [Homo sapiens]
Length=136

 Score = 35.0 bits (79),  Expect = 0.046
 Identities = 17/34 (50%), Positives = 25/34 (73%), Gaps = 0/34 (0%)

Query  192  VRLVCNGVISAHHNLRLWGSSDSPASASRVAGIT  225
            +RL+ +G+I AH +L + G +D PASAS+VA  T
Sbjct  93   LRLLYSGLIIAHCSLEILGRNDPPASASKVAETT  126


>  gi|22748869|ref|NP_689623.1|  PARK2 co-regulated [Homo sapiens]
Length=296

 Score = 35.0 bits (79),  Expect = 0.046
 Identities = 19/32 (59%), Positives = 21/32 (65%), Gaps = 0/32 (0%)

Query  193  RLVCNGVISAHHNLRLWGSSDSPASASRVAGI  224
            RL C+G I A  NL   GSSD P SAS+VA I
Sbjct  211  RLECSGAIMARCNLDHLGSSDPPTSASQVAEI  242

>  gi|21699084|ref|NP_660326.1|  nucleoredoxin [Homo sapiens]
Length=135

 Score = 34.7 bits (78),  Expect = 0.061
 Identities = 19/27 (70%), Positives = 20/27 (74%), Gaps = 0/27 (0%)

Query  193  RLVCNGVISAHHNLRLWGSSDSPASAS  219
            RL C+GVI AH NL L GSSDS A AS
```

```
Sbjct  109  RLECSGVILAHCNLCLLGSSDSLALAS  135

>  gi|109627668|ref|NP_116094.2|  hypothetical protein LOC84791 [Homo sapiens]
Length=124

 Score = 32.7 bits (73),  Expect = 0.23
 Identities = 17/28 (60%), Positives = 20/28 (71%), Gaps = 0/28 (0%)

Query  192  VRLVCNGVISAHHNLRLWGSSDSPASAS  219
            +RL CN   SAH NL L  SS+SPA+AS
Sbjct  97   LRLECNDATSAHCNLCLPDSSNSPATAS  124

>  gi|113421909|ref|XP_001130807.1|  PREDICTED: hypothetical protein [Homo sapiens]
Length=152

 Score = 32.0 bits (71),  Expect = 0.39
 Identities = 30/97 (30%), Positives = 44/97 (45%), Gaps = 17/97 (17%)

Query  138  GRITVFTEQPSAPTWNGNFFPPQMTLLPLP-----PQRPSYHDLVFQCGSDSTTDNQTGV  192
            G++ V+ E+PS    +      ++ + P P     P R      +++   D T  + T
Sbjct  31   GQLRVWWEKPSC---SSEIHKVEIAVAPTPLLWRLPSR------IWEPARDLTAAHWTPE  81

Query  193  ---RLVCNGVISAHHNLRLWGSSDSPASASRVAGITG  226
               RL C   +SA  N     S D PASAS+VAGI G
Sbjct  82   DTQRLECYVAMSARCNPCFLSSCDPPASASQVAGIRG  118


>  gi|113865935|ref|NP_001038943.1|  hypothetical protein LOC644997 [Homo sapiens]
Length=167

 Score = 32.0 bits (71),  Expect = 0.39
 Identities = 16/35 (45%), Positives = 22/35 (62%), Gaps = 0/35 (0%)

Query  193  RLVCNGVISAHHNLRLWGSSDSPASASRVAGITGM  227
            +L  +G + A+ NL L  SSD P  AS+  G+TGM
Sbjct  80   KLERSGTVIAYCNLELLASSDPPVWASQSTGMTGM  114


>  gi|89886187|ref|NP_001034843.1|  UG  hypothetical protein LOC441212 [Homo sapiens]
Length=121

 Score = 31.6 bits (70),  Expect = 0.51
 Identities = 15/19 (78%), Positives = 17/19 (89%), Gaps = 0/19 (0%)

Query  199  VISAHHNLRLWGSSDSPAS  217
            +ISAH +LRL GSSDSPAS
Sbjct  1    MISAHRDLRLPGSSDSPAS  19


 Score = 28.1 bits (61),  Expect = 5.7
 Identities = 14/22 (63%), Positives = 16/22 (72%), Gaps = 0/22 (0%)

Query  206  LRLWGSSDSPASASRVAGITGM  227
            L L  S D PASAS+ AGITG+
Sbjct  53   LELPASGDPPASASQSAGITGV  74
```

>gi|89030285|ref|XP_944216.1| PREDICTED: hypothetical protein [Homo sapiens]
Length=160

 Score = 31.6 bits (70), Expect = 0.51
 Identities = 16/35 (45%), Positives = 19/35 (54%), Gaps = 0/35 (0%)

Query 193 RLVCNGVISAHHNLRLWGSSDSPASASRVAGITGM 227
            RL C+G I AHH L   S+D P AS V   T +
Sbjct 100 RLECSGAIKAHHGLERLRSTDIPDLASPVTRTTAI 134

>gi|42659177|ref|XP_376822.1| PREDICTED: hypothetical protein [Homo sapiens]
Length=160

 Score = 31.6 bits (70), Expect = 0.51
 Identities = 16/35 (45%), Positives = 19/35 (54%), Gaps = 0/35 (0%)

Query 193 RLVCNGVISAHHNLRLWGSSDSPASASRVAGITGM 227
            RL C+G I AHH L   S+D P AS V   T +
Sbjct 100 RLECSGAIKAHHGLERLRSTDIPDLASPVTRTTAI 134

>gi|28212280|ref|NP_777603.1| hypothetical protein LOC283579 [Homo sapiens]
Length=122

 Score = 31.6 bits (70), Expect = 0.51
 Identities = 16/26 (61%), Positives = 19/26 (73%), Gaps = 0/26 (0%)

Query 202 AHHNLRLWGSSDSPASASRVAGITGM 227
            A   L L GSS+ PASAS+ AGITG+
Sbjct 37   AQAGLELLGSSNPPASASQSAGITGV 62

>gi|89886193|ref|NP_001034848.1| hypothetical protein LOC642484 [Homo sapiens]
Length=147

 Score = 31.2 bits (69), Expect = 0.67
 Identities = 16/36 (44%), Positives = 20/36 (55%), Gaps = 0/36 (0%)

Query 194 LVCNGVISAHHNLRLWGSSDSPASASRVAGITGMFL 229
            L C+G I AH +L   S D P   SRVAG G+ +
Sbjct 33   LECSGPIIAHCSLDFPASVDPPTLISRVAGTAGLLI 68

>gi|19882217|ref|NP_598400.1| mitochondrial translation optimization 1 homolog isoform a [Homo
sapiens]
Length=717

 Score = 30.8 bits (68), Expect = 0.88
 Identities = 13/18 (72%), Positives = 14/18 (77%), Gaps = 0/18 (0%)

Query 193 RLVCNGVISAHHNLRLWG 210
            R+ CNG ISAHHNL L G
Sbjct 385 RMECNGAISAHHNLPLPG 402

>gi|21361101|ref|NP_003675.2| MAP kinase interacting serine/threonine kinase 1 isoform 1 [Homo
sapiens]
Length=465

 Score = 29.3 bits (64), Expect = 2.5
 Identities = 13/18 (72%), Positives = 15/18 (83%), Gaps = 0/18 (0%)

Query 210 GSSDSPASASRVAGITGM 227
            GSSD P SAS+VAG TG+
Sbjct 190 GSSDPPTSASQVAGTTGI 207

>gi|21945058|ref|NP_660344.1| hypothetical protein LOC201158 [Homo sapiens]
Length=276

 Score = 28.9 bits (63), Expect = 3.3
 Identities = 14/26 (53%), Positives = 18/26 (69%), Gaps = 0/26 (0%)

Query 202 AHHNLRLWGSSDSPASASRVAGITGM 227
            A   L++ GS D PASA + AGITG+
Sbjct 161 AQTGLKVLGSRDPPASAFQSAGITGV 186

>gi|62243734|ref|NP_060190.2| signal-transducing adaptor protein-2 isoform 1 [Homo sapiens]
Length=449

 Score = 28.9 bits (63), Expect = 3.3
 Identities = 15/26 (57%), Positives = 17/26 (65%), Gaps = 0/26 (0%)

Query 202 AHHNLRLWGSSDSPASASRVAGITGM 227
            A   L L SSD P SAS+ AGITG+
Sbjct 366 AQAGLELLTSSDPPTSASQSAGITGV 391

>gi|113423932|ref|XP_001134334.1| PREDICTED: similar to RNA binding motif protein 19 [Homo sapiens]
Length=969

 Score = 28.1 bits (61), Expect = 5.7
 Identities = 14/32 (43%), Positives = 19/32 (59%), Gaps = 0/32 (0%)

Query 196 CNGVISAHHNLRLWGSSDSPASASRVAGITGM 227
            C ++ +   L L S D PASAS+ AGI G+
Sbjct 431 CFSMLVSQAGLELLTSGDPPASASQSAGIMGV 462

>gi|66348062|ref|NP_001018114.1| fumarylacetoacetate hydrolase domain containing 1 isoform 1 [Homo
sapiens]
Length=248

 Score = 27.3 bits (59), Expect = 9.7
 Identities = 15/28 (53%), Positives = 20/28 (71%), Gaps = 1/28 (3%)

Query 193 RLVCNGVISAHHNLRLWGSSDSPASASR 220

```
            +L C+  I+AH +L L GSS +P SASR
Sbjct  221  KLECSSAITAHCSLELPGSS-NPPSASR  247
```

APPENDIX 3
PROTEINS CONTAINING COOL DOMAIN

NP_003148. Reports NIMA (never in mi...[gi:4507277]

BLink, Conserved Domains, Links

- Next sequence

```
>gi|4507277|ref|NP_003148.1| NIMA (never in mitosis gene a)-related kinase 4 [Homo
sapiens]
MPLAAYCYLRVVGKGSYGEVTLVKHRRDGKQYVIKKLNLRNASSRERRAAEQEAQLLSQLKHPNIVTYKE
SWEGGDGLLYIVMGFCEGGDLYRKLKEQKGQLLPENQVVEWFVQIAMALQYLHEKHILHRDLKTQNVFLT
RTNIIKVGDLGIARVLENHCDMASTLIGTPYYMSPELFSNKPYNYKSDVWALGCCVYEMATLKHAFNAKD
MNSLVYRIIEGKLPAMPRDYSPELAELIRTMLSKRPEERPSVRSILRQPYIKRQISFFLEATKIKTSKNN
IKNGDSQSKPFATVVSGEAESNHEVIHPQPLSSEGSQTYIMGEGKCLSQEKPRASGLLKSPASLKAHTCK
QDLSNTTELATISSVNIDILPAKGRDSVSDGFVQENQPRYLDASNELGGICSISQVEEEMLQDNTKSSAQ
PENLIPMWSSDIVTGEKNEPVKPLQPLIKEQKPKDQSLALSPKLECSGTILAHSNLRLLGSSDSPASASR
VAGITGVCHHAQDQVAGECIIEKQGRIHPDLQPHNSGSEPSLSRQRRQKRREQTEHRGEKRQVRRDLFAF
QESPPRFLPSHPIVGKVDVTSTQKEAENQRRVVTGSVSSSRSSEMSSSKDRPLSARERRRLKQSQEEMSS
SGPSVRKASLSVAGPGKPQEEDQPLPARRLSSDCSVTQERKQIHCLSEDELSSSTSSTDKSDGDYGEGKG
QTNEINALVQLMTQTLKLDSKESCEDVPVANPVSEFKLHRKYRDTLILHGKVAEEAEEIHFKELPSAIMP
GSEKIRRLVEVLRTDVIRGLGVQLLEQVYDLLEEEDEFDREVRLREHMGEKYTTYSVKARQLKFFEENMN
```

NP_150646. Reports alpha-1A-adrenerg...[gi:111118986]

BLink, Conserved Domains, Links

- Previous sequence
- Next sequence

```
>gi|111118986|ref|NP_150646.3| alpha-1A-adrenergic receptor isoform 2 [Homo sapiens]
MVFLSGNASDSSNCTQPPAPVNISKAILLGVILGGLILFGVLGNILVILSVACHRHLHSVTHYYIVNLAV
ADLLLTSTVLPFSAIFEVLGYWAFGRVFCNIWAAVDVLCCTASIMGLCIISIDRYIGVSYPLRYPTIVTQ
RRGLMALLCVWALSLVISIGPLFGWRQPAPEDETICQINEEPGYVLFSALGSFYLPLAIILVMYCRVYVV
AKRESRGLKSGLKTDKSDSEQVTLRIHRKNAPAGGSGMASAKTKTHFSVRLLKFSREKKAAKTLGIVVGC
FVLCWLPFFLVMPIGSFFPDFKPSETVFKIVFWLGYLNSCINPIIYPCSSQEFKKAFQNVLRIQCLCRKQ
SSKHALGYTLHPPSQAVEGQHKDMVRIPVGSRETFYRISKTDGVCEWKFFSSMPRGSARITVSKDQSSCT
TARTKSRSVTRLECSGMILAHCNLRLPGSRDSPASASQAAGTTGMCHQADATRPS
```

NP_009112. Reports mitogen-activated...[gi:6005810]

BLink, Conserved Domains, Links

- Previous sequence
- Next sequence

```
>gi|6005810|ref|NP_009112.1| mitogen-activated protein kinase kinase kinase kinase 1
isoform 2 [Homo sapiens]
MDVVDPDIFNRDPRDHYDLLQRLGGGTYGEVFKARDKVSGDLVALKMVKMEPDDDVSTLQKEILILKTCR
HANIVAYHGSYLWLQKLWICMEFCGAGSLQDIYQVTGSLSELQISYVCREVLQGLAYLHSQKKIHRDIKG
ANILINDAGEVRLADFGISAQIGATLARRLSFIGTPYWMAPEVAAVALKGGYNELCDIWSLGITAIELAE
LQPPLFDVHPLRVLFLMTKSGYQPPRLKEKGKWSAAFHNFIKVTLTKSPKKRPSATKMLSHQLVSQPGLN
RGLILDLLDKLKNPGKGPSIGDIEDEEPELPPAIPRRIRSTHRSSSLGIPDADCCRRHMEFRKLRGMETR
PPANTARLQPPRDLRSSSPRKQLSESSDDDYDDVDIPTPAEDTPPPLPPKPKFRSPSDEGPGSMGDDGQL
SPGVLVRCASGPPPNSPRPGPPPSTSSPHLTAHSEPSLWNPPSRELDKPPLLPPKKEKMKRKGCALLVKL
FNGCPLRIHSTAAWTHPSTKDQHLLLGAEEGIFILNRNDQEATLEMLFPSRTTWVYSINNVLMSLSGKTP
HLYSHSILGLLERKETRAGNPIAHISPHRLLARKNMVSTKIQDTKGCRACCVAEGASSGGPFLCGALETS
VVLLQWYQPMNKFLLVRQVLFPLPTPLSVFALLTGPGSELPAVCIGVSPGRPGKSVLFHTVRFGALSCWL
GEMSTEHRGPVQVTQVEEDMVMVLMDGSVKLVTPEGSPVRGLRTPEIPMTEAVEAVAMVGGQLQAFWKHG
VQVWALGSDQLLQELRDPTLTFRLLGSPRLECSGTISPHCNLLLPGSSNSPASASRVAGITGL
```

NP_060312. Reports hypothetical prot...[gi:8923452]

BLink, Links

- Previous sequence
- Next sequence

```
>gi|8923452|ref|NP_060312.1| hypothetical protein LOC55652 [Homo sapiens]
MPTATGLTLLTSASSAISDPGGEVSAPWGGLRTWTQPLRCWERLLPPPGDPRTVAENTQQDECGLPGSCP
```

ARPLSRKPECGREGILPCCSSSAWPEGSFRPFQMNLFSFLSFFFLFFFFLRWSLTLSPRLECSSAISAHC
NLRLPGSSNSPALASQVAGITGICHHARQIFVFLVETGFCHVGQAGLELLISGDSPASAFQSAGIIGVSH
RARPGSVFLARSEESLYLRPGQQSQEVKV

NP_872301. Reports hypothetical prot...[gi:33438588] BLink, Links

- Previous sequence
- Next sequence

>gi|33438588|ref|NP_872301.1| hypothetical protein LOC120406 [Homo sapiens]
MVEKILIHRILTLFPNAIARKLLLMLTFILIFWIIYLASKDHTKFSFNLENHIILNQGNIFKKYSHSETP
LCPAVSPKETELRIKDIMEKLDQQIPPRPFTHVNTTTSATHSTATILNPQDTYCRGDQLDILLEVRDHLG
HRKQYGGDFLRARMYSTALMAGASGKVTDFNNGTYLVSFTLFWEGQVSLSLLLIHPSEGVSALWRARNQG
CDRIIFTGLFANRSSNVFTECGLTLNTNAELCQYMDDRDQEAFYCVRPQHMPCEALTHMTTRTRNISYLS
KEEWRLFHRSNIGVEMMKNFTPIEVIPCPALFYFIFRDSLTLSPRLECSGMISAHCNLCLPGSSDSPDSA
SHVAGITSVQRHTWL

NP_714912. Reports interleukin 12 re...[gi:24497440] BLink, Links

- Previous sequence
- Next sequence

>gi|24497440|ref|NP_714912.1| interleukin 12 receptor, beta 1 isoform 2 precursor
[Homo sapiens]
MEPLVTWVVPLLFLFLLSRQGAACRTSECCFQDPPYPDADSGSASGPRDLRCYRISSDRYECSWQYEGPT
AGVSHFLRCCLSSGRCCYFAAGSATRLQFSDQAGVSVLYTVTLWVESWARNQTEKSPEVTLQLYNSVKYE
PPLGDIKVSKLAGQLRMEWETPDNQVGAEVQFRHRTPSSPWKLGDCGPQDDDTESCLCPLEMNVAQEFQL
RRRQLGSQGSSWSKWSSPVCVPPENPPQPQVRFSVEQLGQDGRRRLTLKEQPTQLELPEGCQGLAPGTEV
TYRLQLHMLSCPCKAKATRTLHLGKMPYLSGAAYNVAVISSNQFGPGLNQTWHIPADTHTDGMISAHCNL
RLPDSRDSPASASRVAGITGICHHTRLILYF

NP_001011657. Reports zinc finger, matr...[gi:58533176] BLink, Conserved Domains, Links

- Previous sequence
- Next sequence

>gi|58533176|ref|NP_001011657.1| zinc finger, matrin type 1 isoform 1 [Homo sapiens]
MESCSVTRLECSGAISAHCSLHLPGSSDSPASASQIAGTTDAIWNEQEKAELFTDKFCQVCGVMLQFESQ
RISHYEGEKHAQNVSFYFQMHGEQNEVPGKKMKMHVENFQVHRYEGVDKNKFCDLCNMMFSSPLIAQSHY
VGKVHAKKLKQLMEEHDQASPSGFQPEMAFSMRTYVCHICSIAFTSLDMFRSHMQGSEHQIKESIVINLV
KNSRKTQDSYQNECADYINVQKARGLEAKTCFRKMEESSLETRRYREVVDSRPRHRMFEQRLPFETFRTY
AAPYNISQAMEKQLPHSKKTYDSFQDELEDYIKVQKARGLDPKTCFRKMRENSVDTHGYREMVDSGPRSR
MCEQRFSHEASQTYQRPYHISPVESQLPQWLPTHSKRTYDSFQDELEDYIKVQKARGLEPKTCFRKIGDS
SVETHRNREMVDVRPRHRMLEQKLPCETFQTYSGPYSISQVVENQLPHCLPAHDSKQRLDSISYCQLTRD
CFPEKPVPLSLNQQENNSGSYSVESEVYKHLSSENNTADHQAGHKQKHQKRKRHLEEGKERPEKEQSKHK
RKKSYEDTDLDKDKSIRQRKREEDRVKVSSGKLKHRKKKKSHDVPSEKEERKHRKEKKKSVEERTEEEML
WDESILGF

XP_375099. Reports PREDICTED: hypoth...[gi:42660332] BLink, Links

- Previous sequence
- Next sequence

>gi|42660332|ref|XP_375099.1| PREDICTED: hypothetical protein [Homo sapiens]
MYKKQLLYADKADGVFDISSRQQHLKVFQETAKLFSRVFVPFYVSTSNIQVDLTLSPKLECTGMILAHCN
LCLLGSGDSPTSASPVAGTTGMHQFLYF

NP_060313. Reports breast carcinoma ...[gi:58294160] BLink, Links

- Previous sequence
- Next sequence

>gi|58294160|ref|NP_060313.3| breast carcinoma amplified sequence 4 isoform a [Homo
sapiens]
MQRTGGGAPRPGRNHGLPGSLRQPDPVALLMLLVDADQPEPMRSGARELALFLTPEPGAEAKEVEETIEG
MLLRLEEFCSLADLIRSDTSQILEENIPVLKAKLTEMRGIYAKVDRLEAFVKMVGHHVAFLEADVLQAER
DHGAFPQALRRWLGSAGLPSFRNVECSGTIPARCNLRLPGSSDSPASASQVAGITEVTCTGARDVRAAHT
V

: NP_683685. Reports mitochondrial rib...[gi:22547125] BLink, Conserved Domains, Links

- Previous sequence

- Next sequence

>gi|22547125|ref|NP_683685.1| mitochondrial ribosomal protein L10 isoform b [Homo sapiens]
MISAHCNLHLPGSSDSPASASQVAGITGRLPTLQTVRYGSKAVTRHRRVMHFQRQKLMAVTEYIPPKPAI
HPSCLPSPPSPPQEEIGLIRLLRREIAAVFQDNRMIAVCQNVALSAEDKLLMRHQLRKHKILMKVFPNQV
LKPFLEDSKYQNLLPLFVGHNMLLVSEEPKVKEMVRILRTVPFLPLLGGCIDDTILSRQGFINYSKLPSL
PLVQGELVGGLTCLTAQTHSLLQHQPLQLTTLLDQYIREQREKDSVMSANGKPDPDTVPDS

: NP_001003690. Reports MAD2L1 binding pr...[gi:51243063] BLink, Links

- Previous sequence
- Next sequence

>gi|51243063|ref|NP_001003690.1| MAD2L1 binding protein isoform 1 [Homo sapiens]
MARVPLGRSLTLSPRLEHNGMTSAHHNFRLPGSRDSPASASQVAEIIDLEWYEKSEETHASQIELLETSS
TQEPLNASEAFCPRDCMVPVVFPGPVSQEGCCQFTCELLKHIMYQRQQLPLPYEQLKHFYRKPSPQAEEM
LKKKPRATTEVSSRKCQQALAELESVLSHLEDFFARTLVPRVLILLGGNALSPKEFYELDLSLLAPYSVD
QSLSTAACLRRLFRAIFMADAFSELQAPPLMGTVVMAQGHRNCGEDWFRPKLNYRVPSRGHKLTVTLSCG
RPSIRTTAWEDYIWFQAPVTFKGFRE

: NP_056087. Reports hypothetical prot...[gi:56119090] BLink, Conserved Domains, Links

- Previous sequence
- Next sequence

>gi|56119090|ref|NP_056087.1| hypothetical protein LOC23322 [Homo sapiens]
MSGPTDETAGDLPVKDTGLNLFGMGGLQETSTTRTMKSRQAVSRVSREELEDRFLRLHDENILLKQHARK
QEDKIKRMATKLIRLVNDKKRYERVGGGPKRLGRDVEMEEMIEQLQEKVHELEKQNETLKNRLISAKQQL
QTQGYRQTPYNNVQSRINTGRRKANENAGLQECPRKGIKFQDADVAETPHPMFTKYGNSLLEEARGEIRN
LENVIQSQRGQIEELEHLAEILKTQLRRKENEIELSLLQLREQQATDQRSNIRDNVEMIKLHKQLVEKSN
ALSAMEGKFIQLQEKQRTLRISHDALMANGDELNMQLKEQRLKCCSLEKQLHSMKFSERRIEELQDRIND
LEKERELLKENYDKLYDSAFSAAHEEQWKLKEQQLKVQIAQLETALKSDLTDKTEILDRLKTERDQNEKL
VQENRELQLQYLEQKQQLDELKKRIKLYNQENDINADELSEALLLIKAQKEQKNGDLSFLVKVDSEINKD
LERSMRELQATHAETVQELEKTRNMLIMQHKINKDYQMEVEAVTRKMENLQQDYELKVEQYVHLLDIRAA
RIHKLEAQLKDIAYDTKQYKFKPEIMPDDSVDEFGETIHLERGENLFEIHINKVTFSSEVLQASGDKEPV
TFCTYAFYDFELQTTPVVRGLHPEYNFTSQYLVHVNDLFLQYIQKNTITLEVHQAYSTEYETIAACQLKF
HEILEKSGRIFCTASLIGTKGDIPNFGTVEYWFRLRVPMDQAIRLYRERAKALGYITSNFKGPEHMQSLS
QQAPKTAQLSSTDSTDGNLNELHITIRCCNHLQSRASHLQPHPYVVYKFFDFADHDTAIIPSSNDPQFDD
HMYFPVPMNMDLDRYLKSESLSFYVFDDSDTQENIYIGKVNVPLISLAHDRCISGIFELTDHQKHPAGTI
HVILKWKFAYLPPSGSITTEDLGNFIRSEEPEVVQRLPPASSVSTLVLAPRPKPRQRLTPVDKKVSFVDI
MPHQSDETSPPLEDRKEISPEVEHIPEIEINMLTVPHVPKVSQEGSVDEVKENTEKMQQGKDDVSLLSEG
QLAEQSLASSEDETEITEDLEPEVEEDMSASDSDDCIIPGPISKNIKQSLALSPGLGCSSAISAHCNFRL
PGSSDFPASASQVDGITGACHHSQPSEKIRIEIIALSLNDSQVTMDDTIQRLFVECRFYSLPAEETPVSL
PKPKSGQWVYYNYSNVIYVDKENNKAKRDILKAILQKQEMPNRSLRFTVVSDPPEDEQDLECEDIGVAHV
DLADMFQEGRDLIEQNIDVFDARADGEGIGKLRVTVEALHALQSVYKQYRDDLEA

: XP_293581. Reports PREDICTED: simila...[gi:88965894] BLink, Conserved Domains, Links

- Previous sequence
- Next sequence

>gi|88965894|ref|XP_293581.5| PREDICTED: similar to tissue-type vomeronasal neurons putative pheromone receptor V2R2 [Homo sapiens]
MTVILNWKRTQKHENDWFVKAVGKQQAESPGMRHKFLAFLWAELGSEAKEEKEEERTCRLLGKCVDAENH
SLVIGGLFPIDSRTIPANESILEPASAKCEGFNFQRFRWMKAMIHMIKEINKRKDILPNITLGYQIFDTC
FTISKSVEAVLVFLTGQEENRPNFRNSTGAFPAGIVGAGGSFLSVPASRILGLYYLPQVGYTSTCVILSD
KYQFPSYLRVIASDKIQSKAVVKRIQHFHFLTLSPRLECSGAILAHGNLCLPVETGFCHVAQAGLEFLAS
NYLTASASQSAGITGVSHCAWPSTIELWIIQFHIYFRMNCRVTTESRSVAMLEYSGEISAHCHLCLLGSS
NSPASAPLVAGTTGAHHHAQLIFVFLVETGFHHVSQDGLDLSISFPIQCVLMCVLLGLGRGFVQREPICC
FDSIPCADGHVSRKPGERECEQCGEDYWSNAQKSECVLKEVEYLAYDEALGFTLVILSVFGAFVVLAVTA
VYVIHRHTPLVNASDWQLGFLIQVSLIIMLLSSMLFIDKPHNWSCMAGQVTLALGFSLCLSCLLGKTSSL
FLAYRISKSKTQLTSMHPLYRKIIVLISVLAEIGICTAYLILEPPMVYKNMESQNTKIILGCNEISIEFL
YSMFGIDAFLALLCFLTTFVARQLPDNYYEGKCITFGMLVFFIIWMSFVPVYLSTKGKFKMAVEIFAILA
SSHGLLGCIFAPKCLIILLRPERNTSEIVCGRVSTTDNCIQLTSAFVSSELNNTTVSTVLDDRVLIYMCP
LKLQ

: XP_946327. Reports PREDICTED: simila...[gi:88971234] BLink, Conserved Domains, Links

- Previous sequence
- Next sequence

>gi|88971234|ref|XP_946327.1| PREDICTED: similar to tissue-type vomeronasal neurons putative pheromone receptor V2R2 [Homo sapiens]
MGSCISQDQQAESPGMRHKFLAFLWAELGSEAKEEKEEERTCRLLGKCVDAENHSLVIGGLFPIDSRTIP
ANESILEPASAKCEGFNFQRFRWMKAMIHMIKEINKRKDILPNITLGYQIFDTCFTISKSVEAVLVFLTG
QEENRPNFRNSTGAFPAGIVGAGGSFLSVPASRILGLYYLPQVGYTSTCVILSDKYQFPSYLRVIASDKI
QSKAVVKRIQHFHFLTLSPRLECSGAILAHGNLRLPVETGFCHVAQAGLEFLASNYLTASASQSAGITGV
SHCAWPSTIELWIIQFHIYFRMNCRVTTESRSVAMLEYSGEISAHCHLCLLGSSNSPASAPLVAGTTGAH
HHAQLIFVFLVETGFHHVSQDGLDLSISFPIQCVLMCVLLGLGRGFVQREPICCFDSIPCADGHVSRKPG
ERECEQCGEDYWSNAQKSECVLKEVEYLAYDEALGFTLVILSVFGAFVVLAVTAVYVIHRHTPLVNASDW
QLGFLIQVSLIIMLLSSMLFIDKPHNWSCMAGQVTLALGFSLCLSCLLGKTSSLFLAYRISKSKTQLTSM
HPLYRKIIVLISVLAEIGICTAYLILEPPMVYKNMESQNTKIILGCNEISIEFLYSMFGIDAFLALLCFL
TTFVARQLPDNYYEGKCITFGMLVFFIIWMSFVPVYLSTKGKFKMAVEIFAILASSHGLLGCIFAPKCLI
ILLRPERNTSEIVCGRVSTTDNCIQLTSAFVSSELNNTTVSTVLDDRVLIYMCPLKLQ

: NP_777547. Reports intraflagellar tr...[gi:28372523] BLink, Links

- Previous sequence
- Next sequence

>gi|28372523|ref|NP_777547.1| intraflagellar transport protein IFT20 [Homo sapiens]
MAKDILGEAGLHFDELNKLRVLDPEVTQQTIELKEECKDFVDKIGQFQKIVGGLIELVDQLAKEAENEKM
KSLAVSPRLECTGAISAHCKLCLSDSSDSPTSPSRVGGTTGHRCSELAQIYSKAERSSTAATSSPNSRKE
NAARKVSG

: NP_001004345. Reports hypothetical prot...[gi:51972262] BLink, Links

- Previous sequence
- Next sequence

>gi|51972262|ref|NP_001004345.1| hypothetical protein LOC440867 [Homo sapiens]
MKGPCPHLPPPLSSCIMNETAASLLPEVLHFRLGCNGSISAQCNLCFPGSSDSPASASQAAVNTGWSAVV
LCLEFVPAVGFVVLLTSRMKPRTFTRNITLYGCTTVCLSILQVKDMWVVPSAG

: NP_659411. Reports coiled-coil domai...[gi:21699054] BLink, Conserved Domains, Links

- Previous sequence
- Next sequence

>gi|21699054|ref|NP_659411.1| coiled-coil domain containing 122 [Homo sapiens]
MSDNKERKSQGFPKEDNQDTSSLADAVEKVAKQQQSQASEIEKNKKVLFNLKNELHELEKEIAAISAETK
ETERQIYQQDSAIENTKLHCDSLETQIKSLHSENVKLKFDIETAQEDFEEHMIKYNAYYAKIKAHKNSLG
EVESKWSFMTELHEKRDFVKKLKTMKEELMQDLQNPGGNRITQVQEDITNLKDKIITVKESIIEKTCFLE
EEKKTHEKLRKEIEGLAPSPRLECSSAISAHCKLCLPGSRHSPASASGVAGTTGACHHTQLIFCIFSRDG
VSPC

: NP_001013702. Reports hypothetical prot...[gi:61966807] BLink, Links

- Previous sequence
- Next sequence

>gi|61966807|ref|NP_001013702.1| hypothetical protein LOC401233 [Homo sapiens]
MSDPQTEELKVKFYRDNQGHLKGDRLCDHWKREAVDLAFMHLDEDDTGNCTLQVEVAKYQRNGKYEASGR
KCANHRKAPSLRQKRPRRSPSKRRDTSELSSSNTFHPVDFEDGQRRPSRRVKFGPTRRLIVFDRHPAGEP
VSWRNAGAAAHCIQTFDGLIPSPKAGVQWCDLSSLQPLPPSSSDSLTSASQVPGTADVCHHTWLIFFFFY
RVGVSPCCPGWPQTAELKQSAHLSLQKCWDSRWEPSRLAIFKKSLALSPRLECSGAISAHCKLCFPASRH
SPASASRVAGTAGARHQTRLNICIFGRDGVSLCWPGWSRSATSALWEAQGGKIT

: NP_001012677. Reports arginine-fifty ho...[gi:61969666] BLink, Conserved Domains, Links

- Previous sequence
- Next sequence

>gi|61969666|ref|NP_001012677.1| arginine-fifty homeobox [Homo sapiens]
MRNRMAPENPQPDPFINRNYSNMKVIPPQDPASPSFTLLSKLECSGTVSAYCSLNLPGSTDPPTSASRVA
ATTAIRRRHKERTSFTHQQYEELEALFSQTMFPDRNLQEKLALRLDLPESTVKVWFRNRRFKLKKQQQQQ
SAKQRNQILPSKKNVPTSPRTSPSPYAFSPVISDFYSSLPSQPLDPSNWAWNSTFTESSTSDFQMQDTQW
ERLVASVPALYSDAYDIFQIIELYNLPDENEISSSSFHCLYQYLSPTKYQVGGQGSSLSIFAGPAVGLSP
AQTWPNMTSQAFEAYSLTDSLEFQKTSNMVDLGFL

: NP_612412. Reports myosin light chai...[gi:34147532] BLink, Conserved Domains, Links

- Previous sequence
- Next sequence

```
>gi|34147532|ref|NP_612412.2| myosin light chain 2, precursor lymphocyte-specific
[Homo sapiens]
MLLRLVSNSWPQVILPPRPPKVLGLQAPRRARKRAEGTASSNVFSMFDQSQIQEFKESLALSPRLERNGM
ISAHCNLCLTGSSNSPASASQAFTIMDQNRDGFIDKEDLRDTFAALGRINVKNEELEAMVKEAPGPINFT
VFLTMFGEKLKGTDPEETILHAFKVFDTEGKGFVKADVIKEKLMTQADRFSEEEVKQMFAAFPPDVCGNL
DYRNLCYVITHGEEKD
```

: XP_209640. Reports PREDICTED: hypoth...[gi:27480484] BLink, Links

- Previous sequence
- Next sequence

```
>gi|27480484|ref|XP_209640.1| PREDICTED: hypothetical protein [Homo sapiens]
MKDEVLNLNSQLLYAIWKKVKLECSGPILAHCNLCLLGSRHPSTSASQVAGTTGEKTMRSARMMDCHHWG
TGKGLSKSMYVFQSLQNVSDSLKYIFSKCQIQALSTVQF
```

: NP_001003811. Reports testis expressed ...[gi:51477721] BLink, Links

- Previous sequence
- Next sequence

```
>gi|51477721|ref|NP_001003811.1| testis expressed sequence 11 isoform 1 [Homo sapiens]
MISAHCNLRLLCSSDSSASASQVAGTTEVVENLVTNDNSPNIPEAIDRLFSDIANINRESMAEITDIQIE
EMAVNLWNWALTIGGGWLVNEEQKIRLHYVACKLLSMCEASFASEQSIQRLIMMNMRIGKEWLDAGNFLI
ADECFQAAVASLEQLYVKLIQRSSPEADLTMEKITVESDHFRVLSYQAESAVAQGDFQRASMCVLQCKDM
LMRLPQMTSSLHHLCYNFGVETQKNNKYEESSFWLSQSYDIGKMDKKSTGPEMLAKVLRLLATNYLDWDD
TKYYDKALNAVNLANKEHLSSPGLFLKMKILLKGETSNEELLEAVMEILHLDMPLDFCLNIAKLLMDHER
ESVGFHFLTIIHERFKSSENIGKVLILHTDMLLQRKEELLAKEKIEEIFLAHQTGRQLTAESMNWLHNIL
WRQAASSFEVQNYTDALQWYYYSLRFYSTDEMDLDFTKLQRNMACCYLNLQQLDKAKEAVAEAERHDPRN
VFTQFYIFKIAVIEGNSERALQAIITLENILTDEESEDNDLVAERGSPTMLLSLAAQFALENGQQIVAEK
ALEYLAQHSEDQEQVLTAVKCLLRFLLPKIAEMPESEDKKKEMDRLLTCLNRAFVKLSQPFGEEALSLES
RANEAQWFRKTAWNLAVQCDKDPVMMREFFILSYKMSQFCPSDQVILIARKTCLLMAVAVDLEQGRKAST
AFEQTMFLSRALEEIQTCNDIHNFLKQTGTFSNDSCEKLLLLYEFEVRAKLNDPLLESFLESVWELPHLE
TKTFETIAIIAMEKPAHYPLIALKALKKALLLYKKEEPIDISQYSKCMHNLVNLSVPDGASNVELCPLEE
VWGYFEDALSHISRTKDYPEMEILWLMVKSWNTGVLMFSRSKYASAEKWCGLALRFLNHLTSFKESYETQ
MNMLYSQLVEALSNNKGPVFHEHGYWSKSD
```

: NP_001030127. Reports sorbin and SH3 do...[gi:78000165] BLink, Conserved Domains, Links

- Previous sequence
- Next sequence

```
>gi|78000165|ref|NP_001030127.1| sorbin and SH3 domain containing 1 isoform 4 [Homo
sapiens]
MSSECDGGSKAVMNGLAPGSNGQDKATADPLRARSISAVKIIPVKTVKNASGLVLPTDMDPTKICTGKGA
VTLRASSSYRETPSSSPASPQETRQHESKPGLEPEPSSADEWRLSSSADANGNAQPSSLAAKGYRSVHPN
LPSDKSQDATSSSAAQPEVIVVPLYLVNTDRGQEGTARPPTPLGPLGCVPTIPATASAASPLTFPTLDDF
TPPHLQRWPHHSQPARASGSFAPTSQTPPSFSPPPPLVPPAPEDLRRVSEPDLTGAVSSTDSSPLLNEVS
SSLIGTDSQAFPSVSKPSSAYPSTTIVNPTIVLLQHNREQQKRLSSLSDPVSERRVGEQDSAPTQEKPTS
PGKAIEKRAKDDSRRVVKSTQDLSDVSMDEVGIPLRNTERSKDWYKTMFKQIHKLNRDTPEENPYFPTYK
FPELPEIQQTSEETKSCSVMSPRLECSGTVIAHCSLKLLDSSNPPTSASQVAGTADDDSDLYSPRYSFSE
DTKSPLSVPRSKSEMSYIDGEKVVKRSATLPLPARSSSLKSSSERNDWEPPDKKVDTRKYRAEPKSIYEY
QPGKSSVLTNEKMSRDISPEEIDLKNEPWYKFFSELEFGKPPPKKIWDYTPGDCSILPREDRKTNLDKDL
SLCQTELEADLEKMETLNKAPSANVPQSSAISPTPEISSETPGYIYSSNFHAVKRESDGAPGDLTSLENE
RQIYKSVLEGGDIPLQGLSGLKRPSSSASTKDSESPRHFIPADYLESTEEFIRRRHDDKEKLLADQRRLK
REQEEADIAARRHTGVIPTHHQFITNERFGDLLNIDDTAKRKSGSEMRPARAKFDFKAQTLKELPLQKGD
IVYIYKQIDQNWYEGEHHGRVGIFPRTYIELLPPAEKAQPKKLTPVQVLEYGEAIAKFNFNGDTQVEMSF
RKGERITLLRQVDENWYEGRIPGTSRQGIFPITYVDVIKRPLVKNPVDYMDLPFSSSPSRSATASPQPWR
EESGQYERKAERGAGERGPGGPKISKKSCLKPSDVVRCLSTEQRLSDLNTPEESRPGKPLGSAFPGSEAE
QTERHRGGEQAGRKAARRGGSQQPQAQQRRVTPDRSQTSQDLFSYQALYSYIPQNDDELELRDGDIVDVM
EKCDDGWFVGTSRRTKQFGTFPGNYVKPLYL
```

: NP_001009923. Reports hypothetical prot...[gi:58331120] BLink, Conserved Domains, Links

- Previous sequence
- Next sequence

>gi|58331120|ref|NP_001009923.1| hypothetical protein LOC29058 isoform 1 [Homo sapiens]
MQPWALPTVGELWVCGRPGAALRWSLVLSPRLEPSGVISAHCNLHLLASSDSSASASRLCQRVMMPSRTN
LATGIPSSKVKYSRLSSTDDGYIDLQFKKTPPKIPYKAIALATVLFLIGAFLIIIGSLLLSGYISKGGAD
RAVPVLIIGILVFLPGFYHLRIAYYASKGYRGYSYDDIPDFDD

: NP_001012414. Reports tripartite motif-...[gi:60099474] BLink, Conserved Domains, Links

- Previous sequence
- Next sequence

>gi|60099474|ref|NP_001012414.1| tripartite motif-containing 61 [Homo sapiens]
MEFVTALADLRAEASCPICLDYLKDPVTISCGHNFCLSCIIMSWKDLHDSFPCPFCHFCCPERKFISNPQ
LGSLTEIAKQLQIRSKKRKRQEEKHVCKKHNQVLTFFCQKDLELLCPRCSLSTDHQHHCVWPIKKAASYH
RKKLEEYNAPWKERVELIEKVITMQTRKSLELKKKMESPSVTRLECSCTISAHFNLRLPGSSDSSASGS

: NP_113661. Reports carnitine deficie...[gi:34147403] BLink, Conserved Domains, Links

- Previous sequence
- Next sequence

>gi|34147403|ref|NP_113661.2| carnitine deficiency-associated, expressed in ventricle 1 isoform 2 [Homo sapiens]
MSDQIKFIMDSLNKEPFRKNYNLITFDSLEPMQLLQVLSDVLAEIDPKQLVDIREEMPEQTAKRMLSLLG
ILKYKPSGNATDMSTFRQGLVIGSKPVIYPVLHWLLQRTNELKKRAYLARFLIKLEVPSEFLQDETVADT
NKQYEELMEAFKTLHKEYEQLKISGFSTAEIRKDISAMEEEKDQLIKRVEHLKKRVETAQNHQWMLKIAR
QLRVEKEREEYLAQQKQEQKNQLFHAVQRLQRVQNQLKSMRQAAADAKPESLMKRLEEEIKFNLYMVTEK
FPKELENKKKELHFLQKVVSEPAMGHSDLLELESKINEINTEINQLIEKKMMRNEPIEGKLSLYRQQASI
ISRKKEAKAEELQEAKEKLASLEREASVKRNQTREFDGTEVLKGDERQDLTLSPRLECGGVIMAYCSLKL
LGSSDPPTSAS

: XP_001126811. Reports PREDICTED: hypoth...[gi:113421662] BLink, Links

- Previous sequence
- Next sequence

>gi|113421662|ref|XP_001126811.1| PREDICTED: hypothetical protein [Homo sapiens]
MCIQKQNHIPAAVSFDALRKLQRPKLFPEKRSFTGVPALSIDFTNGCDLVGSSSLHNMLVCSSYDINRQD
TFQKDRQRVGPSGASQKTEGFLLRLLYSGLIIAHCSLEILGRNDPPASASKVAETTDSGSLSLANT

: NP_689623. Reports PARK2 co-regulate...[gi:22748869] BLink, Links

- Previous sequence
- Next sequence

>gi|22748869|ref|NP_689623.1| PARK2 co-regulated [Homo sapiens]
MVAEKETLSLNKCPDKMPKRTKLLAQQPLPVHQPHSLVSEGFTVKAMMKNSVVRGPPAAGAFKERPTKPT
AFRKFYERGDFPIALEHDSKGNRIAWKVEIEKLDYHHYLPLFFDGLCEMTFPYEFFARQGIHDMLEHGGN
KILPVLPQLIIPIKNALNLRNRQVICVTLKVLQHLVVSAEMVGKALVPYYRQILPVLNIFKNMNGSYSLP
RLECSGAIMARCNLDHLGSSDPPTSASQVAEIIVNSGDGIDYSQQKRENIGDLIQETLEAFERYGGENAF
INIKYVVPTYESCLLN

: NP_660326. Reports nucleoredoxin [Ho...[gi:21699084] BLink, Conserved Domains, Links

- Previous sequence
- Next sequence

>gi|21699084|ref|NP_660326.1| nucleoredoxin [Homo sapiens]
MVDILGERHLVTCKGATVEAEAALQNKVVALYFAAARCAPSRDFTPLLCDFYTALVAEARRPAPFEVVFV
SADGSCQEMLDFMRELHGAWLALPFHDPYRQRSLALLPRLECSGVILAHCNLCLLGSSDSLALAS

: NP_116094. Reports hypothetical prot...[gi:109627668] BLink, Links

- Previous sequence
- Next sequence

>gi|109627668|ref|NP_116094.2| hypothetical protein LOC84791 [Homo sapiens]
MDKKSTHRNPEDARAGKYEGKHKRKKRRKQNQNQHRSRHRSVTSFSSDDPMFPSSSSSSSGSQTDSSIED
AAKGKIKKKRREKTNKWEKRKSLVLLLRLECNDATSAHCNLCLPDSSNSPATAS

: NP_001012681. Reports solute carrier fa...[gi:61744479] BLink, Conserved Domains, Links

- Previous sequence
- Next sequence

>gi|61744479|ref|NP_001012681.1| solute carrier family 3 (activators of dibasic and neutral amino acid transport), member 2 isoform d [Homo sapiens]
MELQPPEASIAVVSIPRQLPGSHSEAGVQGLSAGDDSETGSDCVTQAGLQLLASSDPPALASKNAEVTGT
MSQDTEVDMKEVELNELEPEKQPMNAASGAAMSLAGAEKNGLVKIKVAEDEAEAAAAAKFTGLSKEELLK
VAGSPGWVRTRWALLLLFWLGWLGMLAGAVVIIVRAPRCRELPAQKWWHTGALYRIGDLQAFQGHGAGNL
AGLKGRLDYLSSLKVKGLVLGPIHKNQKDDVAQTDLLQIDPNFGSKEDFDSLLQSAKKKSIRVILDLTPN
YRGENSWFSTQVDTVATKVKDALEFWLQAGVDGFQVRDIENLKDASSFLAEWQNITKGFSEDRLLIAGTN
SSDLQQILSLLESNKDLLLTSSYLSDSGSTGEHTKSLVTQYLNATGNRWCSWSLSQARLLTSFLPAQLLR
LYQLMLFTLPGTPVFSYGDEIGLDAAALPGQPMEAPVMLWDESSFPDIPGAVSANMTVKGQSEDPGSLLS
LFRRLSDQRSKERSLLHGDFHAFSAGPGLFSYIRHWDQNERFLVVLNFGDVGLSAGLQASDLPASASLPA
KADLLLSTQPGREEGSPLELERLKLEPHEGLLLRFPYAA

: XP_001130807. Reports PREDICTED: hypoth...[gi:113421909] BLink, Links

- Previous sequence
- Next sequence

>gi|113421909|ref|XP_001130807.1| PREDICTED: hypothetical protein [Homo sapiens]
MSVQTAQTQPAIYRSRVALNTLSHNANHKWGQLRVWWEKPSCSSEIHKVEIAVAPTPLLWRLPSRIWEPA
RDLTAAHWTPEDTQRLECYVAMSARCNPCFLSSCDPPASASQVAGIRGGEERKTFWCGLGSNSLEGETAR
VWRGGHPWRDPF

: NP_001038943. Reports hypothetical prot...[gi:113865935] BLink, Links

- Previous sequence
- Next sequence

>gi|113865935|ref|NP_001038943.1| hypothetical protein LOC644997 [Homo sapiens]
MPSQSACPVLSTAPGTPCDLRKHLLNMVSEEKRSPQLSAKTWRRGLRLQKRRNALFLPEGDICVVGSTSG
ARALIPETSKLERSGTVIAYCNLELLASSDPPVWASQSTGMTGMSYRSQPQLGFKSTPPAHSSVFHHSVK
APKEDQAQEAASRPLTSQDGWNPNIKK

: NP_001034843. Reports hypothetical prot...[gi:89886187] BLink, Links

- Previous sequence
- Next sequence

>gi|89886187|ref|NP_001034843.1| hypothetical protein LOC441212 [Homo sapiens]
MISAHRDLRLPGSSDSPASVFPSGWDYRHAPLCLANFVFLVEAGFLHVGQSGLELPASGDPPASASQSAG
ITGVSHRDGLLCFNFLTSPLTHGLVTHVLFSFYILDSSNFLILLLCNLSPS

: XP_944216. Reports PREDICTED: hypoth...[gi:89030285] BLink, Links

- Previous sequence
- Next sequence

>gi|89030285|ref|XP_944216.1| PREDICTED: hypothetical protein [Homo sapiens]
MSKHFLACKVRVFPRPPRAQGCPGPEPQLGRCNCTWEHGGSMVLASRQLGKVQGSCLFLAPAGSVKHAGR
TAPPPLQLALSQWPLQRGHHCHQKFAVSPRLECSGAIKAHHGLERLRSTDIPDLASPVTRTTAILFCSRT
IAGELMQLFDGPRHSSALLG

: XP_376822. Reports PREDICTED: hypoth...[gi:42659177] BLink, Links

- Previous sequence
- Next sequence

>gi|42659177|ref|XP_376822.1| PREDICTED: hypothetical protein [Homo sapiens]
MSKHFLACKVRVFPRPPRAQGCPGPEPQLGRCNCTWEHGGSMVLASRQLCKVQGSCLFLAPAGSVKHAGR
TAPPPLQLALSQWPLQRGHHCHQKFAVSPRLECSGAIKAHHGLERLRSTDIPDLASPVTRTTAILFCSRT
IAGELMQLFDGPRHSSALLG

: NP_777603. Reports hypothetical prot...[gi:28212280] BLink, Links

- Previous sequence
- Next sequence

>gi|28212280|ref|NP_777603.1| hypothetical protein LOC283579 [Homo sapiens]
MGREMKKTGTPRPFRIEDPNQQPTWHDQPEMGSHYFAQAGLELLGSSNPPASASQSAGITGVSHCARPGE
HDLNHTVFQVKDSTFLRHLESDRPEFKSCLPPHFTEPSVSLSTSEGCEDAMG

: NP_001034848. Reports hypothetical prot...[gi:89886193] BLink, Links

- Previous sequence
- Next sequence

>gi|89886193|ref|NP_001034848.1| hypothetical protein LOC642484 [Homo sapiens]
MVTGPCLTCVSSLIERASPNHPTNKGLTLLPWLECSGPIIAHCSLDFPASVDPPTLISRVAGTAGLLILR
FSSASANPETARPIPPLPCPPPRLLHMKTTRMKTFMMIHFHLMNKLQEIIQEERHGGMLESLLSLKVGNP
GSCSCSH

BLink, Conserved Domains, Links

: NP_598400. Reports mitochondrial tra...[gi:19882217]

- Previous sequence
- Next sequence

>gi|19882217|ref|NP_598400.1| mitochondrial translation optimization 1 homolog isoform a [Homo sapiens]
MFYFRGCGRWVAVSFTKQQFPLARLSSDSAAPRTPHFDVIVIGGGHAGTEAATAAARCGSRTLLLTHRVD
TIGQMSCNPSFGGIGKGHLMREVDALDGLCSRICDQSGVHYKVLNRRKGPAVWGLRAQIDRKLYKQNMQK
EILNTPLLTVQEGAVEDLILTEPEPEHTGKCRVSGVVLVDGSTVYAESVILTTGTFLRGMIVIGLETHPA
GRLGDQPSIGLAQTLEKLGFVVGRLKTGTPPRIAKESINFSILNKHIPDNPSIPFSFTNETVWIKPEDQL
PCYLTHTNPRVDEIVLKNLHLNSHVKETTRGPRYCPSIESKVLRFPNRLHQVWLEPEGMDSDLIYPQGLS
MTLPAELQEKMITCIRGLEKAKVIQPDGVLLLLPRMECNGAISAHHNLPLPGYGVQYDYLDPRQITPSLE
THLVQRLFFAGQINGTTGYEEAAAQGVIAGINASLRVSRKPPFVVSRTEGYIGVLIDDLTTLGTSEPYRM
FTSRVEFRLSLRPDNADSRLTLRGYKDAGCVSQQRYERACWMKSSLEEGISVLKSIEFLSSKWKKLIPEA
SISTSRSLPVRALDVLKYEEVDMDSLAKAVPEPLKKYTKCRELAERLKIEATYESVLFHQLQEIKGVQQD
EALQLPKDLDYLTIRDVSLSHEVREKLHFSRPQTIGAASRIPGVTPAAIINLLRFVKTTQRRQSAMNESS
KTDQYLCDADRLQEREL

BLink, Conserved Domains, Links

: NP_003675. Reports MAP kinase intera...[gi:21361101]

- Previous sequence
- Next sequence

>gi|21361101|ref|NP_003675.2| MAP kinase interacting serine/threonine kinase 1 isoform 1 [Homo sapiens]
MVSSQKLEKPIEMGSSEPLPIADGDRRRKKKRRGRATDSLPGKFEDMYKLTSELLGEGAYAKVQGAVSLQ
NGKEYAVKIIEKQAGHSRSRVFREVETLYQCQGNKNILELIEFFEDDTRFYLVFEKLQGGSILAHIQKQK
HFNEREASRVVRDVAAALDFLHTKDKVSLCHLGWSAMAPSGLTAAPTSLGSSDPPTSASQVAGTTGIAHR
DLKPENILCESPEKVSPVKICDFDLGSGMKLNNSCTPITTPELTTPCGSAEYMAPEVVEVFTDQATFYDK
RCDLWSLGVVLYIMLSGYPPFVGHCGADCGWDRGEVCRVCQNKLFESIQEGKYEFPDKDWAHISSEAKDL
ISKLLVRDAKQRLSAAQVLQHPWVQGQAPEKGLPTPQVLQRNSSTMDLTLFAAEAIALNRQLSQHEENEL
AEEPEALADGLCSMKLSPPCKSRLARRRALAQAGRGEDRSPPTAL

BLink, Conserved Domains, Links

: NP_660344. Reports hypothetical prot...[gi:21945058]

- Previous sequence
- Next sequence

>gi|21945058|ref|NP_660344.1| hypothetical protein LOC201158 [Homo sapiens]
MLQQDSNDDTEAVSLFDAEEETTNRPRKAKIRHPVASFFHLFFRVSAIIVCLLCELLSSSFITCMVTIIL
LLSCDFWAVKNVTGRLMVGLRWWNHIDEDGKSHWVFESRKESSQENKTVSEAESRIFWLGLIACSVLWVI
FAFSALFSFTVKWLRRSRHIAQTGLKVLGSRDPPASAFQSAGITGVSRCPGHPSSKFHQVDINSFTRITD
RALYWKPAPRLSSPPLRAAPGNCQQMAPARLFLSLRLWAWRGGGESPNSRGTGEPGPKFHLASGMH

BLink, Conserved Domains, Links

: NP_060190. Reports signal-transducin...[gi:62243734]

- Previous sequence
- Next sequence

>gi|62243734|ref|NP_060190.2| signal-transducing adaptor protein-2 isoform 1 [Homo sapiens]
MASALRPPRVPKPKGVLPSHYYESFLEKKGPCDRDYKKFWAGLQGLTIYFYNSNRDFQHVEKLNLGAFEK
LTDEIPWGSSRDPGTHFSLILRDQEIKFKVETLECREMWKGFILTVVELRVPTDLTLLPGHLYMMSEVLA
KEEARRALETPSCFLKVSRLEAQLLLERYPECGNLLLRPSGDGADGVSVTTRQMHNGTHVVRHYKVKREG
PKYVIDVEQPFSCTSLDAVVNYFVSHTKKALVPFLLDEDYEKVLGYVEADKENGENVWVAPSAPGPGPAP
CTGGPKPLSPASSQDKLPPLPPLPNQEENYVTPIGDGPAVDYENQDVASSSWPVILKPKKLPKPPAKLPK
PPVGPKPVEKGFHHVAQAGLELLTSSDPPTSASQSAGITGVSHHTWPHLSSLPEPKVFNGGLGRKLPVSS
AQPLFPTAGLADMTAELQKKLEKRRALEH

BLink, Conserved Domains, Links

: NP_002385. Reports solute carrier fa...[gi:65506891]

- Previous sequence
- Next sequence

>gi|65506891|ref|NP_002385.3| solute carrier family 3 (activators of dibasic and neutral amino acid transport), member 2 isoform c [Homo sapiens]
MELQPPEASIAVVSIPRQLPGSHSEAGVQGLSAGDDSELGSHCVAQTGLELLASGDPLPSASQNAEMIET
GSDCVTQAGLQLLASSDPPALASKNAEVTGTMSQDTEVDMKEVELNELEPEKQPMNAASGAAMSLAGAEK
NGLVKIKVAEDEAEAAAAAAKFTGLSKEELLKVAGSPGWVRTRWALLLLFWLGWLGMLAGAVVIIVRAPRC
RELPAQKWWHTGALYRIGDLQAFQGHGAGNLAGLKGRLDYLSSLKVKGLVLGPIHKNQKDDVAQTDLLQI
DPNFGSKEDFDSLLQSAKKKSIRVILDLTPNYRGENSWFSTQVDTVATKVKDALEFWLQAGVDGFQVRDI
ENLKDASSFLAEWQNITKGFSEDRLLIAGTNSSDLQQILSLLESNKDLLLTSSYLSDSGSTGEHTKSLVT
QYLNATGNRWCSWSLSQARLLTSFLPAQLLRLYQLMLFTLPGTPVFSYGDEIGLDAAALPGQPMEAPVML
WDESSFPDIPGAVSANMTVKGQSEDPGSLLSLFRRLSDQRSKERSLLHGDFHAFSAGPGLFSYIRHWDQN
ERFLVVLNFGDVGLSAGLQASDLPASASLPAKADLLLSTQPGREEGSPLELERLKLEPHEGLLLRFPYAA

: XP_001134334. Reports PREDICTED: simila...[gi:113423932]

BLink, Conserved Domains, Links

- Previous sequence
- Next sequence

>gi|113423932|ref|XP_001134334.1| PREDICTED: similar to RNA binding motif protein 19 [Homo sapiens]
MSRLIVKNLPNGMKEERFRQLFAAFGTLTDCSLKFTKDGKFRKFGFIGFKSEEEAQKAQKHFNKSFIDTS
RITVEFCKSFGDPAKPRAWSKHAQKPSQPKQPPKDSTTPEIKKDEKKKKVAGQLEKLKEDTEFQEFLSVH
QRRAQAATWANDGLDAEPSKGKSKPASDYLNFDSDSGQESEEEGAGEDLEEEASLEPKAAVQKELSDMDY
LKSKMVKAGSSSSSEEEESEDEAVHCDEGSEAEEEDSSATPVLQERDSKGAGQEQGMPAGKKRPPEARAE
TEKPANQKEPTTCHTTVKLRGAPFNVTEKNVMEFLAPLKPVAIRIVRNAHGNKTGYIFVDFSNEEEVKQA
LKCNREYMGKEALAMCSLCVTAFLRSFISFTRSCTSTITTTKNAQARVLGRAGIGGGLALNRVLSALASP
RGDIGTQTYSCFSMLVSQAGLELLTSGDPPASASQSAGIMGVSHWAVQNIIISTYAQSASDPPSTLNPVL
LKKKKKKKHRAVGGIXSMXEGERHPWNPFPSQPPLQAVGRWEGQQVTWPTANQNSSFPLPQETKGSVAVR
VALGETQLVQEVRRFLIDNGVSLDSFSQAAAERSKTVILVKNLPAGTLAAELQETFGHFGSLGRVLLPEG
GITAIVEFLEPLEARKAFRHLAYSKFHHVPLYLEWAPVGVFSSTAPQKKKLQDTPSEPMEKDPAEPETVP
DGETPEDENPTEEGADNSSAKMEEEEEEEEEEEESLPGCTLFIKNLNFDTTEEKLKEVFSKVGTVKSCSI
SKKKNKAGVLLSMGFGFVEYRKPEQAQKALKQLQGHVVDGHKLEVRISERATKPAVTLARKKQVPRKQTT
SKILVRNIPFQAHSREIRELFSTFGELKTVRLPKKMTGTGTHRGFGFVDFLTKQDAKRAFNALCHSTHLY
GRRLVLEWADSEVTLQALRRKTAAHFHEPPKKKRSVVLDEILEQLEGSDSDSEEQTLQL

: NP_001018114. Reports fumarylacetoaceta...[gi:66348062]

BLink, Conserved Domains, Links

- Previous sequence

>gi|66348062|ref|NP_001018114.1| fumarylacetoacetate hydrolase domain containing 1 isoform 1 [Homo sapiens]
MGIMAASRPLSRFWEWGKNIVCVGRNYADHVREMRSAVLSEPVLFLKPSTAYAPEGSPILMPAYTRNLHH
ELELGVVMGKRCRAVPEAAAMDYVGGYALCLDMTARDVQDECKKKGLPWTLAKSFTASCPVSAFVPKEKI
PDPHKLKLWLKVNGELRQEGETSSMIFSIPYIISYVSKIITLEEGDIILTGTPKGVGPVKENDEIEAGIH
GLRQGLTLSPKLECSSAITAHCSLELPGSSNPPSASRF

APPENDIX 4
ANALYSIS OF COOL DOMAIN

■ Motif Scan Graphic Results: KCNRG_ISOFORM_SHORT

```
  1 mssqelvtln vggkifttrf stikqfpasr larmldgrdq efkmvggqif vdrdgdlfsf
 61 ildflrthql llptefsdyl rlqrealfye lrslvdllnp yllqprpalv evhflsrntq
121 affrvfgscs ktiemltgri tvfteqpsap twngnffppq mtllplppqr psyhdlvfqc
181 gsdsttdnqt gvrlvcngvi sahhnlrlwg ssdspasasr vagitgmfl
```

Description: User-entered sequence
Motifs scanned: All
Stringency: High
Show domains: Yes

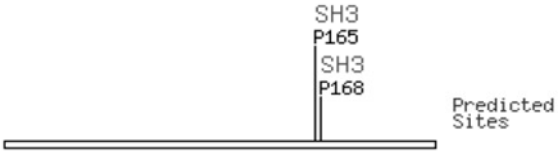

No domains found

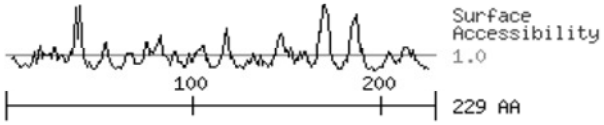

Src homology 3 group (SH3)				
Amphiphysin SH3			Gene Card **AMPH**	
Site	Score	Percentile	Sequence	SA
P168	0.4391	0.049 %	MTLLPLP**P**QRPSYHD	2.370
Cbl-Associated protein C-SH3			Gene Card **N/A**	
Site	Score	Percentile	Sequence	SA
P168	0.5588	0.076 %	MTLLPLP**P**QRPSYHD	2.370
Itk SH3			Gene Card **ITK**	
Site	Score	Percentile	Sequence	SA
P165	0.5555	0.129 %	PPQMTLL**P**LPPQRPS	0.475

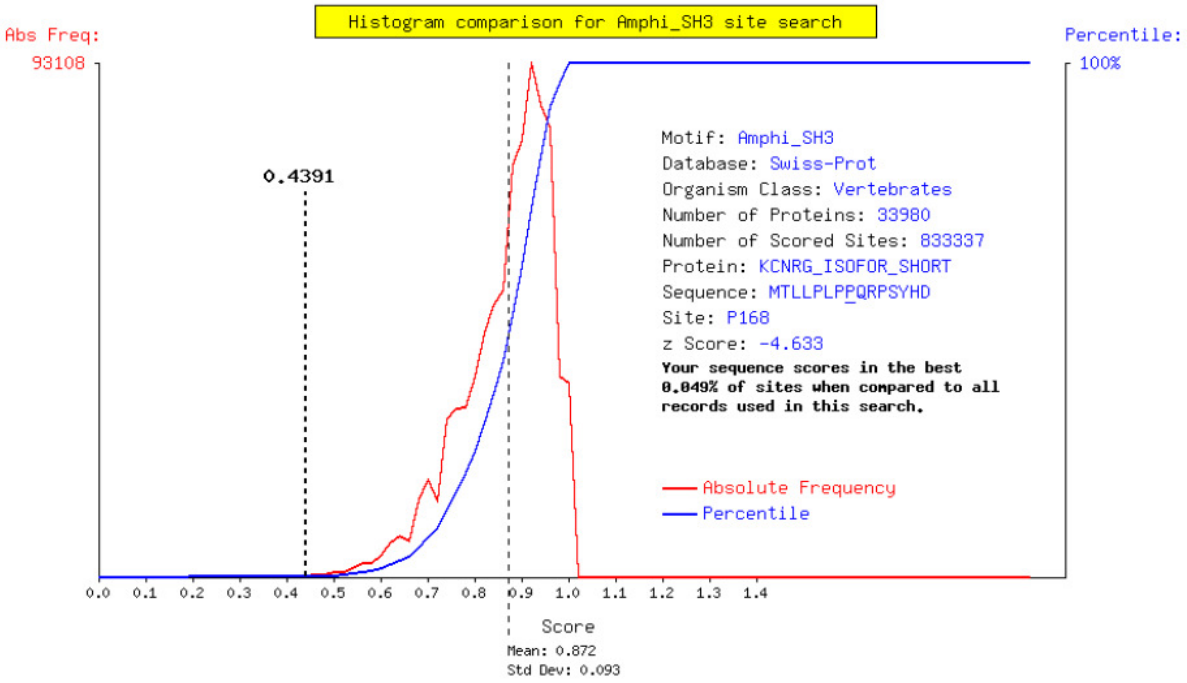

Note: Although the distribution is similar to a normal for searches with many sites, the percentile reported here is computed directly from the histogram, and not from a z table.

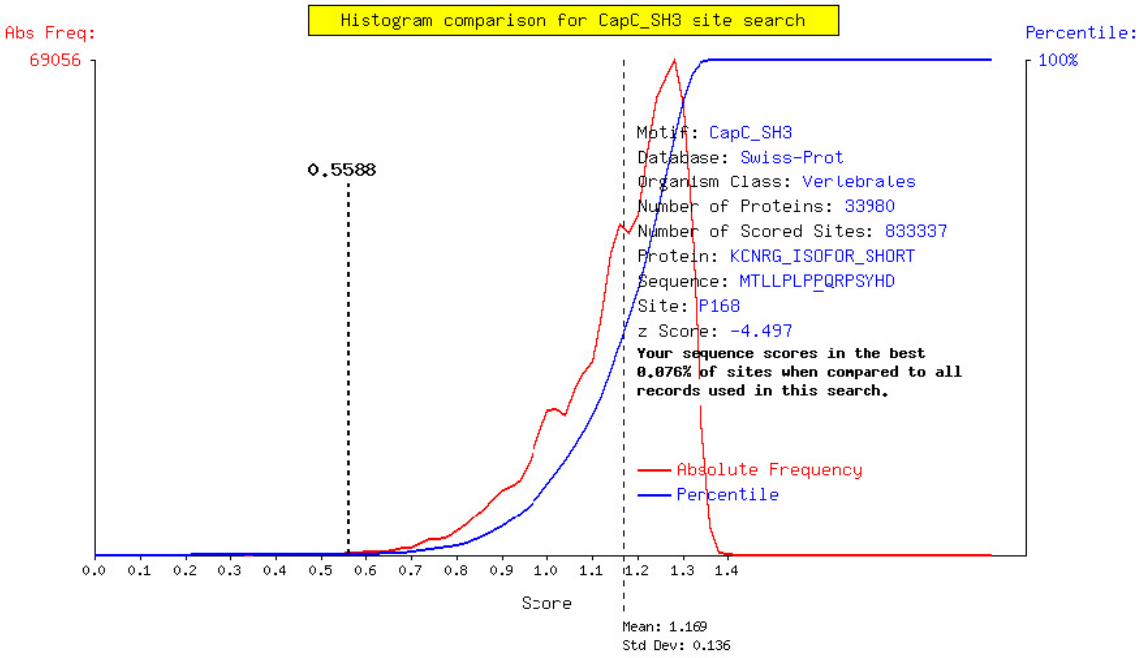

Note: Although the distribution is similar to a normal for searches with many sites, the percentile reported here is computed directly from the histogram, and not from a z table.

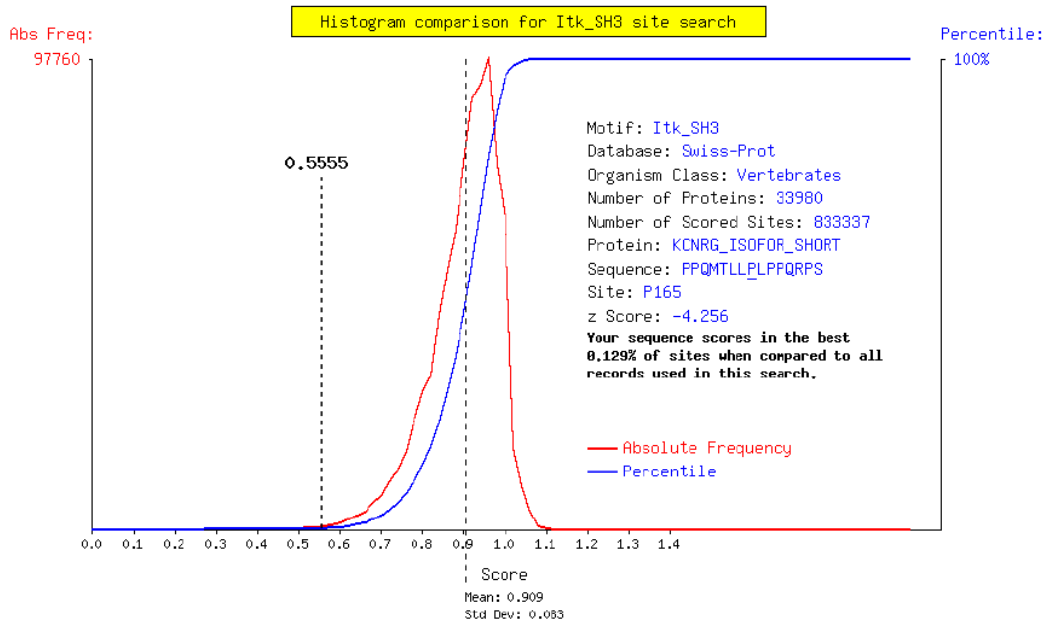

Note: Although the distribution is similar to a normal for searches with many sites, the percentile reported here is computed directly from the histogram, and not from a z table.

NetPhos 2.0 Server - prediction results
Technical University of Denmark

KCNRG 229 Sequence

```
MSSQELVTLNVGGKIFTTRFSTIKQFPASRLARMLDGRDQEFKMVGGQIFVDRDGDLFSFILDFLRTHQLLLPTEFSDYL
80
RLQREALFYELRSLVDLLNPYLLQPRPALVEVHFLSRNTQAFFRVFGSCSKTIEMLTGRITVFTEQPSAPTWNGNFFPPQ
160
MTLLPLPPQRPSYHDLVFQCGSDSTTDNQTGVRLVCNGVISAHHNLRLWGSSDSPASASRVAGITGMFL
240
.....ST.....................................................Y.
80
.....S.....................................T.....................
160
.T.....SY.....S.............................S.....
240

Phosphorylation sites predicted:    Ser: 5  Thr: 3  Tyr: 2
```

Serine predictions

Name	Pos	Context	Score	Pred
		V		
Sequence	2	---MSSQEL	0.012	.
Sequence	3	--MSSQELV	0.004	.
Sequence	21	TTRFSTIKQ	0.992	*S*
Sequence	29	QFPASRLAR	0.121	.
Sequence	59	GDLFSFILD	0.013	.
Sequence	77	PTEFSDYLR	0.005	.
Sequence	93	YELRSLVDL	0.947	*S*

Sequence	116	VHFLSRNTQ	0.015	.
Sequence	128	RVFGSCSKT	0.062	.
Sequence	130	FGSCSKTIE	0.004	.
Sequence	148	TEQPSAPTW	0.010	.
Sequence	172	PQRPSYHDL	0.997	*S*
Sequence	182	FQCGSDSTT	0.017	.
Sequence	184	CGSDSTTDN	0.977	*S*
Sequence	201	NGVISAHHN	0.016	.
Sequence	211	RLWGSSDSP	0.007	.
Sequence	212	LWGSSDSPA	0.443	.
Sequence	214	GSSDSPASA	0.468	.
Sequence	217	DSPASASRV	0.946	*S*
Sequence	219	PASASRVAG	0.311	.

Threonine predictions

Name	Pos	Context	Score	Pred
Sequence	8	QELVTLNVG	0.017	.
Sequence	17	GKIFTTRFS	0.352	.
Sequence	18	KIFTTRFST	0.433	.
Sequence	22	TRFSTIKQF	0.941	*T*
Sequence	67	DFLRTHQLL	0.028	.
Sequence	74	LLLPTEFSD	0.018	.
Sequence	119	LSRNTQAFF	0.219	.
Sequence	132	SCSKTIEML	0.052	.
Sequence	137	IEMLTGRIT	0.859	*T*
Sequence	141	TGRITVFTE	0.322	.
Sequence	144	ITVFTEQPS	0.168	.
Sequence	151	PSAPTWNGN	0.081	.
Sequence	162	PPQMTLLPL	0.550	*T*
Sequence	185	GSDSTTDNQ	0.144	.
Sequence	186	SDSTTDNQT	0.055	.
Sequence	190	TDNQTGVRL	0.061	.
Sequence	225	VAGITGMFL	0.018	.

Tyrosine predictions

Name	Pos	Context	Score	Pred
Sequence	79	EFSDYLRLQ	0.778	*Y*
Sequence	89	EALFYELRS	0.060	.
Sequence	101	LLNPYLLQP	0.009	.
Sequence	173	QRPSYHDLV	0.698	*Y*

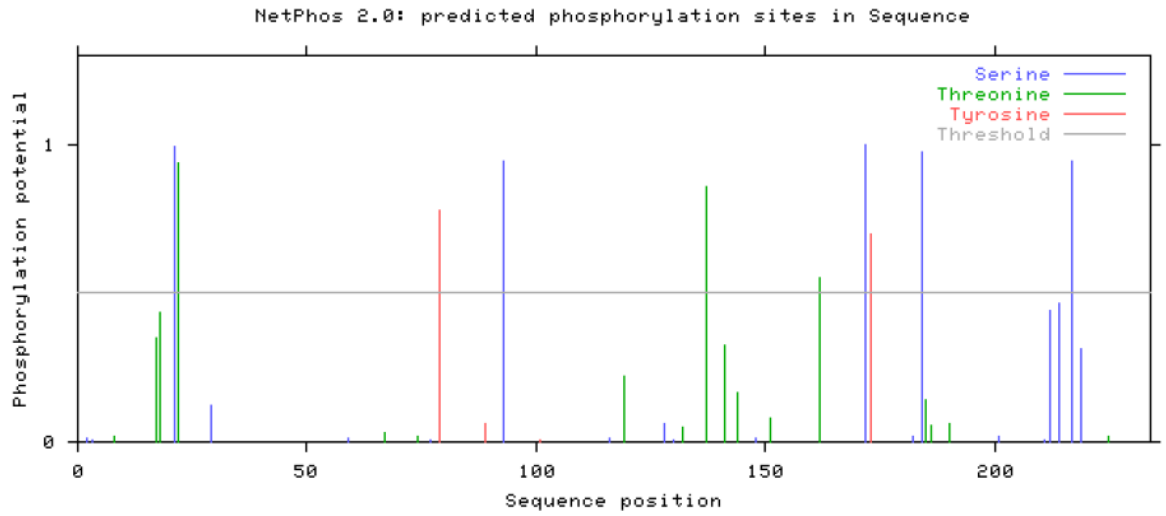

YinOYang 1.2 Prediction Results

(Click here for an explanation of the output)

The predictions for O-GlcNAc sites in 1 sequence

```
Name:  Sequence      Length:  229
MSSQELVTLNVGGKIFTTRFSTIKQFPASRLARMLDGRDQEFKMVGGQIFVDRDGDLFSFILDFLRTHQLLLPTEFSDYL
80
RLQREALFYELRSLVDLLNPYLLQPRPALVEVHFLSRNTQAFFRVFGSCSKTIEMLTGRITVFTEQPSAPTWNGNFFPPQ
160
MTLLPLPPQRPSYHDLVFQCGSDSTTDNQTGVRLVCNGVISAHHNLRLWGSSDSPASASRVAGITGMFL
.GG.......................................................................
80
.............................................................G...G............
160
...............................................GG....G.G..........
```

SeqName	Residue		O-GlcNAc result	Potential	Thresh. (1)	Thresh. (2)
Sequence	2	S	+	0.3617	0.3386	0.4067
Sequence	3	S	+	0.3970	0.3667	0.4446
Sequence	144	T	++	0.6040	0.4207	0.5174
Sequence	148	S	+	0.3554	0.3548	0.4286
Sequence	211	S	++	0.5364	0.3926	0.4796
Sequence	212	S	++	0.5149	0.3730	0.4532
Sequence	217	S	++	0.5239	0.3782	0.4601
Sequence	219	S	+	0.4523	0.4088	0.5014

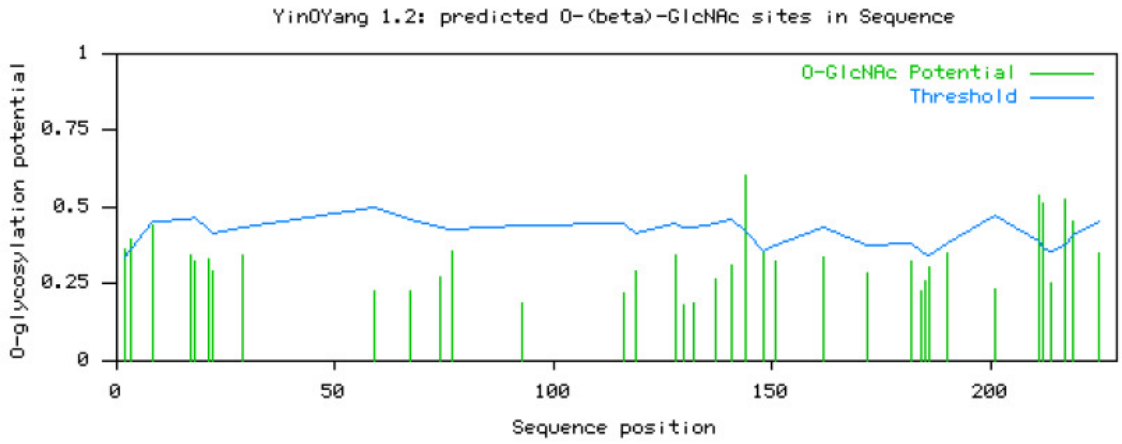

Summary of features reported by ELM.

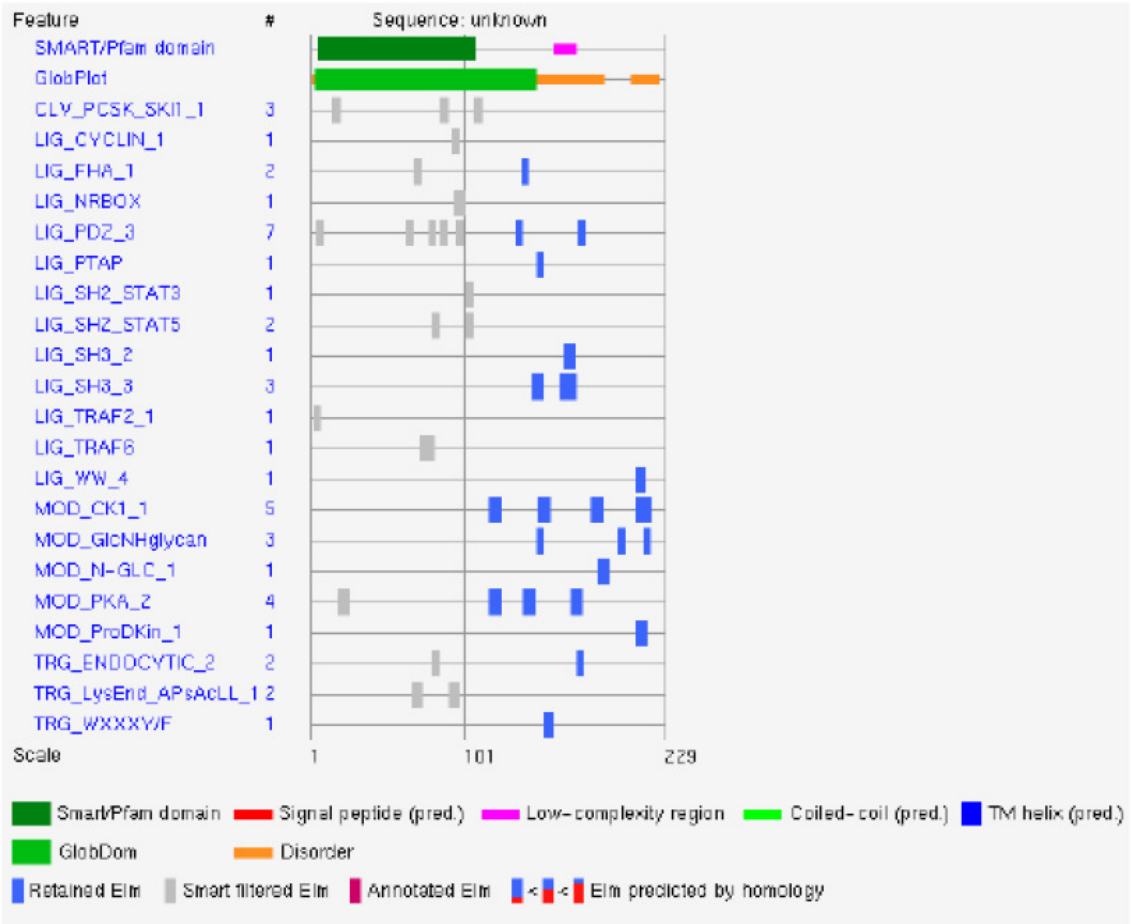

■ Filtering summary

No user supplied cellular location.
User supplied taxon: Homo sapiens
(An ELM is listed as filtered when all its matching instances have been filtered out.)

retained
Species filtered
Smart filtered
Cellular location filtered
all found (before filtering)

Query sequence:

```
>unknown
 MSSQELVTLNVGGKIFTTRFSTIKQFPASRLARMLDGRDQEFKMVGGQIFVDRDGDLFSF
 ILDFLRTHQLLLPTEFSDYLRLQREALFYELRSLVDLLNPYLLQPRPALVEVHFLSRNTQ
 AFFRVFGSCSKTIEMLTGRITVFTEQPSAPTWNGNFFPPQMTLLPLPPQRPSYHDLVFQC
 GSDSTTDNQTGVRLVCNGVISAHHNLRLWGSSDSPASASRVAGITGMFL
```

■ **Globular domains/ TM domains and signal peptide detected by the SMART server**

■ Results of ELM motif search after globular domain filtering and context filtering.

All matches falling inside SMART/PFAM domains are excluded from this list.

Elm Name	Elm Description	Cell Compartment	Pattern
LIG_FHA_1	FHA domain interaction motif 1, threonine phosphorylation is required	nucleus, plasma membrane, cytosol	T..[ILA]
LIG_PDZ_3	Class III PDZ domains binding motif	membrane, plasma membrane, cytosol	.[DE].[IVL]
LIG_PTAP	PTAP alike ligands	not annotated	P[TS]AP
LIG_SH3_2	this is the motif recognized by class II SH3 domains	plasma membrane, focal adhesion, cytosol	P..P.[KR]
LIG_SH3_3	This is the motif recognized by those SH3 domains with a non-canonical class I recognition specificity	plasma membrane, focal adhesion, cytosol	...[PV]..P
LIG_WW_4	Class IV WW domains interaction motif; phosphorylation-dependent interaction.	nucleus, cytosol	...[ST]P.
MOD_CK1_1	CK1 phosphorylation site	nucleus, cytosol	S..([ST])...
MOD_GlcNHglycan	Glycosaminoglycan attachment site	extracellular, Golgi apparatus	D]{0,3}.(S)[GA].

■ List of excluded ELMs falling inside SMART/PFAM domains.

Matches in this list are only likely to be of interest if they are in surface-exposed loops. Consult the SMART or PFAM entries for useful links to solved 3D structures.

Elm Name	Elm Description	Cell Compartment	Pattern
CLV_PCSK_SKI1_1	Subtilisin/kexin isozyme-1 (SKI1) cleavage site ([RK]-X-[hydrophobic]-[LTKF]-|-X)	Golgi apparatus, endoplasmic reticulum lumen, endoplasmic reticulum	[ILMFV][LTKF].
LIG_CYCLIN_1	Substrate recognition site that interacts with cyclin and thereby increases phosphorylation by cyclin/cdk complexes. Predicted protein should have the MOD_CDK site. Also used by cyclin inhibitors.	nucleus, cytosol	[0,1}[FYLIVMP]
LIG_FHA_1	domain interaction motif 1, threonine phosphorylation is required	nucleus, plasma membrane, cytosol	T..[ILA]
LIG_NRBOX	The nuclear receptor box motif (LXXLL) confers binding to nuclear receptors.	nucleus	P][^P](L)(L)[^P]
LIG_PDZ_3	Class III PDZ domains binding motif	membrane, plasma membrane, cytosol	.[DE].[IVL]
LIG_SH2_STAT3	YXXQ motif found in the cytoplasmic region of cytokine Receptors that bind STAT3 SH2 domain.	not annotated	Y..Q
LIG_SH2_STAT5	STAT5 Src Homology 2 (SH2) domain binding motif.	not annotated	Y[VLTFIC]..
LIG_TRAF2_1	Major TRAF2-binding consensus motif. Members of the tumor necrosis factor receptor (TNFR) superfamily initiate intracellular signaling by recruiting the C-domain of the TNFR-associated factors (TRAFs) through their cytoplasmic tails.	cytosol	[PSAT].[QE]E
LIG_TRAF6	TRAF6 binding site. Members of the tumor necrosis factor receptor (TNFR) superfamily initiate intracellular signaling by cruiting the C-domain of the TNFR-associated factors (TRAFs) through their cytoplasmatic tails.	cytosol	.E..[FYWHDE].
MOD_PKA_2	PKA phosphorylation site	cytosol	.R.([ST])...
RG_ENDOCYTIC_2	Tyrosine-based sorting signal responsible for the interaction with mu subunit of AP (Adaptor Protein) complex	plasma membrane, clathrin-coated endocytic vesicle, cytosol	Y..[LMVIF]
LysEnd_APsAcLL_1	Sorting and internalisation signal found in the cytoplasmic juxta-membrane region of type I transmembrane proteins. Targets them from the Trans Golgi Network to the lysosomal-endosomal-melanosomal compartments. Interacts with adaptor protein (AP) complexes	Endocytic vesicle, cytosol	[DER]...L[LVI]

APPENDIX 5
KCNRG VARIANT 2 SEQUENCE

AgttcctcatctgttgctttttcattttgtatactgcaagttcccaggcaactcgaatttgcaaacacagccatggatacactatttaccttacagtagtttcctgggaatctaagtctggtttttgttattcttccctccctccactgcataatcatgtataactagcaacatttatggttatagGttgatttcctaagtgtggctgatggtagcctctagtttgaagtgagggaagaatgagtagtcaggaactggtcactttgaatgtgggagggaagatattcacgacaaggttttctacgataaagcagtttcctgcttctcgtttggcacgcatgttagatggcagagaccaagaattcaagatggttggtggccagatttttgtagacagagatggtgatttgtttagtttcatcttagatttttgagaactcaccagcttttattacccactgaattttcagactatcttaggcttcagagagaggctcttttctatgaacttcgttctctagttgatctcttaaacccatacctgctacagccaagacctgctcttgtggaggtacatttcctaagccggaacactcaagcttttttcagggtgtttggctcttgcagcaaaacaattgagatgctaacagggaggattacagtgtttacagaacaaccttcagcgccgacctggaatggtaacttttttccctcctcagatgaccttacttccactgcctccacaaagaccttcttaccatgacctggttttccagtgtggttctgacagcactactgataaccaaactggagtcaggCTGGTATGCAATGGCGTGATCTCGGCTCACCACAACCTCCGCCTCTGGGGTTCAAGTGATTCTCCTGCCTCAGCCTCCCGAGTAGCTGGGATTACaggtatgtttctataaaacctgataaccgaaaattggccaacggaacaaatgtcctcggcttactgattgacactttattaaaggaaggctttcatttggtcagcactagaacagtatcttctgaagacaaaactgaatgctatagctttgaaaggataaaaagccctgaagtgctcatcacgaatgaaacaccaaaaccagagactatcatcataccagagcaatctcagataaagaaatgaagttgtctatcctcttttaaagagaaattgccatttttcttgtttcattacgtatttagggcatacatgttagccaaatctacactcagcctaactcttggcttcatctgctgccatgccgtctctgggcaaccaggccccaactgtgcttaagccataatgcctgctgctctctagacaactccatgtacttggtgctttggtatatgttctaccttcaatacatctttccctttctcttcttcatgaatgcttatgagccgagattgcgccactgcacactagcttgggtgacagaggaagactgtctcaaaaaaaaaaaaattgatcaaactgatggataccctaagtaccctgacttgatcattacaccttctatgcatgcaacaaaatgccacgtgtaccccataaatatgtagaaatattatatgtaaataaatagttgggccttccgtattttcccactta

Match:516-gap-126

>pcDNA3.1-MycHisA-KCNRG-3ex

TCCTACTTGGCAGTACATCTACGTATTAGTCATCGCTATTACCATGGTGATGCGGTTTTGGCAGTACATCA
ATGGGCGTGGATAGCGGTTTGACTCACGGGGATTTCCAAGTCTCCACCCCATTGACGTCAATGGGAGTTTG
TTTTGGCACCAAAATCAACGGGACTTTCCAAAATGTCGTAACAACTCCGCCCCATTGACGCAAATGGGCGG
TAGGCGTGTACGGTGGGAGGTCTATATAAGCAGAGCTCTCTGGCTAACTAGAGAACCCACTGCTTACTGGC

BamH I

TTATCGAAATTAATACGACTCACTATAGGGAGACCCAAGCTGGCTAGTTAAGCTTGGTACCGAGCTCGGAT

Start

CCagaATGagtagtcaggaactggtcactttgaatgtgggagggaagatattcacgacaaggttttctacg
ataaagcagtttcctgcttctcgtttggcacgcatgttagatggcagagaccaagaattcaagatggttgg
tggccagatttttgtagacagagatggtgatttgtttagtttcatcttagatttttgagaactcaccagc
ttttattacccactgaattttcagactatcttaggcttcagagagaggctcttttctatgaacttcgttct
ctagttgatctcttaaacccatacctgctacagccaagacctgctcttgtggaggtacatttcctaagccg
gaacactcaagcttttttcagggtgtttggctcttgcagcaaaacaattgagatgctaacagggaggatta
cagtgtttacagaacaaccttcagcgccgacctggaatggtaacttttttccctcctcagatgaccttactt
ccactgcctccacaaagaccttcttaccatgacctggttttccagtgtggttctgacagcactactgataa
ccaaactggagtcaggCTGGTATGCAATGGCGTGATCTCGCTCACCACAACCTCCGCCTCTGGGGTTCAAGTGATTCTCCTGCCT
CAGCCTCCCGAGTAGCTGGGATTACaggtatgtttctaCTCGAGTCTAGAGGGC

Xho I

CCTTCGAACAAAAACTCATCTCAGAAGAGGATCTGAATATGCATACCGGT

Stop

CATCATCACCATCACCATTGAGTTTAAACCCGCTGATCAGCCTCGACTGTGCCTTCTAGTTGCC
AGCCATCTGTTGTTTGCCCCTCCCCCGTGCCTTCCTTGACCCTGGAAGGTGCCACTCCCACTGT
CCTTTCCTAATAAAATGAGGAAATTGCATCGCATTGTCTGAGTAGGTGTCATTCTATTCT

(Yellow, and light blue sequences indicate primers)

APPENDIX 6
CELL PROLIFERATION ASSAY: BrdU ELISA

BrdU Results	(48 Hours)			
Cell Line	*All Values compared to EV*			
	Value	% change	Significant?	M-W Pval
RPMI Regular	4453.515	-41%	yes	0.0014763
RPMI EV	3164.89			
R clone S2A11	2211.265	30%	yes	0.0103341
R clone S3A10	2074.04	34%	yes	0.00738151
R clone S1B9	2221.39	30%	yes	0.0103341
RPMI Variant 2	2907.39	8%	no	0.286869
HL60 Regular	13184.14	12%	no	0.0802642
HL60 EV	11678.51			
HL60 V1	8593.26	26%	yes	0.000543901
HL60 V2	10090.51	12%	no	0.0414918
LNCaP Regular	2509.673	-32%	no	0.0524476
LNCaP EV	1564.236			
LNCaP V1	1918.636	38%	yes	0.0034965
LNCaP V2	3314.423	24%	yes	0.0249417

APOPTOSIS ASSAY: CASPACE 3/7

Apoptosis Results	(2 hours)			
Cell Line	*All Values compared to EV*			
	Value	% change	Significant?	M-W Pval
RPMI Regular	42.30375	-33%	YES	0.002331
RPMI TE	31.765			
R clone S2A11	89.0975	-180%	YES	7.77E-05
R clone S3A10	104.085	-228%	YES	7.77E-05
R clone S1B9	75.02	-136%	YES	7.77E-05
RPMI Variant 2	61.5325	-94%	YES	7.77E-05
HL60 Regular	2.101375	56%	YES	7.77E-05
HL60 TE	4.7795			
HL60 V1	15.08625	-216%	YES	7.77E-05
HL60 V2	5.95575	-25%	NO	0.191142
LNCaP Regular	18.6625	1%	NO	0.399223
LNCaP TE	18.9275			
LNCaP V1	27.54729	-46%	YES	0.000155
LNCaP V2	26.77344	-41%	YES	0.000155

APPENDIX 7
FACS ANALYSIS: CELL CYCLE PI

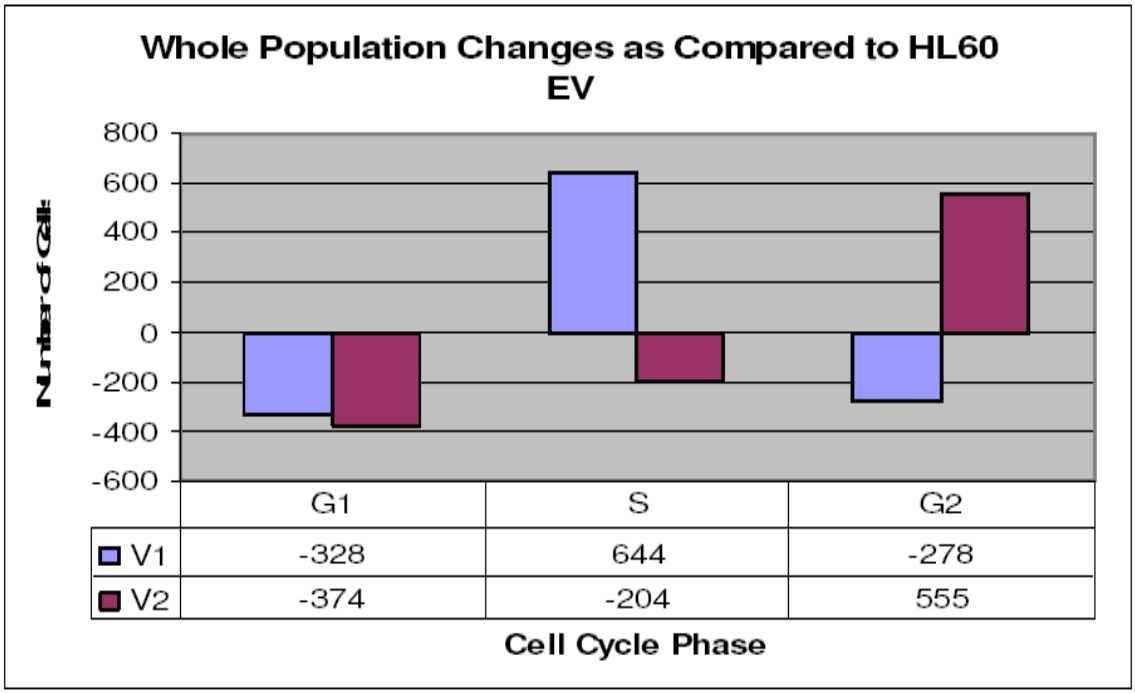

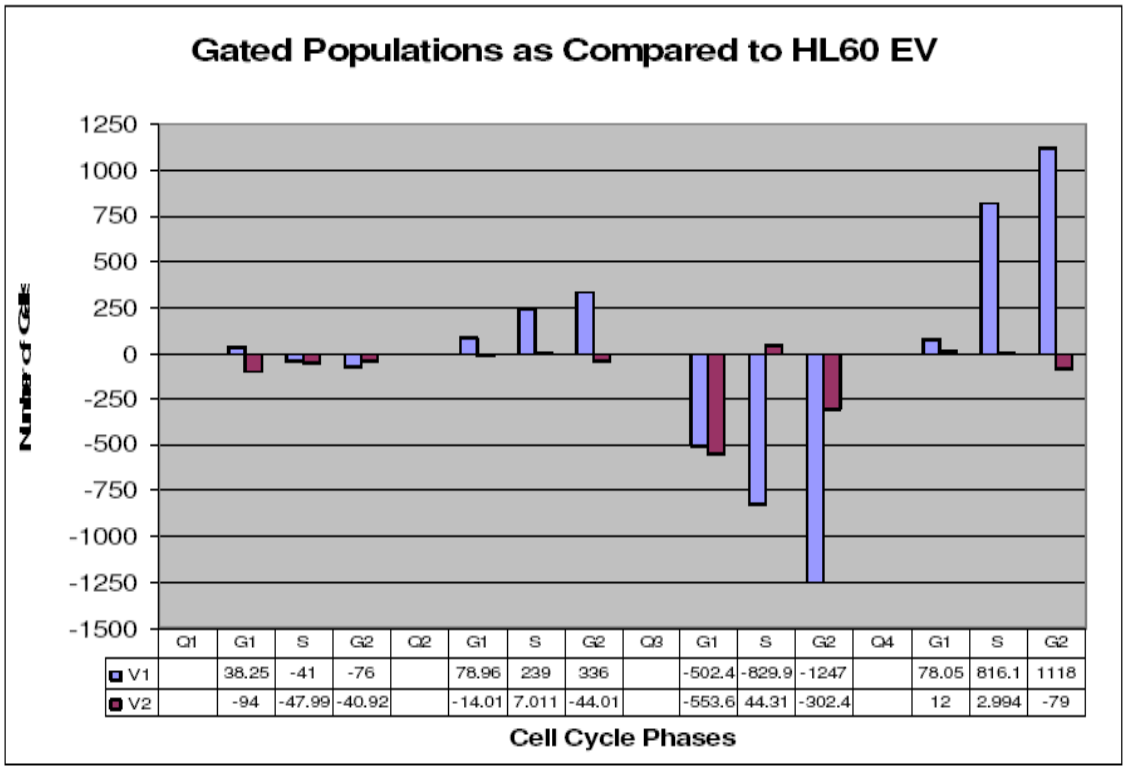

HL60 EV FACS: PI

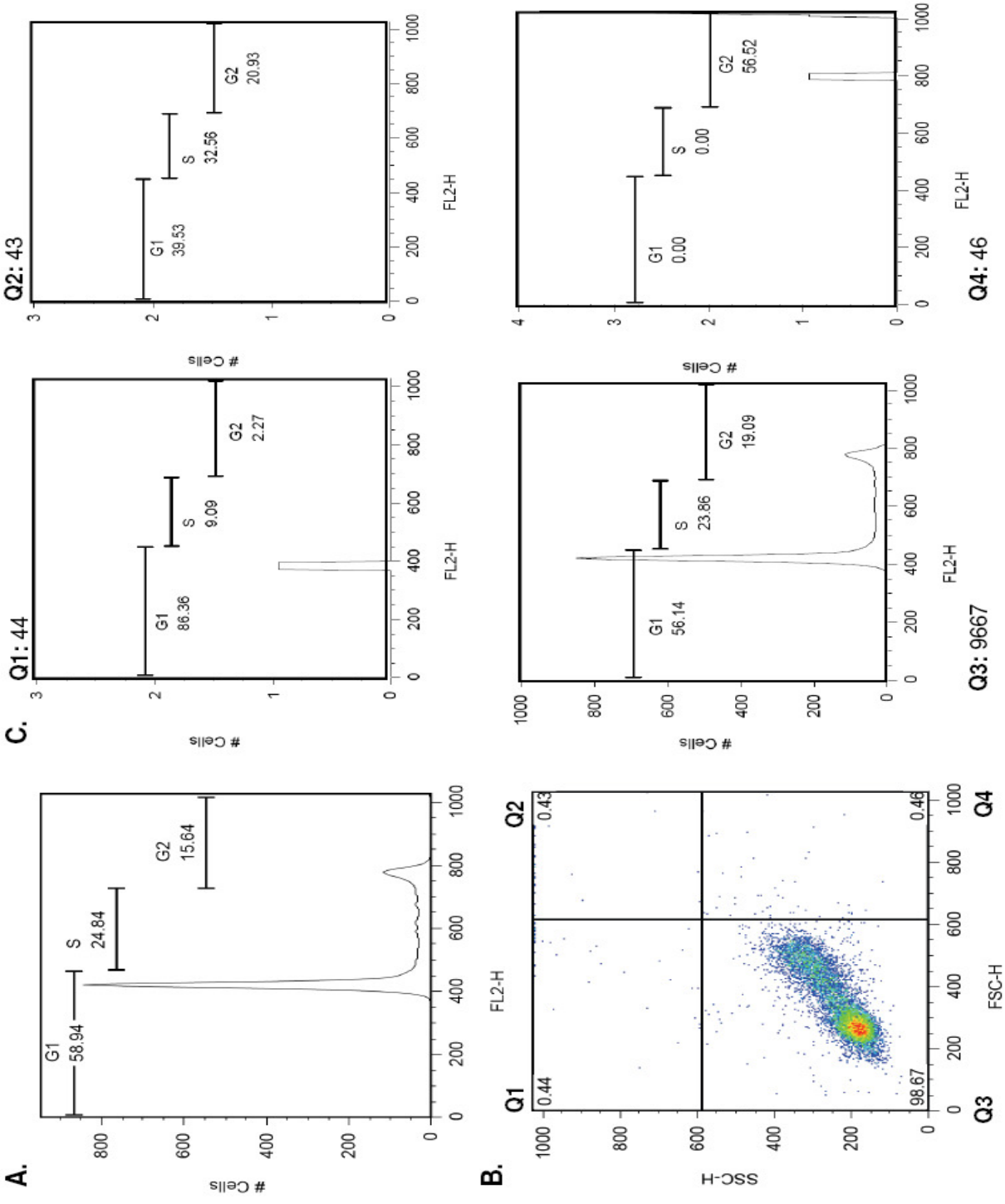

HL60 V1 FACS: PI

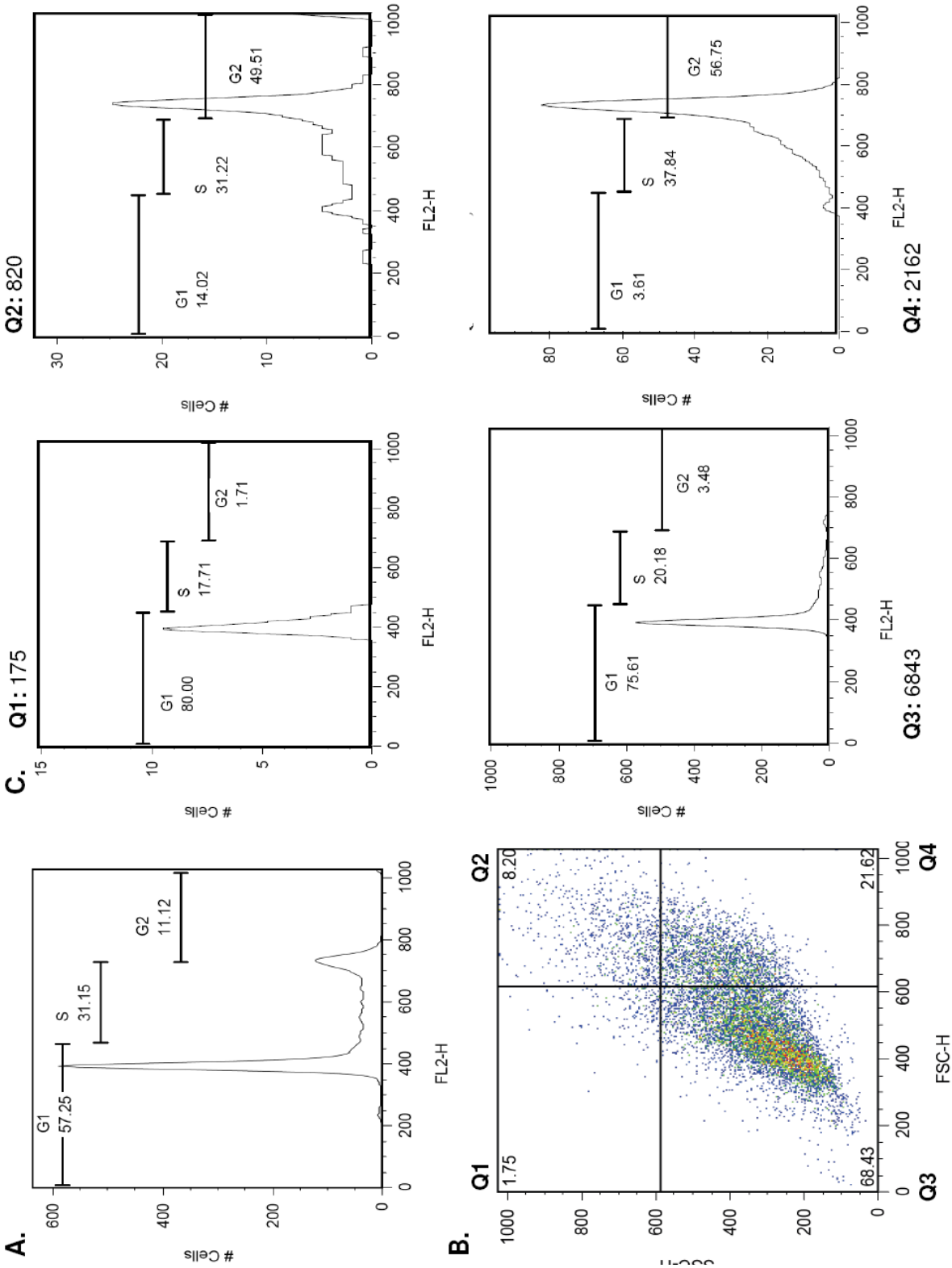

HL60 V2 FACS: PI

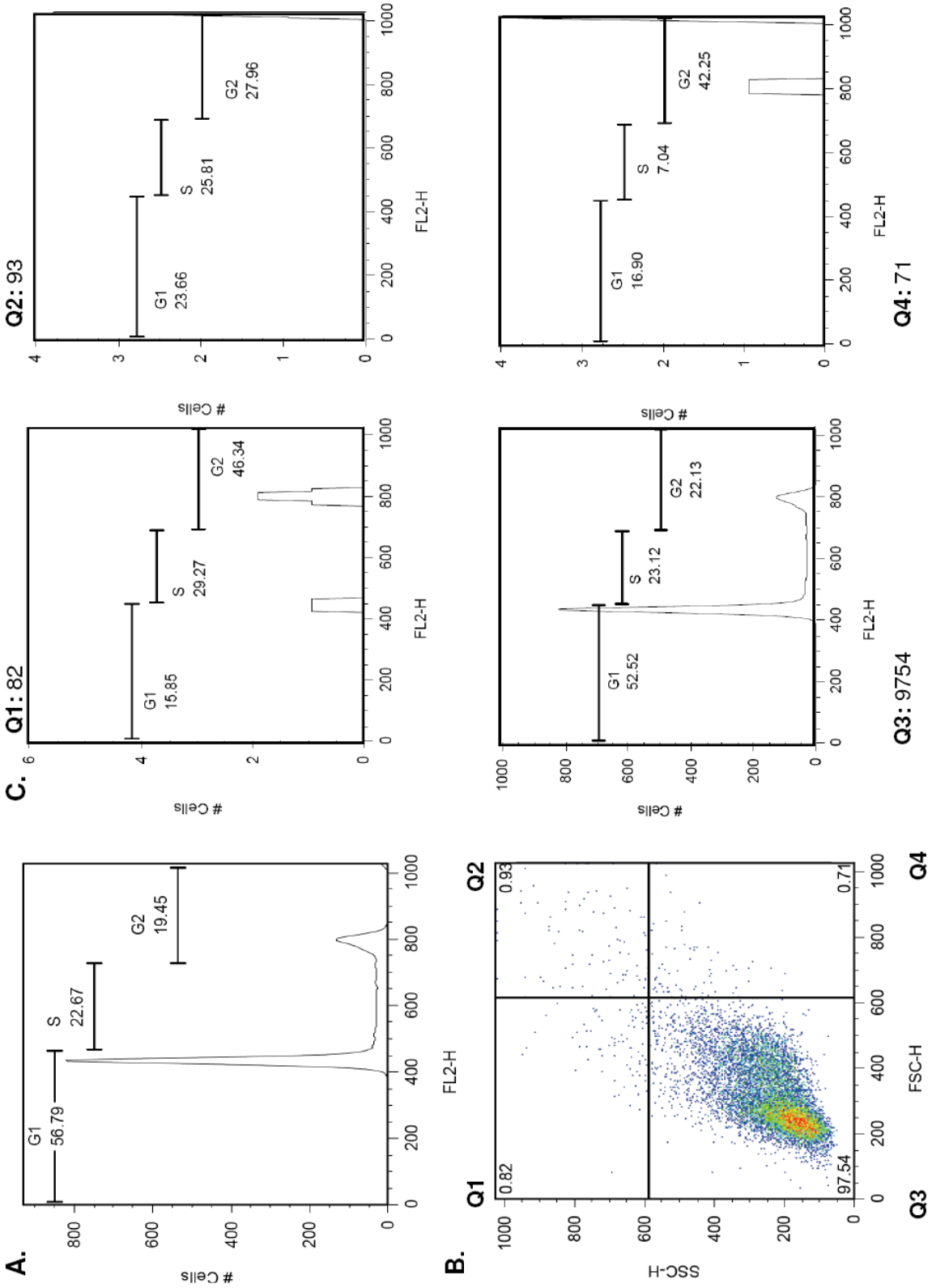

HL60 FACS PI: OVERLAY

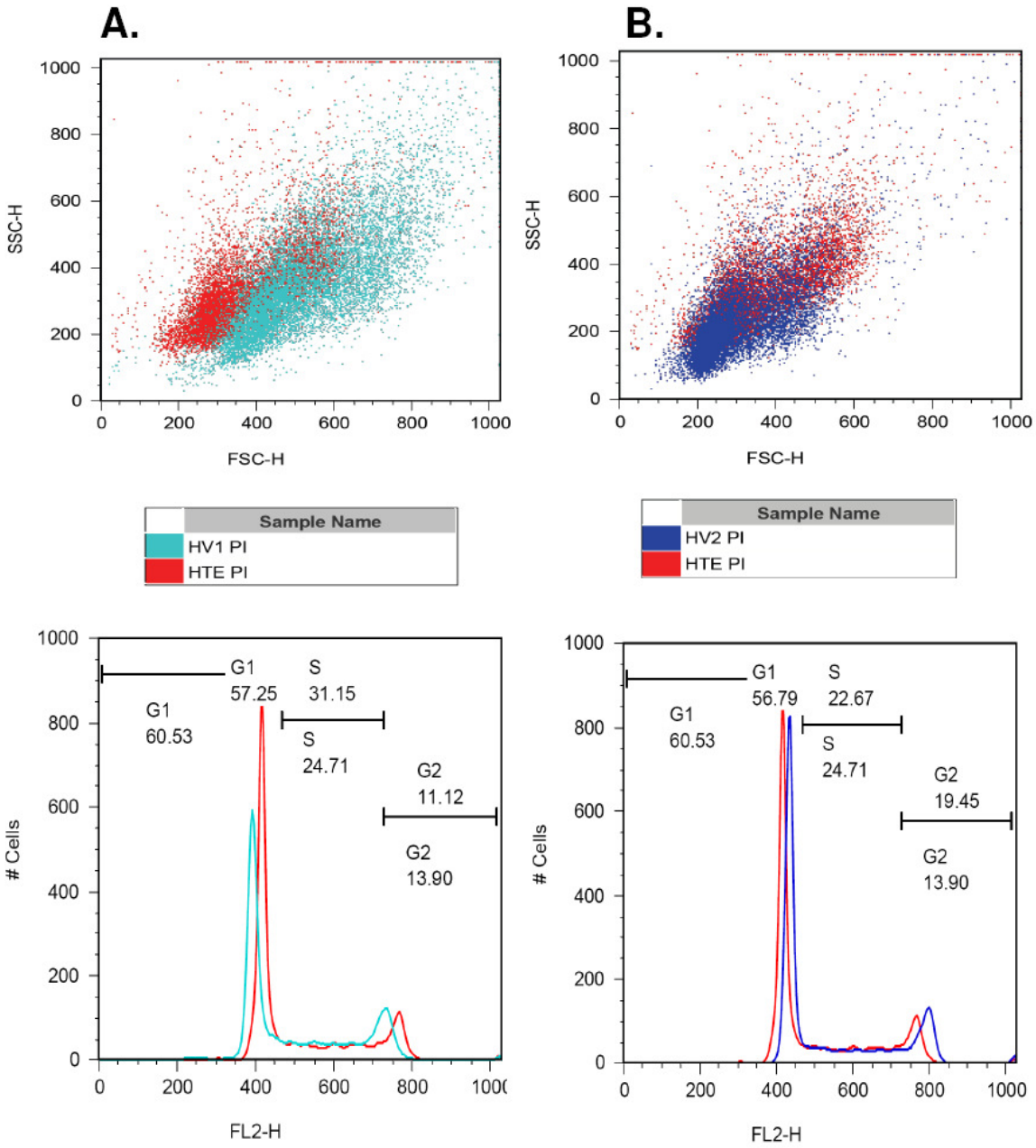

RPMI CELL CYCLE ANALYSIS: FACS PI

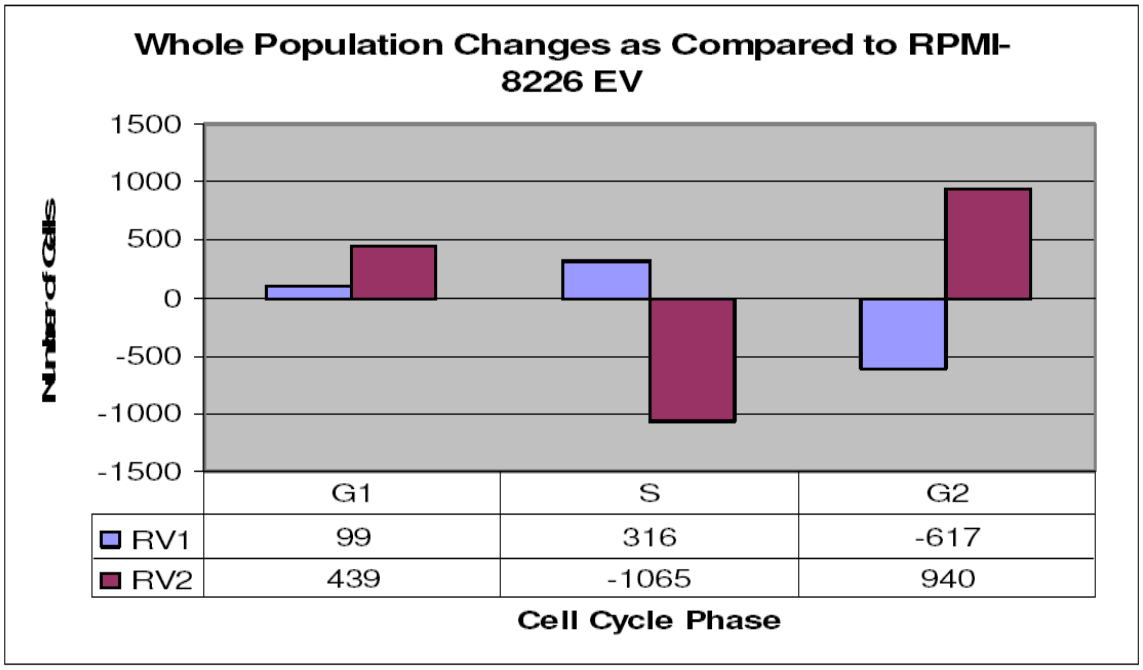

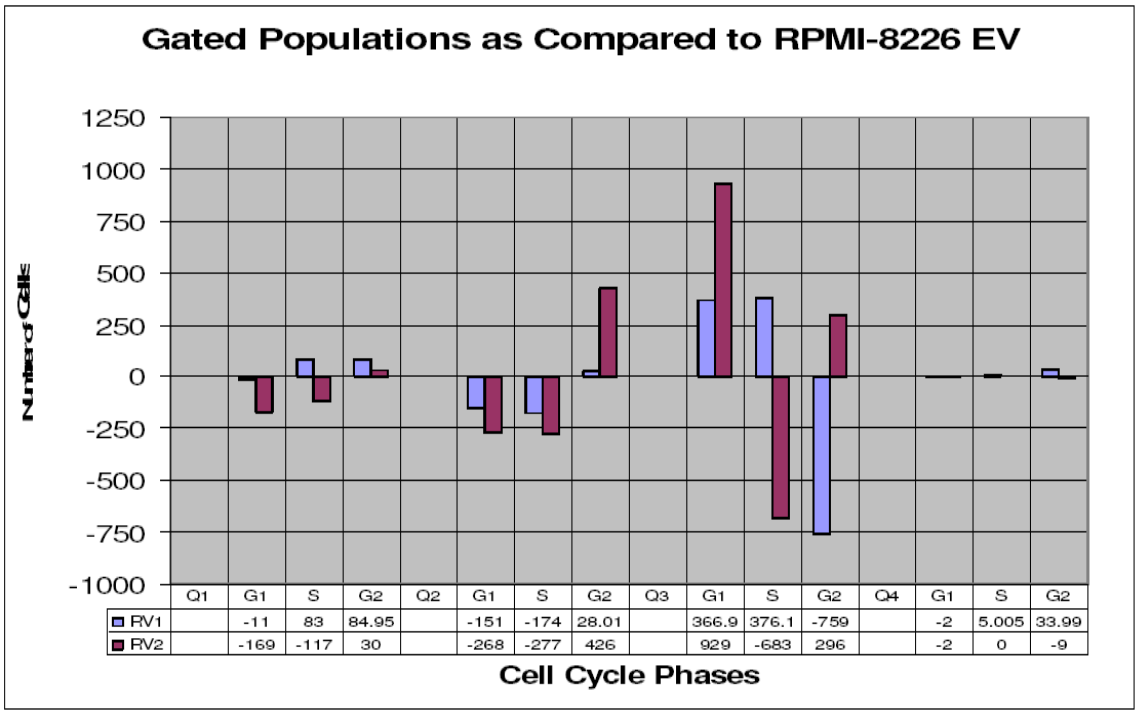

RPMI EV FACS: PI

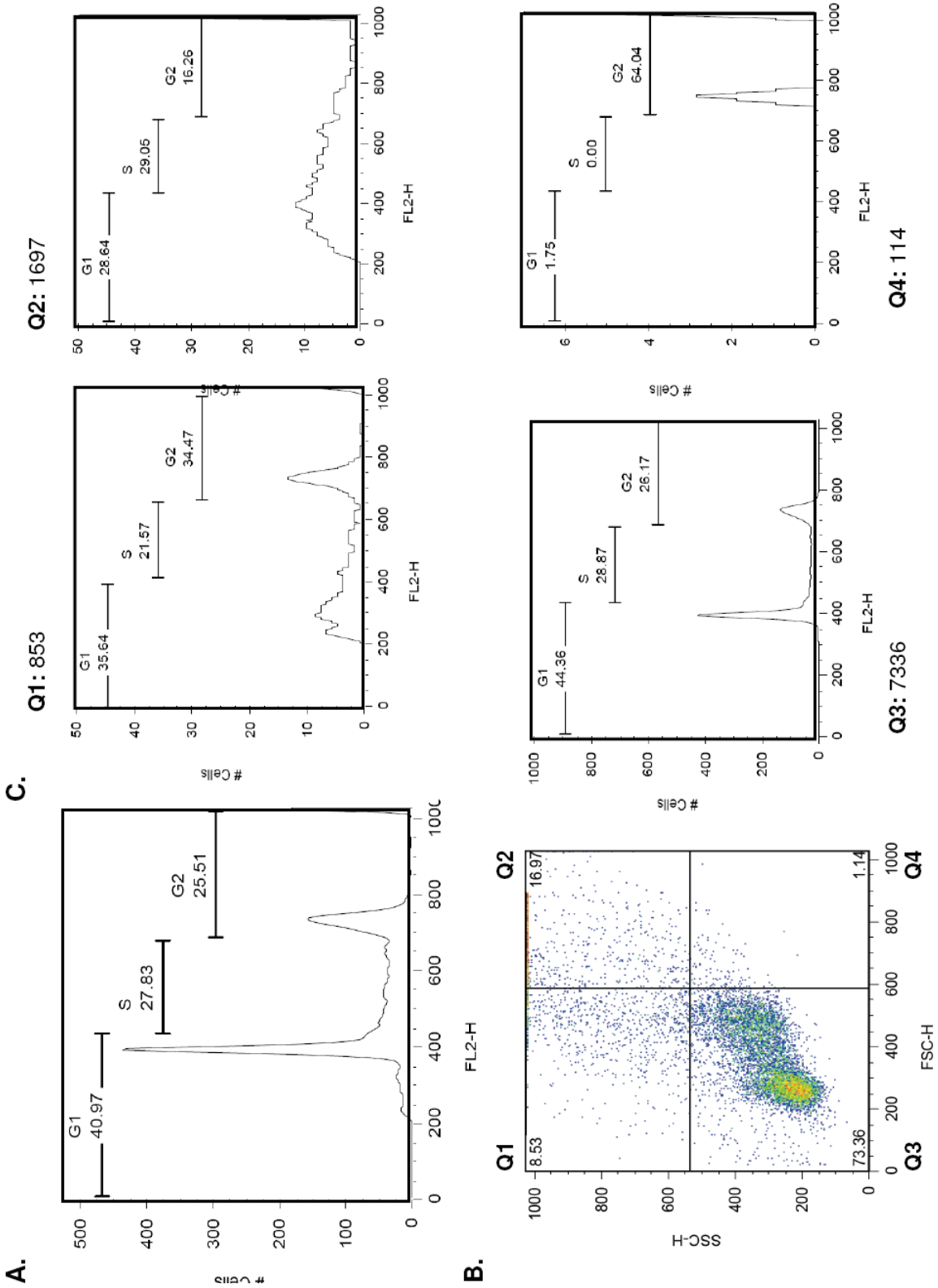

RPMI V1 FACS: PI

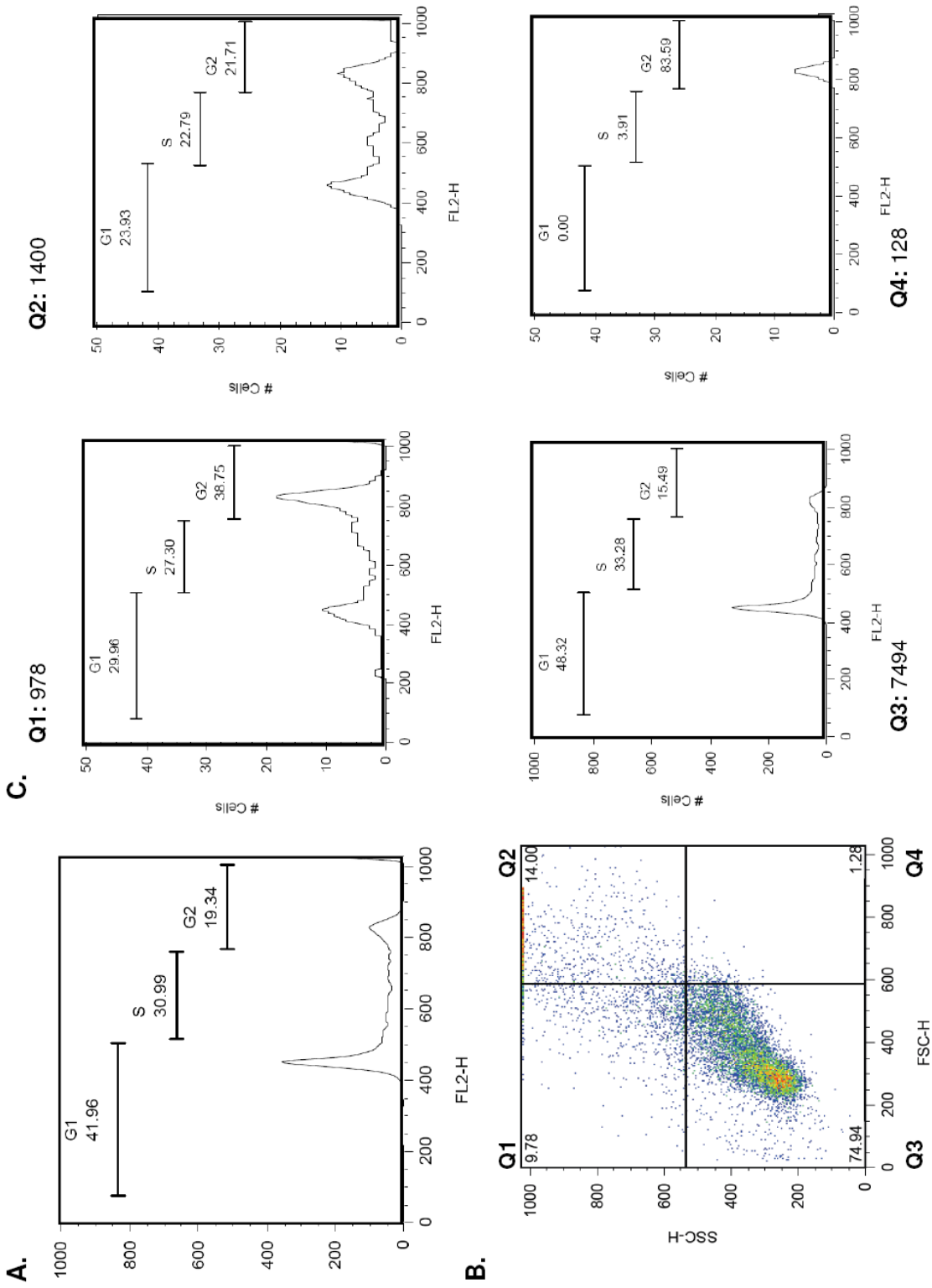

RPMI V2 FACS: PI

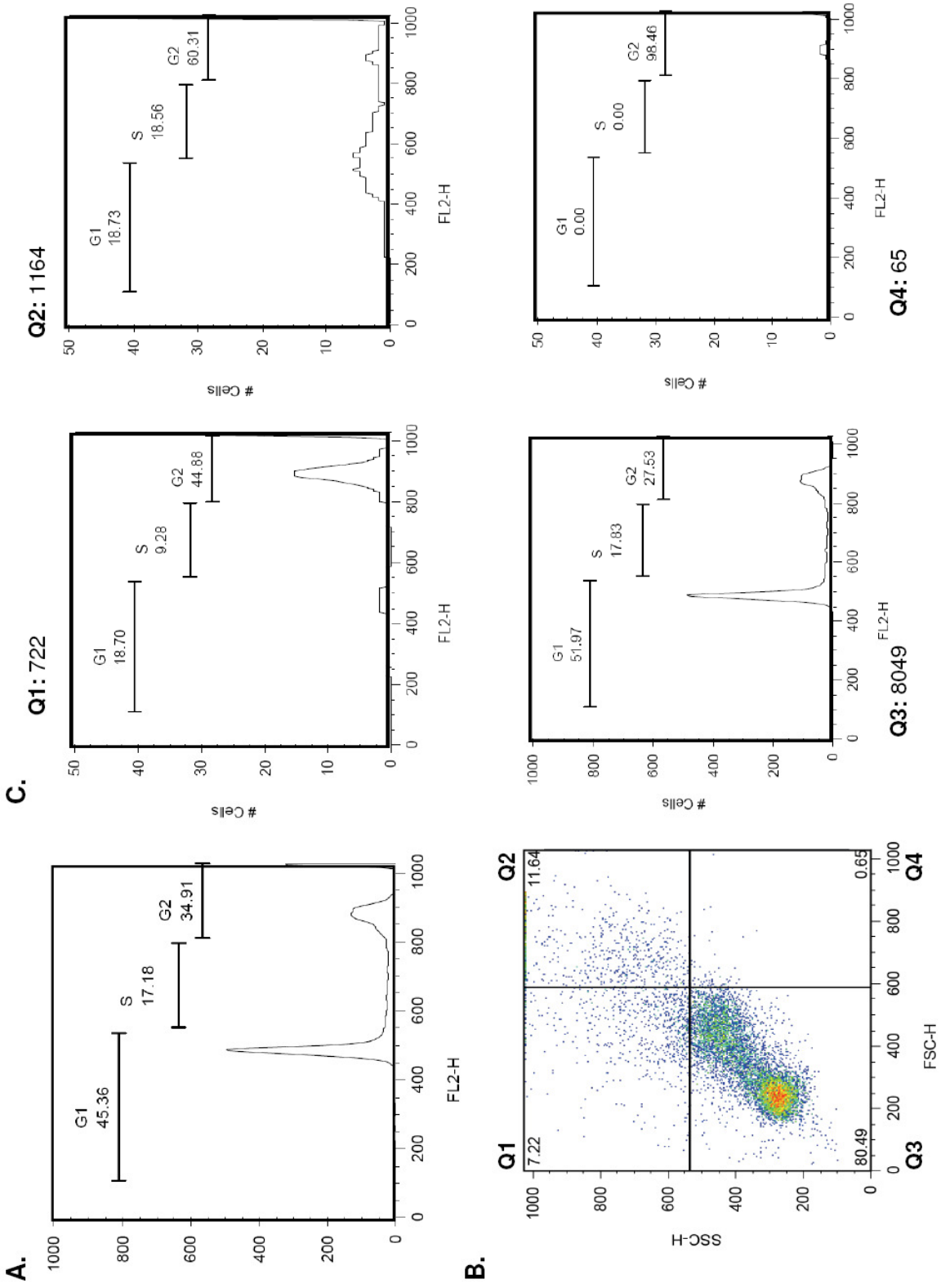

RPMI FACS PI: OVERLAY

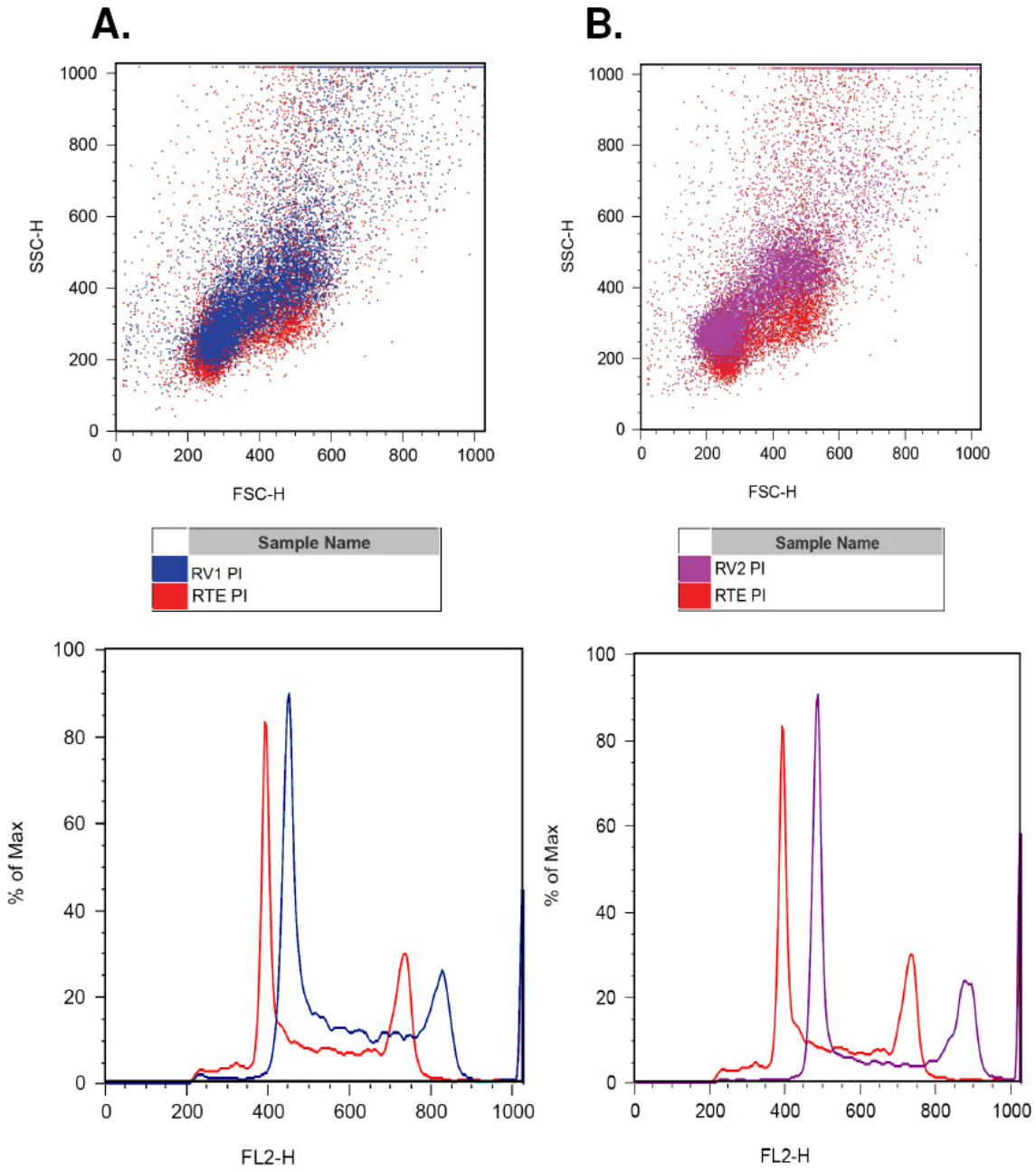

LNCaP CELL CYCLE ANALYSIS: FACS PI

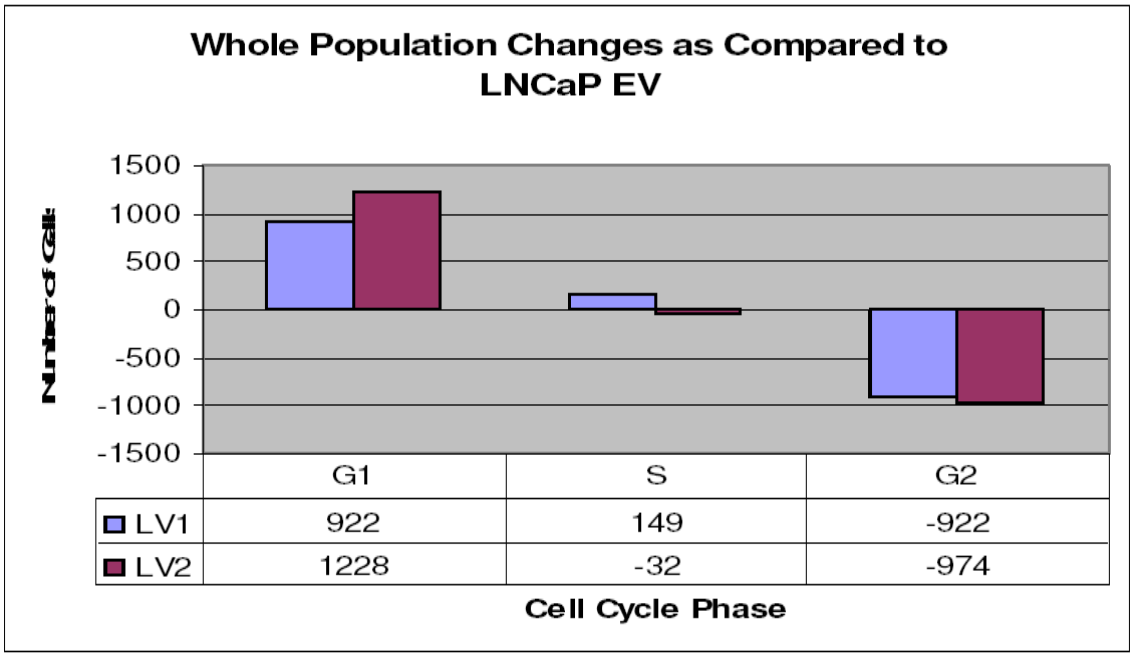

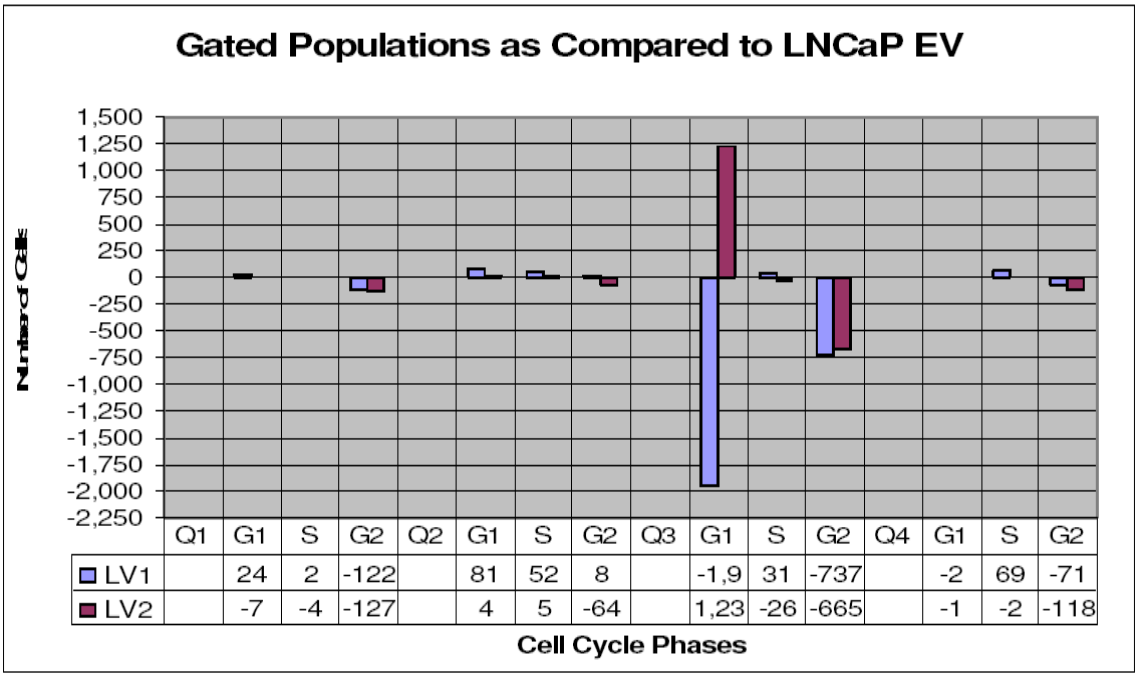

LNCaP EV FACS: PI

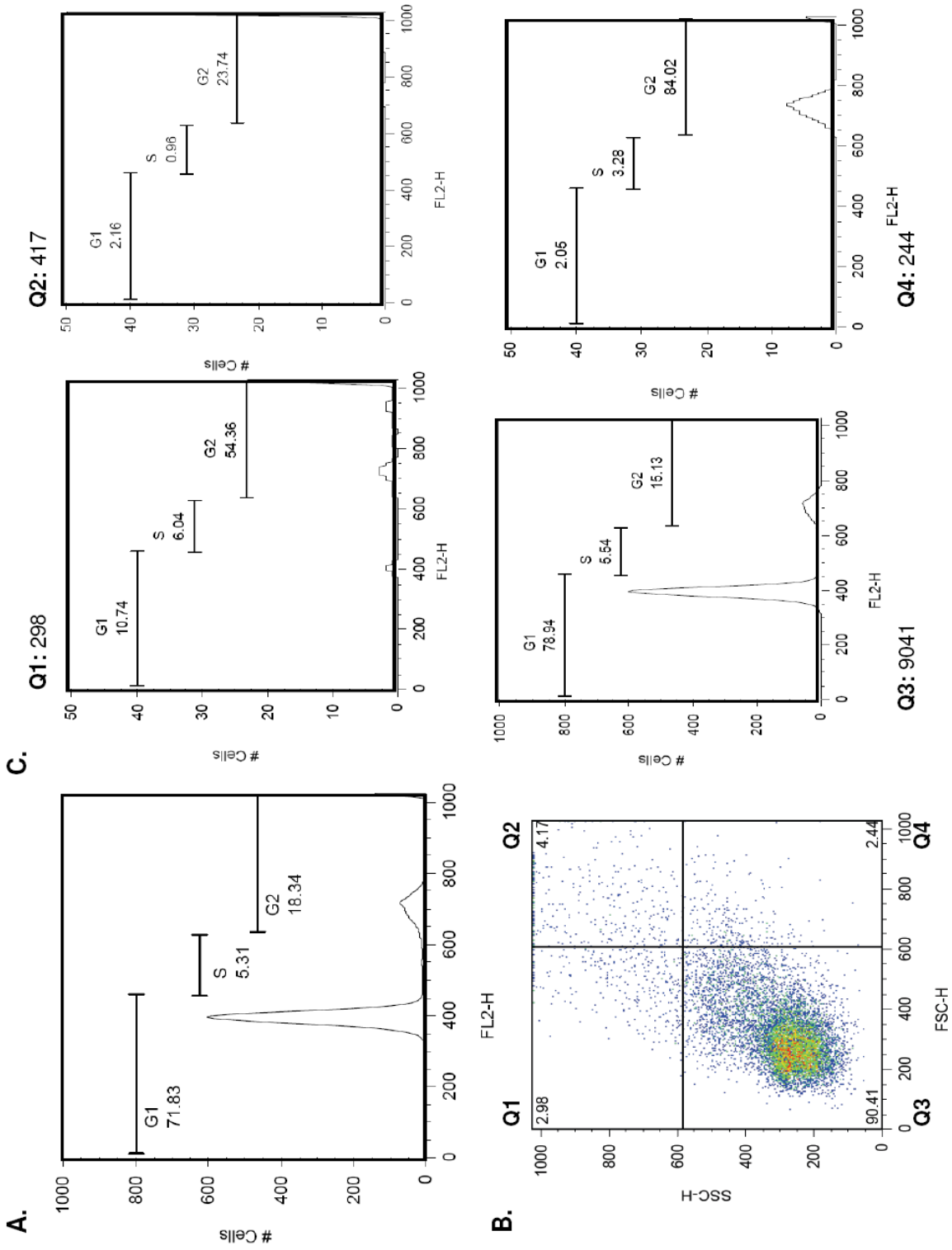

LNCaP V1 FACS: PI

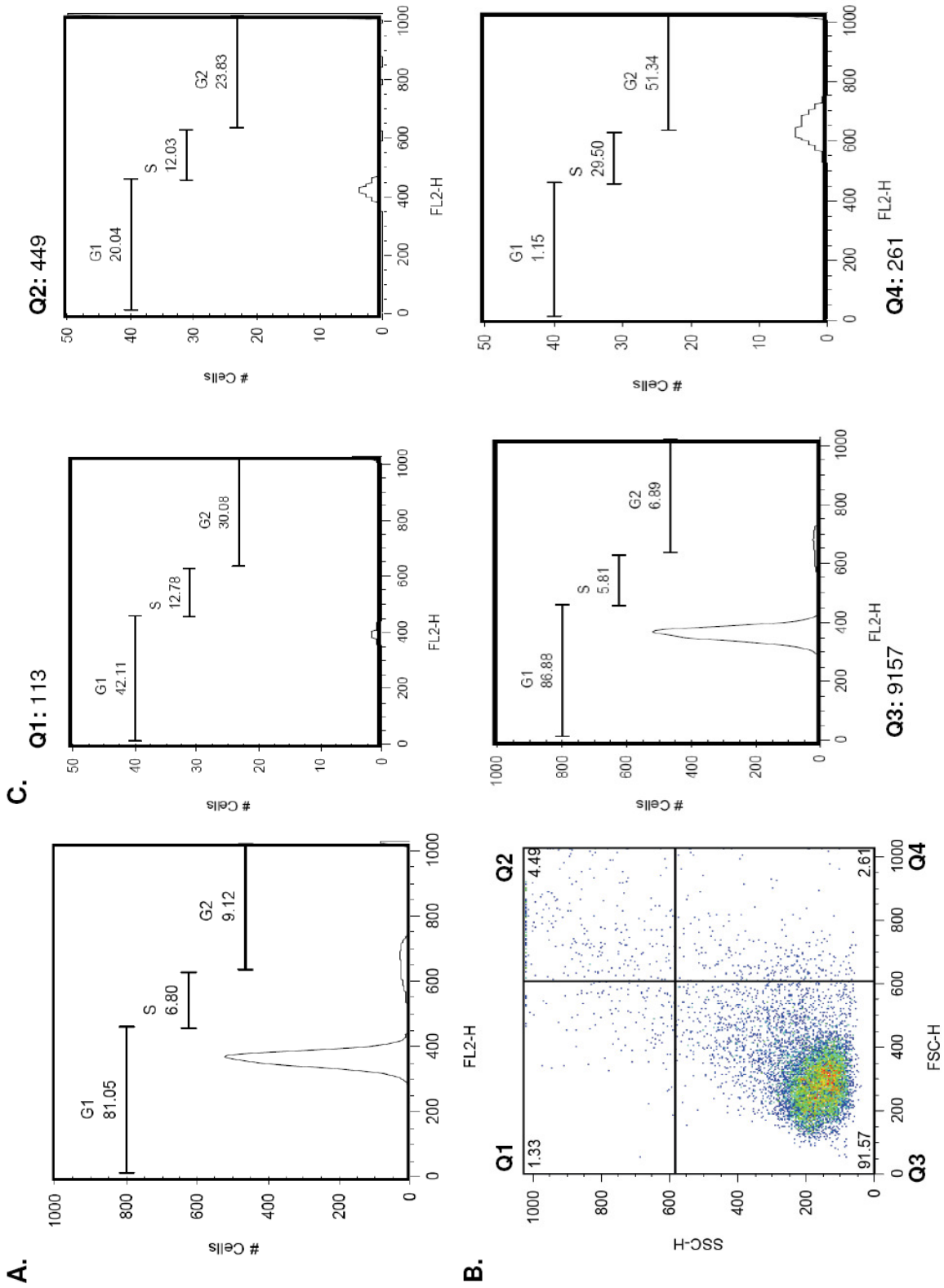

LNCaP V2 FACS: PI

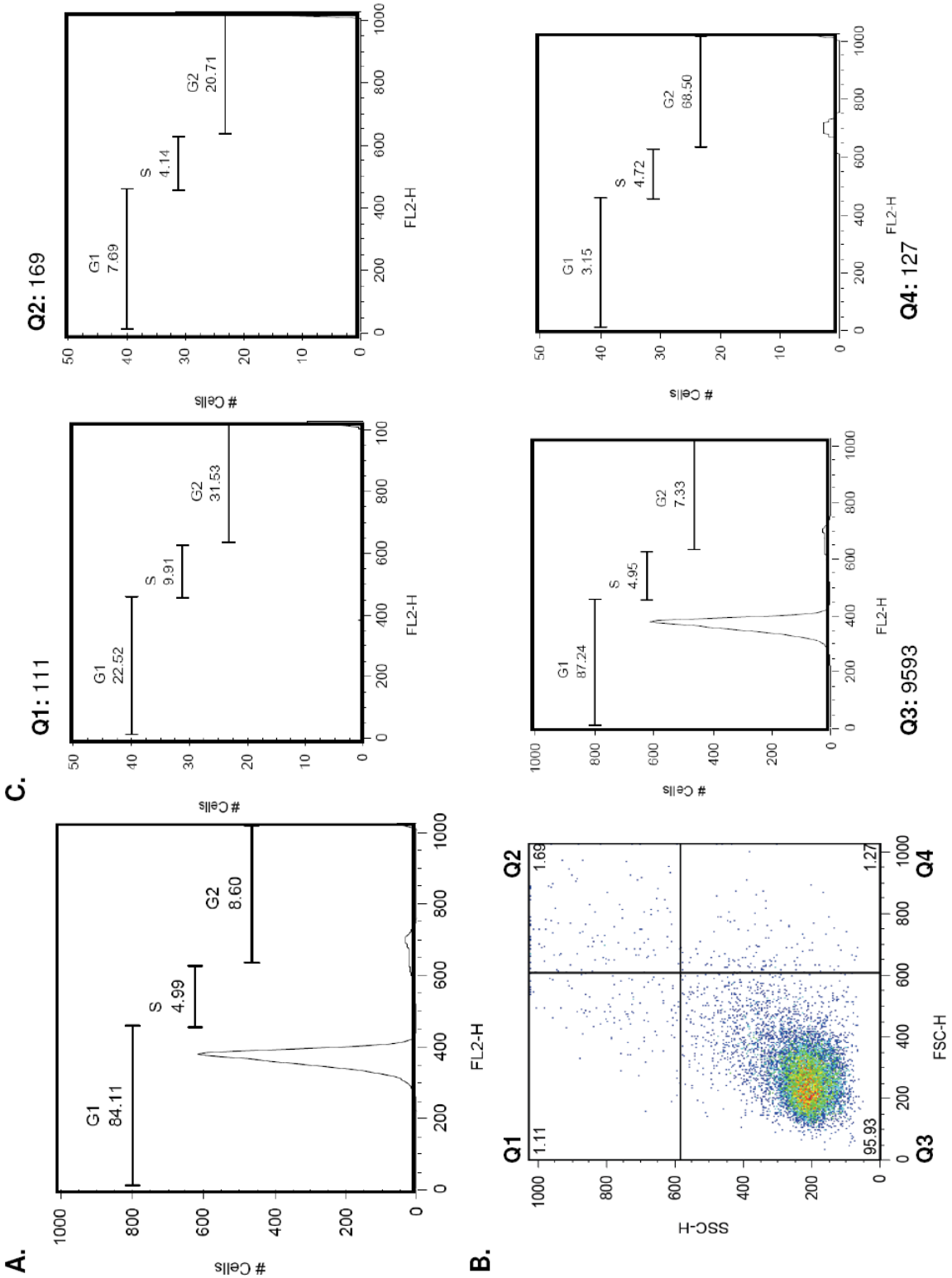

LNCaP FACS PI: OVERLAY

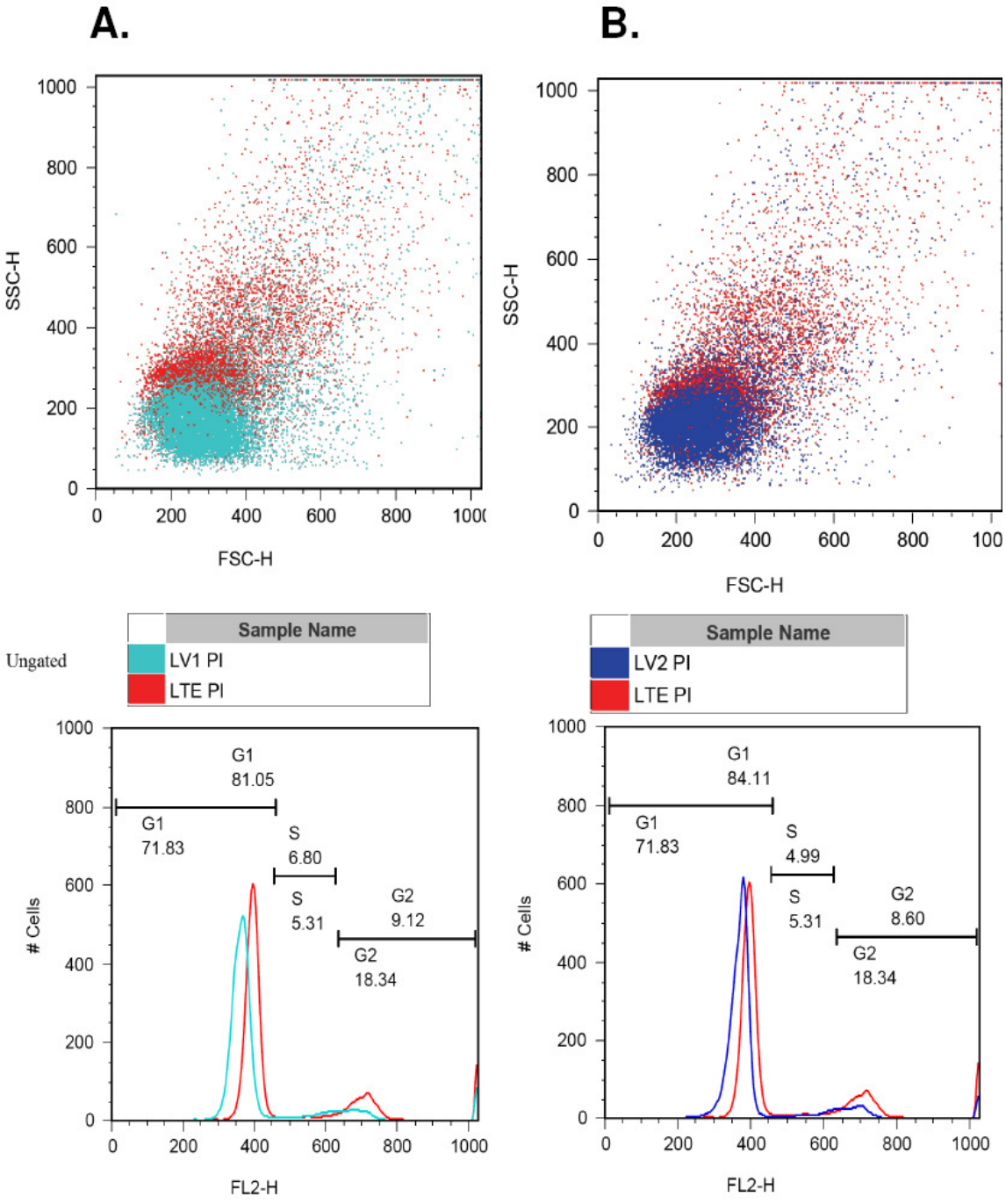

APPENDIX 8
APOPTOSIS FACS ANALYSIS: ANNEXIN V / 7-AAD

HL60 FACS: APOPTOSIS

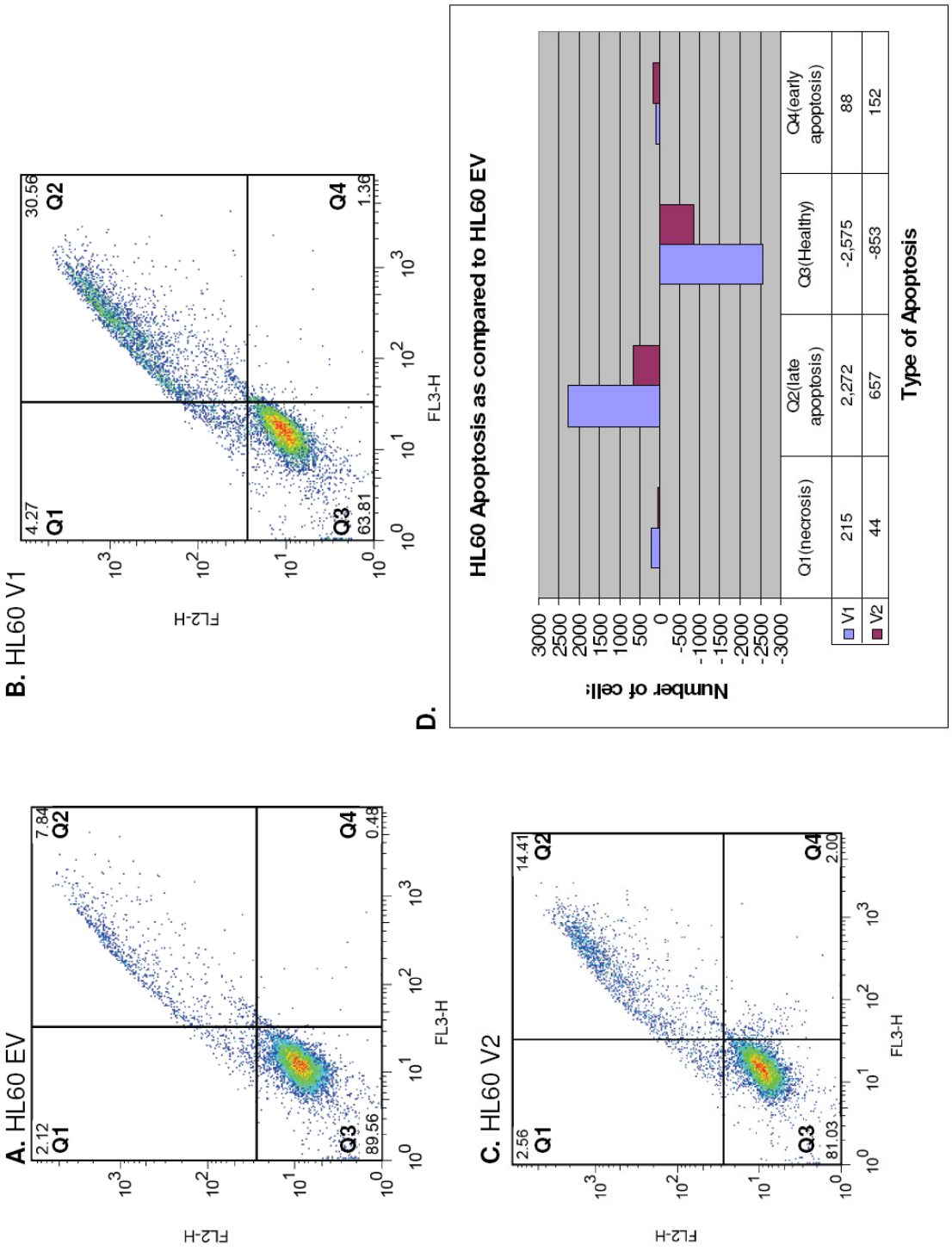

RPMI FACS: APPOPTOSIS

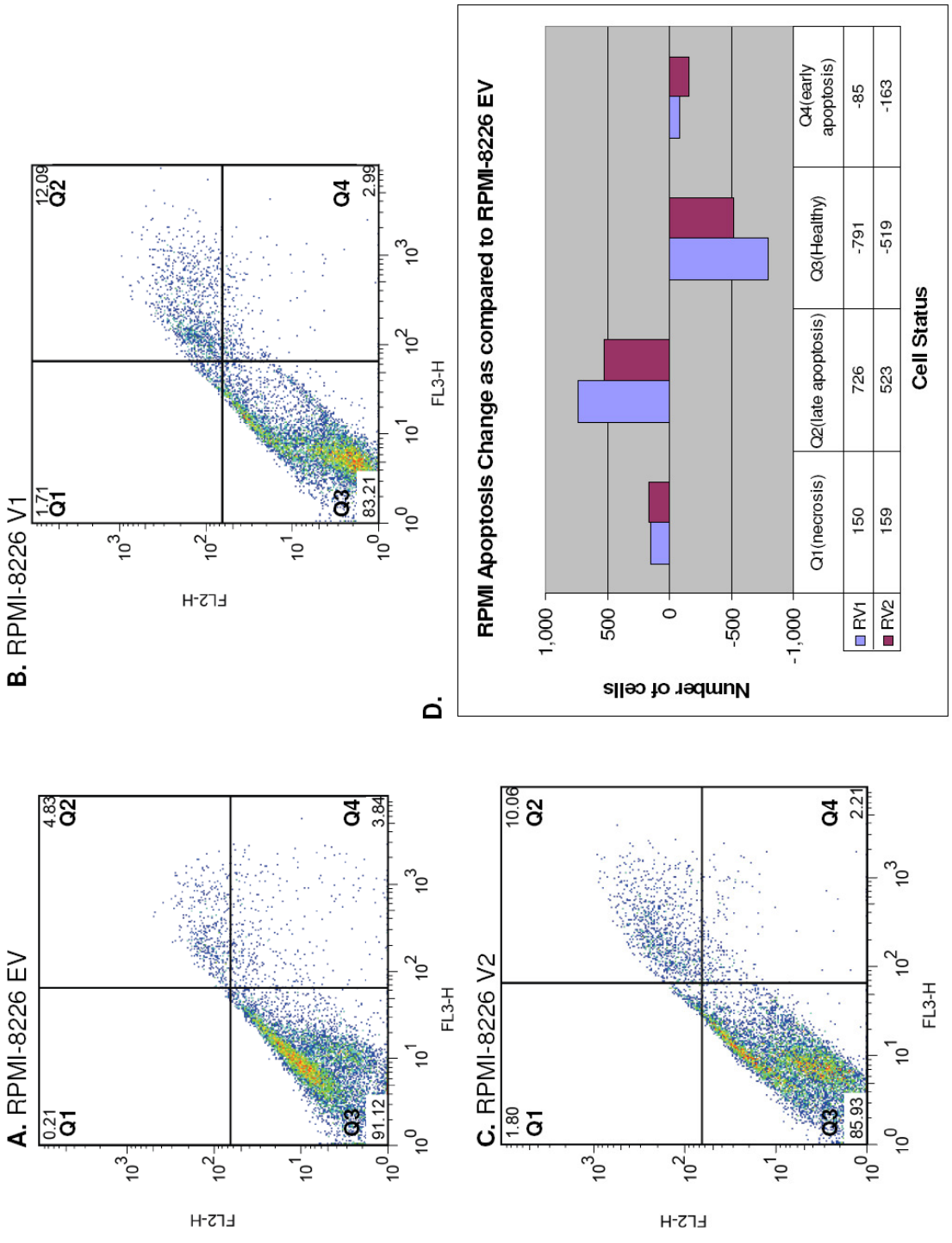

LNCaP FACS: APPOPTOSIS

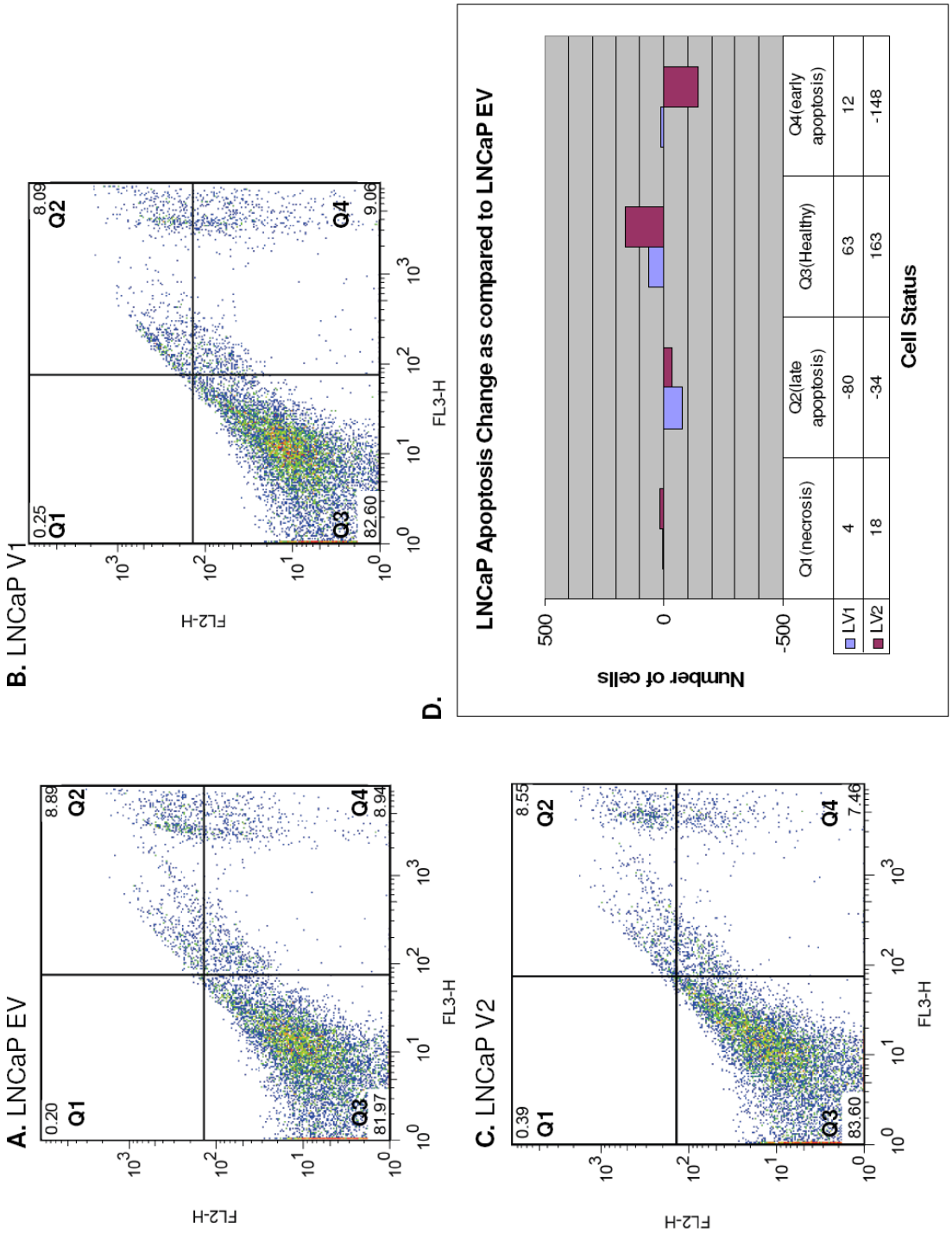

APPENDIX 9
PROTEIN ARRAY: KCNRG V1 & V2 TRANSFECTED CELL LINES

Protein Array For Cells Transfected with KCNRG

FOLD CHANGE AS COMPARED TO REGULARS - AND TRANSFECTED EMPTY WHEN PRESENT

MicroVigene Version 2997.00
Culture en-US
Row 89.00 Column 38.00

Y	Cl Casp6 D162	Cl Casp7 D198	Cl Casp9 D315	Cl Casp9 D330	pEGFR Y992	pIGFIR_IR YYYY	pIRS1 S612	pmTOR S2481	pVEGFR2 Y1175	
RPMI REGULAR										
S1B9	0.96	0.87	0.99	0.90	0.86	0.89	1.24	1.52	0.29	
S2A11	3.29	2.18	1.54	1.68	0.70	2.40	1.52	0.85	1.21	
S3A10	2.14	2.05	1.21	1.07	0.92	1.36	1.10	1.11	0.85	
RPMI V2	1.51	2.12	1.46	1.42	0.68	0.77	1.07	0.85	0.89	
(everything compared to TE)										
HL60 REGULAR	0.42	0.69	0.81	0.80	1.47	1.16	0.64	1.06	0.99	
HL60 TE										
HL60 V1	0.84	0.85	0.95	0.93	0.89	0.86	0.68	0.76	0.49	
HL60 V2	0.51	0.69	0.93	0.79	0.57	0.87	0.62	0.70	0.57	
(everything compared to HR)										
HL60 REGULAR										
HL60 TE	2.41	1.45	1.24	1.25	0.68	0.86	1.57	0.94	1.01	
HL60 V1	2.01	1.23	1.18	1.16	0.60	0.74	1.06	0.71	0.49	
HL60 V2	1.23	1.00	1.16	0.99	0.39	0.75	0.98	0.66	0.57	
LNCaP REGULAR										
LNCaP V1	1.16	1.02	1.08	0.90	0.47	0.49	0.93	0.90	0.93	
LNCaP V2	1.02	1.01	0.95	0.97	0.79	2.16	2.27	1.16	1.39	

Fold properties:

1.) If number is **equal to 1** the two samples are similar in intensity
2.) If the number is **greater than 1**, there is an **increase** in the test sample as compared to the control sample
3.) if the number is **less than 1**, there is a **decrease** in the test sample as compared to the control sample

pcAbl T735	pEGFR Y1148	pEGFR Y1173	pGSK3ab Y279_216	pJAK1 Y1022_23	pMEK1_2 S217_221	pPDGFR b Y716	pShc Y317	pSTAT1 Y701	pBAD S112
1.39	1.15	1.40	1.29	1.37	1.44	1.47	1.54	1.43	0.60
1.02	1.06	1.26	0.60	1.07	0.55	1.73	2.05	0.83	0.54
1.11	1.20	1.19	0.81	1.13	0.96	1.57	1.55	1.11	0.45
1.08	1.14	0.88	1.13	0.85	1.11	1.00	0.90	1.01	1.02
0.90	1.02	1.75	0.63	1.03	0.82	1.17	1.73	0.83	1.21
0.98	0.92	1.73	0.97	0.92	0.94	1.02	1.62	0.95	1.46
0.82	0.85	0.98	0.83	0.75	0.91	0.78	1.06	0.66	2.32
1.11	0.98	0.57	1.59	0.97	1.23	0.85	0.58	1.21	0.83
1.09	0.91	0.99	1.53	0.90	1.15	0.87	0.93	1.15	1.21
0.91	0.84	0.56	1.32	0.73	1.12	0.67	0.61	0.80	1.92
0.77	1.26	1.10	1.00	1.46	0.96	0.98	1.07	1.02	0.82
0.64	1.10	0.98	0.63	1.65	1.33	1.47	1.36	0.79	0.65

pERK T202_Y204	pmTOR S2448	pAKT S473 80ms	pErbB3 Y1289	pSrc Y527	pcAbl Y245	pMAPK pTEpY	pSrc Fam Y416	pAKT T308	pCREB S133
1.00	0.62	1.49	0.66	0.47	1.11	1.55	1.04	0.40	0.73
3.15	0.46	0.90	0.50	0.95	0.72	2.59	2.83	0.46	0.57
1.00	0.37	0.96	0.61	1.87	0.69	1.34	2.39	0.48	0.56
11.05	0.80	0.80	1.17	0.67	0.96	0.99	0.73	0.69	0.89
0.33	0.38	1.31	0.27	0.81	0.87	1.03	1.66	0.89	0.63
0.38	0.59	0.98	1.20	0.85	1.05	0.99	1.14	1.52	1.19
2.04	1.64	1.01	1.65	1.13	1.07	0.87	0.89	1.06	1.44
3.03	2.61	0.76	3.67	1.24	1.15	0.97	0.60	1.12	1.59
1.15	1.54	0.74	4.41	1.05	1.20	0.96	0.69	1.71	1.89
6.18	4.29	0.76	6.04	1.40	1.23	0.84	0.54	1.19	2.29
33.68	0.63	0.48	0.76	0.78	1.07	1.00	0.37	0.47	0.68
175.91	1.01	0.57	0.61	0.42	0.78	2.31	1.55	0.48	0.43

pErbB2 Y1248	pMARCKS S152_156	pSAPK_JNK T183_Y	pCl PARP D214	pGSK3ab S21_9	pIGFIR_IR Y1131_Y1	Cl Casp3 D175	OPN 300ms M 02210	plkBa S32_36
0.93	1.10	0.52	0.54	1.56	0.81	0.94	0.73	0.79
2.30	0.95	0.63	4.38	0.97	0.61	1.87	0.55	0.72
0.92	0.87	0.64	1.73	1.26	0.63	1.30	0.77	0.78
1.35	1.08	0.72	1.93	1.03	0.75	1.30	0.82	1.27
1.13	1.12	0.79	0.15	0.73	0.83	0.42	1.07	0.85
1.67	1.05	0.57	1.21	0.96	0.93	0.92	1.67	0.98
2.64	1.55	1.00	0.38	0.45	0.38	1.12	2.13	1.52
0.88	0.89	1.27	6.71	1.37	1.21	2.38	0.94	1.17
1.48	0.94	0.73	8.11	1.31	1.12	2.20	1.57	1.15
2.33	1.39	1.26	2.57	0.62	0.46	2.68	2.00	1.79
0.53	0.65	0.55	0.57	0.44	0.81	0.88	0.41	0.81
0.99	1.15	0.96	1.08	0.81	1.06	0.63	0.50	0.72

APPENDIX 10
MICROARRAY CANCER PATHWAY: KCNRG V1 TRANSFECTED CELLS

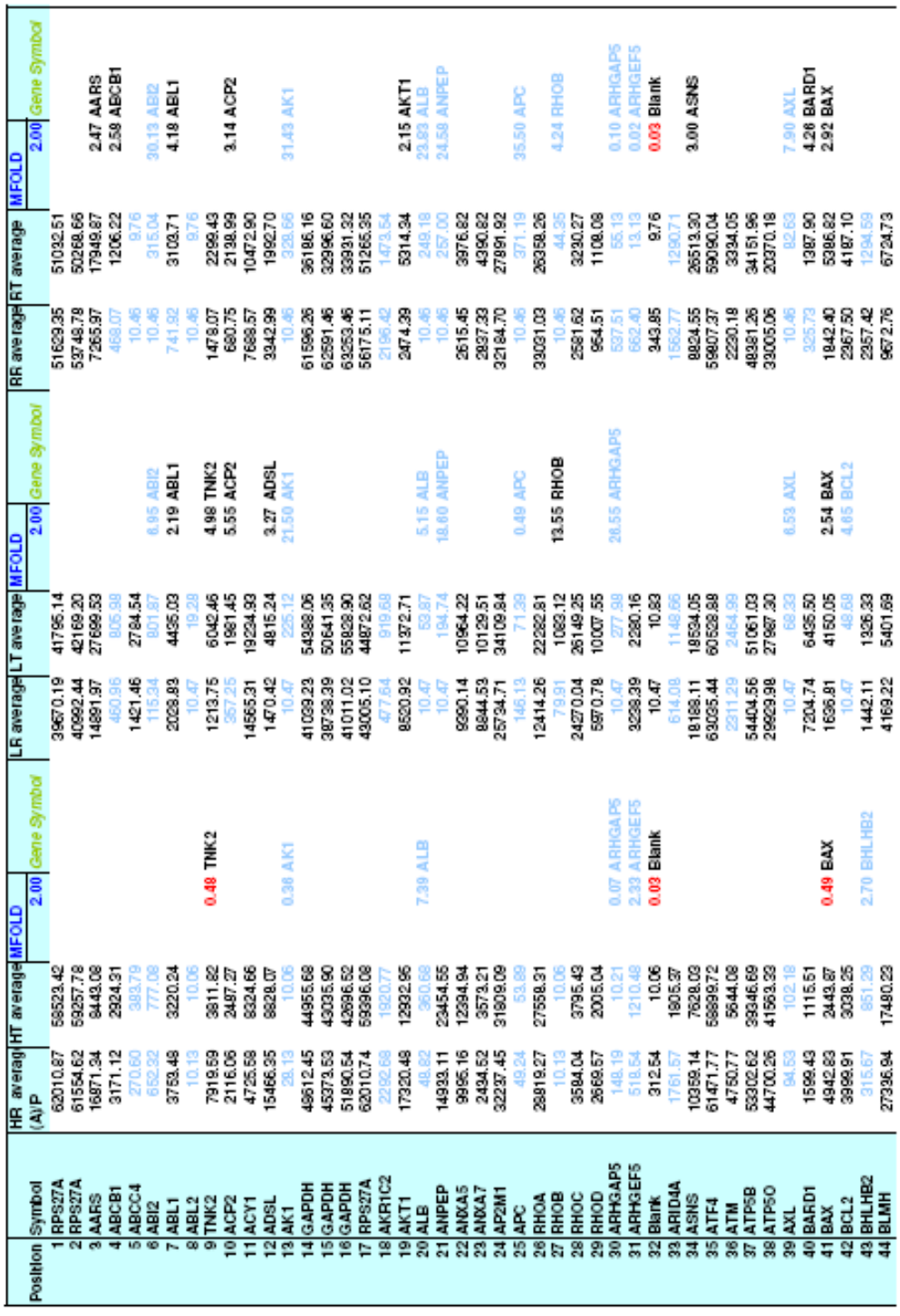

Position	Symbol	HR average (A)/P	HT average	MFOLD 2.00	Gene Symbol	LR average	LT average	MFOLD 2.00	Gene Symbol	RR average	RT average	MFOLD 2.00	Gene Symbol
1	RPS27A	62010.87	58523.42			39670.19	41795.14			51629.35	51032.51		
2	RPS27A	61554.62	59257.78			40992.44	42169.20			53748.78	50268.66		
3	AARS	16871.34	9449.08			14891.97	27699.53			7265.97	17949.87	2.47	AARS
4	ABCB1	3171.12	2924.31			460.96	805.98			468.07	1206.22	2.59	ABCB1
5	ABCC4	270.60	393.79			1421.46	2784.54			10.46	8.76		
6	ABI2	652.92	777.08			115.34	801.87	6.95	ABI2	10.46	315.04	30.13	ABI2
7	ABL1	3793.48	3220.24			2029.93	4435.03	2.19	ABL1	741.92	3103.71	4.18	ABL1
8	ABL2	10.13	10.06			10.47	19.28			10.46	9.76		
9	TNK2	7919.59	3811.82	0.48	TNK2	1213.75	6042.46	4.98	TNK2	1478.07	2299.43		
10	ACP2	2116.06	2497.27			357.25	1981.45	5.55	ACP2	680.75	2139.99	3.14	ACP2
11	ACY1	4725.58	8324.66			14565.31	19234.83			7688.57	10472.90		
12	ADSL	15466.35	8828.07			1470.42	4815.24	3.27	ADSL	3342.99	1992.70		
13	AK1	28.13	10.06	0.36	AK1	10.47	225.12	21.50	AK1	10.46	328.66	31.43	AK1
14	GAPDH	48612.45	44955.68			41039.23	54388.06			61596.26	36196.16		
15	GAPDH	45373.53	43035.90			38738.39	50641.35			62591.46	32996.60		
16	GAPDH	51890.54	42696.52			41011.02	55828.90			63253.46	33931.32		
17	RPS27A	62010.74	59396.08			43005.10	44872.62			56175.11	51265.35		
18	AKR1C2	2292.68	1920.77			477.64	919.68			2196.42	1473.54		
19	AKT1	17320.48	12992.95			8520.92	11372.71			2474.39	5314.34	2.15	AKT1
20	ALB	48.82	360.68	7.39	ALB	10.47	53.87	5.15	ALB	10.46	249.18	23.83	ALB
21	ANPEP	14933.11	23454.55			10.47	194.74	18.60	ANPEP	10.46	257.00	24.58	ANPEP
22	ANXA5	9995.16	12394.94			9290.14	10964.22			2515.45	3976.82		
23	ANXA7	2494.52	3573.21			8844.53	10129.51			2937.33	4390.82		
24	AP2M1	32237.45	31809.09			25734.71	34109.84			32184.70	27891.92		
25	APC	49.24	53.89			146.13	71.39	0.49	APC	10.46	371.19	35.50	APC
26	RHOA	28819.27	27558.31			12414.26	22282.81			3903103	26359.26		
27	RHOB	10.13	10.06			79.91	1083.12	13.55	RHOB	10.46	44.35	4.24	RHOB
28	RHOC	3594.04	3795.43			24270.04	26149.25			2581.62	3230.27		
29	RHOD	2668.57	2005.04			597.0.78	10007.55			964.51	1108.08		
30	ARHGAP5	148.19	10.21	0.07	ARHGAP5	10.47	277.99	26.55	ARHGAP5	537.51	55.13	0.10	ARHGAP5
31	ARHGEF5	518.54	1210.48	2.33	ARHGEF5	3239.39	2280.16			662.40	13.13	0.02	ARHGEF5
32	Blank	312.54	10.06	0.03	Blank	10.47	10.83			343.85	9.76	0.03	Blank
33	ARID4A	1761.57	1805.37			614.08	1148.66			1562.77	1290.71		
34	ASNS	10358.14	7628.09			18188.11	18534.05			8824.55	26513.30	3.00	ASNS
35	ATF4	61471.77	58899.72			63035.44	60528.88			59807.37	59090.04		
36	ATM	4750.77	5544.08			2211.29	2464.99			2230.18	3394.05		
37	ATP5B	53302.62	39346.69			54404.56	51061.03			48381.26	34151.96		
38	ATP5O	44700.26	41563.39			29929.98	27987.30			39005.06	20370.18		
39	AXL	94.53	102.18			10.47	68.33	6.53	AXL	10.46	82.63	7.90	AXL
40	BARD1	1598.43	1115.51			7204.74	6435.50			325.73	1387.90	4.26	BARD1
41	BAX	4942.83	2443.87	0.49	BAX	1696.81	4150.05	2.54	BAX	1842.40	5395.82	2.92	BAX
42	BCL2	3998.91	3038.25			10.47	48.68	4.65	BCL2	2367.50	4187.10		
43	BHLHB2	315.67	851.29	2.70	BHLHB2	1442.11	1335.33			2357.42	1294.59		
44	BLMH	27396.94	17480.23			4169.22	5401.69			967.2.76	6724.73		

45	BRAF	111.27	10.06	0.09 BRAF	10.47	10.12		10.46	9.76		
46	BRCA1	2208.19	1482.36		490.02	912.02		942.32	2104.05	2.23 BRCA1	
47	BRCA2	2083.25	1992.28		308.89	616.45		166.04	529.20	3.19 BRCA2	
48	BTK	12490.63	7895.78		10.47	10.12		2093.77	205.49	0.10 BTK	
49	CANX	29326.64	24438.88		15866.67	17515.96		21087.18	17524.06		
50	CAP1	14423.41	22069.91		10002.84	10379.92		7449.08	11289.28		
51	CAPN1	12483.73	19449.18		15943.67	14222.51		11031.07	12972.30		
52	CAPNS1	18539.72	18396.82		21623.01	31398.68		8040.56	8896.14		
53	CAV1	834.92	697.78		471.52	900.09		1200.18	1153.19		
54	CBFB	2367.53	1896.10		1171.64	1361.06		1847.21	3069.20		
55	CBLB	114.13	357.85	3.14 CBLB	473.04	345.55		10.46	620.47	59.34 CBLB	
56	CCL2	10.13	3016.83	297.80 CCL2	10.47	10.12		10.46	9.76		
57	CCND1	4809.77	2289.32	0.48 CCND1	5256.63	13185.29	2.51 CCND1	17.70	1818.53	102.74 CCND1	
58	CCND2	23860.62	20822.12		10.47	10.12		31685.63	39217.51		
59	CCND3	15853.98	29541.40		6392.61	5213.95		4903.69	5479.37		
60	CCNE1	5213.54	5358.17		1224.63	2187.17		627.62	1346.01	2.14 CCNE1	
61	CCT5	24801.50	28880.84		11568.03	12428.03		6966.44	8803.18		
62	CD24	10.13	10.06		10.47	56.41	5.39 CD24	10.46	9.76		
63	CD44	735.84	108.04	0.15 CD44	10.47	10.12		10.46	9.76		
64	CD59	2467.62	3258.65		1710.82	2014.74		1673.81	2945.47		
65	CDC20	7615.89	10567.24		5852.84	3603.09		3865.91	5761.90		
66	CDC25A	922.62	610.70		385.75	439.04		10.46	486.24	46.50 CDC25A	
67	CDC25B	4082.94	3436.68		3551.48	2066.48		6400.64	9049.83		
68	CDC25C	3442.82	2564.74		1355.51	2749.99	2.03 CDC25C	1043.38	2099.85	2.01 CDC25C	
69	CDC2L5	18988.80	17351.66		28246.67	27797.84		17291.23	21082.66		
70	CDK10	1406.69	940.88		918.00	1958.24	2.13 CDK10	10.46	672.27	64.29 CDK10	
71	CDK4	28934.96	22559.25		20509.28	23637.34		19629.94	27243.18		
72	CDK5	1403.32	1104.83		2007.88	2628.22		547.42	2188.08	4.00 CDK5	
73	CDK9	499.83	618.66		1506.83	1864.37		1021.68	1636.48		
74	CDKL1	557.24	369.29		490.34	347.18		252.93	893.93	3.53 CDKL1	
75	CDKN1A	6479.12	4446.05		38511.66	16732.59	0.43 CDKN1A	2000.57	4333.38	2.17 CDKN1A	
76	CDKN1B	1886.01	2048.39		3413.28	2420.35		2014.98	4156.17	2.06 CDKN1B	
77	CDKN1C	10.13	10.06		10.47	10.12		10.46	9.76		
78	CDKN2A	3662.07	5362.93		1946.76	1966.11		2442.93	3605.36		
79	CDKN2B	10.13	81.41	8.04 CDKN2B	10.47	10.12		10.46	202.53	19.37 CDKN2B	
80	CDKN2D	701.67	937.76		108.99	57.93		10.46	338.35	32.36 CDKN2D	
81	CEBPG	2368.39	1278.11		1773.34	1779.53		10.46	1146.92	109.69 CEBPG	
82	CENPC1	24.27	226.98	9.35 CENPC1	10.47	10.12		10.46	34.93	3.34 CENPC1	
83	CGRRF1	206.37	444.27	2.15 CGRRF1	831.15	459.65		10.46	418.00	39.98 CGRRF1	
84	CHAF1A	5491.76	3743.22		2385.80	1207.01		1527.79	2684.44		
85	CIB1	27770.96	21337.60		27984.36	29464.82		15362.15	18013.30		
86	CKMT1B	14351.70	13020.17		21413.65	21119.52		20671.65	21313.49		
87	CLK1	1001.15	892.07		914.34	312.62	0.34 CLK1	10.46	1202.31	114.98 CLK1	
88	CLK2	7444.00	8524.42		5362.52	4789.12		3743.86	6700.92		
89	CLK3	146.09	226.89		10.47	58.17	5.56 CLK3	12.98	564.87	43.53 CLK3	
90	CLNS1A	41789.72	24819.09		10318.79	12933.50		13852.32	17198.99		

91	CLTC	1789.83	3307.45		738.69	1990.22	2.69 CLTC	10.46	601.09	57.49 CLTC	
92	COL1A1	10.13	10.06		10.47	37.76	3.61 COL1A1	10.46	9.76		
93	COL6A3	10.13	36.59	3.61 COL6A3	10.47	117.26	11.20 COL6A3	10.46	9.76		
94	COX6C	16572.93	22689.11		20731.27	16346.84		8305.28	10681.34		
95	COX7A2	17468.64	35188.89	2.01 COX7A2	28444.33	21277.40		23387.06	23090.74		
96	Crat	1193.17	302.85	0.25 Crat	9851.94	10973.00		2365.67	3281.09		
97	CRHR1	10.13	10.06		10.47	10.12		10.46	9.76		
98	CSF1R	10.13	10.06		10.47	10.12		10.46	9.76		
99	CSK	7683.69	5554.79		1881.54	3820.79	2.03 CSK	3867.75	4586.97		
100	CSNK1G2	11806.19	14327.60		6682.02	7019.59		6278.70	6179.01		
101	CTNNA1	49.24	546.36	11.10 CTNNA1	7568.11	4185.79		3413.60	3802.08		
102	CTNNB1	411.75	267.84		272.92	612.90	2.25 CTNNB1	10.46	444.32	42.49 CTNNB1	
103	CTPS	5767.30	3938.17		1438.98	1671.41		1795.77	2766.77		
104	CTSC	5943.10	9007.49		10.47	239.32	22.86 CTSC	2468.78	3983.66		
105	CTSD	1312.67	2411.13		2666.40	2874.13		747.10	2296.78	3.07 CTSD	
106	CUL1	7002.13	10809.12		6350.99	4322.76		4845.85	8775.16		
107	CYR61	2584.89	1184.36	0.46 CYR61	2026.91	836.05	0.41 CYR61	2081.17	1710.57		
108	DCC	961.98	1282.15		11.82	10.12		10.46	503.87	48.19 DCC	
109	DCN	10.13	10.06		402.40	10.12	0.03 DCN	10.46	9.76		
110	DDX10	3537.73	3205.47		1904.25	1306.42		1325.85	2922.77	2.20 DDX10	
111	DEK	8759.56	8230.53		4483.36	4109.33		3306.07	9142.99	2.77 DEK	
112	DHCR7	14208.79	4697.97	0.33 DHCR7	6090.70	7103.15		10823.18	11060.52		
113	DHRS2	10.13	10.06		10.47	10.12		10.46	9.76		
114	DHX8	4898.62	7188.44		4140.07	5069.66		2097.18	3958.75		
115	DLG3	10.13	98.47	9.72 DLG3	10.47	10.12		10.46	76.65	7.33 DLG3	
116	DVL1	14308.44	9432.59		22292.86	22311.60		10982.44	15144.32		
117	DVL3	3568.71	3168.06		1597.25	2544.76		753.84	2526.70	3.35 DVL3	
118	E2F1	17405.46	7588.49	0.44 E2F1	6782.08	6938.63		1709.69	6236.92	3.65 E2F1	
119	E2F3	2997.81	2451.64		2466.99	1497.99		950.48	4746.68	4.99 E2F3	
120	E2F5	10.13	11.96		42.46	415.52	9.79 E2F5	10.46	75.37	7.21 E2F5	
121	EGFR	406.23	1016.17	2.50 EGFR	156.71	525.54	3.35 EGFR	10.46	9.76		
122	EGR1	1028.10	3628.80	3.53 EGR1	409.05	468.85		58.47	86.58		
123	EIF5	13.55	511.21	37.73 EIF5	10.47	39.13	3.74 EIF5	10.46	9.76		
124	EPHA2	10.13	74.14	7.32 EPHA2	489.54	486.39		57.19	717.44	12.55 EPHA2	
125	ERBB2	49.96	58.35		4089.74	6055.85		10.46	101.06	9.66 ERBB2	
126	ERBB3	746.85	1931.55	2.59 ERBB3	2308.32	2185.12		10.46	60.51	5.79 ERBB3	
127	ERBB4	1389.32	1596.82		101.39	134.24		10.46	113.85	10.89 ERBB4	
128	ERCC3	4133.48	3250.34		4102.47	4453.28		791.26	1976.25	2.50 ERCC3	
129	ETV1	10.13	10.06		57.57	1521.70	26.43 ETV1	10.46	9.76		
130	ETV3	10.13	10.06		10.47	10.12		10.46	16.19		
131	ETV6	1063.26	1958.11		409.47	519.49		10.46	1637.23	156.58 ETV6	
132	F2R	199.69	329.59		10.47	256.73	24.52 F2R	10.46	1172.30	112.11 F2R	
133	FASTK	10.13	146.45	14.46 FASTK	10.47	164.03	15.67 FASTK	10.46	213.62	20.43 FASTK	
134	FBN1	10.13	10.06		10.47	10.12		10.46	9.76		
135	FBN2	10.13	265.53	26.21 FBN2	10.47	10.12		10.46	9.76		
136	FES	1698.66	1586.62		139.36	205.59		10.46	191.67	18.33 FES	

137	FGFR1	10.13	32.71	3.23 FGFR1	27.23	39.13		10.46	9.76		
138	FGR	1331.14	6207.69	4.66 FGR	547.46	473.59		269.93	676.58	2.51 FGR	
139	FKBP8	10.13	10.06		642.85	915.19		10.46	30.35	2.90 FKBP8	
140	FN1	10.13	708.79	69.97 FN1	9523.49	5676.44		22269.03	19442.34		
141	FOS	82.76	1485.04	17.94 FOS	503.43	1176.72	2.34 FOS	432.57	415.14		
142	FOSL1	80.04	807.97	10.09 FOSL1	102.77	196.82		138.11	720.98	5.22 FOSL1	
143	FOSL2	3383.77	1957.53		3317.35	3223.11		1482.28	2442.46		
144	FOXG1A	10.13	10.06		10.47	60.13	5.74 FOXG1A	10.46	9.76		
145	FOXO1A	10.13	10.06		262.83	10.12	0.04 FOXO1A	10.46	296.30	28.34 FOXO1A	
146	FRAP1	4176.91	4809.77		1571.14	2264.28		1104.14	2931.77	2.66 FRAP1	
147	FRZB	624.18	603.84		34.40	389.77	11.33 FRZB	125.04	1191.84	9.53 FRZB	
148	FTL	59408.29	59502.58		35783.44	35857.90		63474.54	58891.76		
149	FZD2	899.14	985.58		587.56	574.01		1257.22	2285.82		
150	C2orf31	59.48	22.33	0.38 C2orf31	173.51	469.40	2.71 C2orf31	10.46	356.07	34.05 C2orf31	
151	FZD9	137.48	136.12		475.62	1133.39	2.38 FZD9	10.46	471.17	45.06 FZD9	
152	XRCC6	30307.51	35398.48		33351.63	40812.90		25871.44	27019.42		
153	GAS6	10.13	10.06		890.51	936.08		19683.85	7468.31	0.38 GAS6	
154	GCN5L2	12449.54	5566.10	0.45 GCN5L2	9251.29	11191.30		8802.14	10879.82		
155	GDF15	1163.46	2268.71		64159.20	61031.65		645.86	2117.32	3.28 GDF15	
156	GNA13	774.28	623.06		2130.69	2290.44		1026.98	1991.55		
157	GNAS	40142.60	43297.38		59620.13	56557.81		50885.43	45050.08		
158	GNB2	2074.41	2308.39		3143.19	3364.91		1726.70	2259.84		
159	GNB2L1	59351.22	59176.02		64006.48	61415.70		63686.35	54674.23		
160	AS1	161.97	79.06	0.49 AS1	110.39	288.16	2.61 AS1	243.25	231.12		
161	GPR39	10.13	10.06		10.47	10.12		10.46	9.76		
162	GRB2	13289.60	13400.55		5274.75	6168.47		3325.06	8645.87	2.60 GRB2	
163	GSK3A	11446.38	23219.08	2.03 GSK3A	11324.29	9440.05		7539.16	9248.92		
164	B2M	37450.21	36190.67		8360.83	4698.70		38574.32	45916.02		
165	GSPT1	8670.39	10204.31		15569.08	10476.73		9460.43	13847.22		
166	GTF2I	16365.88	17249.10		7704.77	12531.20		10292.89	9313.26		
167	H2AFZ	10931.94	10922.33		6555.98	7999.57		1197.70	4855.18	4.05 H2AFZ	
168	HADHA	3604.29	2969.52		1591.03	1818.83		470.74	1331.39	2.83 HADHA	
169	HDAC1	8132.13	9174.44		9492.92	11968.81		5278.75	6546.73		
170	HDGF	27104.82	30700.09		24255.26	22461.49		28113.11	29514.37		
171	HLA-C	52698.96	52969.31		39410.19	41520.08		63739.56	58037.88		
172	HLA-G	39756.43	45071.27		26256.73	22836.04		62080.22	51764.26		
173	HMGA1	56013.29	57496.18		32059.18	30228.68		52928.03	37955.72		
174	HMGB1	24931.28	25345.64		17780.63	18734.40		14175.72	14844.94		
175	HMGN2	18435.35	21307.65		16558.58	17464.75		14416.89	19378.14		
176	AS1	10.13	10.06		10.47	22.93	2.19 AS1	10.46	150.28	14.37 AS1	
177	HMMR	21.76	353.33	16.24 HMMR	231.33	144.05		10.46	436.76	41.77 HMMR	
178	HRB	10.13	10.06		10.47	10.12		10.46	16.43		
179	HSPA4	3023.66	4051.82		5248.35	4453.22		1023.48	3148.21	3.08 HSPA4	
180	HSPA5	2067.48	4265.13	2.06 HSPA5	602.62	663.33		401.01	2223.32	5.54 HSPA5	
181	B2M	37558.23	37820.03		9734.11	4915.33		39909.72	47330.10		
182	HSPA8	40711.32	39551.15		41017.52	42006.54		24156.84	24253.99		

183	HSPB1	49727.31	52298.31		64135.96	62354.49		58394.54	54681.80		
184	HSPH1	8011.22	10373.06		8659.91	8526.06		5371.17	9187.98		
185	HYAL1	10.13	10.06		224.60	318.57		122.07	604.75	4.95	HYAL1
186	HYOU1	10032.66	22547.80	2.25 HYOU1	24615.50	19187.65		27179.46	38044.53		
187	ICAM1	125.23	113.74		217.95	328.36		881.77	1892.88	2.15	ICAM1
188	ID1	14.87	10.06		124.11	146.99		141.05	774.17	5.49	ID1
189	ID2	407.96	696.29		243.86	114.24	0.47 ID2	3111.59	3191.07		
190	IDUA	10.13	67.76	6.69 IDUA	131.74	246.84		10.46	127.76	12.22	IDUA
191	IER3	10.13	10.06		10.47	41.80	3.99 IER3	10.46	143.44	13.72	IER3
192	AS1R1	10.13	10.06		10.47	18.13		10.46	9.76		
193	IFITM1	10.13	10.06		10.47	10.12		13500.14	21959.67		
194	IGF1R	10.13	10.06		10.47	31.83	3.04 IGF1R	10.46	330.24	31.58	IGF1R
195	IGF2R	5362.53	6477.54		7551.34	6545.83		6043.62	13976.18	2.31	IGF2R
196	IGFBP3	72.60	88.95		65.21	349.23	5.36 IGFBP3	1412.62	778.60		
197	IGFBP4	3088.01	1911.07		1048.17	2103.42	2.01 IGFBP4	1219.79	2822.09	2.31	IGFBP4
198	B2M	33754.37	31252.51		9421.88	6393.27		36323.54	44581.76		
199	IGFBP5	58930.64	59077.89		64019.97	62427.59		63730.87	58046.87		
200	IL1B	5318.68	6523.56		6534.80	9477.68		3736.52	7298.15		
201	ILK	4131.21	9964.96	2.41 ILK	10069.83	7322.04		5104.01	9657.32		
202	ING1	396.61	619.99		109.21	231.53	2.12 ING1	10.46	585.36	55.98	ING1
203	IRF3	9749.70	11647.49		10866.01	13762.81		11072.42	15062.46		
204	ITGA3	10.13	10.06		291.58	268.73		99.55	1483.39	14.90	ITGA3
205	ITGA6	10.13	10.06		10.47	206.71	19.74 ITGA6	10.46	9.76		
206	ITGB4	10.13	10.06		219.97	201.94		56.86	283.96	4.99	ITGB4
207	JAK1	10.13	156.21	15.42 JAK1	10.47	45.18	4.31 JAK1	10.46	393.78	37.66	JAK1
208	AS1R2	10.13	10.06		10.47	10.12		10.46	9.76		
209	JARID1A	103.12	1171.68	11.36 JARID1A	10.47	89.68	8.56 JARID1A	137.64	751.24	5.46	JARID1A
210	JUN	6461.34	2539.57	0.39 JUN	700.47	2026.13	2.89 JUN	39.98	1008.30	25.22	JUN
211	JUNB	12370.03	20094.41		7798.49	8879.44		5910.94	10862.14		
212	JUND	10812.67	11944.29		22598.96	23521.78		17141.35	12801.37		
213	K-ALPHA-1	61759.80	58433.53		58417.67	58246.44		57506.58	57857.58		
214	KIAA1026	979.35	758.81		619.58	870.06		527.21	1870.20	3.55	KIAA1026
215	KIT	4858.28	1873.67	0.39 KIT	730.57	911.66		878.82	1831.69	2.08	KIT
216	KITLG	10.13	10.06		305.52	165.52		10.46	118.80	11.36	KITLG
217	KLK10	10.13	602.58	59.48 KLK10	1061.96	1085.87		187.95	1486.73	7.91	KLK10
218	KPNA2	9048.94	12019.67		10059.06	4778.61	0.48 KPNA2	6300.68	9793.24		
219	KRAS	38.20	366.84	9.60 KRAS	745.87	866.25		439.60	1647.28	3.75	KRAS
220	KRT18	10.13	10.06		19350.13	22297.65		7744.84	8498.80		
221	KRT2A	10.13	10.06		10.47	77.93	7.44 KRT2A	10.46	9.76		
222	KRT9	10.13	10.06		10.47	16.35		10.46	9.76		
223	LAMB1	10.13	10.06		10.47	10.12		10.46	9.76		
224	AS1R3	10.13	10.06		10.47	10.12		10.46	9.76		
225	LAMP2	110.35	781.21	7.08 LAMP2	1875.78	1307.55		96.17	1985.78	20.65	LAMP2
226	LCK	190.06	183.69		2247.41	2689.58		10.46	2423.72	231.79	LCK
227	LCN2	25510.02	22064.41		27719.88	59566.37	2.15 LCN2	5435.19	54584.02	10.04	LCN2
228	LEP	398.98	35.16	0.09 LEP	4268.15	3285.55		10.46	1344.11	128.54	LEP

229	LITAF	2570.12	2739.69		2932.33	3507.65		1241.14	3643.34	2.94 LITAF
230	LRPAP1	15780.25	24848.53		19106.36	23296.73		18187.31	27253.06	
231	LTF	10.13	10.06		123.61	176.18		1490.27	6400.07	4.29 LTF
232	LYN	401.42	1598.45	3.98 LYN	455.81	265.28		10.46	9.76	
233	LZTR1	118.42	139.94		481.46	366.79		10.46	67.67	6.47 LZTR1
234	SMAD1	697.25	541.50		2138.42	1697.92		17.70	1529.92	86.43 SMAD1
235	MAP2K2	10169.76	9196.48		16753.36	22175.08		21181.94	19271.39	
236	MAP3K8	10.13	10.06		10.47	241.68	23.08 MAP3K8	10.46	9.76	
237	MAPK12	10.13	10.06		10.47	217.67	20.79 MAPK12	10.46	43.92	4.20 MAPK12
238	MAPK13	10.13	10.06		1065.12	1993.73		1245.37	2161.66	
239	MAPKAPK3	16314.79	15221.05		7296.97	5439.31		2526.75	5171.41	2.05 MAPKAPK3
240	MAPRE1	2962.45	2081.90		1760.75	2600.59		460.44	3373.41	7.33 MAPRE1
241	MARS	9002.61	13510.76		7888.40	10409.53		4020.54	15322.78	3.81 MARS
242	MAS1	10.13	10.06		10.47	66.72	6.37 MAS1	10.46	31.65	3.03 MAS1
243	MCC	295.85	104.41	0.35 MCC	172.05	768.41	4.47 MCC	10.46	585.72	56.02 MCC
244	MCM2	36089.24	23610.87		13767.35	13980.47		14051.64	20644.64	
245	MCM4	725.96	1072.96		10.47	182.41	17.42 MCM4	10.46	269.06	25.73 MCM4
246	MDM2	10.13	10.06		76.86	163.01	2.12 MDM2	10.46	149.72	14.32 MDM2
247	MDM4	3438.73	4822.75		11277.94	6741.49		3219.91	9505.29	2.95 MDM4
248	MET	1904.31	1775.91		341.09	603.04		266.18	1066.51	4.01 MET
249	MGST1	7693.82	11148.46		21713.65	14192.32		6722.23	12508.78	
250	MICB	1865.67	1988.53		2312.52	3093.11		2796.88	6729.51	2.41 MICB
251	MLLT3	10.13	10.06		364.49	598.18		10.46	213.74	20.44 MLLT3
252	MME	10.13	10.06		23029.45	34049.34		10.46	6158.20	588.94 MME
253	MMP1	10.13	10.06		10.47	72.23	6.90 MMP1	10.46	58.61	5.61 MMP1
254	MMP14	10.13	10.06		10.47	10.12		10.46	9.76	
255	MMP17	10.13	10.06		65.34	300.95	4.61 MMP17	10.46	144.54	13.82 MMP17
256	MMP2	14871.74	20964.25		23129.17	32011.13		23124.66	30720.74	
257	MNDA	264.75	2684.79	10.14 MNDA	10.47	10.12		10.46	9.76	
258	MSH2	3178.01	2109.59		10.47	10.12		10.46	1110.29	106.18 MSH2
259	MSH6	7378.75	9731.41		2474.73	2161.56		4142.39	4982.76	
260	MT3	828.43	999.40		466.11	1185.72	2.54 MT3	10.46	1276.14	122.04 MT3
261	MYB	29729.72	36084.55		95.06	55.32		471.14	2050.95	4.35 MYB
262	MYBL1	79.21	10.06	0.13 MYBL1	10.47	66.18	6.32 MYBL1	10.46	111.07	10.62 MYBL1
263	MYBL2	20463.19	11036.36		5907.38	4850.77		7660.11	13331.21	
264	MYC	20378.58	11182.48		4927.05	7224.84		21906.95	13801.49	
265	MYCL1	10.13	10.06		19.44	79.35	4.08 MYCL1	10.46	39.52	3.78 MYCL1
266	MYCN	10.13	10.06		10.47	45.00	4.30 MYCN	10.46	56.76	5.43 MYCN
267	MYD88	7471.49	6854.80		7101.06	7343.38		4843.10	8249.34	
268	MYL9	1937.13	1497.89		3885.63	5043.86		1468.02	3371.12	2.30 MYL9
269	MYLK	10.13	10.06		10.47	69.56	6.64 MYLK	10.46	331.24	31.68 MYLK
270	NEO1	10.13	10.06		308.43	276.76		287.80	807.22	2.80 NEO1
271	NF1	10.13	10.06		10.47	18.13		10.46	9.76	
272	NF2	4792.10	5308.13		10217.22	9020.38		3511.36	4575.56	
273	NFKB1	750.32	2485.27	3.31 NFKB1	5036.09	3199.74		1162.12	1366.53	
274	NFKB2	520.77	10.06	0.02 NFKB2	1349.16	1101.52		2947.30	3062.29	

275	NID1	3609.28	5856.39			5492.21	6896.50			3340.57	7365.48	2.20 NID1
276	NINJ1	11614.10	16373.79			22817.43	17183.30			7571.39	24650.12	3.26 NINJ1
277	NMBR	90.92	21.64	0.24	NMBR	10.47	126.34	12.07	NMBR	10.46	171.24	16.38 NMBR
278	NME1	12434.40	6953.51			17441.90	14295.92			13896.79	12311.12	
279	NME2	25483.38	18267.32			22117.12	19731.38			24704.67	18070.98	
280	NME3	7050.72	3063.55	0.43	NME3	5272.81	14033.22	2.66	NME3	2023.66	5933.09	2.93 NME3
281	NOTCH1	1955.18	3949.60	2.02	NOTCH1	3180.50	1005.81	0.32	NOTCH1	3541.28	2398.62	
282	NOTCH2	1989.66	2355.45			1049.19	504.26	0.48	NOTCH2	4013.70	8394.57	2.09 NOTCH2
283	NOTCH4	1556.41	2131.33			3122.13	3722.98			3911.80	5706.48	
284	NPM1	60089.73	56960.50			59990.79	53797.71			56707.19	35703.80	
285	NQO1	355.17	492.52			6738.42	2662.53	0.40	NQO1	10.46	1072.08	102.53 NQO1
286	NR1D1	23.88	24.89			203.85	265.06			91.30	1739.46	19.05 NR1D1
287	NR2F1	10.13	10.06			10.47	59.24	5.66	NR2F1	10.46	75.30	7.20 NR2F1
288	NR2F6	409.73	338.39			3655.40	3741.32			160.69	966.90	6.02 NR2F6
289	NRAS	55.09	159.40	2.89	NRAS	20.29	18.48			10.46	350.79	33.55 NRAS
290	NRG1	373.16	242.07			10.47	331.60	31.67	NRG1	10.46	442.46	42.31 NRG1
291	YBX1	53220.24	53018.71			38750.84	37416.56			56077.41	49154.54	
292	OSM	211.93	225.76			77.83	136.31			97.87	655.41	6.70 OSM
293	PA2G4	782.91	379.80	0.49	PA2G4	71.18	532.61	7.48	PA2G4	10.46	710.03	67.90 PA2G4
294	PABPC1	56361.12	48665.64			49230.29	53584.06			51454.61	40486.99	
295	PCNA	18934.07	15722.64			12981.02	11262.60			10508.85	15432.05	
296	PCTK1	335.91	406.10			313.89	597.44			172.48	807.76	4.68 PCTK1
297	PCTK2	95.78	131.72			697.44	815.62			435.45	1355.15	3.11 PCTK2
298	PCTK3	10.13	10.06			404.20	411.14			3155.42	4637.23	
299	PDGFA	640.56	1605.72	2.51	PDGFA	2900.75	2523.43			1391.66	3607.98	2.59 PDGFA
300	PDGFB	9952.70	13036.79			15562.54	25588.96			11652.71	13873.78	
301	PDGFRA	10.13	10.06			74.99	133.64			10.46	9.76	
302	PDPK1	804.72	2749.93	3.42	PDPK1	3772.45	3443.26			3186.90	3362.98	
303	PEA15	644.10	1448.98	2.25	PEA15	11210.53	14870.49			7614.59	6946.01	
304	PFDN4	53.54	380.87	7.11	PFDN4	166.03	294.35			10.46	298.37	28.53 PFDN4
305	PFDN5	33780.56	31100.75			22183.90	19470.12			17813.60	14269.10	
306	PGAM1	39412.36	47649.92			42581.02	49875.34			33304.86	24644.88	
307	PHB	4426.24	5049.94			3736.63	4289.48			2492.24	2630.10	
308	PIK3CA	252.50	577.34	2.29	PIK3CA	10.47	84.73	8.09	PIK3CA	323.51	2089.47	6.46 PIK3CA
309	PIK3CB	63.34	377.13	5.95	PIK3CB	275.26	608.40	2.21	PIK3CB	10.46	129.38	12.37 PIK3CB
310	PIK3CG	9475.69	18514.53			16686.23	19360.42			5236.07	15934.12	3.04 PIK3CG
311	PIM1	439.86	114.09	0.26	PIM1	6828.95	1305.40	0.19	PIM1	5383.86	3605.65	
312	PKM2	25351.96	48691.94			27059.29	43426.65			60543.65	53629.57	
313	PKMYT1	9434.80	4295.79	0.46	PKMYT1	2251.43	1621.72			5156.83	8675.04	
314	PLK2	10.13	10.06			1334.23	2562.58			10.46	415.88	39.77 PLK2
315	PPARD	22315.48	33281.23			39784.29	48243.36			37941.45	44717.63	
316	PPARG	607.25	1506.69	2.48	PPARG	798.89	511.39			10.46	174.09	16.65 PPARG
317	PPP2R5A	66.30	120.09			695.85	737.95			10.46	427.10	40.85 PPP2R5A
318	PRDX2	7598.68	6822.15			37284.33	44282.79			27040.65	15198.63	
319	PRDX4	6649.28	14645.48	2.20	PRDX4	13493.16	15215.93			47161.80	43109.97	
320	PRKAR1A	22501.56	17147.92			23536.46	24553.97			28864.32	26547.55	

321	PRKCBP1	1236.91	2081.85		550.39	838.25		87.05	1504.58	17.28	PRKCBP1
322	PRNP	907.39	811.24		3018.51	2985.05		77.08	3025.76	39.26	PRNP
323	PRSS15	26074.45	33821.83		31303.42	24587.35		16165.94	38506.11	2.38	PRSS15
324	PSMA1	7822.29	8364.53		3568.74	5707.84		669.37	3035.70	4.54	PSMA1
325	PTCH	10.13	418.55	41.32 PTCH	1338.60	3713.26	2.77 PTCH	29.78	442.09	14.85	PTCH
326	PTEN	2119.58	2681.67		3599.15	1440.04	0.40 PTEN	2116.28	2869.43		
327	PTGS1	6440.83	5081.16		5138.02	11480.28	2.23 PTGS1	5862.16	3539.21		
328	PTMA	43740.11	27277.95		35937.70	26442.85		38898.56	26240.65		
329	PTN	10.13	10.06		10.47	10.12		10.46	67.74	6.48	PTN
330	PTPRN	10.13	10.06		10.47	10.12		10.46	9.76		
331	RAB5A	2015.30	3133.81		5075.09	3750.74		1124.45	2517.75	2.24	RAB5A
332	RAC1	1955.02	1984.68		3978.54	5256.63		2720.07	4259.01		
333	RAD50	10.13	10.06		10.47	42.87	4.09 RAD50	61.02	9.76	0.16	RAD50
334	RAF1	7623.53	8669.93		9622.43	8330.20		7086.19	6305.96		
335	RALBP1	662.20	565.28		70.59	324.79	4.60 RALBP1	363.58	623.82		
336	RAP1A	11104.09	16548.17		9158.30	7643.26		5277.63	7389.23		
337	RARA	17120.83	27217.75		24057.52	28679.33		21440.85	31870.33		
338	RARB	10.13	10.06		10.47	68.34	6.53 RARB	10.46	185.67	17.76	RARB
339	RASGRF1	6073.52	11836.67		11223.89	11135.61		5402.73	9931.10		
340	RB1	14118.67	24114.84		26282.19	29699.93		20912.55	29101.38		
341	RBBP4	11478.11	11108.66		14339.48	11407.08		15594.74	18736.49		
342	RBL2	505.68	728.14		583.24	870.32		10.46	504.10	48.21	RBL2
343	PHB2	32958.38	24507.73		21145.16	14482.37		23939.31	16311.19		
344	REL	311.96	180.12		19.61	44.61	2.28 REL	10.46	300.68	28.76	REL
345	RELA	2970.35	2308.82		2144.84	2743.82		1510.53	4543.78	3.01	RELA
346	RELB	1611.23	2093.33		3163.16	966.70	0.31 RELB	4091.02	6770.61		
347	RET	2330.17	238.35	0.10 RET	158.67	134.35		33.89	146.09	4.31	RET
348	RFC2	467.41	82.70	0.18 RFC2	10.47	10.12		10.46	176.13	16.84	RFC2
349	RGS19	18721.94	13724.67		56.77	210.98	3.72 RGS19	1229.31	1598.16		
350	RIPK1	10.13	10.06		52.81	156.78	2.97 RIPK1	125.62	280.19	2.23	RIPK1
351	RPN2	14669.45	23474.51		19295.03	16470.97		32826.92	40095.14		
352	RPS6KB1	557.56	67.60	0.12 RPS6KB1	873.63	534.00		319.43	448.93		
353	RRM1	13173.76	6908.85		4509.97	4283.72		422.21	2394.71	5.67	RRM1
354	SARS	3495.76	3143.72		15148.48	5769.25	0.38 SARS	1392.82	7004.10	5.03	SARS
355	SELENBP1	10.13	10.06		35345.73	31621.98		10.46	68.45	6.55	SELENBP1
356	SEMA3C	10.13	10.06		406.34	466.39		10.46	277.33	26.52	SEMA3C
357	SEMA4D	2974.41	4294.52		402.88	532.69		58.85	808.00	13.73	SEMA4D
358	SEPP1	10.13	10.06		10.47	434.88	41.53 SEPP1	10.46	1869.42	178.78	SEPP1
359	SEPT6	1856.56	794.30	0.43 SEPT6	10.47	201.42	19.24 SEPT6	897.14	2563.81	2.86	SEPT6
360	SERPINH1	10.13	10.06		10.47	10.12		10.46	281.99	26.97	SERPINH1
361	SFN	47.13	10.21	0.22 SFN	10.47	87.58	8.36 SFN	6477.77	1953.68	0.30	SFN
362	SFPQ	876.20	720.21		1290.74	1266.46		1344.94	2154.31		
363	HSPCB	50288.72	41457.92		55534.59	48535.17		53709.82	47434.90		
364	SFRS7	1061.40	748.19		652.07	1239.31		216.12	166.49		
365	SHB	10.13	10.06		553.33	227.39	0.41 SHB	120.84	9.76	0.08	SHB
366	SHH	10.13	10.06		10.47	167.48	15.99 SHH	29.88	41.96		

367	SIAH2	3393.88	1794.94		2556.63	1867.05		7668.47	7116.17		
368	SIVA	34188.58	31011.00		12012.75	10072.55		6811.07	6472.50		
369	SKI	10.13	10.06		10.47	10.12		10.46	9.76		
370	SKIL	10.13	10.06		10.47	10.12		10.46	50.77	4.86	SKIL
371	SLC16A1	162.61	588.91	3.62 SLC16A1	1230.63	2841.23	2.31 SLC16A1	10.46	1087.64	104.02	SLC16A1
372	SLC1A4	1220.59	2824.28	2.31 SLC1A4	10.47	10.12		2744.12	5024.35		
373	SLC20A1	11321.55	21587.20		6961.12	2134.48	0.31 SLC20A1	1889.19	3936.78	2.08	SLC20A1
374	SMO	10.13	10.06		10.47	390.36	37.28 SMO	10.46	9.76		
375	SMPD1	15.91	11.56		152.96	306.66	2.00 SMPD1	10.46	206.34	19.73	SMPD1
376	SNAI2	10.13	10.06		29.77	53.01		127.63	415.80	3.26	SNAI2
377	SND1	41483.02	26634.59		18639.45	14194.06		53440.87	41987.76		
378	HSPCB	50617.41	40255.03		54395.60	49769.49		55093.15	48173.34		
379	SNRPB2	3867.02	6302.73		4092.72	2305.16		3036.64	3014.05		
380	SOCS1	10.13	10.06		842.89	193.58	0.23 SOCS1	344.36	790.62	2.30	SOCS1
381	SOCS3	10.13	10.06		332.88	285.11		10.46	38.94	3.72	SOCS3
382	SOD1	25836.60	39559.79		49159.90	43009.46		32194.74	28405.89		
383	SORT1	10.13	10.06		298.20	277.54		46.07	256.21	5.56	SORT1
384	SPINT2	10.13	10.06		26308.15	25401.64		17793.27	17165.24		
385	SPRY2	10.13	274.76	27.12 SPRY2	10.47	10.12		10.46	9.76		
386	SRC	10.13	10.06		10.47	10.12		10.46	68.25	6.53	SRC
387	SRPX	345.27	10.06	0.03 SRPX	10.47	10.12		10.46	329.34	31.50	SRPX
388	STAT1	1772.83	605.65	0.34 STAT1	507.71	193.55	0.38 STAT1	1165.16	7427.92	6.38	STAT1
389	STAT2	716.60	2804.29	3.91 STAT2	923.38	922.18		269.93	1705.64	6.32	STAT2
390	STAT3	88.33	748.80	8.48 STAT3	1327.79	1370.05		10.46	590.37	56.46	STAT3
391	STAT5B	10.13	10.06		10.47	10.12		10.46	9.76		
392	STC1	478.53	62.57	0.13 STC1	786.13	655.75		484.39	959.24		
393	HSPCB	51105.23	41935.57		52730.90	49152.25		52262.11	49735.78		
394	TAF1	1025.22	1025.70		816.54	2076.15	2.54 TAF1	1488.83	1096.04		
395	TBL3	10.13	10.06		100.57	12.25	0.12 TBL3	10.46	9.76		
396	TBRG4	21299.28	19119.48		14582.36	9871.62		15736.85	11339.61		
397	TCF1	2770.93	3285.85		4996.08	3563.12		3692.44	3740.30		
398	TCF7L2	992.39	2766.10	2.79 TCF7L2	4713.58	3125.18		8356.53	9325.02		
399	TFAP2C	10.13	10.06		1342.90	1116.70		10.46	9.76		
400	TFDP1	7652.78	8833.30		2122.91	1314.81		2594.91	3658.07		
401	TFDP2	327.88	150.78	0.46 TFDP2	10.47	10.12		10.46	9.76		
402	TGFA	10.13	120.34	11.88 TGFA	10.47	10.12		10.46	15.41		
403	TGFB1	10.13	10.06		10.47	10.12		10.46	20.97	2.01	TGFB1
404	TGFBI	10.13	10.06		10.47	10.12		10.46	9.76		
405	TGFBR2	1372.08	1229.42		659.84	1328.50	2.01 TGFBR2	487.63	1154.13	2.37	TGFBR2
406	TGFBR3	10.13	10.06		29.86	73.67	2.47 TGFBR3	10.46	9.76		
407	THBS1	203.57	106.42		1495.34	670.70	0.45 THBS1	10.46	370.67	35.45	THBS1
408	HSPCB	53907.53	43715.00		55051.06	52824.22		52039.39	50581.97		
409	TIE1	628.77	630.93		1172.31	1119.25		1166.78	1413.78		
410	TIMP1	6002.92	27295.90	4.55 TIMP1	659.99	1205.01		24658.73	10996.24	0.45	TIMP1
411	TIMP3	10.13	10.06		10.47	10.12		10.46	9.76		
412	TJP1	10.13	10.06		5835.82	3466.43		10.46	9.76		

413	TK1	9636.57	4491.86	0.47 TK1	13758.64	6803.32	0.49 TK1	12109.74	12011.46		
414	TLE1	10.13	10.06		2711.27	1336.34	0.49 TLE1	10.46	224.20	21.44 TLE1	
415	TNF	468.58	18098.31	38.62 TNF	10.47	10.12		10.46	9.76		
416	TNFRSF10A	231.13	3815.42	16.51 TNFRSF10A	10.47	112.38	10.73 TNFRSF10A	10.46	275.79	26.38 TNFRSF10A	
417	TNFRSF10B	8177.10	13133.19		16649.29	10262.34		3796.95	7325.12		
418	TNFRSF1A	12008.03	27168.69	2.26 TNFRSF1A	9066.39	8484.75		3204.38	4832.77		
419	TNFRSF1B	21809.46	23111.55		10.47	10.12		7116.63	6388.17		
420	FAS	10.13	10.06		10.47	10.12		10.46	75.56	7.23 FAS	
421	TNFSF7	361.29	109.02	0.30 TNFSF7	10.47	10.12		10.46	1405.00	134.37 TNFSF7	
422	TNK1	139.78	108.45		537.63	1282.50	2.39 TNK1	10.46	422.97	40.45 TNK1	
423	TOB1	10.13	103.83	10.25 TOB1	2474.07	2856.80		111.42	650.03	5.83 TOB1	
424	TP53	10.13	10.06		11523.15	18538.65		3175.63	7650.33	2.41 TP53	
425	TP53BP2	1351.76	2280.88		1070.66	482.03	0.45 TP53BP2	10.46	32.86	3.14 TP53BP2	
426	TP53I3	10.13	10.06		412.54	32.63	0.08 TP53I3	10.46	9.76		
427	TP73	10.13	10.06		10.47	10.12		10.46	9.76		
428	TPBG	128.17	27.79	0.22 TPBG	17.91	10.12		130.21	461.19	3.54 TPBG	
429	TPT1	59793.29	56799.89		44454.16	43000.93		41247.93	32501.50		
430	TRADD	1604.53	3674.10	2.29 TRADD	3287.33	3720.34		11552.60	7661.48		
431	TRAM1	10.13	724.17	71.48 TRAM1	119.78	302.69	2.53 TRAM1	10.46	439.32	42.01 TRAM1	
432	TRRAP	10.13	10.06		10.47	120.65	11.52 TRRAP	10.46	9.76		
433	ACTB	45376.94	58233.20		51338.91	38144.75		48264.05	36605.72		
434	TSG101	3645.12	4912.98		5787.27	4747.74		1696.68	3003.73		
435	TUFM	29232.87	33090.64		25025.76	19467.53		36180.58	23062.17		
436	TXNRD1	2226.27	3253.78		3072.21	3462.02		363.62	1937.61	5.33 TXNRD1	
437	TYRO3	1742.57	1098.62		1299.99	1467.88		50.83	1273.11	25.04 TYRO3	
438	UBC	41357.15	57862.80		62742.33	58200.35		60535.68	58175.67		
439	UBE2L6	10458.01	5335.92		1586.71	1206.72		15310.25	35618.95	2.33 UBE2L6	
440	UCHL1	10.13	10.06		10.47	10.12		10.46	85.85	8.21 UCHL1	
441	USP7	1605.45	2658.28		1541.57	1609.62		2476.41	3937.93		
442	VDAC1	6375.03	5813.14		10660.73	9233.11		13443.38	4586.50	0.34 VDAC1	
443	VEGF	10.13	10.06		10.47	10.12		10.46	9.76		
444	VHL	44.85	163.09	3.64 VHL	47.54	10.12	0.21 VHL	10.46	9.76		
445	PUC18	64.59	23.66	0.37 PUC18	10.47	10.12		10.46	9.76		
446	Pol1	10.13	10.06		10.47	10.12		10.46	9.76		
447	Luc1	10.13	10.06		132.41	41.04	0.31 Luc1	125.19	40.36	0.32 Luc1	
448	Luc2	10.13	10.06		10.47	10.12		10.46	9.76		
449	ACTB	43790.80	57981.99		51935.11	36758.38		48453.90	34877.03		
450	Blank	158.89	466.11	2.93 Blank	568.69	298.96		368.88	241.03		
451	Blank	69.54	185.79	2.67 Blank	62.53	10.12	0.16 Blank	10.46	87.73	8.39 Blank	
452	VIL2	1227.47	2455.93	2.00 VIL2	590.91	687.05		1759.16	1597.78		
453	WEE1	1213.56	1818.79		1831.88	691.29	0.38 WEE1	10.46	584.28	55.88 WEE1	
454	WNT1	2548.15	6719.58	2.64 WNT1	1864.30	2955.80		1506.23	5007.99	3.32 WNT1	
455	WNT2	10.13	10.06		10.47	10.12		395.92	82.15	0.21 WNT2	
456	WNT2B	10.13	10.06		10.47	10.12		10.46	9.76		
457	WNT3	10.13	10.06		10.47	10.12		10.46	9.76		
458	WNT5A	10.13	10.06		10.47	10.12		10.46	9.76		

459	WT1	2058.24	3048.48			10.47	10.12			10.46	9.76		
460	18SrRNA	258.94	563.08	2.17	18SrRNA	3472.53	1404.60	0.40	18SrRNA	2059.88	2348.33		
461	PPIH	3269.05	3289.30			607.20	612.71			1075.67	1968.81		
462	M6PR	7480.88	8233.58			2549.74	1159.19	0.45	M6PR	2521.88	4923.44		
463	NONO	26568.71	16306.42			25073.51	18601.48			16632.13	16271.81		
464	LDHA	20671.48	22371.75			20191.34	40057.31			40166.40	14309.32	0.36	LDHA
465	ACTB	45789.84	57386.32			50616.06	33985.27			48283.48	35687.94		
466	ACTB	34632.45	55468.42			51389.34	36382.10			47534.42	35833.58		
467	ACTB	35760.43	57230.41			52979.78	38768.97			47983.00	38431.71		
468	XRCC1	5468.43	3113.62			1125.13	397.37	0.35	XRCC1	1592.39	1603.42		
469	XRCC4	10.13	80.19	7.92	XRCC4	187.43	10.12	0.05	XRCC4	10.46	320.33	30.63	XRCC4
470	XRCC5	6825.08	9970.55			6022.44	5524.78			2849.74	4476.30		
471	YES1	332.61	750.64	2.26	YES1	1687.70	2226.74			231.67	1043.53	4.50	YES1
472	YWHAB	6323.80	10700.38			8924.23	9410.65			2657.30	2824.31		
473	YWHAZ	886.49	1595.23			2702.39	2778.48			113.68	1463.73	12.88	YWHAZ
474	ZAP70	10.13	10.06			10.47	10.12			10.46	9.76		
475	ZNF9	15762.44	12940.61			11125.11	6063.17			5673.01	9066.46		
476	BAS2C	10.13	10.06			10.47	10.12			10.46	9.76		
477	BAS2C	10.13	10.06			10.47	10.12			10.46	9.76		
478	BAS2C	971.20	280.54	0.29	BAS2C	647.22	1080.73			1663.47	1675.88		
479	BAS2C	14151.57	13680.56			16299.43	14166.91			27402.04	21758.21		
480	BAS2C	55665.37	54479.48			60707.95	55707.77			63724.06	55593.68		
Present Genes:				*111.00*	53.00			*123.00*	41.00			*215.00*	82.00
ABSENT				58.00				82.00				133.00	
Mann-Whitney valid hits:					25.00				17.00				93.00

Avg. after normalization

HR 1	HR 2	HR 3	HR 4	HT 1	HT 2	HT 3	HT 4	LR 1	LR 2	LR 3	LR 4
8,498.24	8,544.15	8,532.60	7,853.74	10,456.19	9,381.27	7,489.03	8,096.06	-	8,668.43	8,362.62	7,760.64

	8,498.24		8,855.64		8,263.90
Stdev for H	934.93	10.9%			
Stdev for L	3,451.63	57.5%			
Stdev for R	3,229.50	53.0%			

Hochberg Test													
Genes rejected	43	53	73	21	60	62	19	23	-	63	57	33	
Position	Symbol	*HR 1 12.21* test result	*HR 2 01.11.* test result	*HR 3 02.15.(* test result	*HR 4 02.20.07.jp* test result	*HT 1 12.21.* test result	*HT 2 01.11.* test result	*HT 3 02.15.(* test result	*HT 4 02.20.07.jp* test result	*LR 1 12.21.(* test result	*LR 2 01.11.0* test result	*LR 3 02.15.(* test result	*LR 4 02.20.07.jp* test result
1	RPS27A		Reject					Reject					
2	RPS27A		Reject					Reject					
3	AARS												
4	ABCB1		Reject			Reject							
5	ABCC4												

APPENDIX 11
RT-ARRAY vs. MICROARRAY: CANCER PATHWAY PLATFORM

		Up-Down Regulation (comparing to control group)		Microarray
Well	Symbol	HV1	HV2	H
A01	ABL1	-6.1903	-2.2974	-1.16558912
A02	AKT1	1.0792	-1.4142	-1.33925177
A09	BAX	-1.9588	-1.7411	-2.022543207
A11	BCL2	-2.4116	-3.0314	-1.316519303
C07	BRAF	-1.9319	-1.6245	-11.05802705
E07	FAS	1.5369	-1.1487	-1.006762592
E11	IGF1R	-3.8906	-2.1435	-1.006762592
F06	TNF	-25.9921	-10.5561	38.62389015
F07	TNFRSF1(	1.6702	1.5157	16.50798612
F08	TNFRSF1(	-6.2333	-2.4623	1.606093025
F10	TNFRSF1A	-3.6553	-3.7321	2.262543553
G06	TP53	1.057	-1.3195	-1.006762592
G07	TP53BP2	-2.6945	-1.3195	1.687334569
G08	TP73	2.362	-1.3195	-1.006762592
G09	TRADD	-1.7171	-1.6245	2.289834341
H01	B2M	-2.7702	-1.8661	-1.034802804
H04	GAPDH	-3.6301	-1.3195	-1.081341684
H05	ACTB	1	1	1.283321382

		Up-Down Regulation (comparing to control group)		Microarray
Well	Symbol	LV1	LV2	L
A01	ABL1	-1.4044	-1.0718	2.185999865
A02	AKT1	-1.0425	1	1.334681369
A09	BAX	-2.2974	1.5157	2.535447111
A11	BCL2	1.2483	12.1257	4.648702103
C07	BRAF	-1.7777	1.8661	-1.034452454
E07	FAS	-2.0279	-1.7411	-1.034452454
E11	IGF1R	1.8921	1.7411	3.039949607
F06	TNF	1.9185	1.3195	-1.034452454
F07	TNFRSF1(	-1.3566	-1.1487	10.73324837
F08	TNFRSF1(	-1.5369	-1.2311	-1.622368183
F10	TNFRSF1A	-1.9862	1.6245	-1.068550273
G06	TP53	-2.514	-1.7411	1.60881744
G07	TP53BP2	-1.0281	1	-2.221144753
G08	TP73	3.8106	3.0314	-1.034452454
G09	TRADD	1.2058	1.4142	1.131719518
H01	B2M	-1.1173	1.8661	-1.779393103
H04	GAPDH	-2.9282	1.2311	1.325269948
H05	ACTB	1	1	-1.345897174

		Up-Down Regulation (comparing to control group)				Microarray
Well	Symbol	S1B9	S2A11	S3A10	RV2	R
A01	ABL1	9.9866	14.42	6.5887	5.8159	1.781965
A02	AKT1	2	5.3517	4	5.6962	1.590361
A09	BAX	2.7511	8.0556	3.6301	2.3457	1.921616
A11	BCL2	1.2483	1.4044	-1.057	-1.3851	1.323882
C07	BRAF	1.2924	3.4343	1.0497	1.5263	-1.543789
E07	FAS	4.0558	6.6346	1.014	-1.5583	1.17741
E11	IGF1R	2.1585	2.9485	-1.2226	-1.8404	1.874575
F06	TNF	4.084	2.4967	1.5476	-1.0718	-1.655046
F07	TNFRSF1(	1.2058	2.2658	1.4845	1.9588	1.152906
F08	TNFRSF1(	-1.1647	3.4822	1.6021	3.2944	1.587053
F10	TNFRSF1A	1.2311	2.6027	-1.2311	1.4948	1.234229

G06	TP53	1.8277	1.9185	1.3851	1.3104	1.87554
G07	TP53BP2	-2.0279	1.5052	-3.0738	-2.3295	-1.367506
G08	TP73	-1.5476	6.774	3.6553	1.879	-1.627263
G09	TRADD	-1.6472	2.2815	-1.7654	1.1647	-1.492684
H01	B2M	1.8277	-1.434	-1.3472	-1.0867	1.214584
H04	GAPDH	3.2043	1.6935	-1.014	-1.7171	-1.629071
H05	ACTB	1	1	1	1	-1.26931

REFERENCES

REFERENCES

Aerts JL, Gonzales MI, Topalian SL. Selection of appropriate control genes to assess expression of tumor antigens using real-time RT-PCR. Biotechniques. 2004 Jan;36(1):84-6, 88, 90-1. PMID: 14740490

Aravind L, Koonin EV. Fold prediction and evolutionary analysis of the POZ domain: structural and evolutionary relationship with the potassium channel tetramerization domain. J Mol Biol. 1999 Jan 29;285(4):1353-61.

Argenti B, Gallo R, Di Marcotullio L, Ferretti E, Napolitano M, Canterini S, De Smaele E, Greco A, Fiorenza MT, Maroder M, Screpanti I, Alesse E, Gulino A. Hedgehog antagonist REN(KCTD11) regulates proliferation and apoptosis of developing granule cell progenitors. J Neurosci. 2005 Sep 7;25(36):8338-46.

Argenti B, Gallo R, Di Marcotullio L, Ferretti E, Napolitano M, Canterini S, De Smaele E, Greco A, Fiorenza MT, Maroder M, Screpanti I, Alesse E, Gulino A.Hedgehog antagonist REN(KCTD11) regulates proliferation and apoptosis of developing granule cell progenitors. J Neurosci. 2005 Sep 7;25(36):8338-46. PMID: 16148242

Attali B, Honoré E, Lesage F, Lazdunski M, Barhanin J. Regulation of a major cloned voltage-gated K+ channel from human T lymphocytes. FEBS Lett. 1992 Jun 1;303(2-3):229-32. PMID: 1607023

Avdonin V, Kasuya J, Ciorba MA, Kaplan B, Hoshi T, Iverson L. Apoptotic proteins Reaper and Grim induce stable inactivation in voltage-gated K+ channels. Proc Natl Acad Sci U S A. 1998 Sep 29;95(20):11703-8. PMID: 9751729

Baranova A, Hammarsund M, Ivanov D, Skoblov M, Sangfelt O, Corcoran M, Borodina T, Makeeva N, Pestova A, Tyazhelova T, Nazarenko S, Gorreta F, Alsheddi T, Schlauch K, Nikitin E, Kapanadze B, Shagin D, Poltaraus A, Ivanovich Vorobiev A, Zabarovsky E, Lukianov S, Chandhoke V, Ibbotson R, Oscier D, Einhorn S, Grander D, Yankovsky N. Distinct organization of the candidate tumor suppressor gene RFP2 in human and mouse: multiple mRNA isoforms in both species- and human-specific antisense transcript RFP2OS. Gene. 2003 Dec 4;321:103-12.

Baranova A, Hammarsund M, Ivanov D, Skoblov M, Sangfelt O, Corcoran M, Borodina T, Makeeva N, Pestova A, Tyazhelova T, Nazarenko S, Gorreta F, Alsheddi T, Schlauch

K, Nikitin E, Kapanadze B, Shagin D, Poltaraus A, Ivanovich Vorobiev A, Zabarovsky E, Lukianov S, Chandhoke V, Ibbotson R, Oscier D, Einhorn S, Grander D, Yankovsky N. Distinct organization of the candidate tumor suppressor gene RFP2 in human and mouse: multiple mRNA isoforms in both species- and human-specific antisense transcript RFP2OS. Gene. 2003 Dec 4;321:103-12. PMID: 14636997

Barcellona ML, Cardiel G, Gratton E. Time-resolved fluorescence of DAPI in solution and bound to polydeoxynucleotides. Biochem Biophys Res Commun. 1990 Jul 16;170(1):270-80. PMID: 2372293

Bärlund M, Monni O, Weaver JD, Kauraniemi P, Sauter G, Heiskanen M, Kallioniemi OP, Kallioniemi A. Cloning of BCAS3 (17q23) and BCAS4 (20q13) genes that undergo amplification, overexpression, and fusion in breast cancer. Genes Chromosomes Cancer. 2002 Dec;35(4):311-7. PMID: 12378525

Bardwell VJ, Treisman R. The POZ domain: a conserved protein-protein interaction motif. Genes Dev. 1994 Jul 15;8(14):1664-77.

Barton K, Nucifora G. AML1 haploinsufficiency, gene dosage, and the predisposition to acute leukemia. Bioessays. 2000 Mar;22(3):214-8.

Bayón Y, Trinidad AG, de la Puerta ML, Del Carmen Rodríguez M, Bogetz J, Rojas A, De Pereda JM, Rahmouni S, Williams S, Matsuzawa S, Reed JC, Crespo MS, Mustelin T, Alonso A.KCTD5, a putative substrate adaptor for cullin3 ubiquitin ligases. FEBS J. 2008 Aug;275(15):3900-10. Epub 2008 Jun 28. PMID: 18573101

Beghini A, Magnani I, Roversi G, Piepoli T, Di Terlizzi S, Moroni RF, Pollo B, Fuhrman Conti AM, Cowell JK, Finocchiaro G, Larizza L.The neural progenitor-restricted isoform of the MARK4 gene in 19q13.2 is upregulated in human gliomas and overexpressed in a subset of glioblastoma cell lines. Oncogene. 2003 May 1;22(17):2581-91. PMID: 12735302

Binet JL, Auquier A, Dighiero G, et al. A new prognostic classification of chronic lymphocytic leukemia derived from a multivariate survival analysis. Cancer. 1981;48:198

Bixby K.A. , Nanao M.H. , Shen N.V. , Kreusch A. , Bellamy H. , Pfaffinger P.J. , Choe S. Zn2+-binding and molecular determinants of tetramerization in voltage-gated K+ channels. Nat. Struct. Biol. 6 38-43 1999 [PubMed: 9886290]

Bonnet S, Rochefort G, Sutendra G, Archer SL, Haromy A, Webster L, Hashimoto K, Bonnet SN, Michelakis ED. The nuclear factor of activated T cells in pulmonary arterial hypertension can be therapeutically targeted. Proc Natl Acad Sci U S A. 2007 Jul 3;104(27):11418-23. Epub 2007 Jun 27. PMID: 17596340

Bouyge-Moreau I, Rondeau G, Avet-Loiseau H, André MT, Bézieau S, Chérel M, Saleün S, Cadoret E, Shaikh T, De Angelis MM, Arcot S, Batzer M, Moisan JP, Devilder MC. Construction of a 780-kb PAC, BAC, and cosmid contig encompassing the minimal critical deletion involved in B cell chronic lymphocytic leukemia at 13q14.3. Genomics. 1997 Dec 1;46(2):183-90. PMID: 9417905

Brajenovic M, Joberty G, Küster B, Bouwmeester T, Drewes G. Comprehensive proteomic analysis of human Par protein complexes reveals an interconnected protein network. J Biol Chem. 2004 Mar 26;279(13):12804-11.

Brevet M, Ahidouch A, Sevestre H, Merviel P, El Hiani Y, Robbe M, Ouadid-Ahidouch H. Expression of K+ channels in normal and cancerous human breast. Histol Histopathol. 2008 Aug;23(8):965-72. PMID: 18498071

Brito-Babapulle V, Baou M, Matutes E, Morilla R, Atkinson S, Catovsky D. Deletions of D13S25, D13S319 and RB-1 mapping to 13q14.3 in T-cell prolymphocytic leukaemia. Br J Haematol. 2001 Aug;114(2):327-32. PMID: 11529851

Brodianskiĭ VM, Sulimova GE, Udina IG, Aitova SS, Shaĭkhaev GO, Zakhar'ev VM, Fedorova LI, Zelenin AV, Eĭnkhorn S, Baush Ch, et al. [Screening of YAC-clones and creation of a contig covering the region of human chromosome 13, often deleted in B-cell chronic lymphocytic leukemia] Mol Biol (Mosk). 1995 Sep-Oct;29(5):1126-36.

Brookman-Amissah N, Nariculam J, Freeman A, Willamson M, Kirby RS, Masters JR, Feneley MR. Allelic imbalance at 13q14.2 approximately q14.3 in localized prostate cancer is associated with early biochemical relapse. Cancer Genet Cytogenet. 2007 Dec;179(2):118-26. PMID: 18036398

Bueso-Ramos CE, Ferrajoli A, Medeiros LJ, Keating MJ, Estrov Z. Aberrant morphology, proliferation, and apoptosis of B-cell chronic lymphocytic leukemia cells. Hematology. 2004 Aug;9(4):279-86.

Byrd JC, Stilgenbauer S, Flinn IW. Chronic lymphocytic leukemia. Hematology (Am Soc Hematol Educ Program). 2004;:163-83.

Cahalan MD, Lewis RS. Functional roles of ion channels in lymphocytes. Semin Immunol. 1990 Mar;2(2):107-17. Review. PMID: 1717052

Caligaris-Cappio F, Hamblin TJ. B-cell chronic lymphocytic leukemia: a bird of a different feather. J Clin Oncol. 1999 Jan;17(1):399-408. Review. PMID: 10458259

Calin GA, Croce CM. Genomics of chronic lymphocytic leukemia microRNAs as new players with clinical significance. Semin Oncol. 2006 Apr;33(2):167-73. Review. PMID: 16616063

Calin GA, Dumitru CD, Shimizu M, Bichi R, Zupo S, Noch E, Aldler H, Rattan S, Keating M, Rai K, Rassenti L, Kipps T, Negrini M, Bullrich F, Croce CM. Frequent deletions and down-regulation of micro- RNA genes miR15 and miR16 at 13q14 in chronic lymphocytic leukemia. Proc Natl Acad Sci U S A. 2002 Nov 26;99(24):15524-9. Epub 2002 Nov 14. PMID: 12434020

Calin GA, Ferracin M, Cimmino A, Di Leva G, Shimizu M, Wojcik SE, Iorio MV, Visone R, Sever NI, Fabbri M, Iuliano R, Palumbo T, Pichiorri F, Roldo C, Garzon R, Sevignani C, Rassenti L, Alder H, Volinia S, Liu CG, Kipps TJ, Negrini M, Croce CM. A MicroRNA signature associated with prognosis and progression in chronic lymphocytic leukemia. N Engl J Med. 2005 Oct 27;353(17):1793-801. Erratum in: N Engl J Med. 2006 Aug 3;355(5):533. PMID: 16251535

Campos L, Sabido O, Viallet A, Vasselon C, Guyotat D.Expression of apoptosis-controlling proteins in acute leukemia cells.Leuk Lymphoma. 1999 May;33(5-6):499-509.PMID: 10342577

Caporaso N, Marti GE, Goldin L. Perspectives on familial chronic lymphocytic leukemia: genes and the environment. Semin. Hematol. 2004 Jul;41(3):201-6.

Cauchi S, Proença C, Choquet H, Gaget S, De Graeve F, Marre M, Balkau B, Tichet J, Meyre D, Vaxillaire M, Froguel P; D.E.S.I.R. Study Group.Analysis of novel risk loci for type 2 diabetes in a general French population: the D.E.S.I.R. study. J Mol Med. 2008 Mar;86(3):341-8. Epub 2008 Jan 22. PMID: 18210030

Chen L, Li J, Xu W, Qiu H, Zhu Y, Zhang Y, Duan L, Qian S, Lu H. Molecular cytogenetic aberrations in patients with multiple myeloma studied by interphase fluorescence in situ hybridization. Exp Oncol. 2007 Jun;29(2):116-20. PMID: 17704743

Chendrimada TP, Gregory RI, Kumaraswamy E, Norman J, Cooch N, Nishikura K, Shiekhattar R. TRBP recruits the Dicer complex to Ago2 for microRNA processing and gene silencing. Nature. 2005 Aug 4;436(7051):740-4. Epub 2005 Jun 22. PMID: 15973356

Chiorazzi N, Ferrarini M. Evolving view of the in-vivo kinetics of chronic lymphocytic leukemia B cells. Hematology Am Soc Hematol Educ Program. 2006;:273-8, 512.

Cho YG, Kim CJ, Song JH, Rhie DJ, Park YK, Kim SY, Nam SW, Yoo NJ, Lee JY, Park WS. Genetic and expression analysis of the KCNRG gene in hepatocellular carcinomas.Exp Mol Med. 2006 Jun 30;38(3):247-55. PMID: 16819283

Choo KB, Chen HH, Liu TY, Chang CP. Different modes of regulation of transcription and pre-mRNA processing of the structurally juxtaposed homologs, Rnf33 and Rnf35, in

eggs and in pre-implantation embryos. Nucleic Acids Res. 2002 Nov 15;30(22):4836-44. PMID: 12433986

Chouinard SW, Wilson GF, Schlimgen AK, Ganetzky B. A potassium channel beta subunit related to the aldo-keto reductase superfamily is encoded by the Drosophila hyperkinetic locus. Proc Natl Acad Sci U S A. 1995 Jul 18;92(15):6763-7. PMID: 7542775

Corcoran MM, Hammarsund M, Zhu C, Lerner M, Kapanadze B, Wilson B, Larsson C, Forsberg L, Ibbotson RE, Einhorn S, Oscier DG, Grandér D, Sangfelt O. DLEU2 encodes an antisense RNA for the putative bicistronic RFP2/LEU5 gene in humans and mouse. Genes Chromosomes Cancer. 2004 Aug;40(4):285-97. PMID: 15188451

Corcoran MM, Rasool O, Liu Y, Iyengar A, Grander D, Ibbotson RE, Merup M, Wu X, Brodyansky V, Gardiner AC, Juliusson G, Chapman RM, Ivanova G, Tiller M, Gahrton G, Yankovsky N, Zabarovsky E, Oscier DG, Einhorn S. Detailed molecular delineation of 13q14.3 loss in B-cell chronic lymphocytic leukemia. Blood. 1998 Feb 15;91(4):1382-90. PMID: 9454769

Cuneo A, Bigoni R, Rigolin GM, Roberti MG, Bardi A, Cavazzini F, Milani R, Minotto C, Tieghi A, Della Porta M, Agostini P, Tammiso E, Negrini M, Castoldi G. Late appearance of the 11q22.3-23.1 deletion involving the ATM locus in B-cell chronic lymphocytic leukemia and related disorders. Clinico-biological significance. Haematologica. 2002 Jan;87(1):44-51.

Cuneo A, Bigoni R, Rigolin GM, Roberti MG, Bardi A, Piva N, Milani R, Bullrich F, Veronese ML, Croce C, Birg F, Döhner H, Hagemeijer A, Castoldi G. Cytogenetic profile of lymphoma of follicle mantle lineage: correlation with clinicobiologic features. Blood. 1999 Feb 15;93(4):1372-80. PMID: 9949181

Cushman SJ, Nanao MH, Jahng AW, DeRubeis D, Choe S, Pfaffinger PJ. Voltage dependent activation of potassium channels is coupled to T1 domain structure. Nat Struct Biol. 2000 May;7(5):403-7. PMID: 10802739

Dahlén A, Debiec-Rychter M, Pedeutour F, Domanski HA, Höglund M, Bauer HC, Rydholm A, Sciot R, Mandahl N, Mertens F. Clustering of deletions on chromosome 13 in benign and low-malignant lipomatous tumors. Int J Cancer. 2003 Feb 20;103(5):616-623. Review. PMID: 12494468

Danilov AV, Danilova OV, Klein AK, Huber BT. Molecular pathogenesis of chronic lymphocytic leukemia. Curr. Mol. Med. 2006 Sep;6(6):665-75.

Devilder MC, François S, Bosic C, Moreau A, Mellerin MP, Le Paslier D, Bataille R, Moisan JP. Deletion cartography around the D13S25 locus in B cell chronic lymphocytic

leukemia and accurate mapping of the involved tumor suppressor gene.Cancer Res. 1995 Mar 15;55(6):1355-7. PMID: 7882336

Di Marcotullio L, Ferretti E, De Smaele E, Argenti B, Mincione C, Zazzeroni F, Gallo R, Masuelli L, Napolitano M, Maroder M, Modesti A, Giangaspero F, Screpanti I, Alesse E, Gulino A.REN(KCTD11) is a suppressor of Hedgehog signaling and is deleted in human medulloblastoma. Proc Natl Acad Sci U S A. 2004 Jul 20;101(29):10833-8. Epub 2004 Jul 12. PMID: 15249678

Dighiero G, Maloum K, Desablens B, et al. Chlorambucil in indolent chronic lymphocytic leukemia. N Engl J Med. 1998;21:1506.

Ding XF, Luo C, Ren KQ, Zhang J, Zhou JL, Hu X, Liu RS, Wang Y, Gao X, Zhang J.Characterization and expression of a human KCTD1 gene containing the BTB domain, which mediates transcriptional repression and homomeric interactions. DNA Cell Biol. 2008 May;27(5):257-65. PMID: 18358072

Dohner H, Stilgenbauer S, Dohner K, Bentz M, Lichter P. Chromosome aberrations in B-cell chronic lymphocytic leukemia: reassessment based on molecular cytogenetic analysis. J Mol Med. 1999 Feb;77(2):266-81. Review.

Dohner, Hartmut, Stilgenbauer, Stephan, Benner, Axel, Leupolt, Elke, Krober, Alexander, Bullinger, Lars, Dohner, Konstanze, Bentz, Martin, Lichter, Peter. Genomic Aberrations and Survival in Chronic Lymphocytic Leukemia. N Engl J Med 2000 343: 1910-1916.

Dong JT, Boyd JC, Frierson HF Jr. Loss of heterozygosity at 13q14 and 13q21 in high grade, high stage prostate cancer. Prostate. 2001 Nov 1;49(3):166-71. PMID: 11746261

Elnenaei MO, Hamoudi RA, Swansbury J, Gruszka-Westwood AM, Brito-Babapulle V, Matutes E, Catovsky D. Delineation of the minimal region of loss at 13q14 in multiple myeloma. Genes Chromosomes Cancer. 2003 Jan;36(1):99-106. PMID: 12461754

F.S. Collins. Of needles and haystacks: finding human disease genes by positional cloning. Clin. Res., 1991, 39(4), 615-623.

Felipe A, Vicente R, Villalonga N, Roura-Ferrer M, Martínez-Mármol R, Solé L, Ferreres JC, Condom E. Potassium channels: new targets in cancer therapy. Cancer Detect Prev. 2006;30(4):375-85. Epub 2006 Sep 12. Review. PMID: 16971052

Fiserova A, Hajek R, Holubova V, Buchler T, Sobotka J, Kovarova R, Musilova R, Bourkova L, Bulikova A, Mareschova I, Janackova Z, Vanova P, Kuglik P, Vorlicek J, Penka M. Detection of 13q abnormalities in multiple myeloma using immunomagnetically selected plasma cells. Neoplasma. 2002;49(5):300-6.

Gale RP, Foon KA. Biology of chronic lymphocytic leukemia. Semin Hematol. 1987 Oct;24(4):209-29. Review

Gallo R, Zazzeroni F, Alesse E, Mincione C, Borello U, Buanne P, D'Eugenio R, Mackay AR, Argenti B, Gradini R, Russo MA, Maroder M, Cossu G, Frati L, Screpanti I, Gulino A.REN: a novel, developmentally regulated gene that promotes neural cell differentiation. J Cell Biol. 2002 Aug 19;158(4):731-40. Epub 2002 Aug 19. PMID: 12186855

Gao Q, Xue S, Doneanu CE, Goodlett DR, Nelson SD. Minimize the detection of false positives by the software program DetectShift for (18)O-labeled cross-linked peptide analysis. Eur J Mass Spectrom (Chichester, Eng). 2008;14(5):275-280. PMID: 19023145

Giallourakis C, Henson C, Reich M, Xie X, Mootha VK. Disease gene discovery through integrative genomics. Annu Rev Genomics Hum Genet. 2005;6:381-406. Review. PMID: 16124867

Gillies RJ, Robey I, Gatenby RA. Causes and consequences of increased glucose metabolism of cancers. J Nucl Med. 2008 Jun;49 Suppl 2:24S-42S. Review. PMID: 18523064

Grace, M.B., McLeland, C.B., Gagliardi, S.J., Smith, J.M., Jackson, W.E., Blakely, W.F., 2003. Quantitative RT-PCR assay using simultaneous measurement of four fluorophores for radiation-responsive gene targets. Clin. Chem. 49, 1467– 1475.

Gulbis JM, Mann S, MacKinnon R. Structure of a voltage-dependent K+ channel beta subunit. Cell. 1999 Jun 25;97(7):943-52. PMID: 10399921

Gulbis JM, Zhou M, Mann S, MacKinnon R. Structure of the cytoplasmic beta subunit-T1 assembly of voltage-dependent K+ channels. Science. 2000 Jul 7;289(5476):123-7. PMID: 10884227

Harrison CJ, Mazzullo H, Cheung KL, Gerrard G, Jalali GR, Mehta A, Osier DG, Orchard KH. Cytogenetics of multiple myeloma: interpretation of fluorescence in situ hybridization results. Br J Haematol. 2003 Mar;120(6):944-52. PMID: 12648063

Haslinger C, Schweifer N, Stilgenbauer S, Dohner H, Lichter P, Kraut N, Stratowa C, Abseher R. Microarray gene expression profiling of B-cell chronic lymphocytic leukemia subgroups defined by genomic aberrations and VH mutation status.J Clin Oncol. 2004 Oct 1;22(19):3937-49.

Hawthorn LA, Chapman R, Oscier D, Cowell JK. The consistent 13q14 translocation breakpoint seen in chronic B-cell leukaemia (BCLL) involves deletion of the D13S25

locus which lies distal to the retinoblastoma predisposition gene. Oncogene. 1993 Jun;8(6):1415-9. PMID: 8502470

Hayashi K, Igarashi H, Ogawa M, Sakaguchi N. Activity and substrate specificity of the murine STK2 Serine/Threonine kinase that is structurally related to the mitotic regulator protein NIMA of Aspergillus nidulans. Biochem Biophys Res Commun. 1999 Oct 22;264(2):449-56. PMID: 10529384

He H, Tan CK, Downey KM, So AG.A tumor necrosis factor alpha- and interleukin 6-inducible protein that interacts with the small subunit of DNA polymerase delta and proliferating cell nuclear antigen. Proc Natl Acad Sci U S A. 2001 Oct 9;98(21):11979-84. PMID: 11593007

Heginbotham L, Lu Z, Abramson T, MacKinnon R. Mutations in the K+ channel signature sequence. Biophys J. 1994;66:1061–1067.

Ho K, Nichols CG, Lederer WJ, Lytton J, Vassilev PM, Kanazirska MV, Hebert SC. Cloning and expression of an inwardly rectifying ATP-regulated potassium channel. Nature. 1993;362:31–38.

Igarashi A, Segoshi K, Sakai Y, Pan H, Kanawa M, Higashi Y, Sugiyama M, Nakamura K, Kurihara H, Yamaguchi S, Tsuji K, Kawamoto T, Kato Y.Selection of common markers for bone marrow stromal cells from various bones using real-time RT-PCR: effects of passage number and donor age. Tissue Eng. 2007 Oct;13(10):2405-17. PMID: 17596118

Iglesias-Serret D, de Frias M, Santidrian AF, Coll-Mulet L, Cosialls AM, Barragan M, Domingo A, Gil J, Pons G. Regulation of the proapoptotic BH3-only protein BIM by glucocorticoids, survival signals and proteasome in chronic lymphocytic leukemia cells. Leukemia. 2007 Feb;21(2):281-7.

Ivanov DV, Tyazhelova TV, Lemonnier L, Kononenko N, Pestova AA, Nikitin EA, Prevarskaya N, Skryma R, Panchin YV, Yankovsky NK, Baranova AV. A new human gene KCNRG encoding potassium channel regulating protein is a cancer suppressor gene candidate located in 13q14.3. FEBS Lett. 2003 Mar 27;539(1-3):156-60. PMID: 12650944

Jabbar SA, Ganeshaguru K, Wickremasinghe RG, Hoffbrand AV, Foroni L. Deletion of chromosome 13 (band q14) but not trisomy 12 is a clonal event in B-chronic lymphocytic leukaemia (CLL). Br J Haematol. 1995 Jun;90(2):476-8. PMID: 7794777

Junior Barrera, Roberto M Cesar, Jr, Carlos Humes, Jr, David C Martins, Jr, Diogo FC Patrão, Paulo JS Silva, and Helena Brentani. A feature selection approach for

identification of signature genes from SAGE data.BMC Bioinformatics. 2007; 8: 169. Published online 2007 May 22. doi: 10.1186/1471-2105-8-169. PMCID: PMC1891113

Kapanadze B, Kashuba V, Baranova A, Rasool O, van Everdink W, Liu Y, Syomov A, Corcoran M, Poltaraus A, Brodyansky V, Syomova N, Kazakov A, Ibbotson R, van den Berg A, Gizatullin R, Fedorova L, Sulimova G, Zelenin A, Deaven L, Lehrach H, Grander D, Buys C, Oscier D, Zabarovsky ER, Einhorn S, Yankovsky N. A cosmid and cDNA fine physical map of a human chromosome 13q14 region frequently lost in B-cell chronic lymphocytic leukemia and identification of a new putative tumor suppressor gene, Leu5. FEBS Lett. 1998 Apr 17;426(2):266-70. PMID: 9599022

Kapanadze B, Makeeva N, Corcoran M, Jareborg N, Hammarsund M, Baranova A, Zabarovsky E, Vorontsova O, Merup M, Gahrton G, Jansson M, Yankovsky N, Einhorn S, Oscier D, Grandér D, Sangfelt O. Comparative sequence analysis of a region on human chromosome 13q14, frequently deleted in B-cell chronic lymphocytic leukemia, and its homologous region on mouse chromosome 14. Genomics. 2000 Dec 15;70(3):327-34. PMID: 11161783

Kapanadze BI, Brodianskiĭ VM, Semov AB, Baranova AV, Sulimova GE, Aitova SS, Udina IG, Ptitsyna SN, Sal'nikova LE, Chudinov OS, Borbiev TE, Kashuba VV, Gizatullin R, Zabarovskaia V, Zabarovskiĭ ER, Fedorova LI, Zelenin AV, L'iu I, Rasul O, Eĭnkhorn S, van Everdink W, van den Berg A, Buys C, Corcoran M, Iankovskiĭ NK, et al. [Cosmid contig and cDNA map of the 13q14 region is frequently deleted in human B-cell chronic lymphocytic leukemia] Mol Biol (Mosk). 1997 May-Jun;31(3):515-9. Russian. No abstract available. PMID: 9297097

Karlsson A, Miller-Podraza H, Johansson P, Karlsson KA, Dahlgren C, Teneberg S. Different glycosphingolipid composition in human neutrophil subcellular compartments. Glycoconj J. 2001 Mar;18(3):231-43. PMID: 11602807

Kim, Y. H., J. J. Proust, M. J. Buchholz, F. J. Chrest, and A. A. Nordin. Expression of the murine homologue of the cell cycle control protein p34cdc2 in T lymphocytes. J. Immunol. 1992;149:17-23.

Knudson A.G.. Mutation and Cancer: Statistical Study of Retinoblastoma Proc. Natl. Acad. Sci., 1971, 68, 820-823.

Knudson A.G. Retinoblastoma: a prototypic hereditary neoplasm. Semin. Oncol., 1978, 5, 57-60.

Kobertz WR, Miller C. K+ channels lacking the 'tetramerization' domain: implications for pore structure. Nat Struct Biol. 1999 Dec;6(12):1122-5.

Kowanetz K, Husnjak K, Höller D, Kowanetz M, Soubeyran P, Hirsch D, Schmidt MH, Pavelic K, De Camilli P, Randazzo PA, Dikic I.CIN85 associates with multiple effectors controlling intracellular trafficking of epidermal growth factor receptors. Mol Biol Cell. 2004 Jul;15(7):3155-66. Epub 2004 Apr 16. PMID: 15090612

Kubista M, Akerman B, Nordén B. Characterization of interaction between DNA and 4',6-diamidino-2-phenylindole by optical spectroscopy. Biochemistry. 1987 Jul 14;26(14):4545-53. PMID: 3663606

Legdeur MC, Bontje PM, Ossenkoppele GJ, Beelen RH, van de Loosdrecht AA, Broekhoven MG, Langenhuijsen MM, Thijsen SF, Hofstee H, Schuurhuis GJ.The role of BCL-2 and bax protein in monocyte-mediated apoptosis in human leukemic cell lines.Exp Hematol. 1996 Nov;24(13):1530-9.PMID: 8950237

Lerner M, Corcoran M, Cepeda D, Nielsen ML, Zubarev R, Pontén F, Uhlén M, Hober S, Grandér D, Sangfelt O. The RBCC gene RFP2 (Leu5) encodes a novel transmembrane E3 ubiquitin ligase involved in ERAD. Mol Biol Cell. 2007 May;18(5):1670-82. Epub 2007 Feb 21. PMID: 17314412

Lewis RS, Cahalan MD. Potassium and calcium channels in lymphocytes. Annu Rev Immunol. 1995;13:623-53. Review. PMID: 7612237

Lin MC, Lee NP, Zheng N, Yang PH, Wong OG, Kung HF, Hui CK, Luk JM, Lau GK.Tumor necrosis factor-alpha-induced protein 1 and immunity to hepatitis B virus. World J Gastroenterol. 2005 Dec 28;11(48):7564-8. PMID: 16437679

Linsley PS, Schelter J, Burchard J, Kibukawa M, Martin MM, Bartz SR, Johnson JM, Cummins JM, Raymond CK, Dai H, Chau N, Cleary M, Jackson AL, Carleton M, Lim L. Transcripts targeted by the microRNA-16 family cooperatively regulate cell cycle progression. Mol Cell Biol. 2007 Mar;27(6):2240-52. Epub 2007 Jan 22. PMID: 17242205

Liu JP, Liu NS, Yuan HY, Guo Q, Lu H, Li YY. Human homologue of SETA binding protein 1 interacts with cathepsin B and participates in TNF-Induced apoptosis in ovarian cancer cells. Mol Cell Biochem. 2006 Nov;292(1-2):189-95.

Liu Y, Corcoran M, Rasool O, Ivanova G, Ibbotson R, Grandér D, Iyengar A, Baranova A, Kashuba V, Merup M, Wu X, Gardiner A, Mullenbach R, Poltaraus A, Hultström AL, Juliusson G, Chapman R, Tiller M, Cotter F, Gahrton G, Yankovsky N, Zabarovsky E, Einhorn S, Oscier D. Cloning of two candidate tumor suppressor genes within a 10 kb region on chromosome 13q14, frequently deleted in chronic lymphocytic leukemia. Oncogene. 1997 Nov 13;15(20):2463-73. PMID: 9395242

Liu Y, Grandér D, Söderhäll S, Juliusson G, Gahrton G, Einhorn S. Retinoblastoma gene deletions in B-cell chronic lymphocytic leukemia. Genes Chromosomes Cancer. 1992 Apr;4(3):250-6. PMID: 1382567

Liu Y, Hermanson M, Grandér D, Merup M, Wu X, Heyman M, Rasool O, Juliusson G, Gahrton G, Detlofsson R, Nikiforova N, Buys C, Söderhäll S, Yankovsky N, Zabarovsky E, Einhorn S. 13q deletions in lymphoid malignancies. Blood. 1995 Sep 1;86(5):1911-5. PMID: 7655020

Long SB, Campbell EB, Mackinnon R. Crystal structure of a mammalian voltage-dependent Shaker family K+ channel. Science. 2005 Aug 5;309(5736):897-903. Epub 2005 Jul 7. PMID: 16002581

Lu W, Takahashi H, Furusato M, Maekawa S, Nakano M, Meng C, Kikuchi Y, Sudo A, Hano H. Allelotyping analysis at chromosome 13q of high-grade prostatic intraepithelial neoplasia and clinically insignificant and significant prostate cancers. Prostate. 2006 Mar 1;66(4):405-12. PMID: 16302266

Luneau C. , Wiedmann R. , Smith J.S. , Williams J.B. Shaw-like rat brain potassium channel cDNA's with divergent 3' ends. FEBS Lett. 288 163-167 1991 [PubMed: 1879548]

Lyng MB, Laenkholm AV, Pallisgaard N, Ditzel HJ. Identification of genes for normalization of real-time RT-PCR data in breast carcinomas. BMC Cancer. 2008 Jan 22;8:20. PMID: 18211679

Ma E, Wang X, Li Y, Sun X, Tai W, Li T, Gou T.Induction of apoptosis by furanodiene in HL60 leukemia cells through activation of TNFR1 signaling pathway.Cancer Lett. 2008 Jul 28. [Epub ahead of print]PMID: 18667267

Mahaffy RE, Pollard TD.Influence of phalloidin on the formation of actin filament branches by Arp2/3 complex.Biochemistry. 2008 Jun 17;47(24):6460-7. Epub 2008 May 20.PMID: 18489122

Matsuda A, Suzuki Y, Honda G, Muramatsu S, Matsuzaki O, Nagano Y, Doi T, Shimotohno K, Harada T, Nishida E, Hayashi H, Sugano S. Large-scale identification and characterization of human genes that activate NF-kappaB and MAPK signaling pathways. Oncogene. 2003 May 22;22(21):3307-18. PMID: 12761501

McCormack T, McCormack K. Shaker K+ channel beta subunits belong to an NAD(P)H-dependent oxidoreductase superfamily. Cell. 1994 Dec 30;79(7):1133-5. No abstract available. PMID: 8001150

Mengubas K, Riordan FA, Hoffbrand AV, Wickremasinghe RG.Co-ordinated downregulation of bcl-2 and bax expression during granulocytic and macrophage-like differentiation of the HL60 promyelocytic leukaemia cell line.FEBS Lett. 1996 Oct 7;394(3):356-60.PMID: 8830674

Mertens D, Wolf S, Bullinger L, Ohl S, Schaffner C, Döhner H, Stilgenbauer S, Lichter P. BCMSUN, a candidate gene for B-cell chronic lymphocytic leukemia and mantle-cell lymphoma, has an independently expressed homolog on 1p22-p31, BCMSUN-like. Int J Cancer. 2000 Dec 1;88(5):692-7. PMID: 11072235

Migliazza A, Bosch F, Komatsu H, Cayanis E, Martinotti S, Toniato E, Guccione E, Qu X, Chien M, Murty VV, Gaidano G, Inghirami G, Zhang P, Fischer S, Kalachikov SM, Russo J, Edelman I, Efstratiadis A, Dalla-Favera R. Nucleotide sequence, transcription map, and mutation analysis of the 13q14 chromosomal region deleted in B-cell chronic lymphocytic leukemia. Blood. 2001 Apr 1;97(7):2098-104.

Mikael Lerner, Martin Corcoran, Diana Cepeda, Michael L. Nielsen, Roman Zubarev, Fredrik Pontén, Mathias Uhlén, Sophia Hober, Dan Grandér, and Olle Sangfelt. The RBCC Gene RFP2 (Leu5) Encodes a Novel Transmembrane E3 Ubiquitin Ligase Involved in ERAD Mol Biol Cell. 2007 May; 18(5): 1670–1682. doi: 10.1091/mbc.E06-03-0248. PMCID: PMC1855009

Mikael Lerner. On 13q14 deletions in chronic lymphocytic leukemia. Department of Oncology – Pathology, Cancer Center Karolinska, Karolinska Institutet, Stockholm, Sweden. ISBN 978-91-7409-067-3. 2008.

Miller C. An overview of the potassium channel family. Genome Biol. 2000;1(4):REVIEWS0004. Epub 2000 Oct 13. Review. PMID: 11178249

Minor DL, Lin YF, Mobley BC, Avelar A, Jan YN, Jan LY, Berger JM. The polar T1 interface is linked to conformational changes that open the voltage-gated potassium channel. Cell. 2000 Sep 1;102(5):657-70. PMID: 11007484

Montserrat E. Assessing prognosis in patients with chronic lymphocytic leukemia a quarter of a century after Rai and Binet staging systems. Ann Oncol. 2004 Oct;15(10):1450-1.

Narita T, Nishimura T, Yoshizaki K, Taniyama T.CIN85 associates with TNF receptor 1 via Src and modulates TNF-alpha-induced apoptosis. Exp Cell Res. 2005 Mar 10;304(1):256-64. Epub 2004 Dec 1. PMID: 15707590

O'Connor SJ, Su'ut L, Morgan GJ, Jack AS. The relationship between typical and atypical B-cell chronic lymphocytic leukemia. A comparative genomic hybridization-based study. Am J Clin Pathol. 2000 Sep;114(3):448-58.

Oda T, Namba K, Maéda Y.Position and orientation of phalloidin in F-actin determined by X-ray fiber diffraction analysis.Biophys J. 2005 Apr;88(4):2727-36. Epub 2005 Jan 14.PMID: 15653738

Olivier M, Hussain SP, Caron de Fromentel C, Hainaut P, Harris CC. TP53 mutation spectra and load: a tool for generating hypotheses on the etiology of cancer. IARC Sci Publ. 2004;(157):247-70. Review. PMID: 15055300

Ougolkov AV, Bone ND, Fernandez-Zapico ME, Kay NE, Billadeau DD. Inhibition of glycogen synthase kinase-3 activity leads to epigenetic silencing of nuclear factor {kappa}B target genes and induction of apoptosis in chronic lymphocytic leukemia B cells. Blood. 2007 Jul 15;110(2):735-42.

Pamela L Paris, Matthias D Hofer, Giancarlo Albo, Rainer Kuefer, Juergen E Gschwend, Richard E Hautmann, Jane Fridyland, Jeffrey Simko, Peter R Carroll, Mark A Rubin, and Colin Collins. Genomic Profiling of Hormone-Naïve Lymph Node Metastases in Patients with Prostate Cancer. Neoplasia. 2006 December; 8(12): 1083–1089. PMCID: PMC1783716

Papazian DM, Schwarz TL, Tempel BL, Jan YN, Jan LY. Cloning of genomic and complementary DNA from Shaker, a putative potassium channel gene from Drosophila. Science. 1987;237:749–753.

Parcej DN, Scott VE, Dolly JO. Oligomeric properties of alpha-dendrotoxin-sensitive potassium ion channels purified from bovine brain. Biochemistry. 1992 Nov 17;31(45):11084-8. PMID: 1445846

Pearl A. Campbell, Carolina Perez-Iratxeta, Miguel A. Andrade-Navarro, and Michael A. Rudnicki. Oct4 Targets Regulatory Nodes to Modulate Stem Cell Function. PLoS ONE. 2007; 2(6): e553. Published online 2007 June 20. doi: 10.1371/journal.pone.0000553. PMCID: PMC1891092

Perney T.M. , Kaczmarek L.K. The molecular biology of K+ channels. Curr. Opin. Cell Biol. 3 663-670 1991 [PubMed: 1772658]

Pongs O, Kecskemethy N, Müller R, Krah-Jentgens I, Baumann A, Kiltz HH, Canal I, Llamazares S, Ferrus A. Shaker encodes a family of putative potassium channel proteins in the nervous system of Drosophila. . EMBO J. 1988;7:1087–1096.

Rai KR, Sawitsky A, Cronkite EP, Chanana AD, Levy RN, Pasternack BS. Clinical staging of chronic lymphocytic leukemia. Blood. 1975 Aug;46(2):219-34.

Rai KR. Chronic lymphocytic leukemia in the elderly population. Clin Geriatr Med. 1997 May;13(2):245-9.

Raveche ES, Salerno E, Scaglione BJ, Manohar V, Abbasi F, Lin YC, Fredrickson T, Landgraf P, Ramachandra S, Huppi K, Toro JR, Zenger VE, Metcalf RA, Marti GE. Abnormal microRNA-16 locus with synteny to human 13q14 linked to CLL in NZB mice. Blood. 2007 Jun 15;109(12):5079-86. Epub 2007 Mar 9. PMID: 17351108

Redaelli A, Laskin BL, Stephens JM, Botteman MF, Pashos CL. The clinical and epidemiological burden of chronic lymphocytic leukaemia. Eur J Cancer Care (Engl). 2004 Jul;13(3):279-87.

Rehm H, Lazdunski M. Purification and subunit structure of a putative K+-channel protein identified by its binding properties for dendrotoxin I. Proc Natl Acad Sci U S A. 1988 Jul;85(13):4919-23. PMID: 2455300

Resendes BL, Kuo SF, Robertson NG, Giersch AB, Honrubia D, Ohara O, Adams JC, Morton CC.Isolation from cochlea of a novel human intronless gene with predominant fetal expression. J Assoc Res Otolaryngol. 2004 Jun;5(2):185-202. PMID: 15357420

Rødningen OK, Overgaard J, Alsner J, Hastie T, Børresen-Dale AL.Microarray analysis of the transcriptional response to single or multiple doses of ionizing radiation in human subcutaneous fibroblasts. Radiother Oncol. 2005 Dec;77(3):231-40. Epub 2005 Nov 17. PMID: 16297999

Rosenwald A, Ott G, Krumdiek AK, Dreyling MH, Katzenberger T, Kalla J, Roth S, Ott MM, Muller-Hermelink HK. A biological role for deletions in chromosomal band 13q14 in mantle cell and peripheral t-cell lymphomas? Genes Chromosomes Cancer. 1999 Nov;26(3):210-4.

Rowntree C, Duke V, Panayiotidis P, Kotsi P, Palmisano GL, Hoffbrand AV, Foroni L.Deletion analysis of chromosome 13q14.3 and characterisation of an alternative splice form of LEU1 in B cell chronic lymphocytic leukemia. Leukemia. 2002 Jul;16(7):1267-75.

Rybalchenko V, Prevarskaya N, Van Coppenolle F, Legrand G, Lemonnier L, Le Bourhis X, Skryma R. Verapamil inhibits proliferation of LNCaP human prostate cancer cells influencing K+ channel gating. Mol Pharmacol. 2001 Jun;59(6):1376-87. PMID: 11353796

S Stilgenbauer, L Bullinger, A Benner, K Wildenberger, M Bentz, K Döhner, A D Ho, P Lichter and H Döhner. Incidence and clinical significance of 6q deletions in B cell chronic lymphocytic leukemia. Leukemia. 1999 Sep; Vol. 13. No 9, p.1331-1334.

Sambrook, J., Fritsch, E.F., Maniatis, T., 1989. Molecular Cloning: A Laboratory Manual Cold Spring Harbor Laboratory Press, Cold Spring Harbor, NY

Sansal I, Sellers WR. The biology and clinical relevance of the PTEN tumor suppressor pathway. J Clin Oncol. 2004 Jul 15;22(14):2954-63. Review. PMID: 15254063

Sansom M.S. Potassium channels: watching a voltage-sensor tilt and twist. Curr. Biol. 10 R206-R209 2000 [PubMed: 10712896]

Santarosa M, Ashworth A. Haploinsufficiency for tumour suppressor genes: when you don't need to go all the way. Biochim Biophys Acta. 2004 Jun 7;1654(2):105-22. Review. PMID: 15172699

Scaglione BJ, Salerno E, Balan M, Coffman F, Landgraf P, Abbasi F, Kotenko S, Marti GE, Raveche ES. Murine models of chronic lymphocytic leukaemia: role of microRNA-16 in the New Zealand Black mouse model. Br J Haematol. 2007 Dec;139(5):645-57. Epub 2007 Oct 17. Review. PMID: 17941951

Scanlan MJ, Gordan JD, Williamson B, Stockert E, Bander NH, Jongeneel V, Gure AO, Jäger D, Jäger E, Knuth A, Chen YT, Old LJ.Antigens recognized by autologous antibody in patients with renal-cell carcinoma. Int J Cancer. 1999 Nov 12;83(4):456-64. PMID: 10508479

Schwarz T.L. , Tempel B.L. , Papazian D.M. , Jan Y.N. , Jan L.Y. Multiple potassium-channel components are produced by alternative splicing at the Shaker locus in Drosophila. Nature 331 137-142 1988 [PubMed: 2448635]

Scott VE, Rettig J, Parcej DN, Keen JN, Findlay JB, Pongs O, Dolly JO. Primary structure of a beta subunit of alpha-dendrotoxin-sensitive K+ channels from bovine brain. Proc Natl Acad Sci U S A. 1994 Mar 1;91(5):1637-41. PMID: 8127858

Sewing S, Roeper J, Pongs O. Kv beta 1 subunit binding specific for shaker-related potassium channel alpha subunits. Neuron. 1996 Feb;16(2):455-63. PMID: 8789960

Sharpless NE. INK4a/ARF: a multifunctional tumor suppressor locus. Mutat Res. 2005 Aug 25;576(1-2):22-38. Review. PMID: 15878778

Shaw GR, Kronberger DL.TP53 deletions but not trisomy 12 are adverse in B-cell lymphoproliferative disorders. Cancer Genet Cytogenet. 2000 Jun;119(2):146-54. PMID: 10867151

Short KM, Cox TC. Subclassification of the RBCC/TRIM superfamily reveals a novel motif necessary for microtubule binding. J Biol Chem. 2006 Mar 31;281(13):8970-80. Epub 2006 Jan 23. PMID: 16434393

Short KM, Hopwood B, Yi Z, Cox TC. MID1 and MID2 homo- and heterodimerise to tether the rapamycin-sensitive PP2A regulatory subunit, alpha 4, to microtubules:

implications for the clinical variability of X-linked Opitz GBBB syndrome and other developmental disorders. BMC Cell Biol. 2002;3:1. Epub 2002 Jan 4. PMID: 11806752

Sirover MA. New nuclear functions of the glycolytic protein, glyceraldehyde-3-phosphate dehydrogenase, in mammalian cells. J Cell Biochem. 2005 May 1;95(1):45-52. Review. PMID: 15770658

Skoblov M, Shakhbazov K, Oshchepkov D, Ivanov D, Guskova A, Ivanov D, Rubtsov P, Prasolov V, Yankovsky N, Baranova A. Human RFP2 gene promoter: unique structure and unusual strength. Biochem Biophys Res Commun. 2006 Apr 14;342(3):859-66. Epub 2006 Feb 17. PMID: 16499869

Smith GA, Tsui HW, Newell EW, Jiang X, Zhu XP, Tsui FW, Schlichter LC. Functional up-regulation of HERG K+ channels in neoplastic hematopoietic cells. J Biol Chem. 2002 May 24;277(21):18528-34. Epub 2002 Mar 13. PMID: 11893742

Stilgenbauer S, Döhner K, Bentz M, Lichter P, Döhner H. Molecular cytogenetic analysis of B-cell chronic lymphocytic leukemia. Ann Hematol. 1998 Mar-Apr;76(3-4):101-10. Review. PMID: 9619726

Stogios PJ, Downs GS, Jauhal JJ, Nandra SK, Privé GG.Sequence and structural analysis of BTB domain proteins. Genome Biol. 2005;6(10):R82. Blood. 2007 Jun 15;109(12):5079-86. Epub 2007 Mar 9.

Stuhmer W. , Ruppersberg J.P. , Schroter K.H. , Sakmann B. , Stocker M. , Giese K.P., Perschke A. , Baumann A. , Pongs O. Molecular basis of functional diversity of voltage-gated potassium channels in mammalian brain. EMBO J. 8 3235-3244 1989 [PubMed: 2555158]

Suehara Y, Kondo T, Seki K, Shibata T, Fujii K, Gotoh M, Hasegawa T, Shimada Y, Sasako M, Shimoda T, Kurosawa H, Beppu Y, Kawai A, Hirohashi S.Pfetin as a prognostic biomarker of gastrointestinal stromal tumors revealed by proteomics. Clin Cancer Res. 2008 Mar 15;14(6):1707-17. PMID: 18347171

Tan YD, Fornage M, Xu H.Ranking analysis of F-statistics for microarray data. BMC Bioinformatics. 2008 Mar 6;9:142. PMID: 18325100

Tanious FA, Veal JM, Buczak H, Ratmeyer LS, Wilson WD.DAPI (4',6-diamidino-2-phenylindole) binds differently to DNA and RNA: minor-groove binding at AT sites and intercalation at AU sites. Biochemistry. 1992 Mar 31;31(12):3103-12. PMID: 1372825

Tara L Naylor, Joel Greshock, Yan Wang, Theresa Colligon, QC Yu, Virginia Clemmer, Tal Z Zaks, and Barbara L Weber. High resolution genomic analysis of sporadic breast cancer using array-based comparative genomic hybridization. Breast Cancer Res. 2005;

7(6): R1186–R1198. Published online 2005 November 24. doi: 10.1186/bcr1356. PMCID: PMC1410746

Tiazhelova TV, Ivanov DV, Makeeva NV, Kapanadze BI, Nikitin EA, Semov AB, Sangfeldt O, Grander D, Vorob'ev AI, Einhorn S, Iankovskiĭ NK, Baranova AV. Transcription map of the 13q14 region, frequently deleted in B-cell chronic lymphocytic leukemia patients. Genetika. 2001 Nov;37(11):1530-7. PMID: 11771308

Tusher VG, Tibshirani R, Chu G. Significance analysis of microarrays applied to the ionizing radiation response. Proc Natl Acad Sci U S A. 2001 Apr 24;98(9):5116-21. Epub 2001 Apr 17. Erratum in: Proc Natl Acad Sci U S A 2001 Aug 28;98(18):10515. PMID: 11309499

Tyybakinoja A, Vilpo J, Knuutila S. High-resolution oligonucleotide array-CGH pinpoints genes involved in cryptic losses in chronic lymphocytic leukemia. Cytogenet Genome Res. 2007;118(1):8-12.

Unteregger G, Profit S. Quantitative Measurement of Cell Proliferation Using the BrdU ELISA: A Comparison Between Colorimetric and Chemiluminescent Detection. BIochemica. 2001. No 4, p.33-35.

Van Bogaert P, Azizieh R, Désir J, Aeby A, De Meirleir L, Laes JF, Christiaens F, Abramowicz MJ.Mutation of a potassium channel-related gene in progressive myoclonic epilepsy. Ann Neurol. 2007 Jun;61(6):579-86. PMID: 17455289

van Everdink WJ, Baranova A, Lummen C, Tyazhelova T, Looman MW, Ivanov D, Verlind E, Pestova A, Faber H, van der Veen AY, Yankovsky N, Vellenga E, Buys CH. RFP2, c13ORF1, and FAM10A4 are the most likely tumor suppressor gene candidates for B-cell chronic lymphocytic leukemia. Cancer Genet Cytogenet. 2003 Oct 1;146(1):48-57. PMID: 14499696

Wang G, Covarrubias M. Voltage-dependent gating rearrangements in the intracellular T1-T1 interface of a K+ channel. J Gen Physiol. 2006 Apr;127(4):391-400. Epub 2006 Mar 13. PMID: 16533897

Wang M, Windgassen D, Papoutsakis ET.Comparative analysis of transcriptional profiling of CD3+, CD4+ and CD8+ T cells identifies novel immune response players in T-cell activation. BMC Genomics. 2008 May 16;9:225. PMID: 18485203

Watanabe S, Take H, Takeda K, Yu ZX, Iwata N, Kajigaya S.Characterization of the CIN85 adaptor protein and identification of components involved in CIN85 complexes. Biochem Biophys Res Commun. 2000 Nov 11;278(1):167-74. PMID: 11071869

Weger S, Hammer E, Götz A, Heilbronn R.Identification of a cytoplasmic interaction partner of the large regulatory proteins Rep78/Rep68 of adeno-associated virus type 2 (AAV-2). Virology. 2007 May 25;362(1):192-206. Epub 2007 Jan 17. PMID: 17239418

Wieland T. Modification of actins by phallotoxins. Naturwissenschaften. 1977 Jun;64(6):303-9.PMID: 18683

Wolf S, Mertens D, Schaffner C, Korz C, Döhner H, Stilgenbauer S, Lichter P. B-cell neoplasia associated gene with multiple splicing (BCMS): the candidate B-CLL gene on 13q14 comprises more than 560 kb covering all critical regions. Hum Mol Genet. 2001 Jun 1;10(12):1275-85. PMID: 11406609

Xu B, Wilson BA, Lu L. Induction of human myeloblastic ML-1 cell G1 arrest by suppression of K+ channel activity. Am J Physiol. 1996 Dec;271(6 Pt 1):C2037-44. PMID: 8997206

Yang LP, Zhou AD, Li H, Zhang WF, Wu YY, Zhang J, Han M.[Expression profile in the cell lines of human TNFAIP1 gene] Yi Chuan. 2006 Aug;28(8):918-22. Chinese. PMID: 16870576

Yu W, Xu J, Li M. NAB domain is essential for the subunit assembly of both alpha-alpha and alpha-beta complexes of shaker-like potassium channels. Neuron. 1996 Feb;16(2):441-53. PMID: 8789959

Zawlik I, Zakrzewska M, Witusik M, Golanska E, Kulczycka-Wojdala D, Szybka M, Piaskowski S, Wozniak K, Zakrzewski K, Papierz W, Liberski PP, Rieske P.KCTD11 expression in medulloblastoma is lower than in adult cerebellum and higher than in neural stem cells. Cancer Genet Cytogenet. 2006 Oct 1;170(1):24-8. PMID: 16965951

Zerangue N, Jan YN, Jan LY. An artificial tetramerization domain restores efficient assembly of functional Shaker channels lacking T1. Proc Natl Acad Sci U S A. 2000 Mar 28;97(7):3591-5.

Zhang W, McIntosh AL, Xu H, Wu D, Gruninger T, Atshaves B, Liu JC, Schroeder F.Structural analysis of sterol distributions in the plasma membrane of living cells.Biochemistry. 2005 Mar 1;44(8):2864-84. Erratum in: Biochemistry. 2005 May 17;44(19):7388.

Zhou J, Ren K, Liu X, Xiong X, Hu X, Zhang J.A novel PDIP1-related protein, KCTD10, that interacts with proliferating cell nuclear antigen and DNA polymerase delta. Biochim Biophys Acta. 2005 Jul 10;1729(3):200-3. PMID: 15982757

Zhou Q, Kwan HY, Chan HC, Jiang JL, Tam SC, Yao X. Blockage of voltage-gated K+ channels inhibits adhesion and proliferation of hepatocarcinoma cells. Int J Mol Med. 2003 Feb;11(2):261-6.

Zwiebel JA, Cheson BD. Chronic lymphocytic leukemia: staging and prognostic factors. Semin Oncol. 1998;25:42.

CURRICULUM VITAE

Aybike Birerdinc graduated from the International School of Islamabad, Islamabad, Pakistan, in 1994. She received her Bachelor of Science from Trinity College in 1999, and received her Master of Science in Biochemistry with a specialization in Biotechnology from Georgetown University in 2001.